

UNCLASSIFIED

AD NUMBER

AD882624

LIMITATION CHANGES

TO:

Approved for public release; distribution is unlimited.

FROM:

Distribution authorized to U.S. Gov't. agencies only; Test and Evaluation; APR 1971. Other requests shall be referred to Arnold Engineering Development Center, Arnold AFB, TN.

AUTHORITY

AEDC ltr 12 Apr 1976

THIS PAGE IS UNCLASSIFIED

QJ

**LONGITUDINAL STATIC STABILITY AND DRAG  
CHARACTERISTICS OF A-7D AND F-4E  
AIRCRAFT WITH VARIOUS EXTERNAL  
STORE CONFIGURATIONS  
AT TRANSONIC SPEEDS**

**APPROVED FOR RELEASE - 9 Apr 1976**



OFFICE OF INFORMATION  
ARNOLD ENGINEERING DEVELOPMENT CENTER  
ARNOLD AIR FORCE STATION, TENN. 37389

**Ronald E. Davis**

**ARO, Inc.**

**April 1971**

This document contains information that is being released  
its distribution is unlimited. *PW AF Fitter dtd.  
12 April 76 - Welham  
Cole -*

Distribution limited to U. S. Government agencies only;  
contains information covering the test and evaluation of  
military hardware; April 1971; other requests for this  
document must be referred to AFATL (DLII), Eglin AFB,  
Florida 82542.

**PROPULSION WIND TUNNEL FACILITY  
ARNOLD ENGINEERING DEVELOPMENT CENTER  
AIR FORCE SYSTEMS COMMAND  
ARNOLD AIR FORCE STATION, TENNESSEE**

PROPERTY OF U. S. AIR FORCE

F40300-71-C-0002

# ***NOTICES***

When U. S. Government drawings specifications, or other data are used for any purpose other than a definitely related Government procurement operation, the Government thereby incurs no responsibility nor any obligation whatsoever, and the fact that the Government may have formulated, furnished, or in any way supplied the said drawings, specifications, or other data, is not to be regarded by implication or otherwise, or in any manner licensing the holder or any other person or corporation, or conveying any rights or permission to manufacture, use, or sell any patented invention that may in any way be related thereto.

Qualified users may obtain copies of this report from the Defense Documentation Center.

References to named commercial products in this report are not to be considered in any sense as an endorsement of the product by the United States Air Force or the Government.

LONGITUDINAL STATIC STABILITY AND DRAG  
CHARACTERISTICS OF A-7D AND F-4E  
AIRCRAFT WITH VARIOUS EXTERNAL  
STORE CONFIGURATIONS  
AT TRANSONIC SPEEDS

Ronald E. Davis  
ARO, Inc.

This document has been approved for public release  
its distribution is unlimited. *Per AF letter dtg  
12 April 1976 -  
William O. Cole -*

~~Distribution limited to U. S. Government agencies only;  
contains information covering the test and evaluation of  
military hardware; April 1971; other requests for this  
document must be referred to AFATL (DLI), Eglin AFB,  
Florida 32542.~~



APPROVED FOR RELEASE

OFFICE OF INFORMATION  
ARNOLD ENGINEERING DEVELOPMENT CENTER  
ARNOLD AIR FORCE STATION, TENN. 37389

*9 Apr 1976*

## FOREWORD

The work reported herein was sponsored by the Air Force Armament Laboratory (AFATL), Air Force Systems Command (AFSC), under Program Element 62602F, Project 2567.

The test results presented were obtained by ARO, Inc. (a subsidiary of Sverdrup & Parcel and Associates, Inc.), contract operator of the Arnold Engineering Development Center (AEDC), AFSC, Arnold Air Force Station, Tennessee, under Contract F40600-71-C-0002. The tests were conducted during the period November 9 to 17, 1970, under ARO Project No. PC0114, and the manuscript was submitted for publication on February 4, 1971.

This technical report has been reviewed and is approved.

George F. Garey  
Lt Colonel, USAF  
AF Representative, PWT  
Directorate of Test

Joseph R. Henry  
Colonel, USAF  
Director of Test

**ABSTRACT**

Longitudinal aerodynamic characteristics of 0.05-scale models of A-7D and F-4E aircraft were obtained at Mach numbers from 0.50 to 1.30 to determine the effects of store configuration and location on stability and drag. Prototypes, as well as a family of proposed store configurations, were tested.

## CONTENTS

	<u>Page</u>
ABSTRACT . . . . .	iii
NOMENCLATURE . . . . .	viii
I. INTRODUCTION . . . . .	1
II. APPARATUS . . . . .	
2.1 Test Facility . . . . .	1
2.2 Test Articles . . . . .	1
2.3 Instrumentation . . . . .	2
III. TEST DESCRIPTION . . . . .	
3.1 Test Conditions and Procedures . . . . .	2
3.2 Corrections . . . . .	2
3.3 Precision of Measurements . . . . .	3
IV. RESULTS AND DISCUSSION . . . . .	
4.1 Data Presentation . . . . .	3
4.2 A-7D Configurations . . . . .	3
4.3 F-4E Configurations . . . . .	4
V. CONCLUSIONS . . . . .	5

## APPENDIXES

### I. ILLUSTRATIONS

#### Figure

1. Schematic of the Tunnel Test Section Showing Model Location . . . . .	9
2. Sketch of the Aircraft Models . . . . .	
a. A-7D Model . . . . .	10
b. F-4E Model . . . . .	11
3. Details and Dimensions of the Aircraft Model Pylons . . . . .	
a. A-7D Model . . . . .	12
b. F-4E Model . . . . .	13
4. Details and Dimensions of the Aircraft TER and MER Models . . . . .	
a. A-7D Model TER . . . . .	14
b. A-7D Model MER . . . . .	15
c. F-4E Model TER . . . . .	16
d. F-4E Model MER . . . . .	17
5. Details and Dimensions of the 370-gal Fuel Tank Model on the Outboard F-4E Pylon . . . . .	18
6. Details and Dimensions of the MK-82 Bomb Model . . . . .	19
7. Details and Dimensions of the M-117 Bomb Model . . . . .	20
8. Schematic of the TER and MER Store Stations and Orientation . . . . .	21
9. Details and Dimensions of the Various Parametric Shape Configurations . . . . .	22

<u>Figure</u>	<u>Page</u>
10. A-7D and F-4E Models Installed in the Tunnel Test Section	
a. Configuration F401 . . . . .	23
b. Configuration F411 . . . . .	24
c. Configuration A713 . . . . .	25
d. Configuration A704 . . . . .	26
11. Variation of Dynamic Pressure and Reynolds Number with Mach Number . . .	27
12. Lift Coefficient Variation with Angle of Attack for Configurations A701, A702, A703, and A704 . . . . .	28
13. Pitching-Moment Coefficient Variation with Lift Coefficient for Configurations A701, A702, A703, and A704 . . . . .	32
14. Drag Coefficient Variation with Lift Coefficient for Configurations A701, A702, A703, and A704 . . . . .	36
15. Drag Coefficient Variation with Mach Number at $C_L = 0$ for Configurations A701, A702, A703, and A704 . . . . .	40
16. Lift Coefficient Variation with Angle of Attack for Configurations A701, A707, and A710 . . . . .	41
17. Pitching-Moment Coefficient Variation with Lift Coefficient for Configurations A701, A707, and A710 . . . . .	45
18. Drag Coefficient Variation with Lift Coefficient for Configurations A701, A707, and A710 . . . . .	49
19. Drag Coefficient Variation with Mach Number at $C_L = 0$ for Configurations A701, A707, and A710 . . . . .	53
20. Lift Coefficient Variation with Angle of Attack for Configurations A701, A711, A712, and A713 . . . . .	54
21. Pitching-Moment Coefficient Variation with Lift Coefficient for Configurations A701, A711, A712, and A713 . . . . .	58
22. Drag Coefficient Variation with Lift Coefficient for Configurations A701, A711, A712, and A713 . . . . .	62
23. Drag Coefficient Variation with Mach Number at $C_L = 0$ for Configurations A701, A711, A712, and A713 . . . . .	66
24. Lift Coefficient Variation with Angle of Attack for Configurations A701, A705, A706, and A707 . . . . .	67
25. Pitching-Moment Coefficient Variation with Lift Coefficient for Configurations A701, A705, A706, and A707 . . . . .	71
26. Drag Coefficient Variation with Lift Coefficient for Configurations A701, A705, A706, and A707 . . . . .	75
27. Drag Coefficient Variation with Mach Number at $C_L = 0$ for Configurations A701, A705, A706, and A707 . . . . .	79
28. Lift Coefficient Variation with Angle of Attack for Configurations A701, A707, and A713 . . . . .	80
29. Pitching-Moment Coefficient Variation with Lift Coefficient for Configurations A701, A707, and A713 . . . . .	84
30. Drag Coefficient Variation with Lift Coefficient for Configurations A701, A707, and A713 . . . . .	88



<u>Figure</u>	<u>Page</u>
31. Drag Coefficient Variation with Mach Number at $C_L = 0$ for Configurations A701, A707, and A713 . . . . .	92
32. Lift Coefficient Variation with Angle of Attack for Configurations F401, F402, F403, and F404 . . . . .	93
33. Pitching-Moment Coefficient Variation with Lift Coefficient for Configurations F401, F402, F403, and F404 . . . . .	99
34. Drag Coefficient Variation with Lift Coefficient for Configurations F401, F402, F403, and F404 . . . . .	105
35. Drag Coefficient Variation with Mach Number at $C_L = 0.30$ , $M_\infty < 1.0$ and $C_L = 0.1$ , $M_\infty > 1.0$ for Configurations F401, F402, F403, and F404 . . . . .	111
36. Lift Coefficient Variation with Angle of Attack for Configurations F401, F412, F415, and F418 . . . . .	112
37. Pitching-Moment Coefficient Variation with Lift Coefficient for Configurations F401, F412, F415, and F418 . . . . .	118
38. Drag Coefficient Variation with Lift Coefficient for Configurations F401, F412, F415, and F418 . . . . .	124
39. Drag Coefficient Variation with Mach Number at $C_L = 0.30$ , $M_\infty < 1.0$ and $C_L = 0.1$ , $M_\infty > 1.0$ for Configurations F401, F412, F415, and F418 . . . . .	130
40. Lift Coefficient Variation with Angle of Attack for Configurations F401, F405, F406, and F407 . . . . .	131
41. Pitching-Moment Coefficient Variation with Lift Coefficient for Configurations F401, F405, F406, and F407 . . . . .	137
42. Drag Coefficient Variation with Lift Coefficient for Configurations F401, F405, F406, and F407 . . . . .	143
43. Drag Coefficient Variation with Mach Number at $C_L = 0.30$ , $M_\infty < 1.0$ and $C_L = 0.1$ , $M_\infty > 1.0$ for Configurations F401, F405, F406, and F407 . . . . .	149
44. Lift Coefficient Variation with Angle of Attack for Configurations F401, F408, F407, F410, and F411 . . . . .	150
45. Pitching-Moment Coefficient Variation with Lift Coefficient for Configurations F401, F408, F407, F410, and F411 . . . . .	156
46. Drag Coefficient Variation with Lift Coefficient for Configurations F401, F408, F407, F410, and F411 . . . . .	162
47. Drag Coefficient Variation with Mach Number at $C_L = 0.30$ , $M_\infty < 1.0$ and $C_L = 0.1$ , $M_\infty > 1.0$ for Configurations F401, F408, F407, F410, and F411 . . . . .	168
48. Lift Coefficient Variation with Angle of Attack for Configurations F401, F411, and F419 . . . . .	169
49. Pitching-Moment Coefficient Variation with Lift Coefficient for Configurations F401, F411, and F419 . . . . .	175
50. Drag Coefficient Variation with Lift Coefficient for Configurations F401, F411, and F419 . . . . .	181

<u>Figure</u>	<u>Page</u>
51. Drag Coefficient Variation with Mach Number at $C_L = 0.30$ , $M_\infty < 1.0$ and $C_L = 0.1$ , $M_\infty > 1.0$ for Configurations F401, F411, and F419 . . . . .	187
52. Lift Coefficient Variation with Angle of Attack for Configurations F401, F419, and F420 . . . . .	188
53. Pitching-Moment Coefficient Variation with Lift Coefficient for Configurations F401, F419, and F420 . . . . .	194
54. Drag Coefficient Variation with Lift Coefficient for Configurations F401, F419, and F420 . . . . .	200
55. Drag Coefficient Variation with Mach Number at $C_L = 0.30$ , $M_\infty < 1.0$ and $C_L = 0.1$ , $M_\infty > 1.0$ for Configurations F401, F419, and F420 . . . . .	206

## II. TABLES

I. Aircraft Load Configurations . . . . .	207
II. Guide to Figure Interpretation . . . . .	208

## NOMENCLATURE

$A_b$	Base area, 0.0201 sq ft for A-7D and 0.0747 sq ft for F-4E
BL	Buttock line from plane of symmetry, in.
$C_A$	Measured axial-force coefficient, measured axial force/ $q_\infty S$
$C_{A,b}$	Base axial-force coefficient, $(p_\infty - p_b)A_b/q_\infty S$
$C_{A,F}$	Forebody axial-force coefficient, $C_A - C_{A,b}$
$C_D$	Forebody-drag coefficient, forebody drag/ $q_\infty S$
$C_m$	Pitching-moment coefficient, pitching moment/ $q_\infty S d$ , moment reference at FS 16.173 and WL 5.00 for A-7D and FS 16.233 and WL 1.55 for F-4E
$C_L$	Forebody-lift coefficient, forebody lift/ $q_\infty S$
$C_N$	Normal-force coefficient, normal force/ $q_\infty S$
$\bar{c}$	Mean aerodynamic chord, 0.542 ft for the A-7D and 0.802 ft for the F-4E aircraft
FS	Fuselage station, in.

$M_\infty$	Free-stream Mach number
$p_\infty$	Free-stream static pressure, psf
$p_b$	Model base pressure, psf
$q_\infty$	Free-stream dynamic pressure, $0.7 p_\infty M_\infty^2$ , psf
S	Wing reference area, 0.9375 sq ft for A-7D and 1.3250 sq ft for F-4E
WL	Waterline from reference horizontal plane, in.
$\alpha$	Angle of attack, angle between a model waterline and the free-stream velocity vector, deg

## **SECTION I INTRODUCTION**

External carriage of weapons has been used for many years to increase the striking power of fighter-type aircraft. At low speeds, the drag penalties have been acceptable as trade-offs for the added payload. However, for present-day aircraft with transonic and supersonic cruise speeds, the added drag and the destabilizing pitching moments produced by stores carried beneath the wing and/or fuselage can be critical to the success of the mission. Therefore, at the request of the Air Force Armament Laboratory (AFATL), Eglin Air Force Base, Florida, tests utilizing 0.05-scale models of the F-4E and A-7D aircraft were conducted in the Aerodynamic Wind Tunnel (4T), Propulsion Wind Tunnel Facility (PWT), to evaluate the effect of external stores upon aircraft stability and drag. Several new weapon configurations were tested as well as the Triple Ejection Racks (TER) and Multiple Ejection Racks (MER) configured with M-82 and M-117 bombs, all of which are carried by pylons. The new weapon configurations consist of a family of shapes with a common body diameter and ogive nose employing three base region contours and various control and lifting surfaces, hereafter referred to as parametric shapes. These weapon configurations are a proposed means of multiple weapon carriage. Data were obtained for the F-4E and A-7D models over Mach number from ranges 0.5 to 1.30 and 0.5 to 1.05, respectively.

## **SECTION II APPARATUS**

### **2.1 TEST FACILITY**

The Aerodynamic Wind Tunnel (4T) is a closed-loop, continuous flow, variable density tunnel capable of being operated at Mach numbers from 0.20 to 1.30. At all Mach numbers, the stagnation pressure can be varied from 400 to 3400 psfa. The test section is 4 ft square and 12.5 ft long with perforated, variable porosity (0.5 to 10 percent) walls. It is completely enclosed in a plenum chamber from which the air can be evacuated, allowing part of the tunnel airflow to be removed through the perforated walls of the test section. The wall perforations are 0.50-in.-diam holes inclined 60 deg from the normal to the wall surface. This design allows control of wave attenuation and blockage effects. The tunnel model support system consists of a pitch sector, strut, and sting attachment receptacle, and the system has a pitch capability of -12 to 28 deg with respect to the tunnel centerline. A schematic of the test section showing the location of the models is presented in Fig. 1, Appendix I.

### **2.2 TEST ARTICLES**

The test articles were 0.05-scale models of the A-7D and F-4E aircraft and various stores. Dimensional sketches of the A-7D and F-4E models are shown in Fig. 2. The horizontal tail settings for the A-7D and F-4E models were both at zero-degree incidence with respect to model waterline during testing. The wing-root chord of the A-7D and F-4E models have -1.0- and 1.0-deg incidence, respectively, with respect to waterline. Wing and vertical tail surfaces were set at zero-degree deflection on both models. All tests were conducted with free transition.

The locations of the forward end of the pylons, to which the various store carriage racks and stores were mounted, are shown in Fig. 2. Details and dimensions of the pylons are shown in Fig. 3 and the TER and MER are shown in Fig. 4. The TER and MER were mounted on the pylons as required by the store configurations. Shown in Figs. 5, 6, and 7 are dimensional sketches of the 370-gal fuel tank, MK-82 bomb, and M-117 bomb, respectively. Figure 8 shows the numbering sequence of the TER and MER stations and the roll orientation of the MK-82 and M-117 bombs mounted on each station. Dimensional sketches of the seven geometrically related shapes are presented in Fig. 9.

Photographs of four configurations installed in the test section are shown in Fig. 10. A list of the configurations tested is presented in Table I, Appendix II.

## 2.3 INSTRUMENTATION

Two six-component, internal strain-gage balances of different capacity were used during the test to obtain the force and moment data for the A-7D and F-4E models. Base pressure measurements were obtained with pressure transducers connected to two orifices located on the sting inside the base of the aircraft model.

## SECTION III TEST DESCRIPTION

### 3.1 TEST CONDITIONS AND PROCEDURES

Force data were obtained on various store configurations of the A-7D and F-4E aircraft. The Mach number range was from 0.5 to 1.3. Tunnel stagnation pressure ranged from 3200 psfa at  $M_\infty = 0.50$  to 2200 psfa at  $M_\infty = 1.30$ , and the total temperature varied from 90 to 110°F. Reynolds number and dynamic pressure variations with Mach number are presented in Fig. 11. The test section wall porosity was varied with free-stream Mach number in order to achieve the minimum lift interference while reducing blockage effects.

The tunnel conditions were held constant at the prescribed Mach number and total pressure while the angle of attack was varied through the range of -4 to 15 deg. Data were recorded at each of 28 discrete angles of attack. Data were obtained for both the A-7D and F-4E configurations at Mach numbers of 0.50, 0.70, 0.80, 0.90, 0.95, and 1.05 and in addition at Mach numbers of 1.10, 1.20, and 1.30 for the F-4E.

### 3.2 CORRECTIONS

Balance and sting deflections caused by the aerodynamic loads on the model were accounted for in the data reduction program to determine the angle of attack. Model weight tare corrections were made to calculate net aerodynamic forces on the model.

To determine the wind tunnel flow angularity, configuration F401 was run in an upright and inverted position. A flow angle deviation that varied with Mach number was

determined. All data were corrected for this flow angularity which varied from 0.30-deg upwash at Mach number 0.50 to 0.10-deg upwash at Mach number 1.20.

### 3.3 PRECISION OF MEASUREMENTS

Although the data in this report were determined from single-sample measurements, the uncertainties for these data were estimated by methods based on statistical analysis. Errors arising from setting free-stream test conditions were determined from tunnel calibration data. Other effects considered include instrument precision and balance calibration curve-fit deviation. For a 95-percent confidence level, the uncertainties in the data presented herein are as follows:

$C_D (C_L = 0.3)$	$C_L$	$C_m$	$M_\infty$	$q_\infty$	$\alpha$
$\pm 0.0015$	$\pm 0.006$	$\pm 0.001$	$\pm 0.002$	$\pm 10$	$\pm 0.1$

## SECTION IV RESULTS AND DISCUSSION

### 4.1 DATA PRESENTATION

Force and moment coefficients were plotted by machine and faired with straight lines. The data have been presented in the following format and order for each group of data: (1)  $C_L$  versus  $\alpha$ , (2)  $C_D$  versus  $C_L$ , (3)  $C_m$  versus  $C_L$ , and (4)  $C_D$  versus  $M_\infty$ . The effect of  $M_\infty$  on  $C_D$  for the A-7D stores is plotted for  $C_L = 0$  and for the F-4E stores is plotted at  $C_L = 0.3$  and  $C_L = 0.1$  for  $M_\infty < 1.0$  and  $M_\infty > 1.0$ , respectively.

The data have been presented to illustrate primarily the effect of (1) parametric-shape configuration variation, (2) parametric-shape carriage position, and (3) parametric-shape configuration addition on aircraft stability and performance. Data for the clean-aircraft configurations A701 and F401 are presented in each figure for comparison. Presented in Table II is a configuration key to assist in figure interpretation. Data for the A-7D and F-4E are presented in Figs. 12 through 31 and Figs. 32 through 55, respectively. Data are presented only for selected Mach numbers except to show the effect of Mach number on drag coefficient.

### 4.2 A-7D CONFIGURATIONS

The addition of stores resulted in only small changes in the lift curve slope for all configurations as shown in Figs. 12, 16, 20, 24, and 28.

All aircraft configurations were statically stable over the Mach number range (Figs. 13, 17, 21, 25, and 29). In general, the addition of stores reduced the stability of the aircraft, except for the addition of configuration A704 (M-117 bomb on TER), which increased the stability at the high Mach numbers (Fig. 13). However, when the M-117 bomb was carried on the MER (configuration A702), the aircraft stability was decreased.

The addition of lifting surfaces to the blunt-base parametric-shape store reduced aircraft stability at all Mach numbers (Fig. 17) for configurations A707 and A710. The addition of canards (Configuration A707) to the midwing-store configuration, A710, reduced the aircraft stability at subsonic Mach numbers and had no effect at  $M_\infty = 1.05$ .

When stores were carried on one wing, movement of the store from the inboard to the outboard wing station had no effect on aircraft stability (Fig. 21). However, when the stores were carried on both wings, the movement of the stores from the inboard to the outboard wing stations decreased the aircraft stability as Mach number was increased, except at  $M_\infty = 1.05$  where there was no effect (Fig. 25).

The effect of loading stores at the same wing station, on either one or both wings, is shown in Fig. 29. The aircraft stability was decreased when both wings were loaded.

The addition of stores produced large increases in drag coefficient at all Mach numbers for all configurations (Figs. 14, 18, 22, 16, and 32). In some cases, the addition of stores increased the drag coefficient at zero lift by as much as 150 percent of the clean-aircraft drag coefficient (Fig. 14b). As the number of stores was increased the subsonic drag level increased, and the drag rise occurred at progressively lower Mach numbers as shown in Fig. 15. Comparison of the results for similar store configurations (A702 and A703) indicates that the increase in drag coefficient is proportional to the increase in frontal area. With both wings loaded, the inboard carriage positions resulted in the largest increase in drag coefficient as shown in Fig. 27.

### 4.3 F-4E CONFIGURATIONS

The addition of stores to the F-4E resulted in small changes in lift-curve slope and produced a small positive shift in the zero-lift angle of attack for most configurations as shown in Figs. 32, 36, 40, 44, 48, and 52. All aircraft configurations were statically stable over the Mach number range except at the high values of lift coefficient as shown in Figs. 33, 37, 41, 45, 49, and 53.

In general, all configurations exhibited similar changes in stability with Mach number. The addition of stores reduced the aircraft stability, especially at the low subsonic Mach numbers.

Figure 33 indicates that the aircraft is more stable when three MK-82 bombs are carried on the TER than when three M-117 bombs are carried at the high subsonic Mach numbers. As shown in Figs. 41 and 45, with parametric-shape stores on the left and right wings, changing the store-base geometry or adding store lifting surfaces did not affect the aircraft stability characteristics. With both wings loaded with the parametric-shape store, the most outboard carriage position (F419) produced the most favorable stability characteristics at subsonic Mach numbers as shown in Fig. 49. Increasing the number of parametric-shape stores carried on the wings reduced the aircraft stability as illustrated in Fig. 53.

The addition of stores produced large increases in drag coefficient at all Mach numbers, for all configurations, as seen in Figs. 34, 38, 42, 46, 50, and 54.

The incremental drag (produced by changing the base geometry of the parametric-shape stores) for stores carried on both wings is small. It is greatest for the ogive-shaped base (F405) and least for the blunt-shaped base (F407) as shown in Figs. 42 and 43.

The changes in incremental drag, produced by the addition of lifting surfaces to the blunt-base parametric-shape store, were almost as great as the increase produced by the addition of the store at subsonic Mach numbers as shown in Fig. 43 (configuration F407) and in Fig. 47 (all store configurations). With both wings loaded, the most inboard carriage position (F411) produced the most favorable drag characteristics as shown in Figs. 50 and 51. As shown in Fig. 54, comparison of the results for the parametric stores loaded on one wing (F420) and on two wings (F419) shows that the incremental drag coefficient was generally proportional to the increase in aircraft frontal area.

## SECTION V CONCLUSIONS

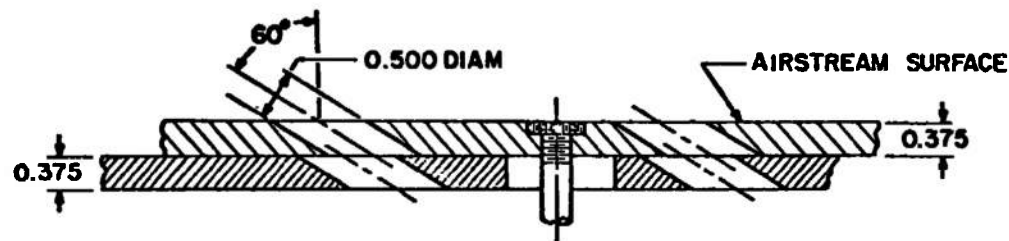
Based on the results of the test to determine the longitudinal static stability and drag characteristics of A-7D and F-4E aircraft with various external store configurations, the following conclusions are made:

1. The addition of stores degrades the stability and drag characteristics of both the A-7D and F-4E aircraft.
2. With stores carried on both wings of an aircraft, movement of the carriage position from the inboard to outboard stations decreases the stability of the A-7D and increases the stability of the F-4E.
3. The incremental drag coefficient increase is generally proportional to the incremental increase in aircraft frontal area when similar stores are added to either the A-7D or F-4E aircraft.
4. With both wings of the aircraft loaded with similar stores, the most inboard carriage position produces the most favorable drag characteristics for the F-4E aircraft and the least favorable drag characteristics for the A-7D aircraft.
5. The increase in incremental drag coefficient, produced by the addition of lifting surfaces to the store, is almost as large as the increase in drag coefficient produced by the addition of the store for the F-4E aircraft at subsonic speeds.



## **APPENDIXES**

- I. ILLUSTRATIONS**
- II. TABLES**



TYPICAL PERFORATED WALL CROSS SECTION

ALL DIMENSIONS AND TUNNEL STATIONS IN INCHES

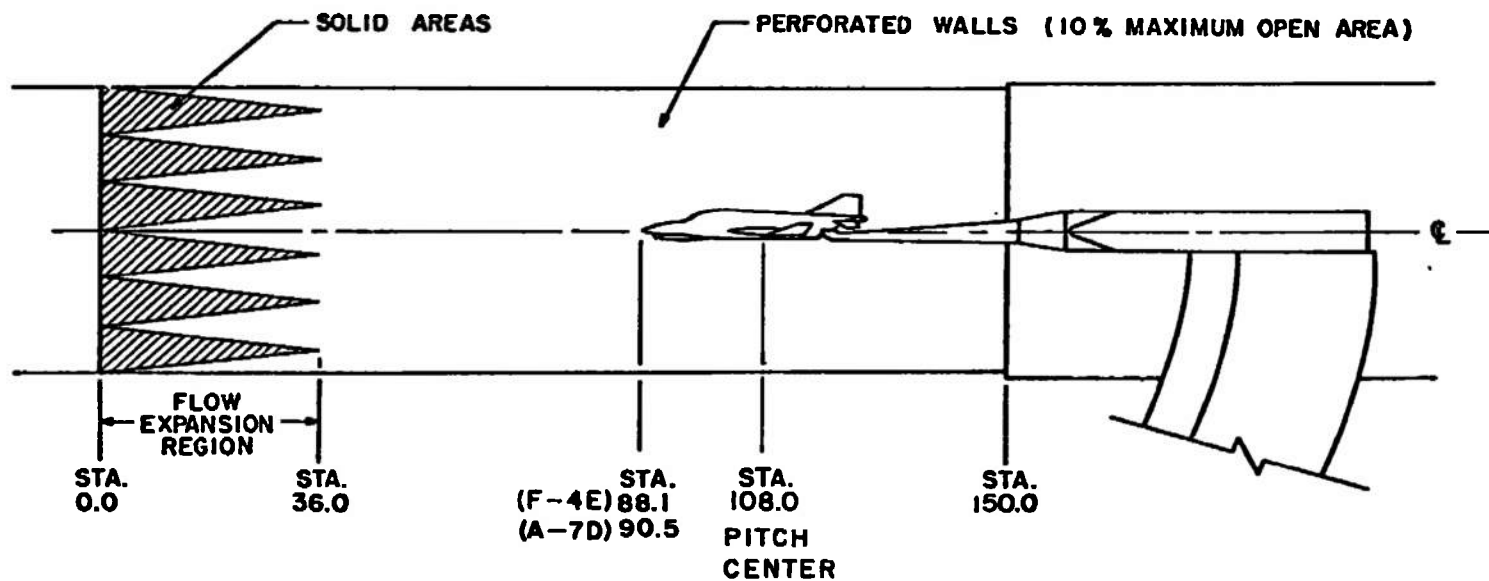
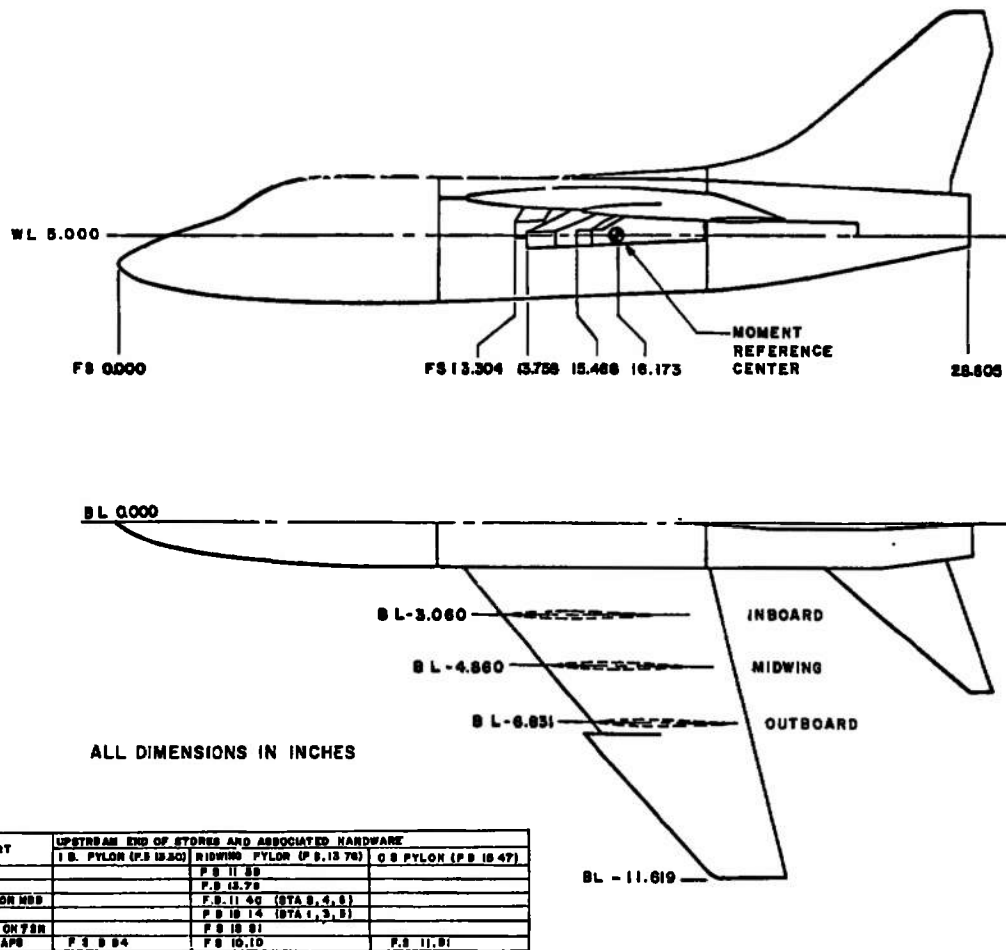
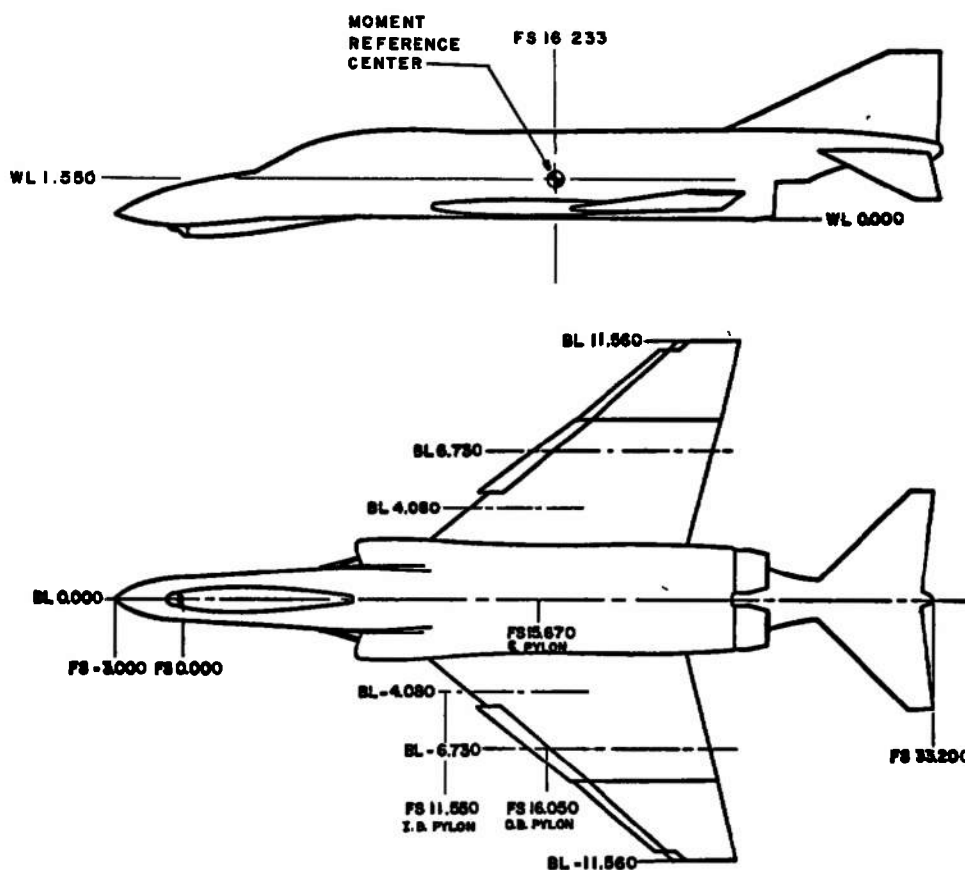


Fig. 1 Schematic of the Tunnel Test Section Showing Model Location



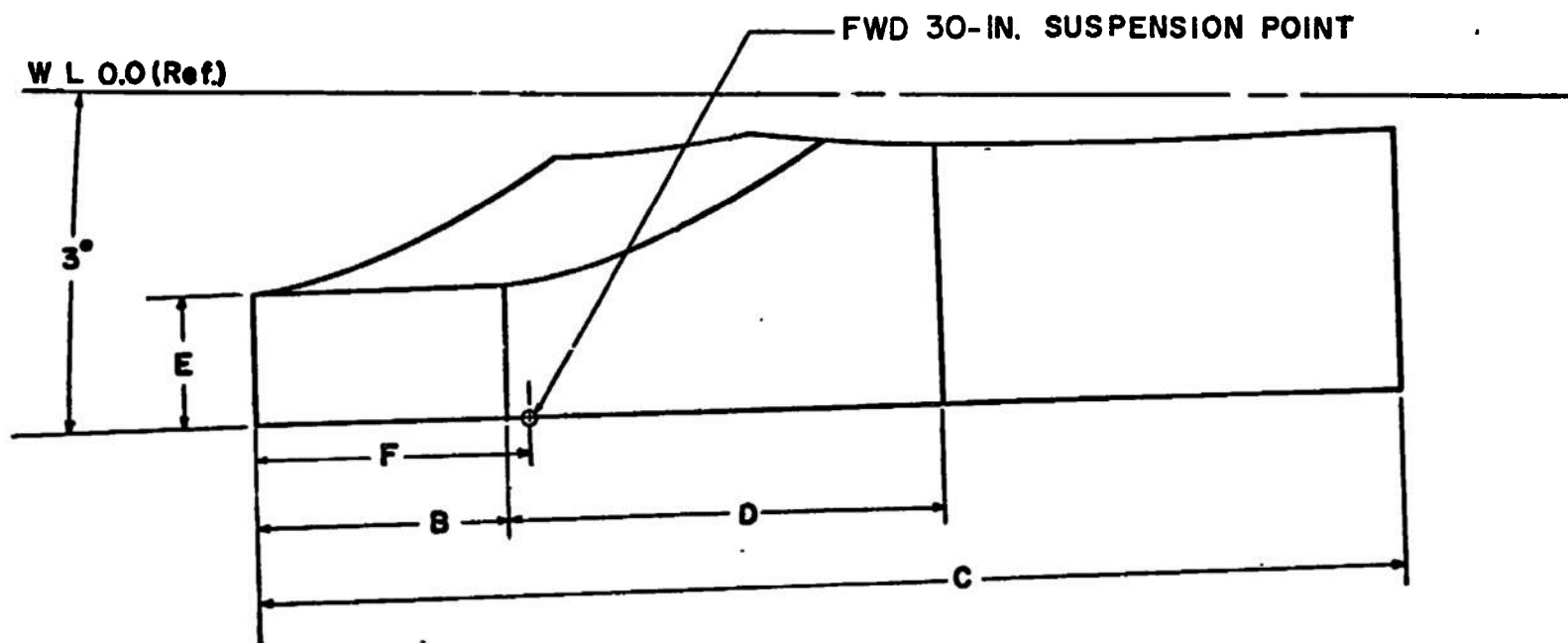
a. A-7D Model  
Fig. 2 Sketch of the Aircraft Models



PART	UPSTREAM END OF STORES AND ASSOCIATED HARDWARE		
	I. PYLON (FS 16.67)	I.B. PYLON (FS 11.56)	O.B. PYLON (FS 16.05)
TER	-	FS 11.51	-
WER	FS 12.51	-	-
WKE ON TER	-	FS 11.87	-
370 GAL TANK	-	-	FS 19.88
MW7 BOMB ON TER	-	FS 11.88	-
PARN SHAPE	-	FS 7.88	FS 18.40

ALL DIMENSIONS IN INCHES

b. F-4E Model  
Fig. 2 Concluded

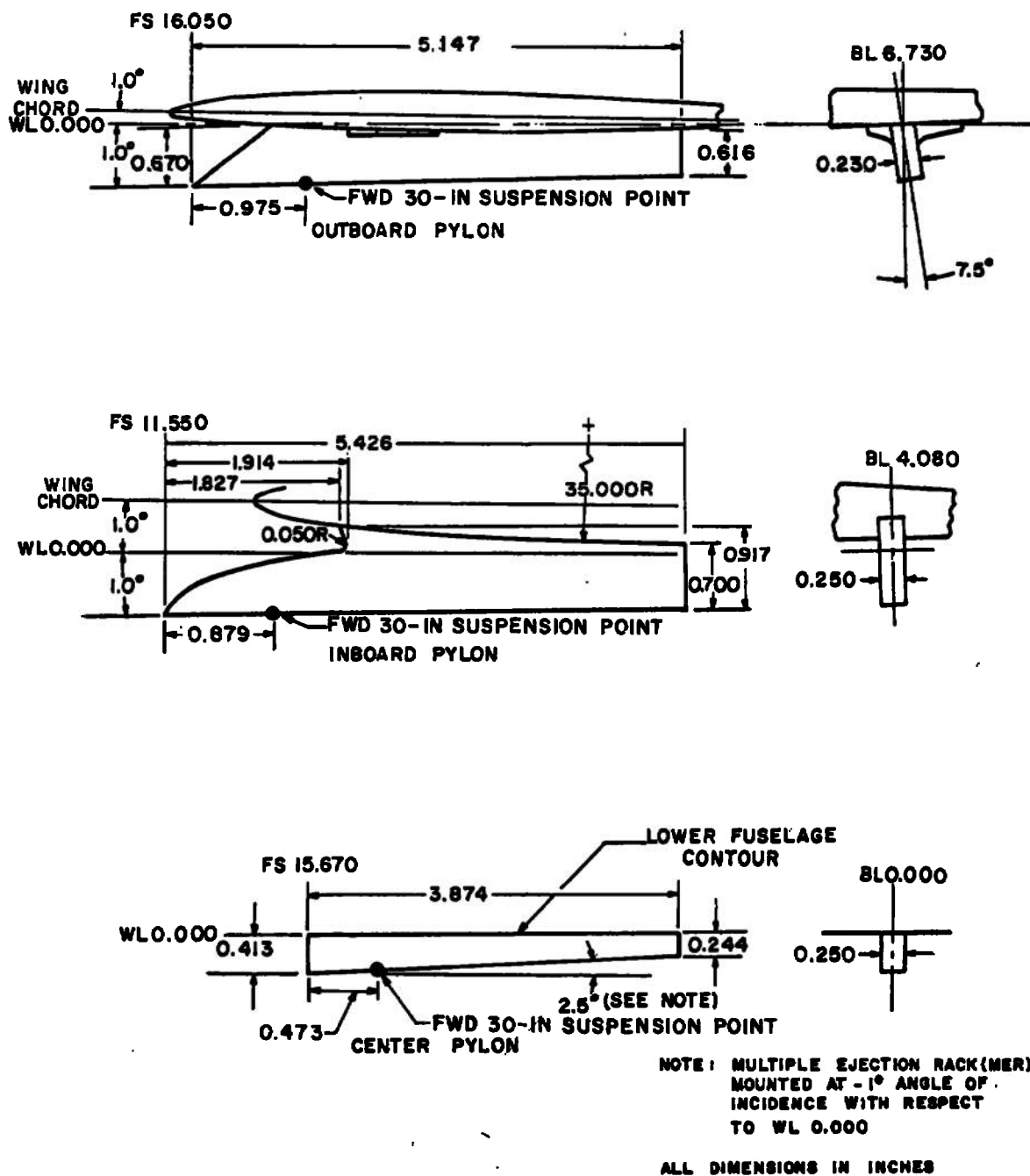


	INBOARD	CENTER	OUTBOARD
B	1.030	1.030	0.515
C	4.580	4.850	4.437
D	1.630	1.905	2.008
E	0.575	0.575	0.513
F	0.950	0.950	0.750

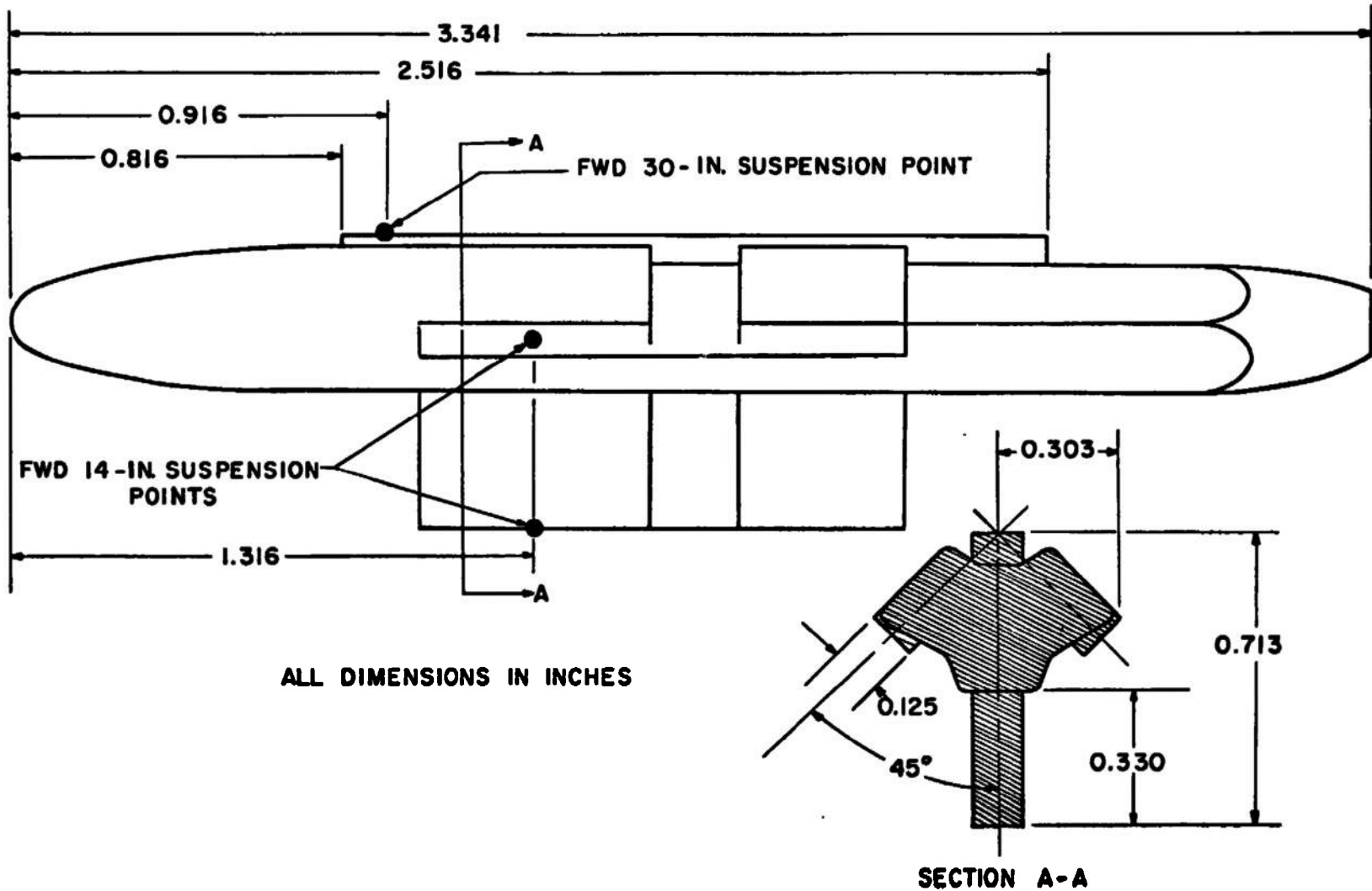
ALL DIMENSIONS IN INCHES

a. A-7D Model

Fig. 3 Details and Dimensions of the Aircraft Model Pylons

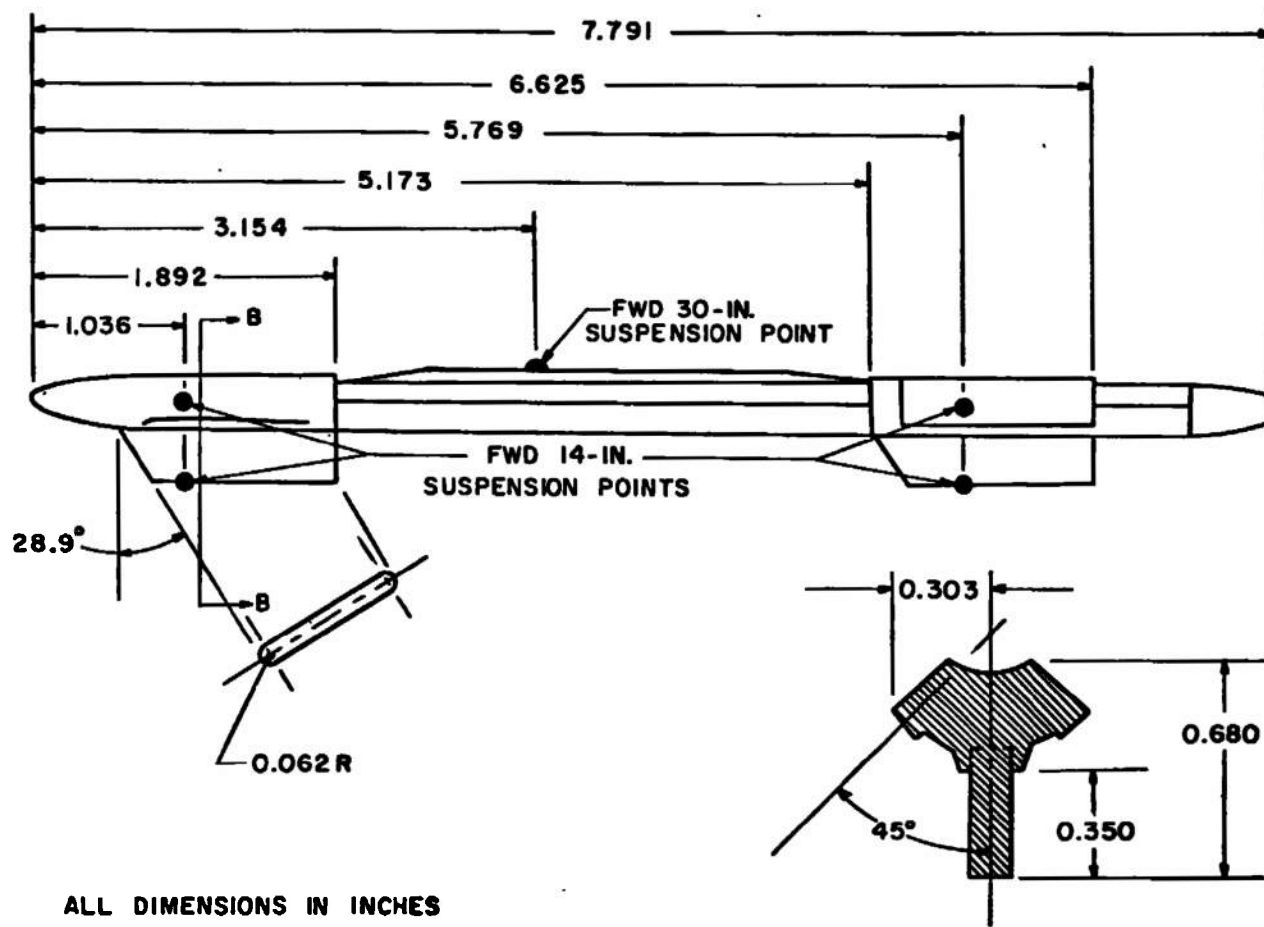


b. F-4E Model  
Fig. 3 Concluded



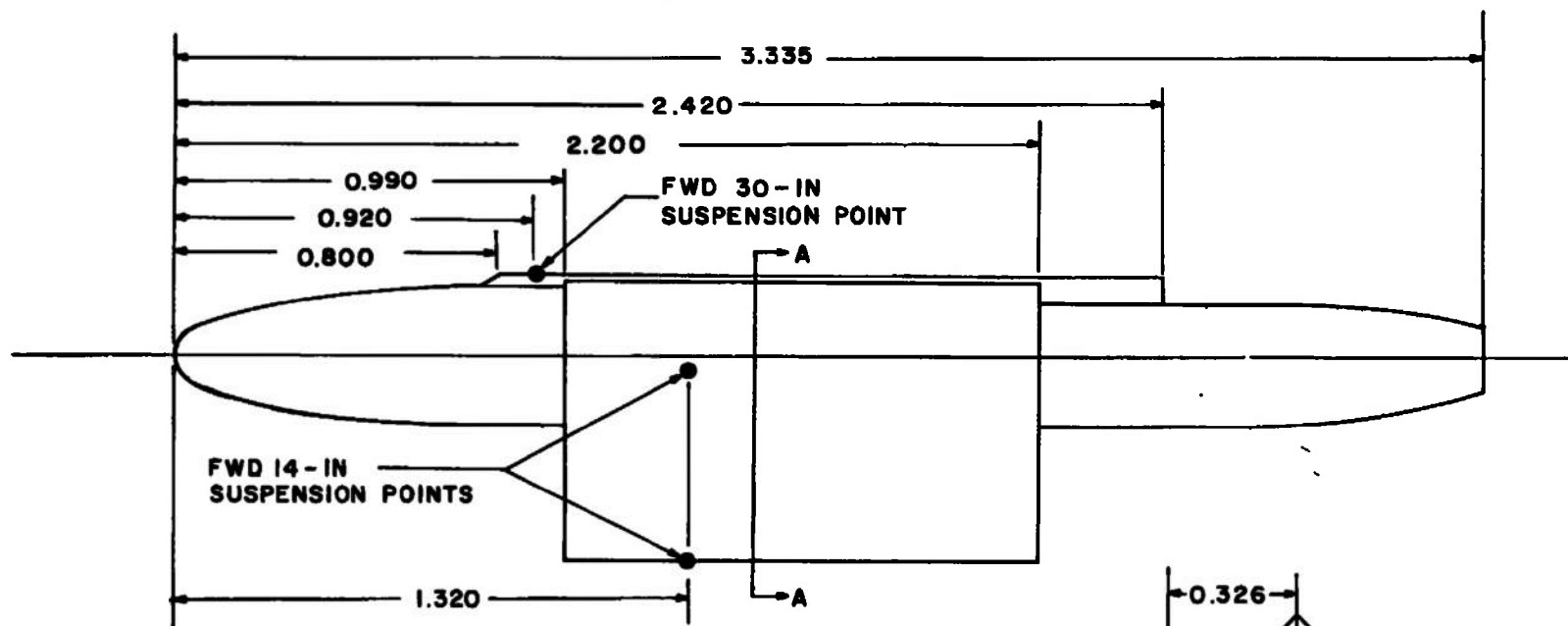
a. A-7D Model TER

Fig. 4 Details and Dimensions of the Aircraft TER and MER Models

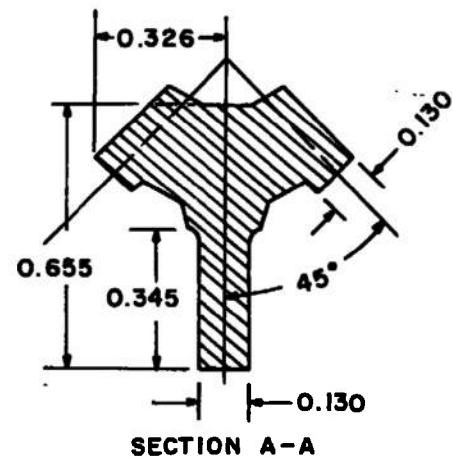


b. A-7D Model MER  
Fig. 4 Continued

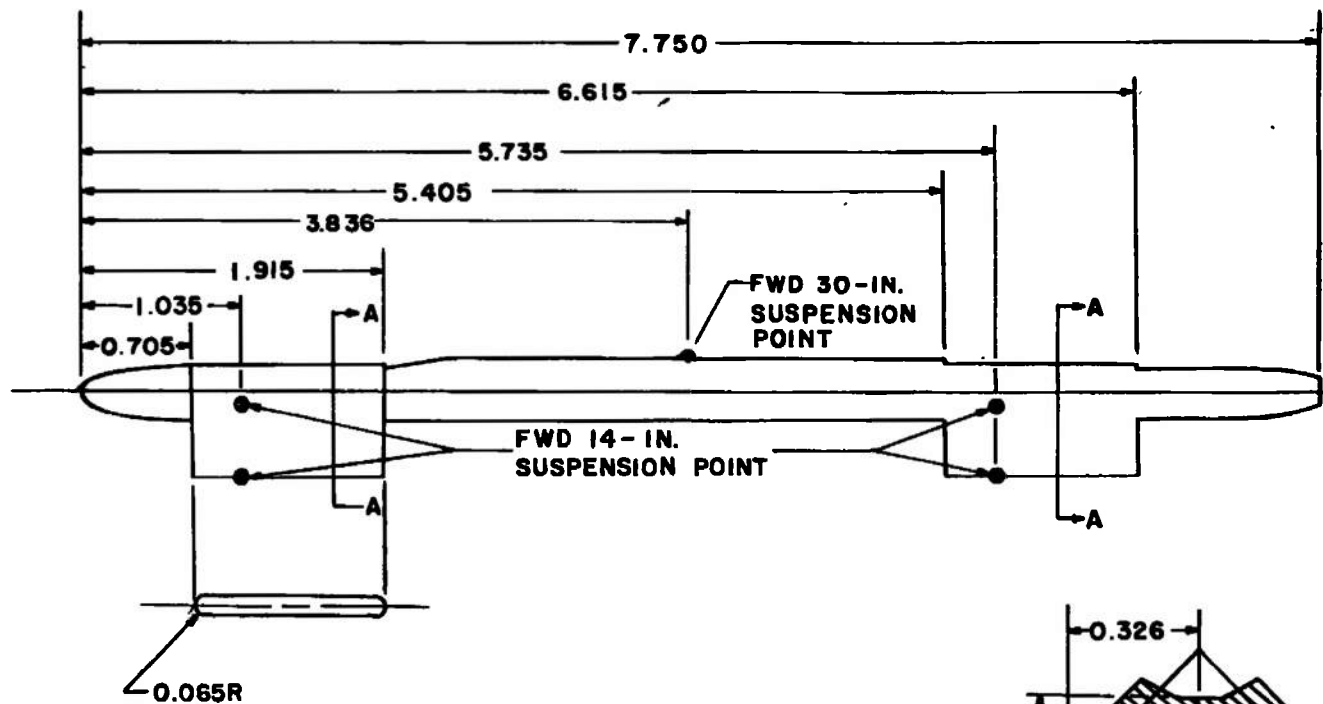




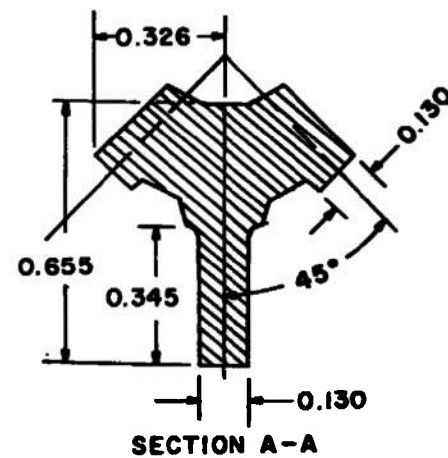
ALL DIMENSIONS IN INCHES



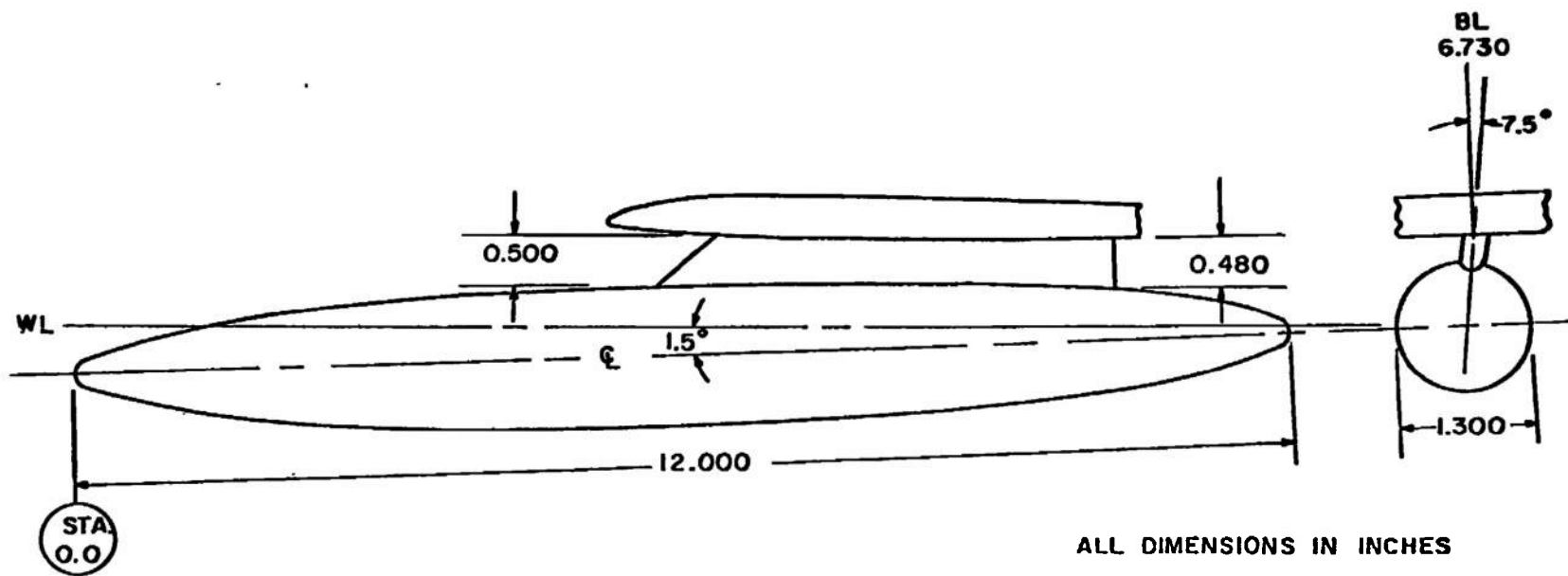
c. F-4E Model TER  
Fig. 4 Continued



ALL DIMENSIONS IN INCHES



d. F-4E Model MER  
Fig. 4 Concluded

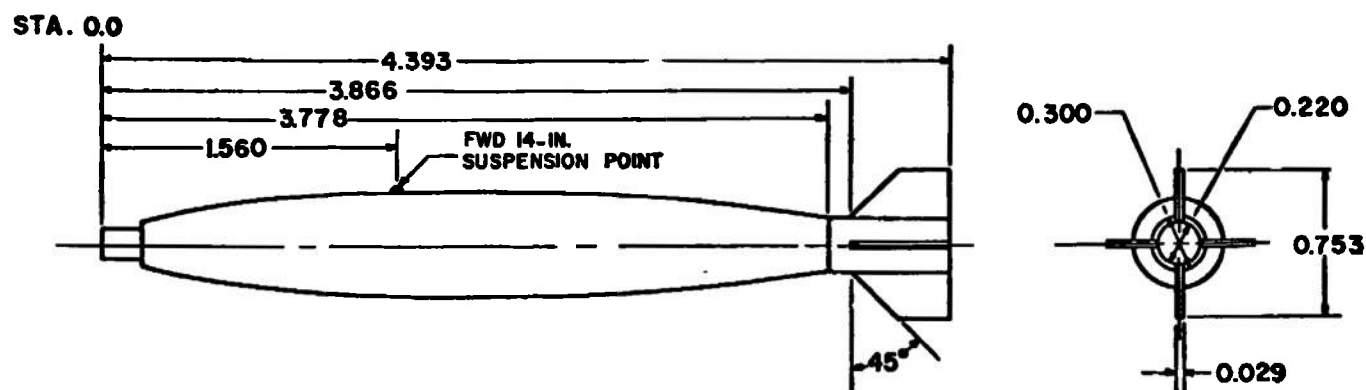


BODY CONTOUR, TYPICAL BOTH ENDS

STATION	BODY DIAM	STATION	BODY DIAM
0.000	0.000	2.500	1.116
0.025	0.100	2.750	1.156
0.050	0.144	3.000	1.190
0.150	0.258	3.250	1.218
0.250	0.340	3.500	1.242
0.500	0.498	3.750	1.260
0.750	0.622	4.000	1.274
1.000	0.724	4.250	1.286
1.250	0.812	4.500	1.294
1.500	0.890	4.750	1.298
1.750	0.958	5.000	1.300
2.000	1.016	6.000	1.300
2.250	1.070		

Fig. 5 Details and Dimensions of the 370-gal Fuel Tank Model on the Outboard F-4E Pylon

STA.	DIAM
0.000	0.150
0.210	0.150
0.212	0.231
0.312	0.282
0.412	0.322
0.512	0.361
0.612	0.391
0.712	0.421
0.812	0.445
0.912	0.465
1.012	0.483
1.112	0.497
1.212	0.510
1.312	0.520
1.412	0.525
1.512	0.530
1.612	0.532
1.712	0.533
1.812	0.535
1.912	0.537
2.312	0.537
2.412	0.535
2.512	0.525
2.612	0.520
2.712	0.510
2.812	0.497
2.912	0.483
3.012	0.465
3.173	0.438



ALL DIMENSIONS IN INCHES

Fig. 6 Details and Dimensions of the MK-82 Bomb Model

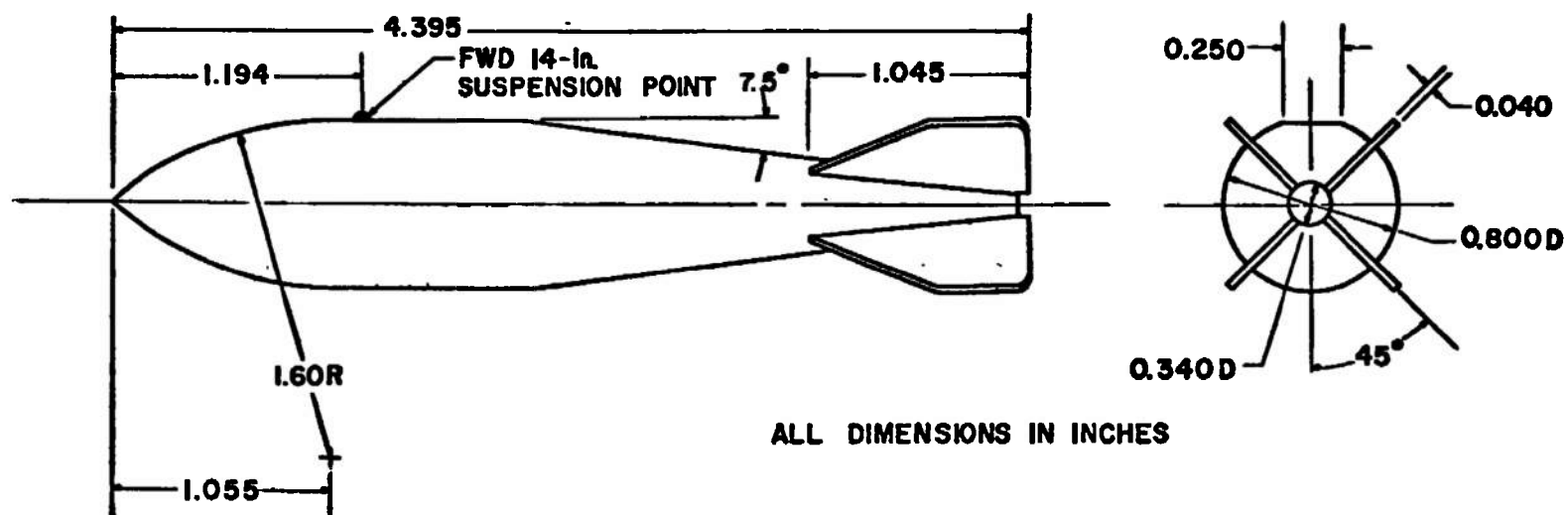
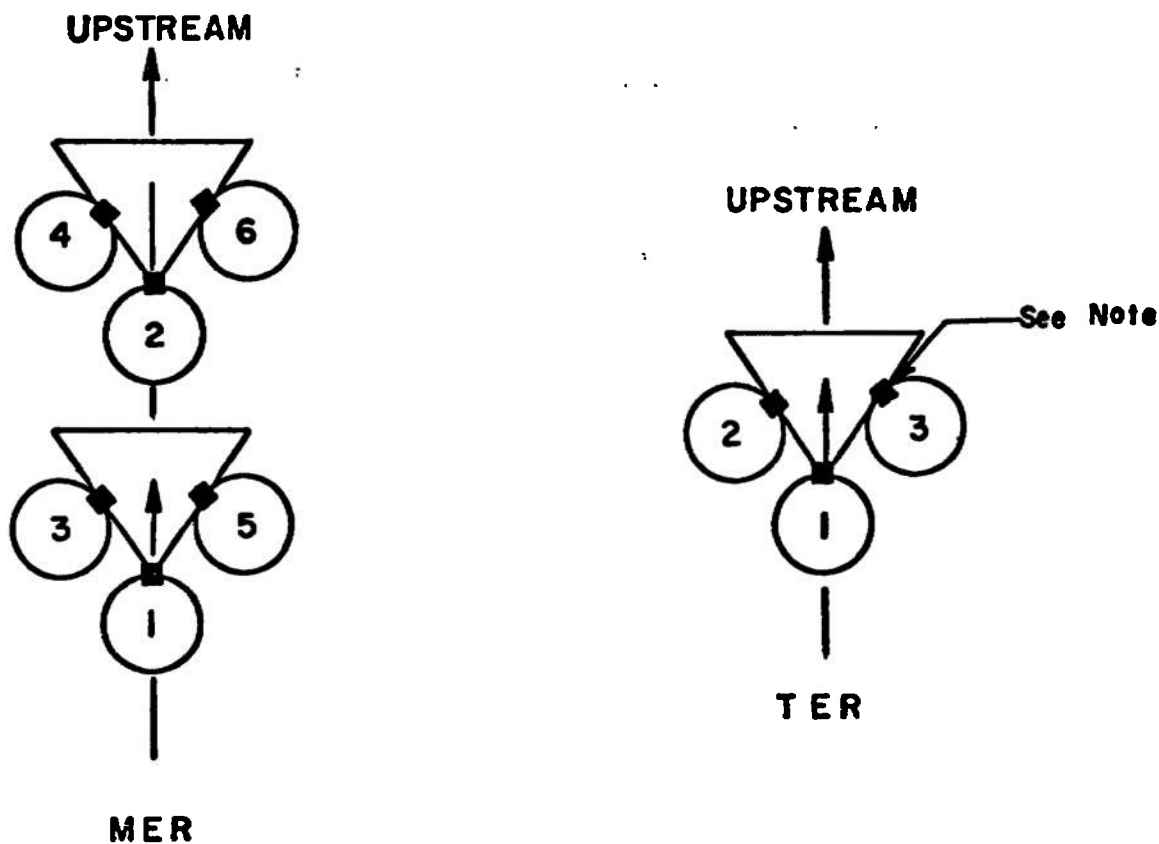


Fig. 7 Details and Dimensions of the M-117 Bomb Model



**NOTE:** The square indicates the orientation of the suspension lugs

TYPE RACK	STATION	ROLL ORIENTATION, deg
<b>MER</b> ↓	<b>1</b>	<b>0</b>
	<b>2</b>	<b>0</b>
	<b>3</b>	<b>45</b>
	<b>4</b>	<b>45</b>
	<b>5</b>	<b>-45</b>
	<b>6</b>	<b>-45</b>
<b>TER</b> ↓	<b>1</b>	<b>0</b>
	<b>2</b>	<b>45</b>
	<b>3</b>	<b>-45</b>

**Fig. 8 Schematic of the TER and MER Store Stations and Orientation**

ALL DIMENSIONS IN INCHES

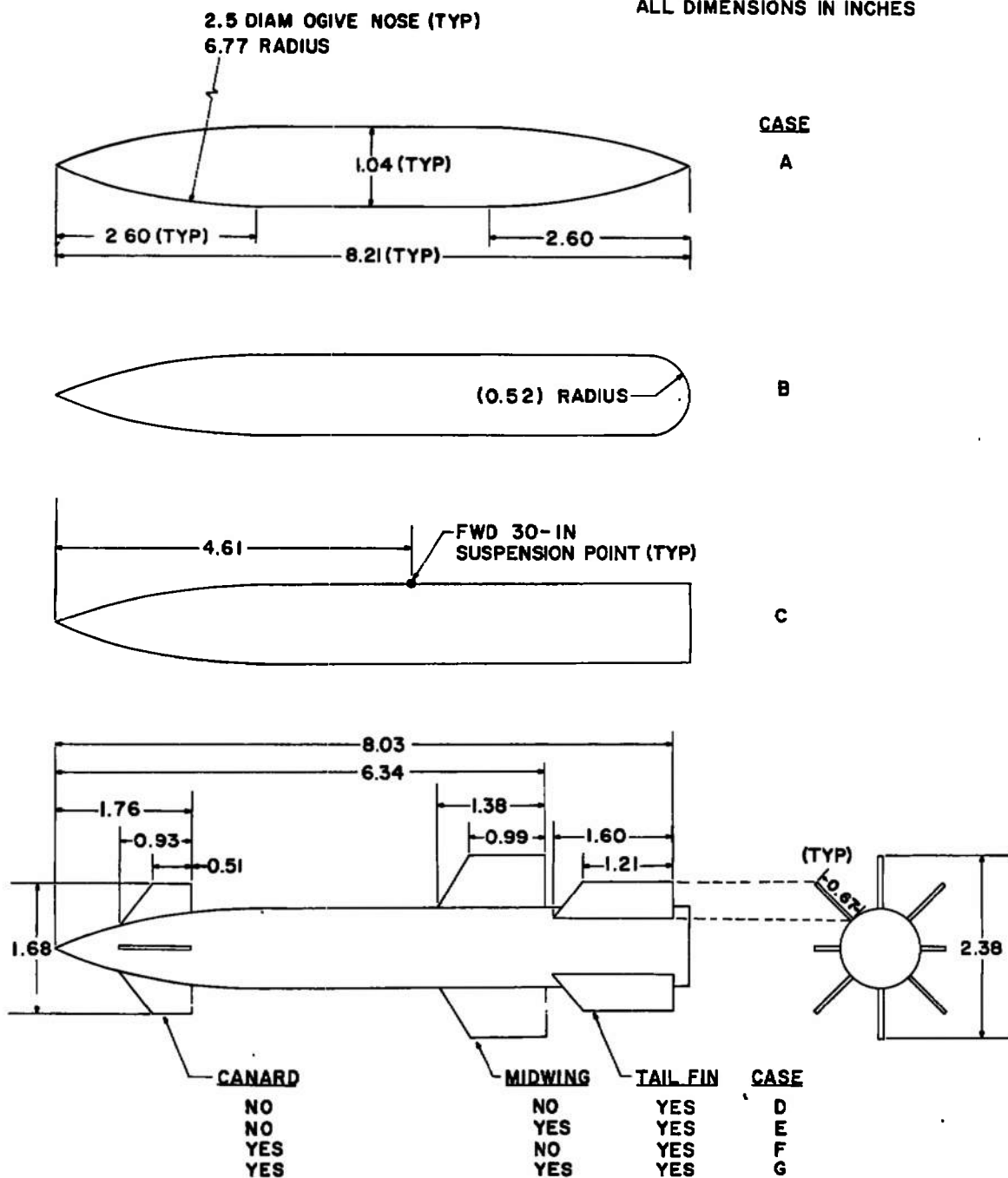
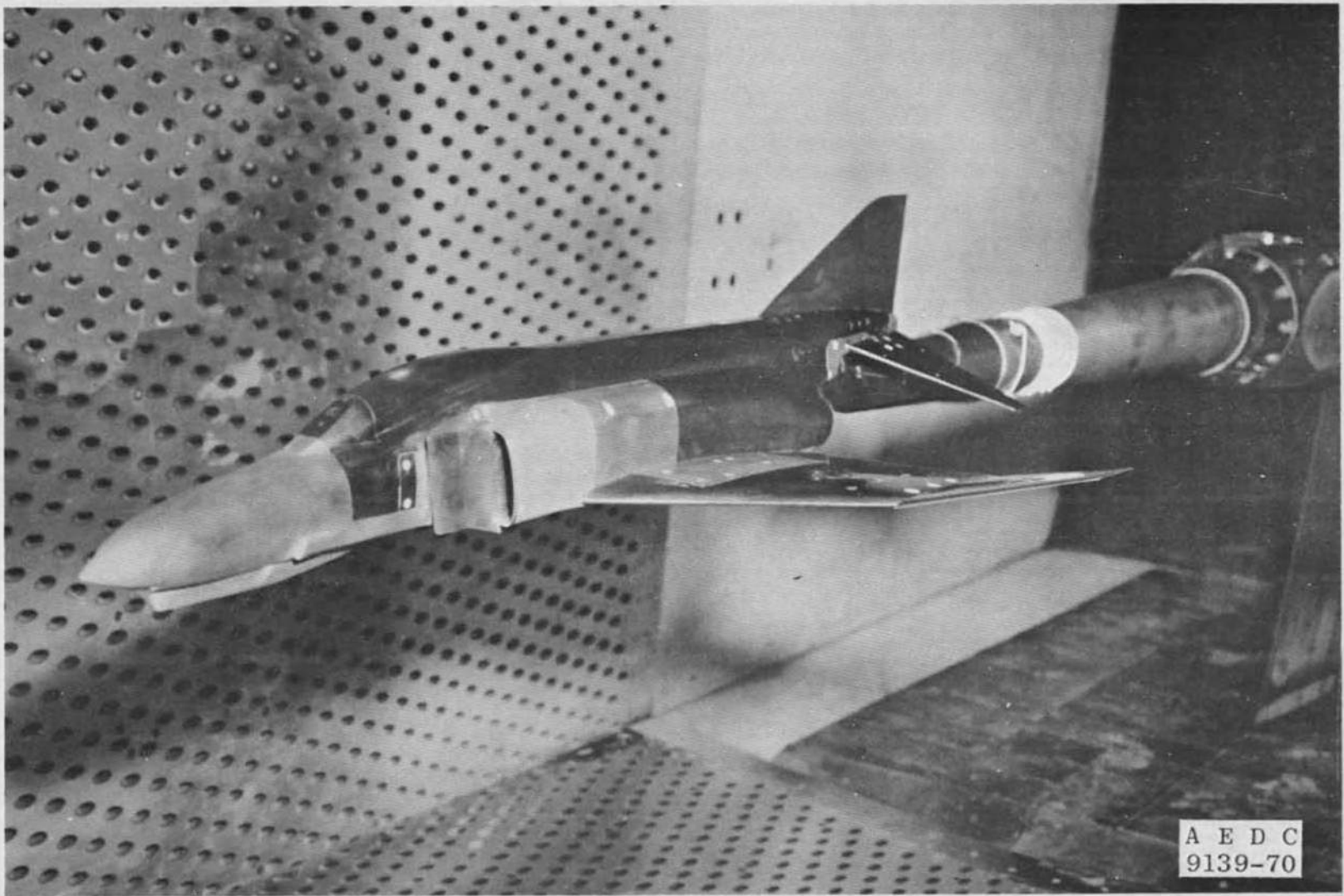


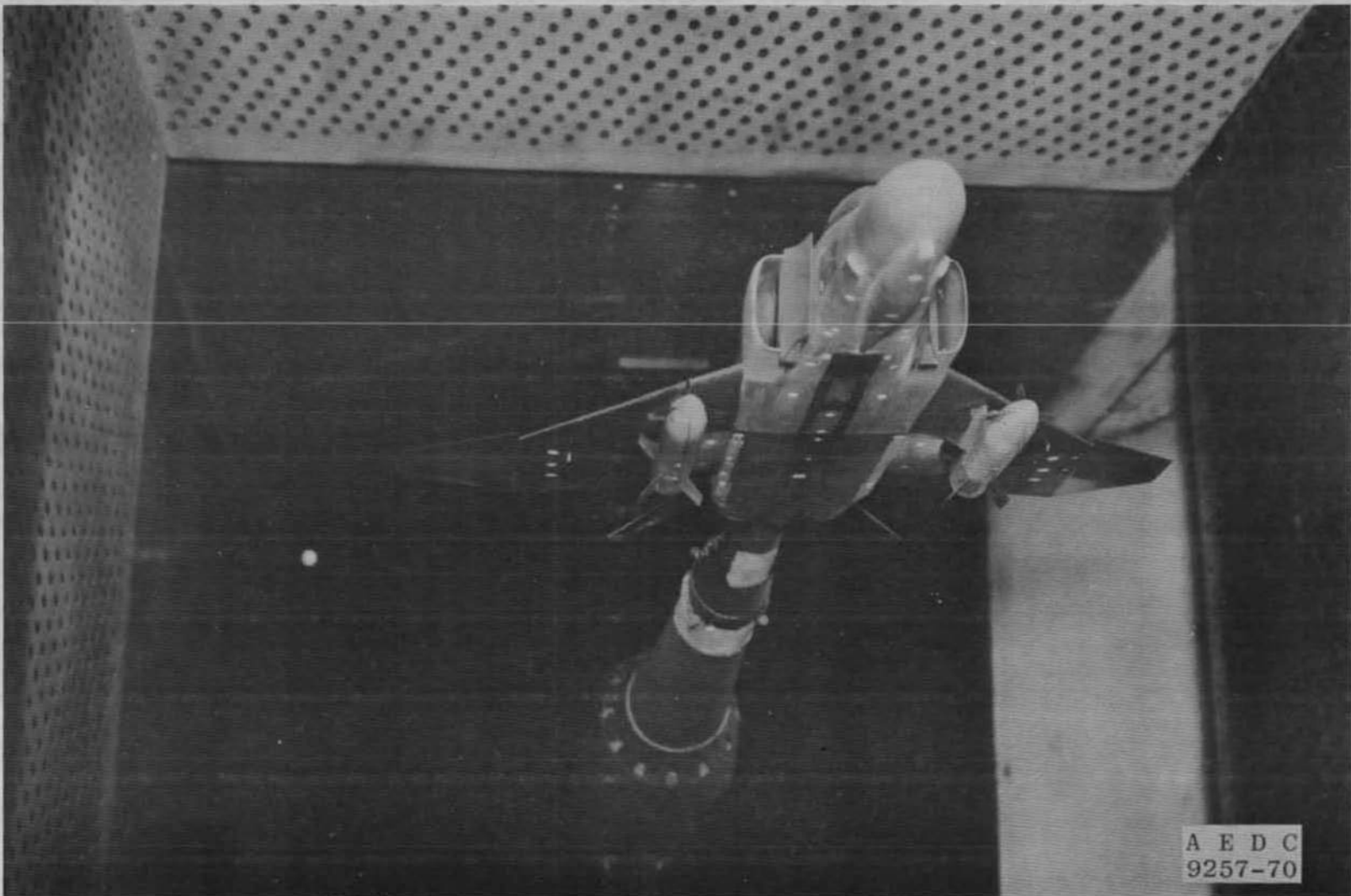
Fig. 9 Details and Dimensions of the Various Parametric Shape Configurations



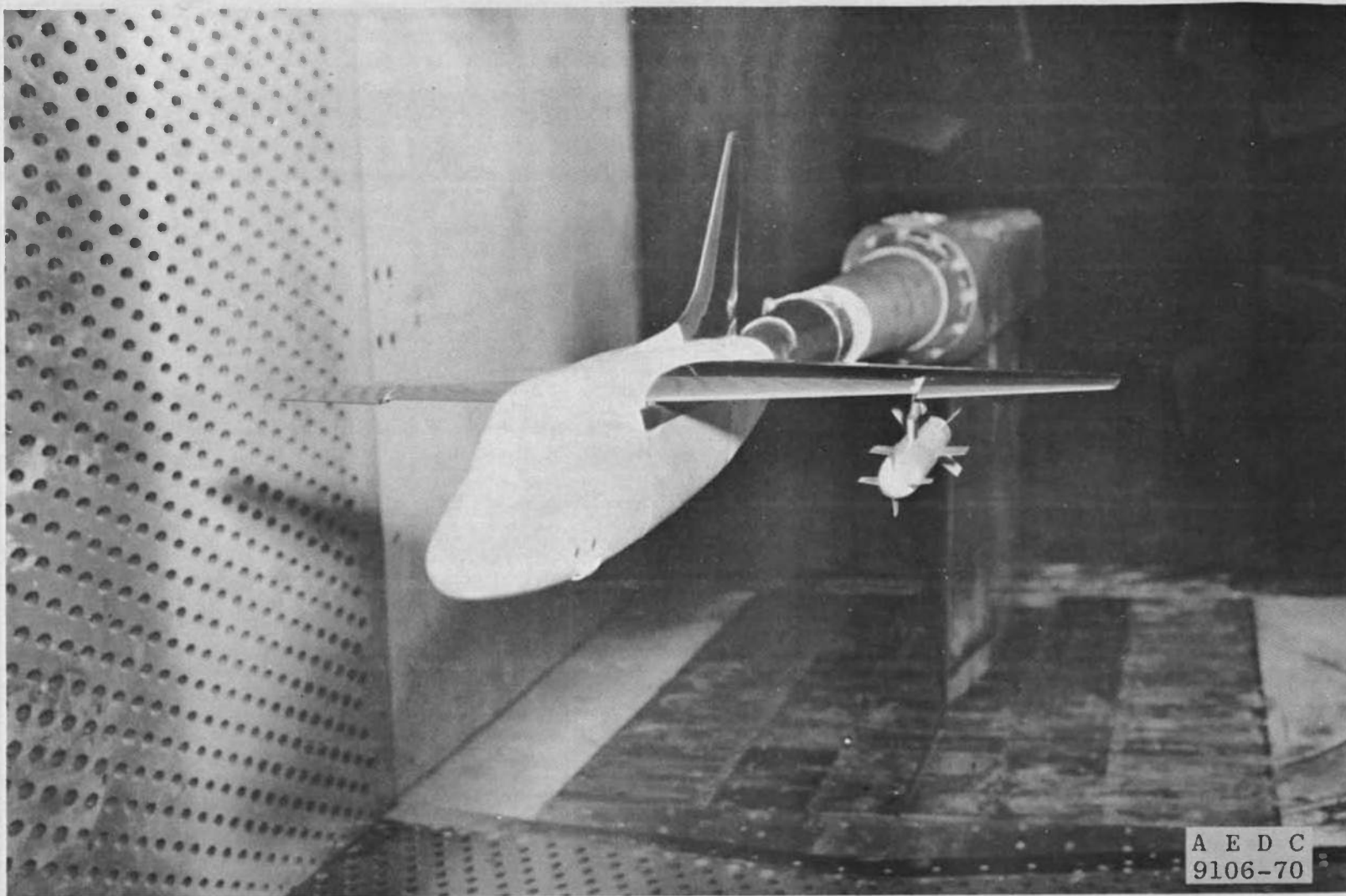
a. Configuration F401

Fig. 10 A-7D and F-4E Models Installed in the Tunnel Test Section

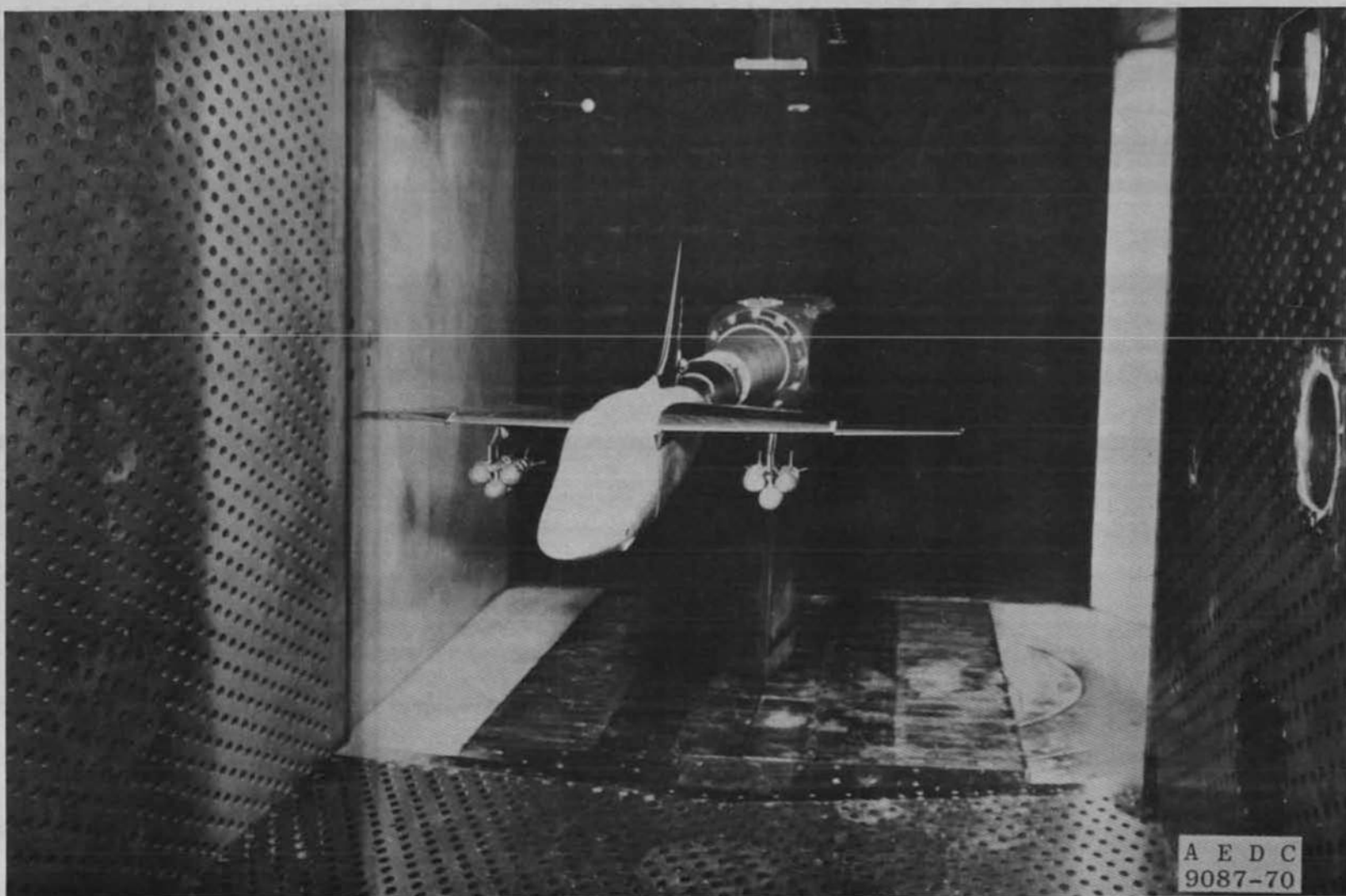




b. Configuration F411  
Fig. 10 Continued



c. Configuration A713  
Fig. 10 Continued



d. Configuration A704  
Fig. 10 Concluded

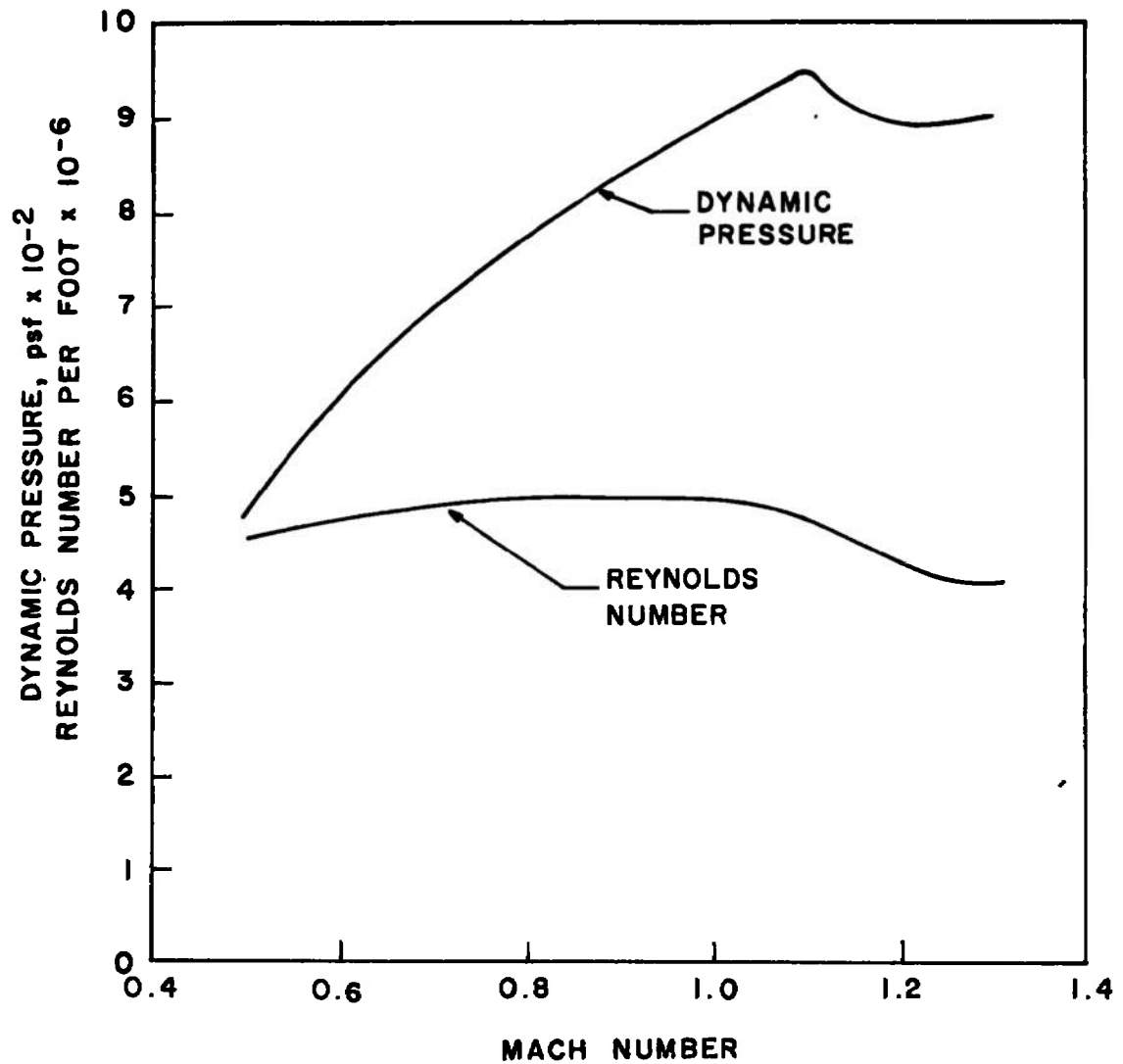
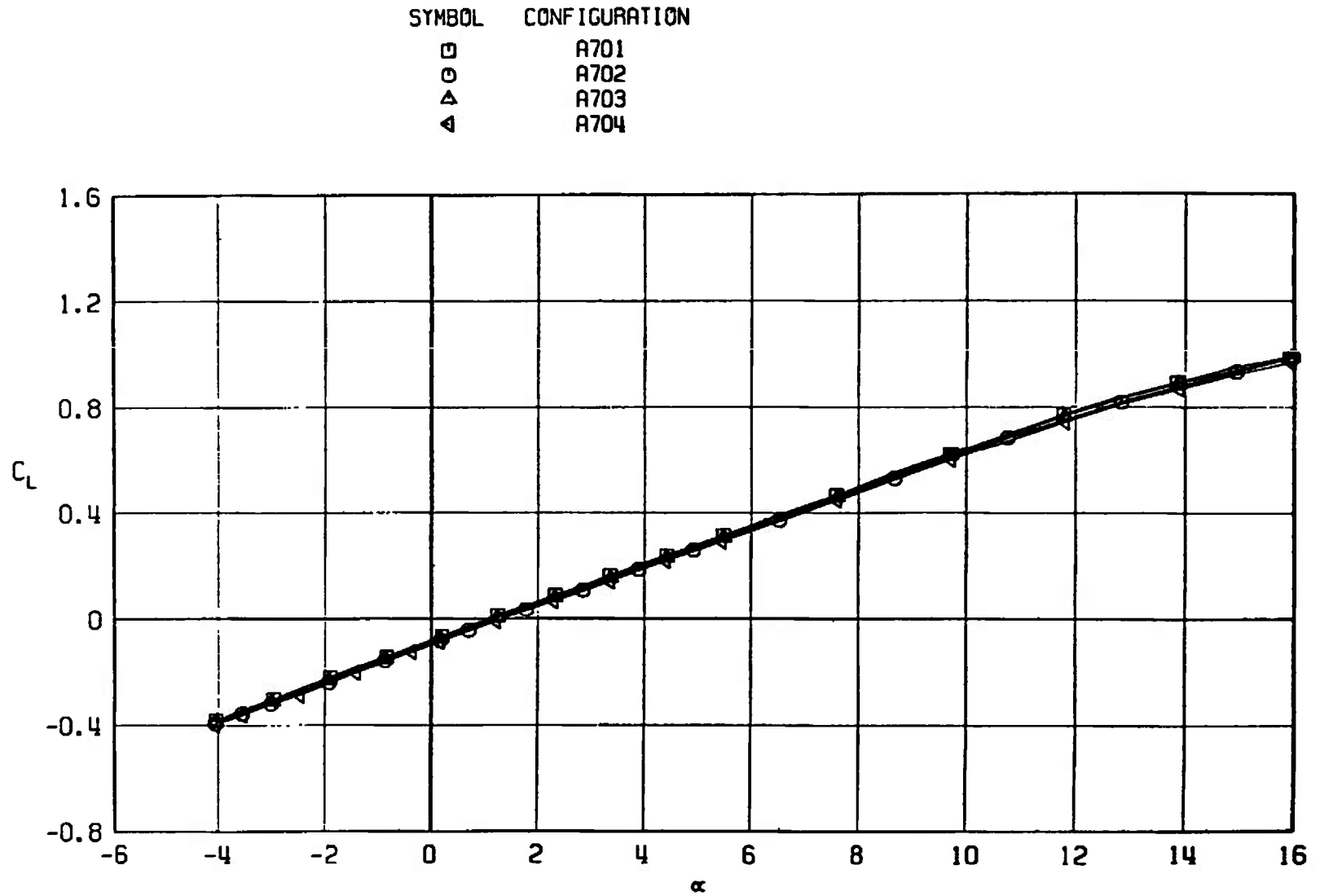


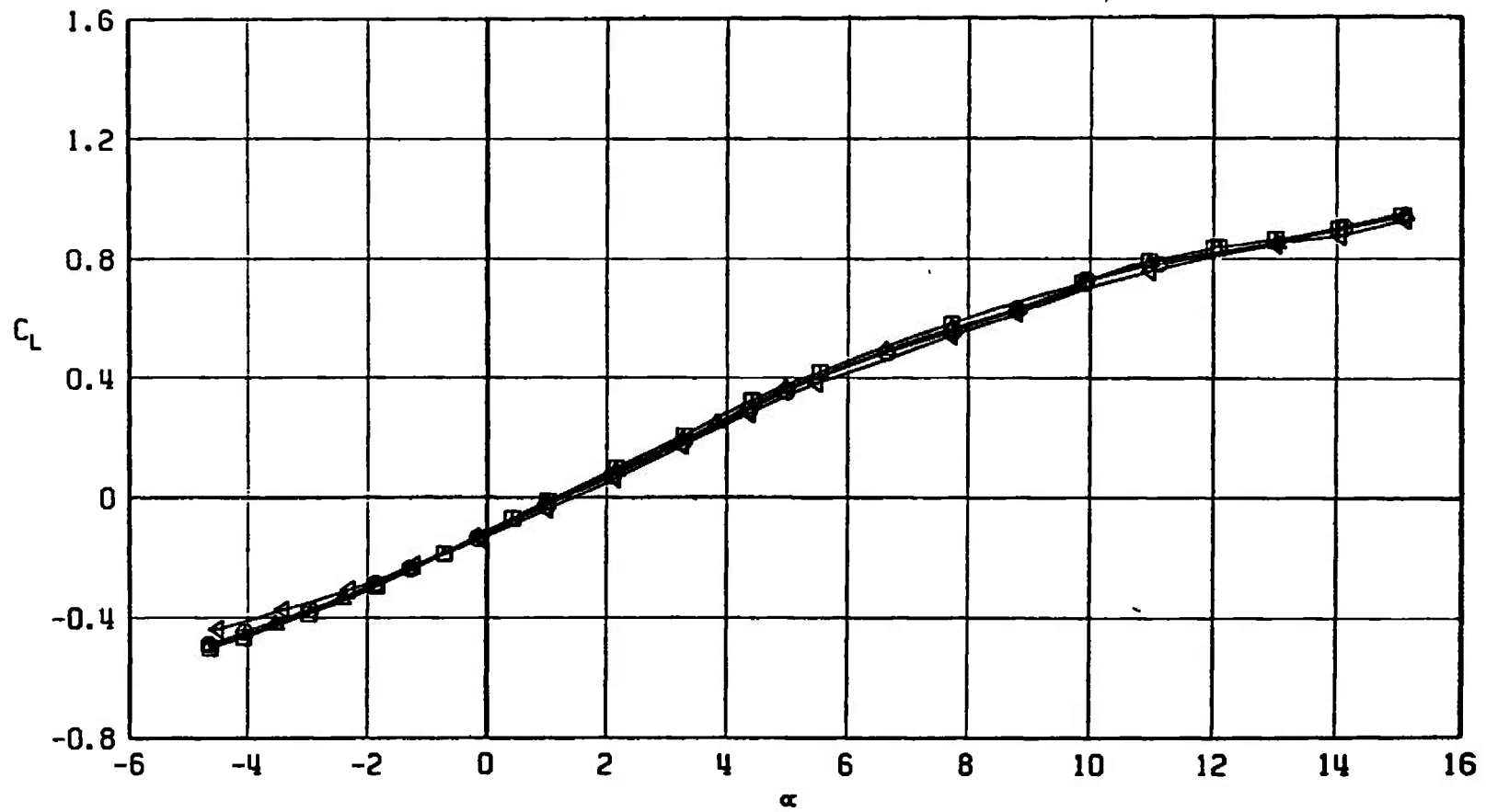
Fig. 11 Variation of Dynamic Pressure and Reynolds Number with Mach Number



a.  $M_\infty = 0.50$

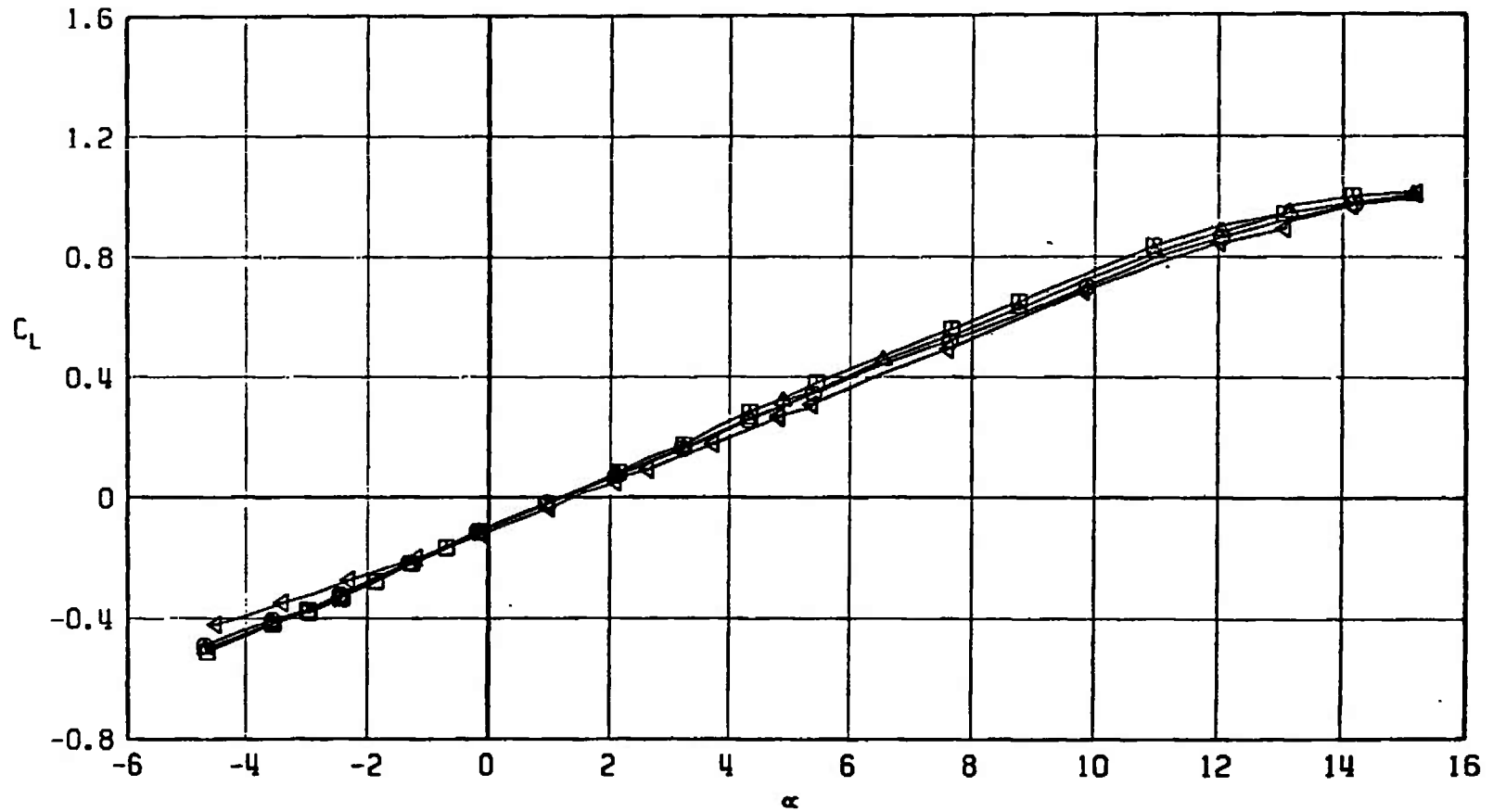
Fig. 12 Lift Coefficient Variation with Angle of Attack for Configurations A701, A702, A703, and A704

SYMBOL	CONFIGURATION
□	A701
○	A702
△	A703
◀	A704



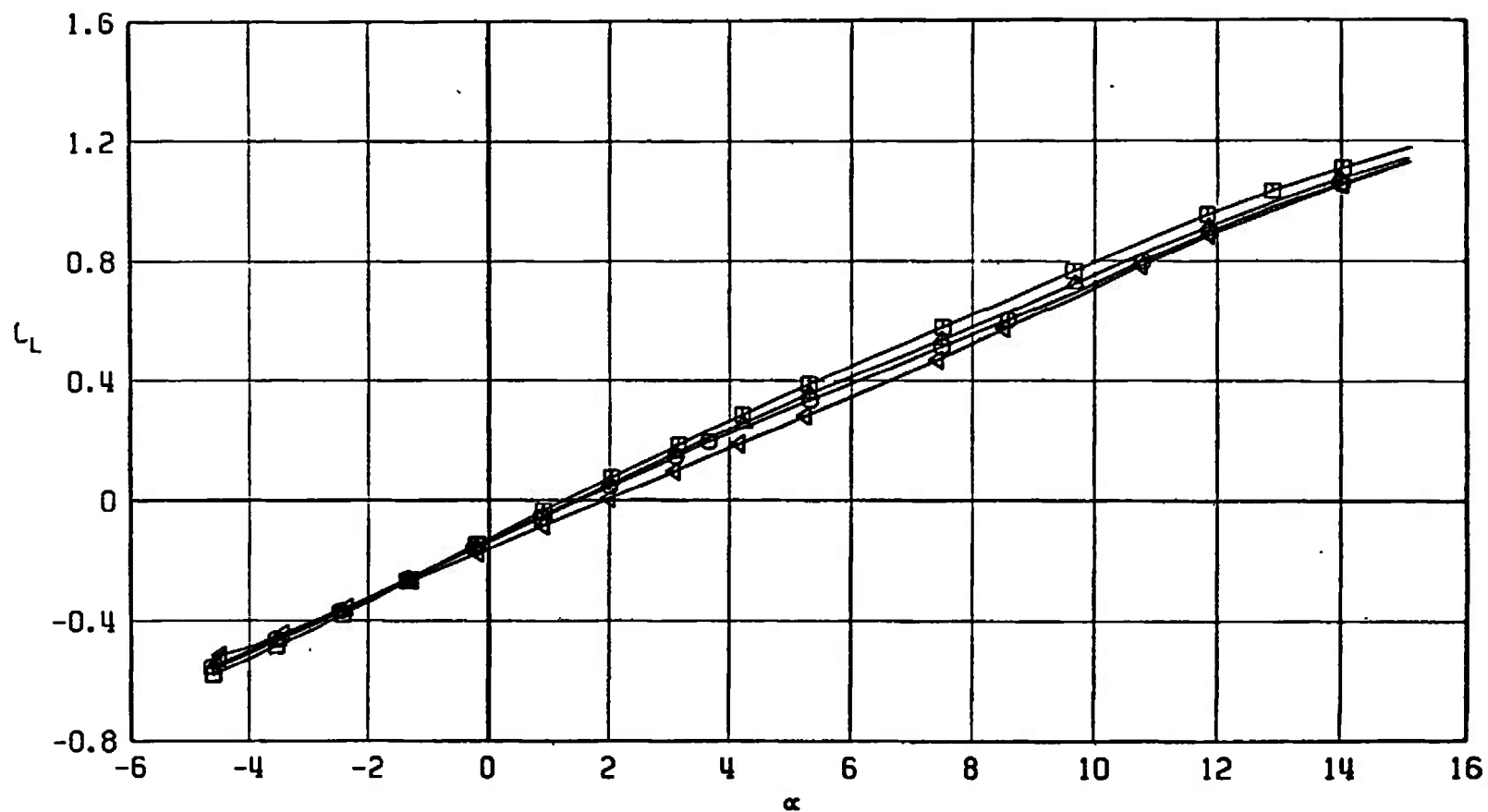
b.  $M_\infty = 0.90$   
Fig. 12 Continued

SYMBOL	CONFIGURATION
□	A701
●	A702
△	A703
▽	A704



c.  $M_\infty = 0.95$   
Fig. 12 Continued

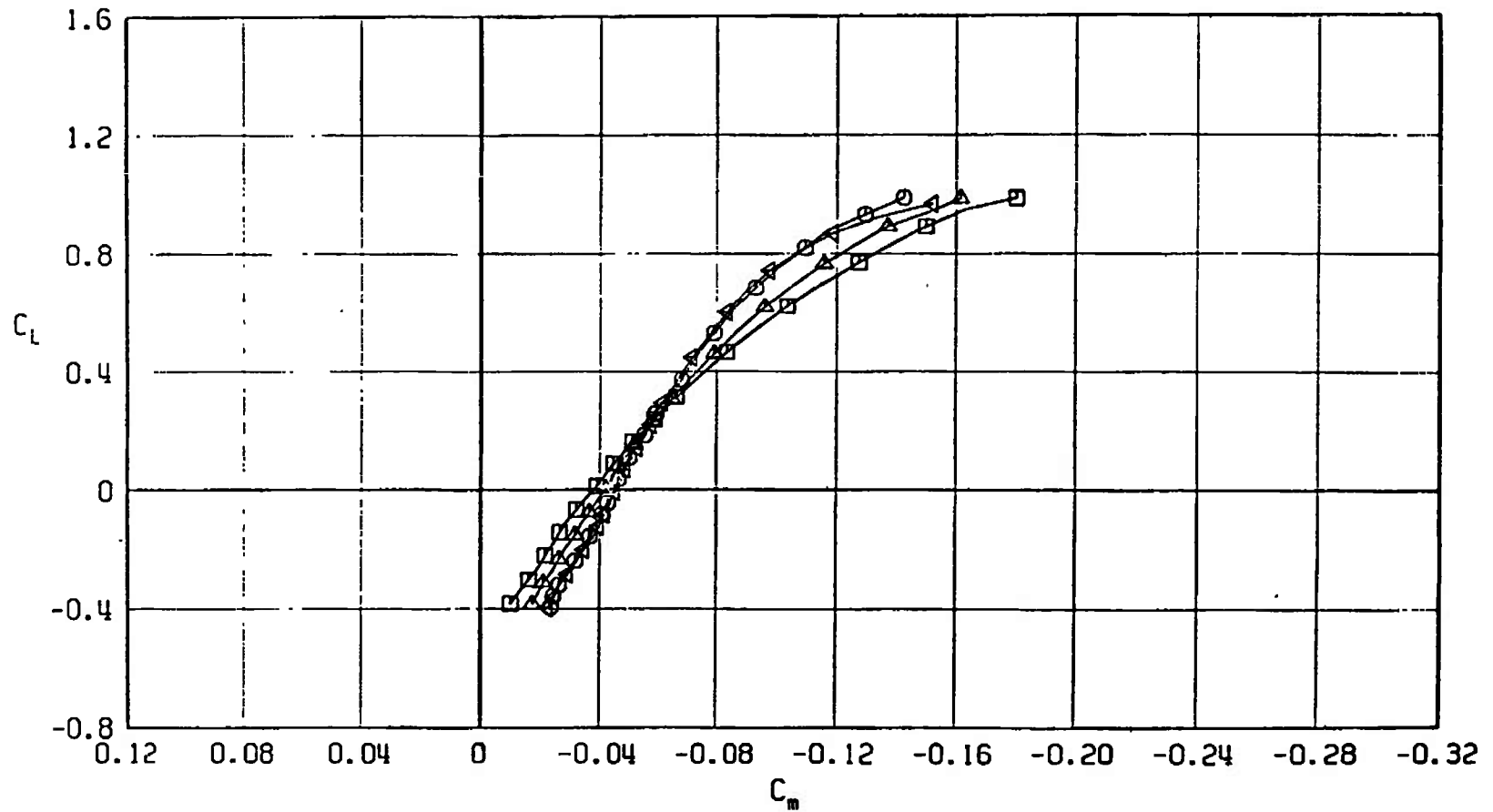
SYMBOL	CONFIGURATION
□	A701
○	A702
△	A703
◊	A704



d.  $M_\infty = 1.05$   
Fig. 12 Concluded



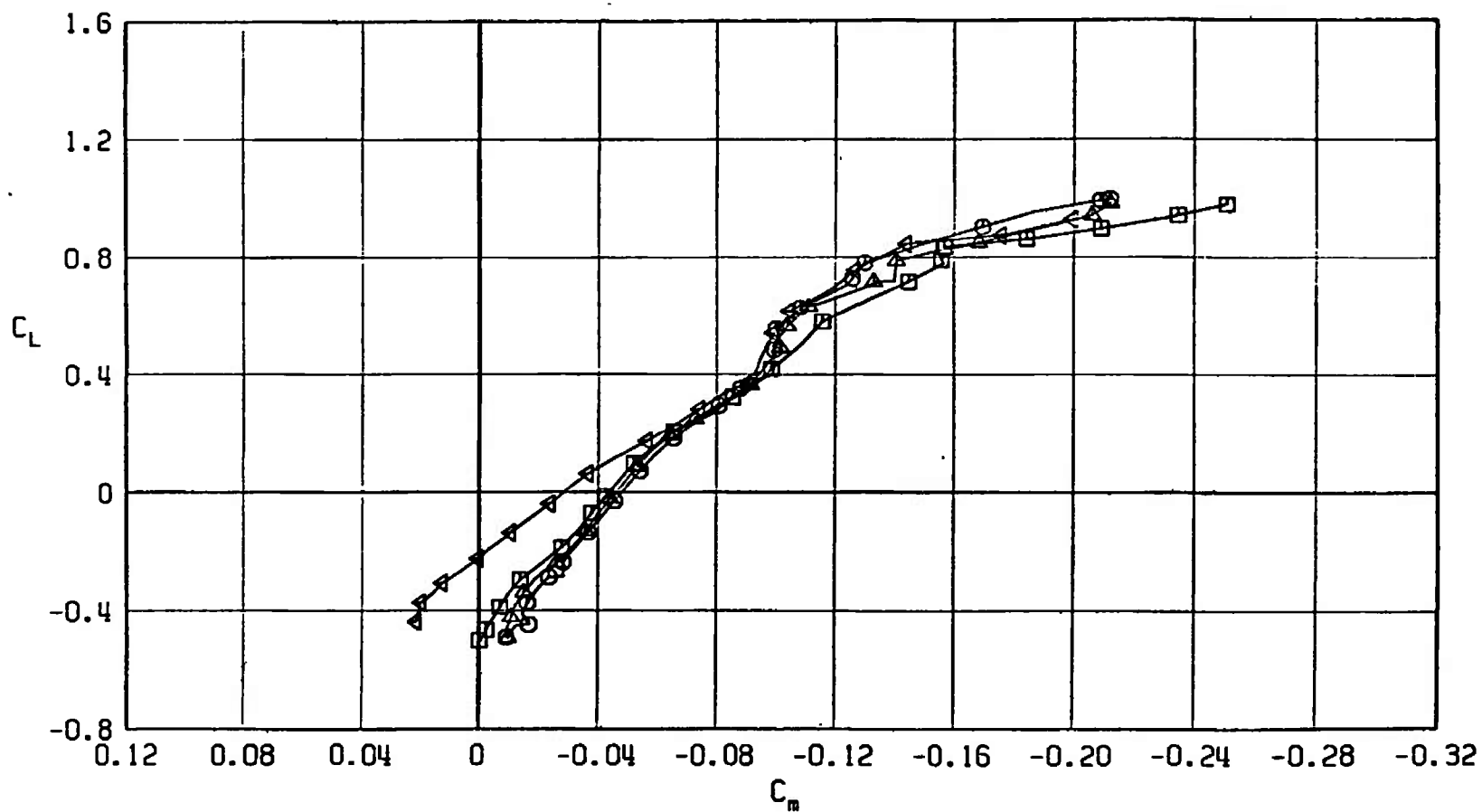
SYMBOL	CONFIGURATION
□	A701
○	A702
△	A703
▽	A704



a.  $M_\infty = 0.50$

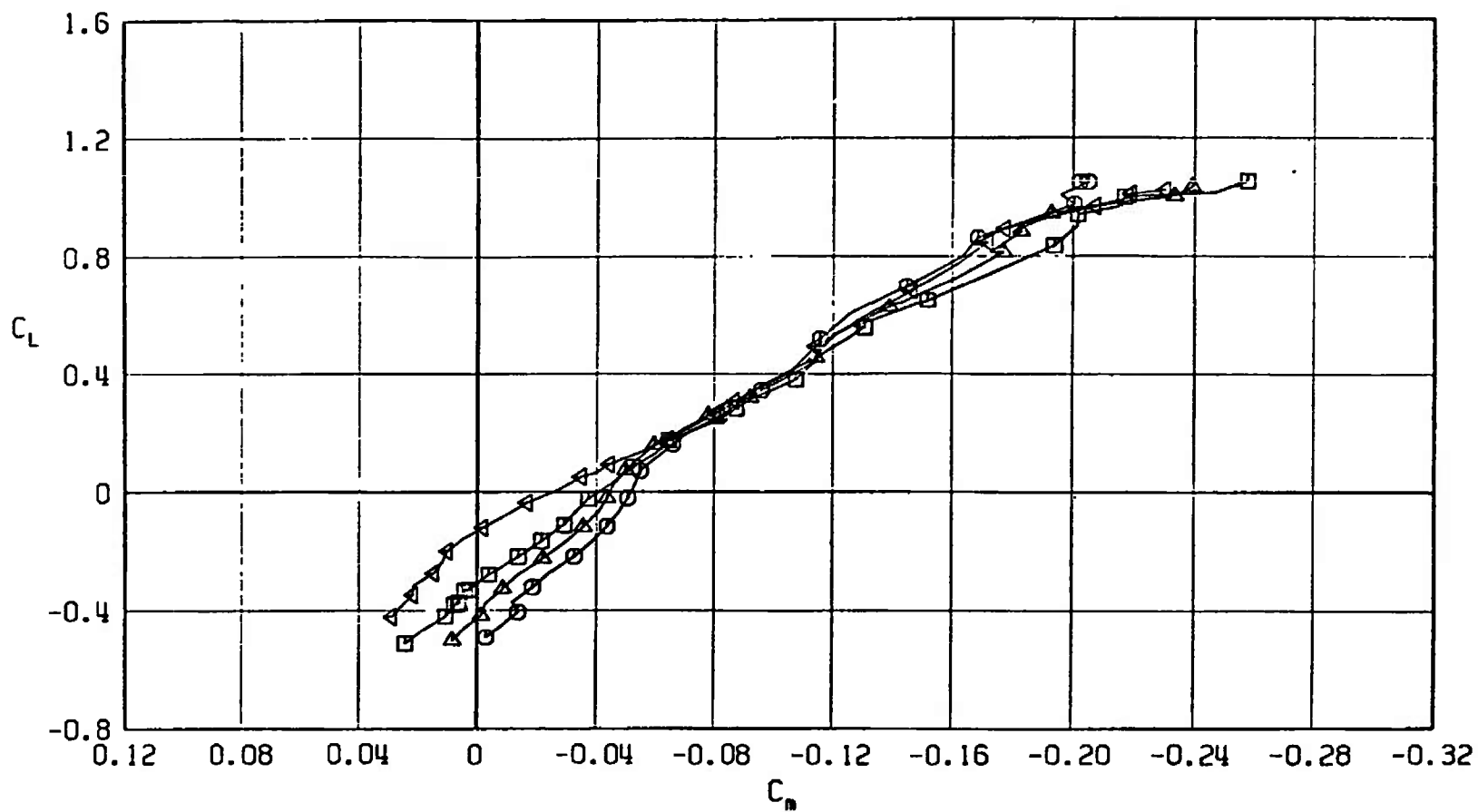
Fig. 13 Pitching-Moment Coefficient Variation with Lift Coefficient for Configurations A701, A702, A703, and A704

SYMBOL	CONFIGURATION
□	A701
○	A702
△	A703
◁	A704



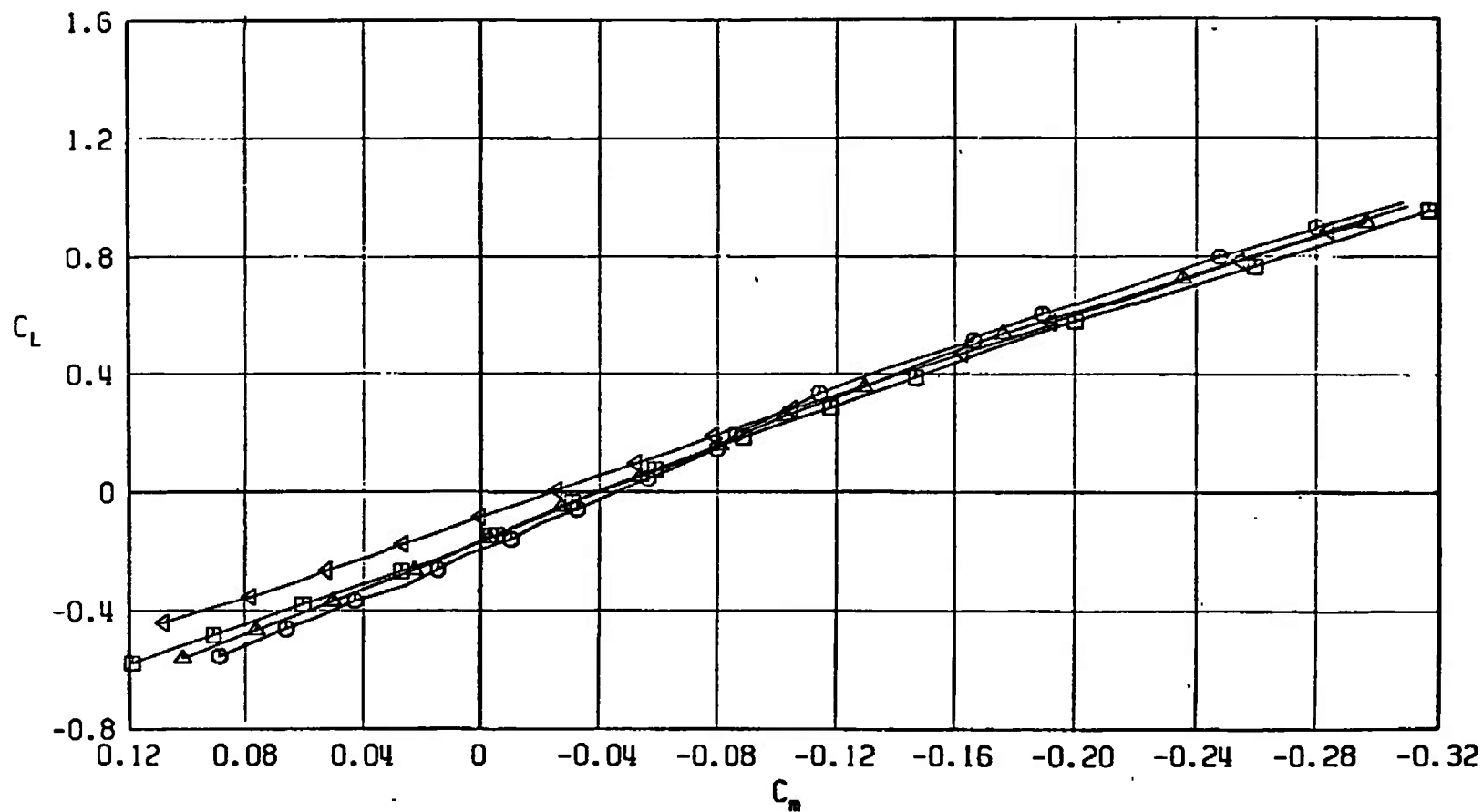
b.  $M_\infty = 0.90$   
Fig. 13 Continued

SYMBOL	CONFIGURATION
□	A701
○	A702
△	A703
▽	A704



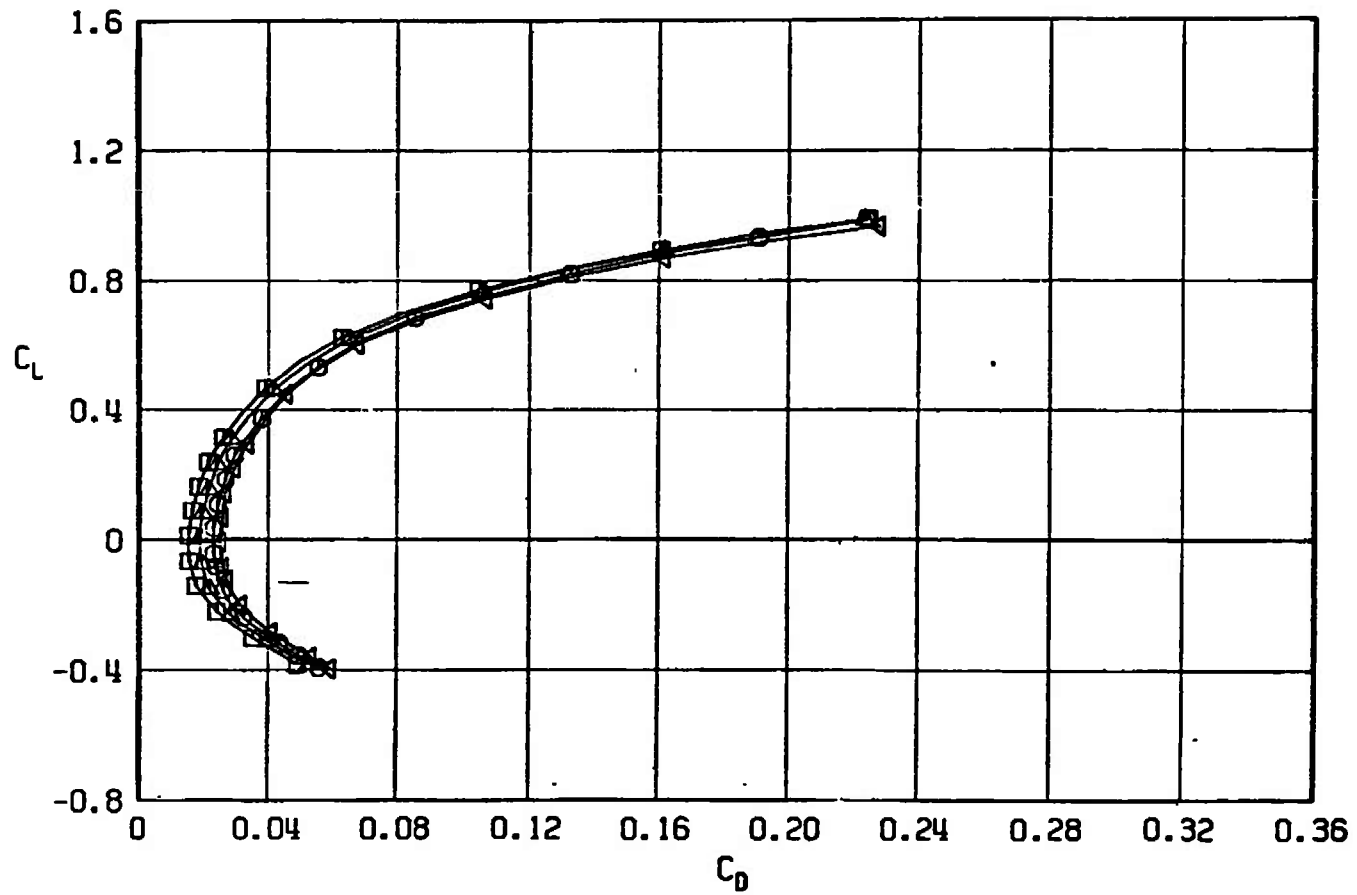
c.  $M_\infty = 0.95$   
Fig. 13 Continued

SYMBOL	CONFIGURATION
□	A701
○	A702
△	A703
◄	A704



d.  $M_\infty = 1.05$   
Fig. 13 Concluded

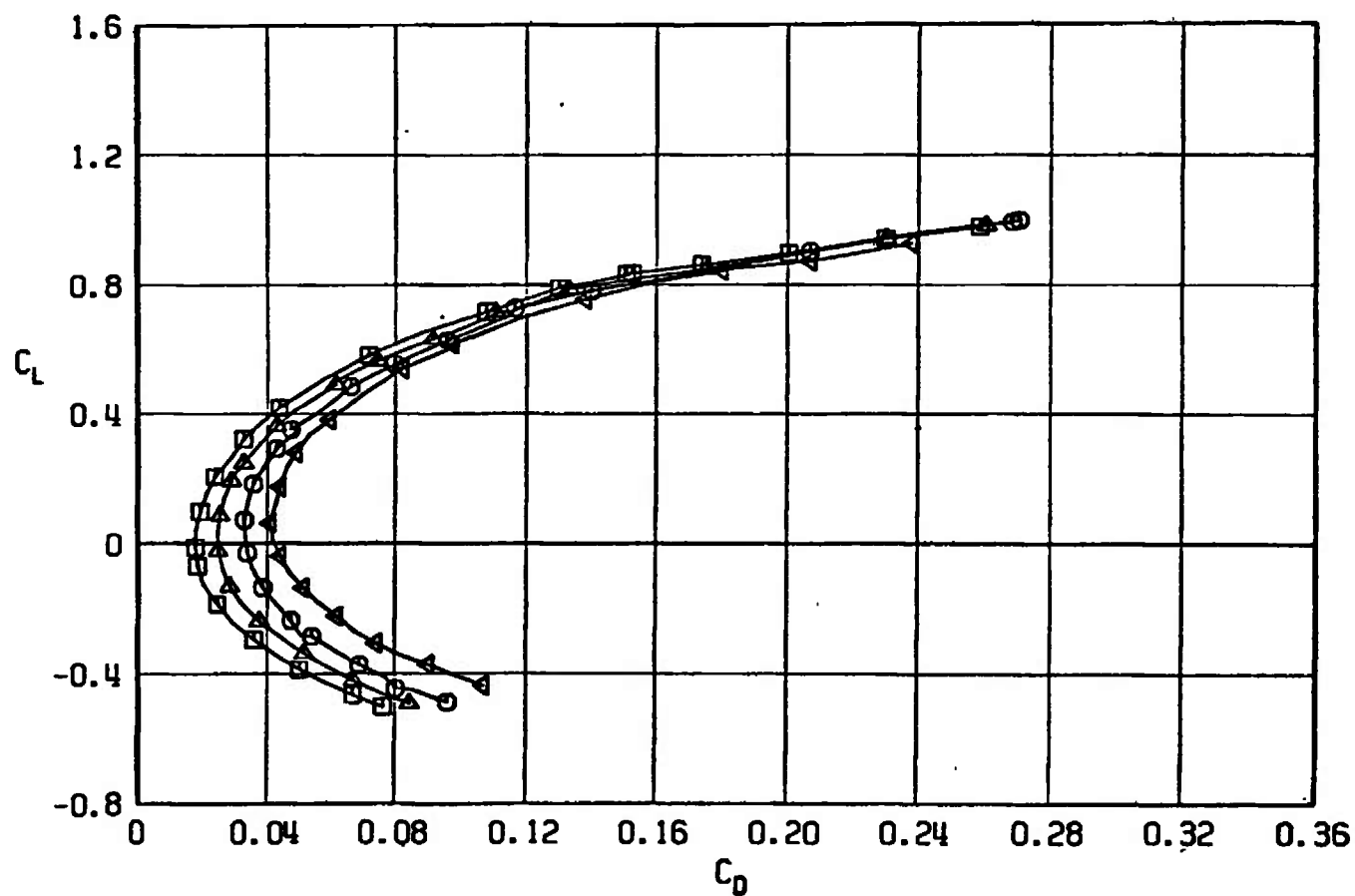
SYMBOL	CONFIGURATION
□	A701
○	A702
△	A703
▽	A704



a.  $M_\infty = 0.50$

Fig. 14 Drag Coefficient Variation with Lift Coefficient for Configurations A701, A702, A703, and A704

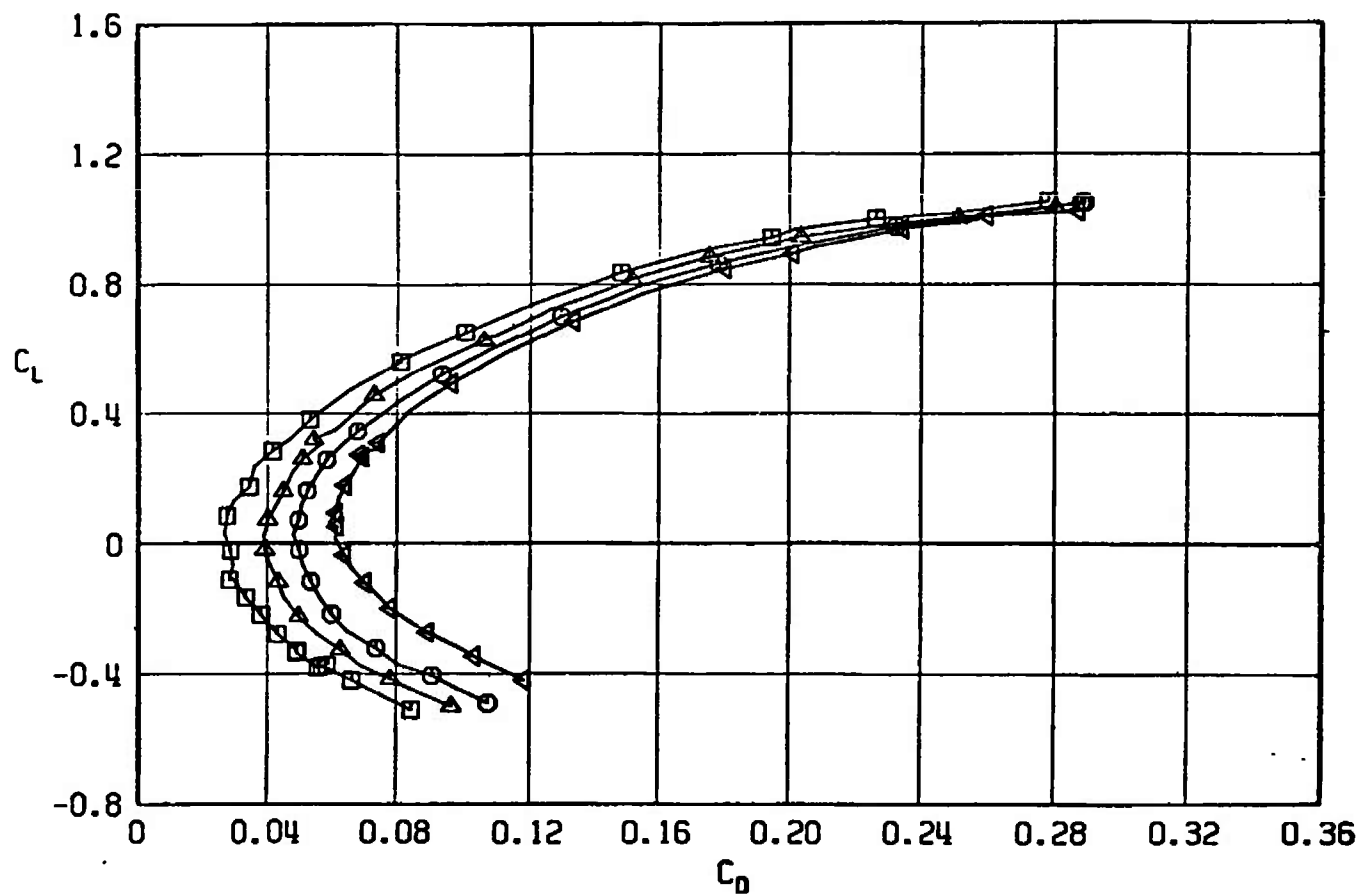
SYMBOL	CONFIGURATION
□	A701
○	A702
△	A703
◀	A704



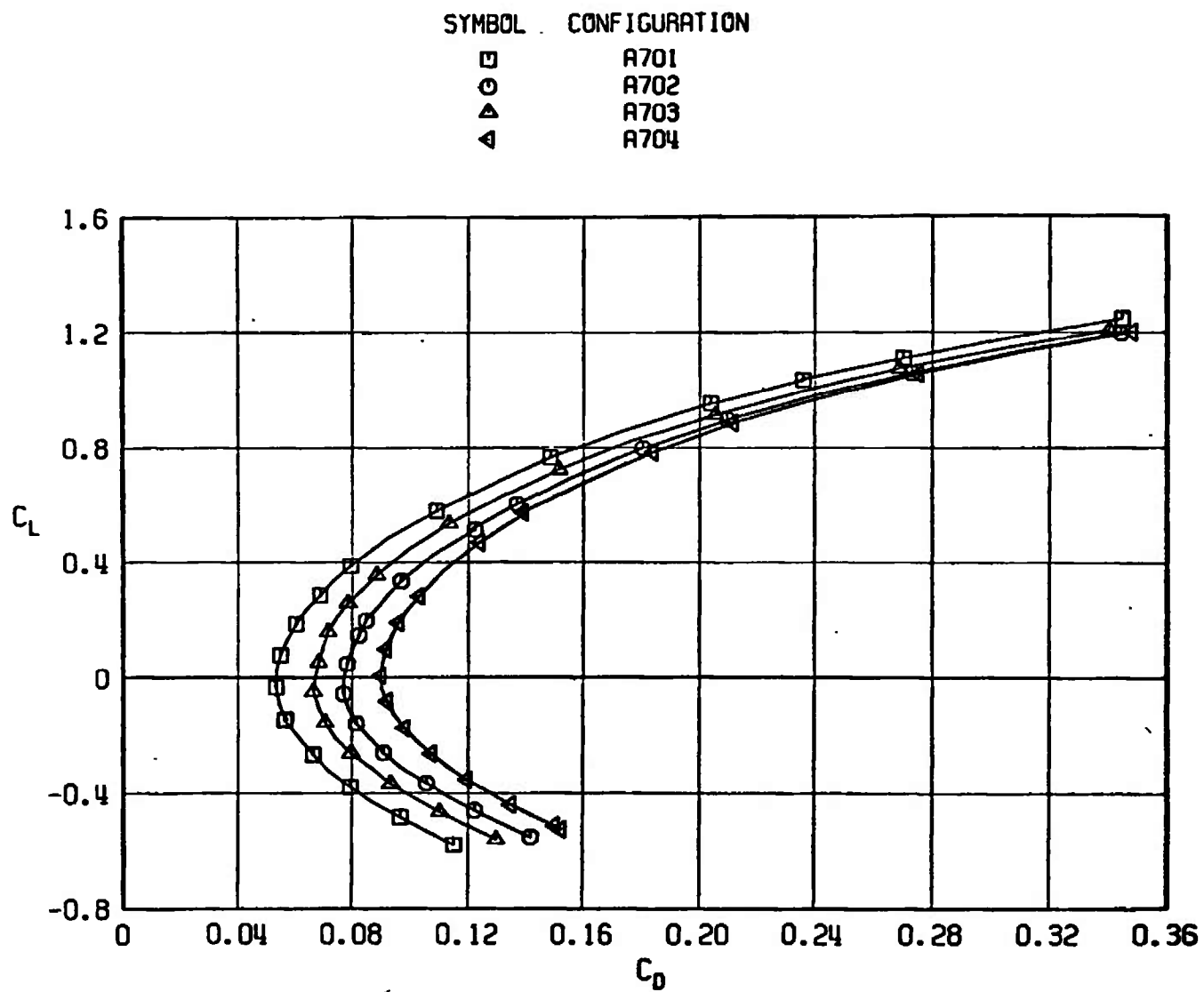
b.  $M_\infty = 0.90$   
Fig. 14 Continued

SYMBOL	CONFIGURATION
--------	---------------

□	A701
○	A702
△	A703
▽	A704



c.  $M_\infty = 0.95$   
Fig. 14 Continued



d.  $M_\infty = 1.05$   
Fig. 14 Concluded



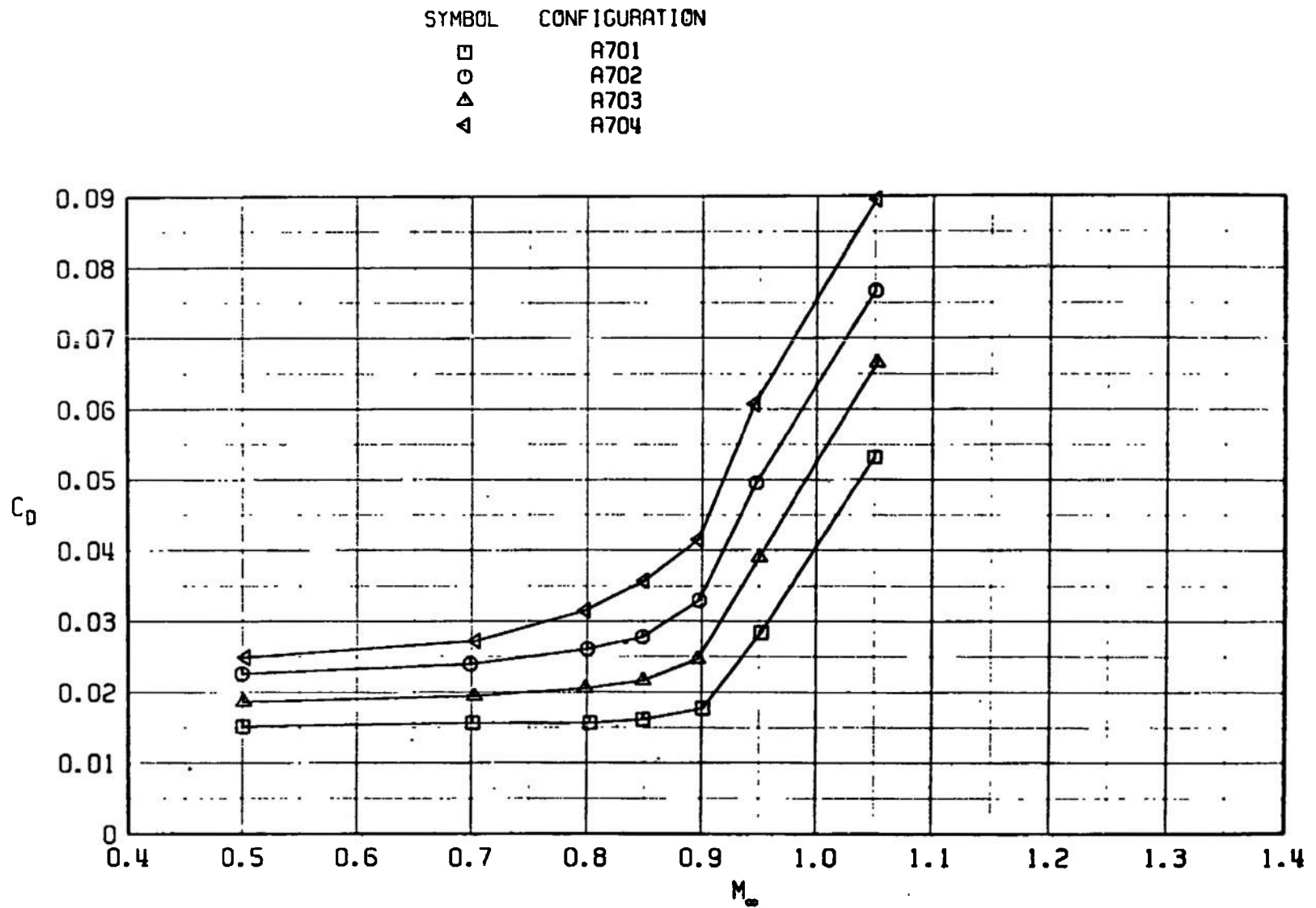
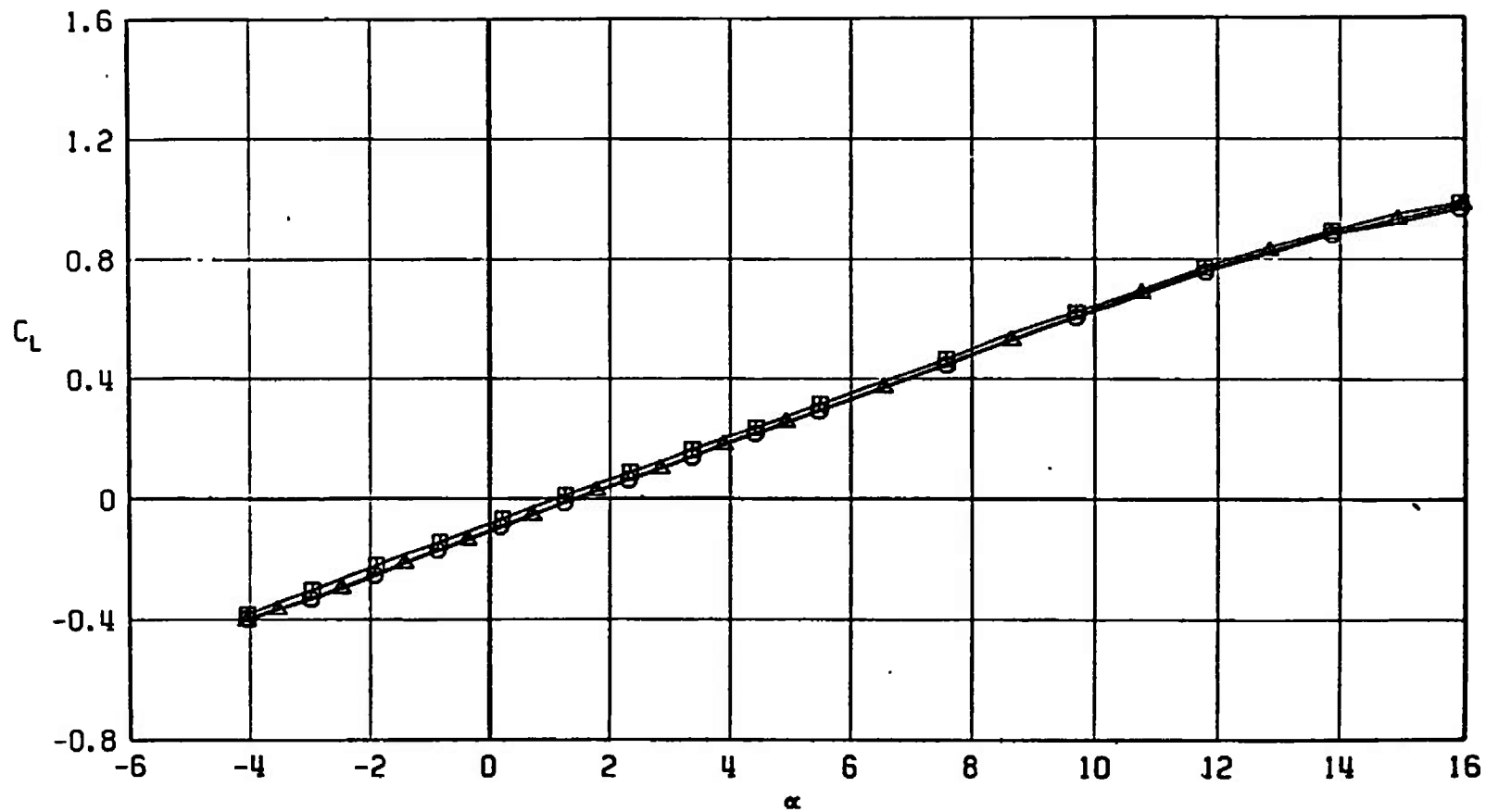


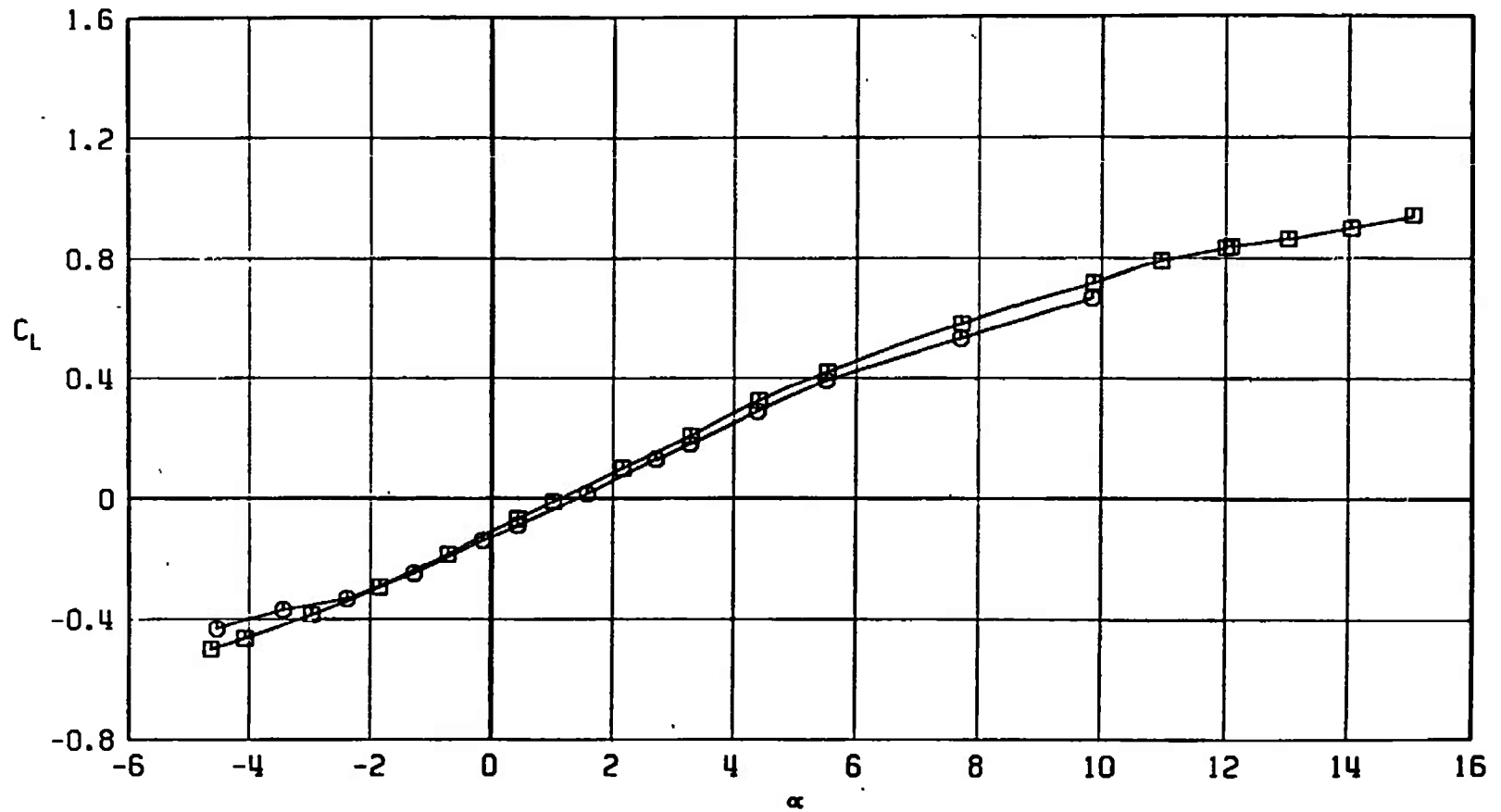
Fig. 15 Drag Coefficient Variation with Mach Number at  $C_L = 0$  for Configurations A701, A702, A703, and A704

SYMBOL	CONFIGURATION
□	A701
○	A710
△	A707



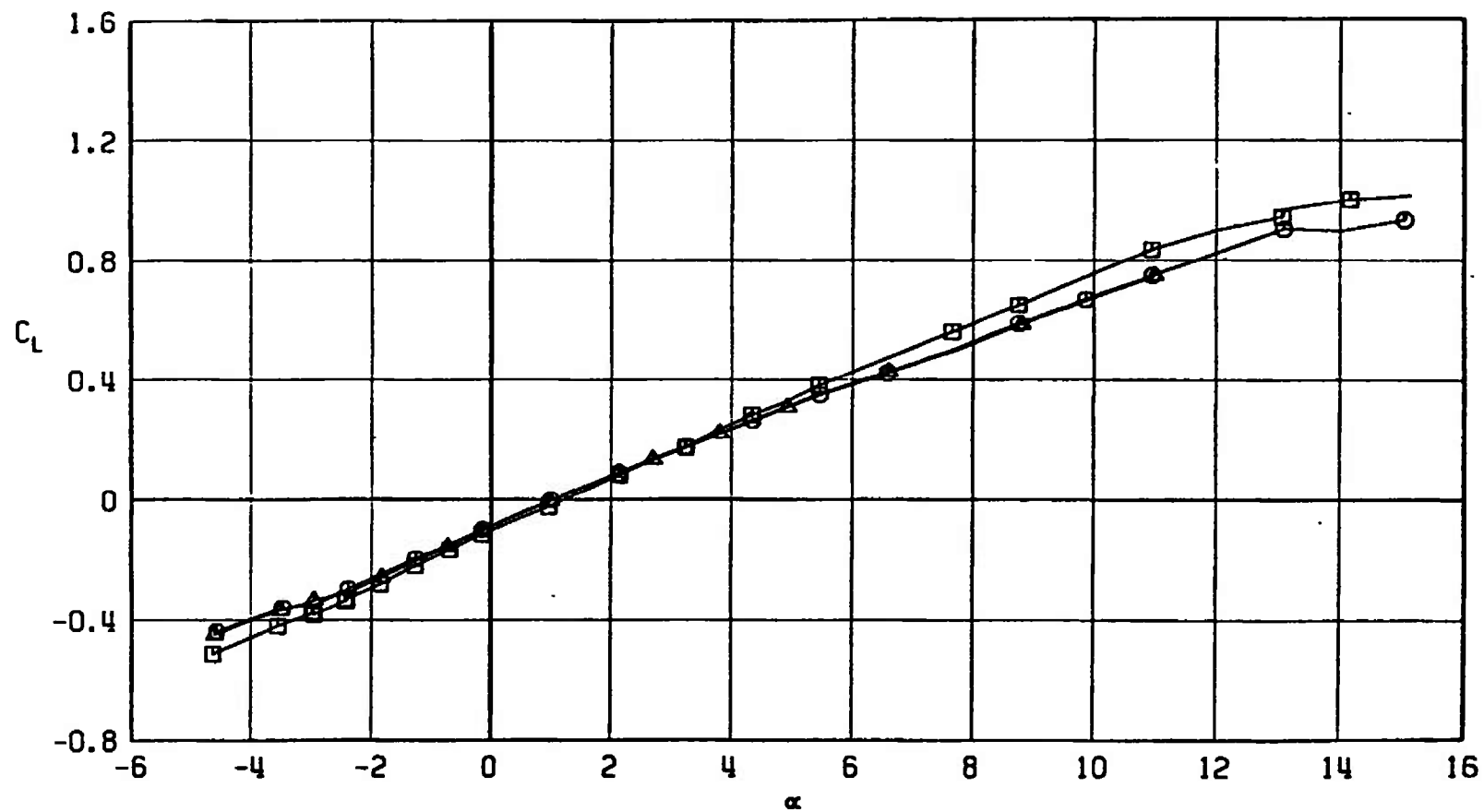
a.  $M_\infty = 0.50$   
 Fig. 16 Lift Coefficient Variation with Angle of Attack for Configurations A701, A707, and A710

SYMBOL	CONFIGURATION
□	A701
○	A710



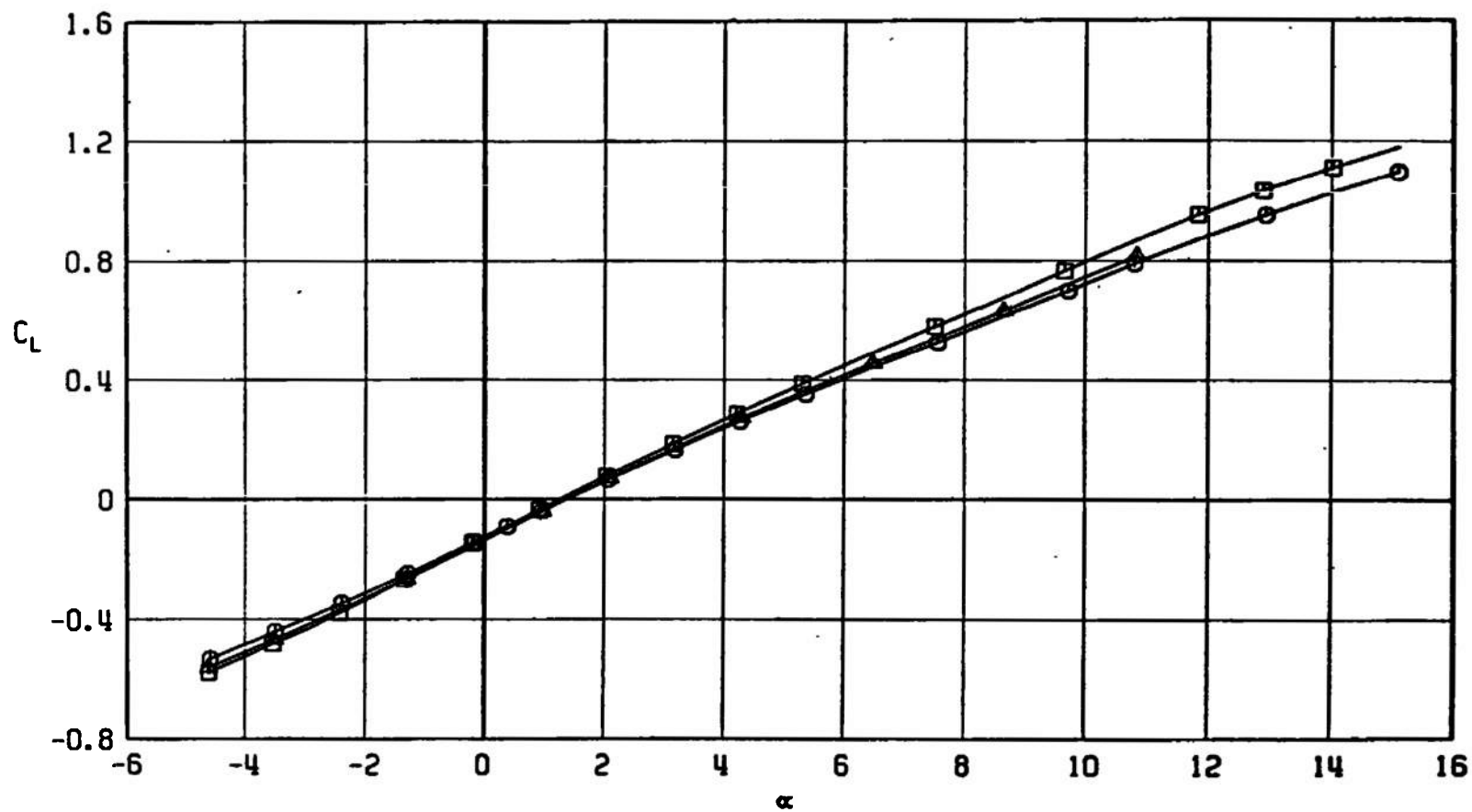
b.  $M_\infty = 0.90$   
Fig. 16 Continued

SYMBOL	CONFIGURATION
□	A701
○	A710
△	A707



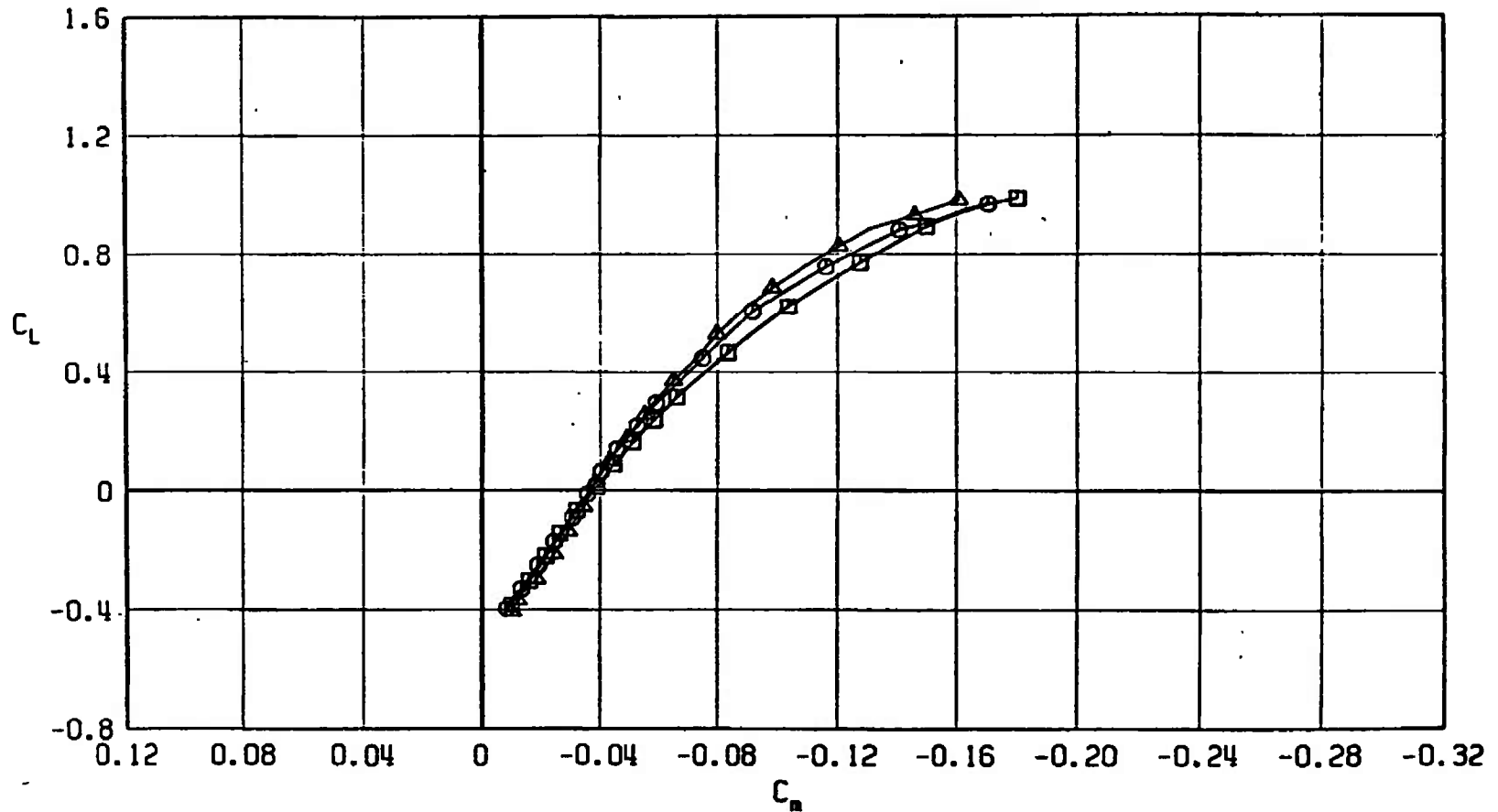
c.  $M_\infty = 0.95$   
Fig. 16 Continued

SYMBOL	CONFIGURATION
□	A701
○	A710
△	A707



d.  $M_\infty = 1.05$   
Fig. 16 Concluded

SYMBOL	CONFIGURATION
□	A701
○	A710
△	A707



a.  $M_\infty = 0.50$

Fig. 17 Pitching-Moment Coefficient Variation with Lift Coefficient for Configurations A701, A707, and A710

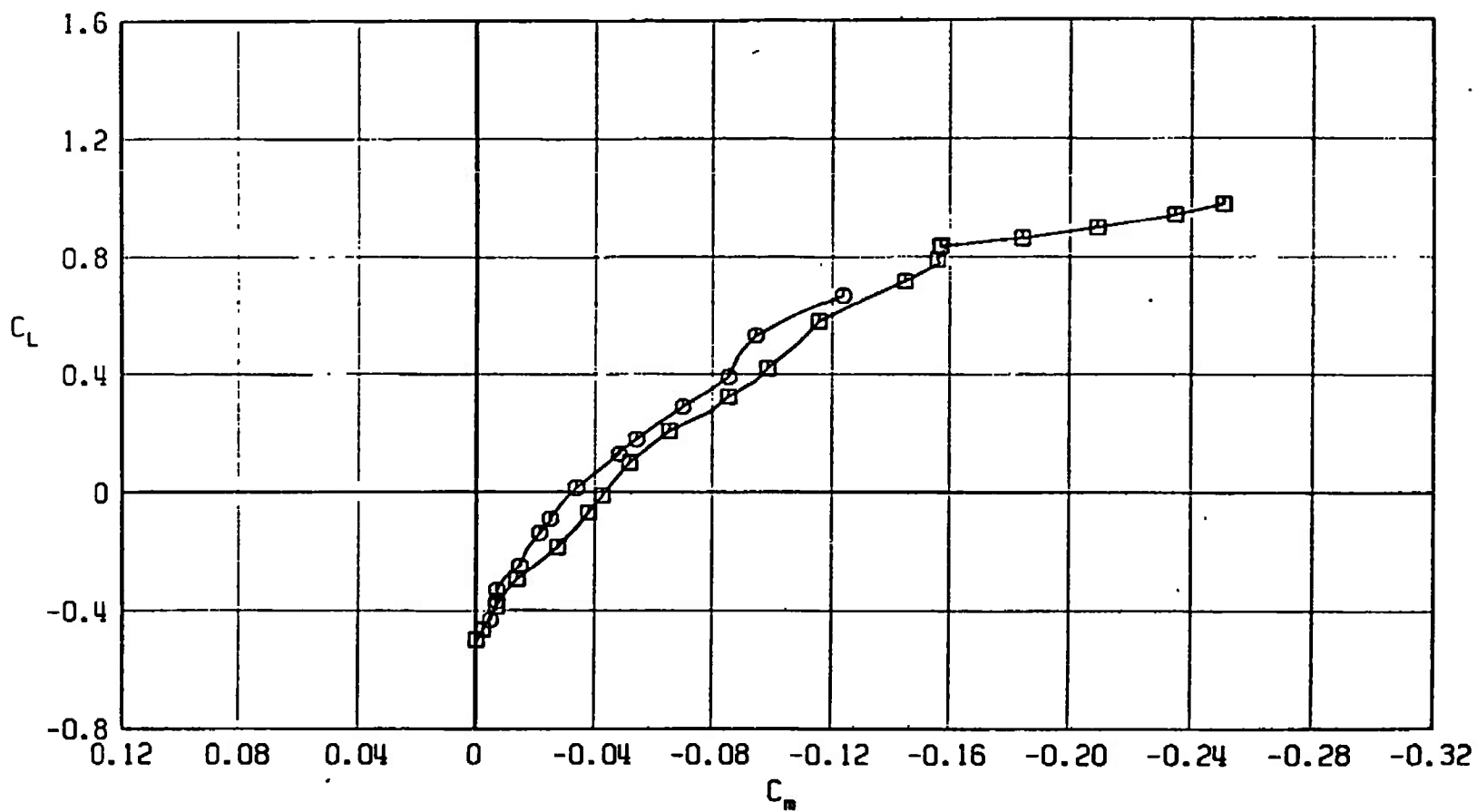
SYMBOL    CONFIGURATION

□

A701

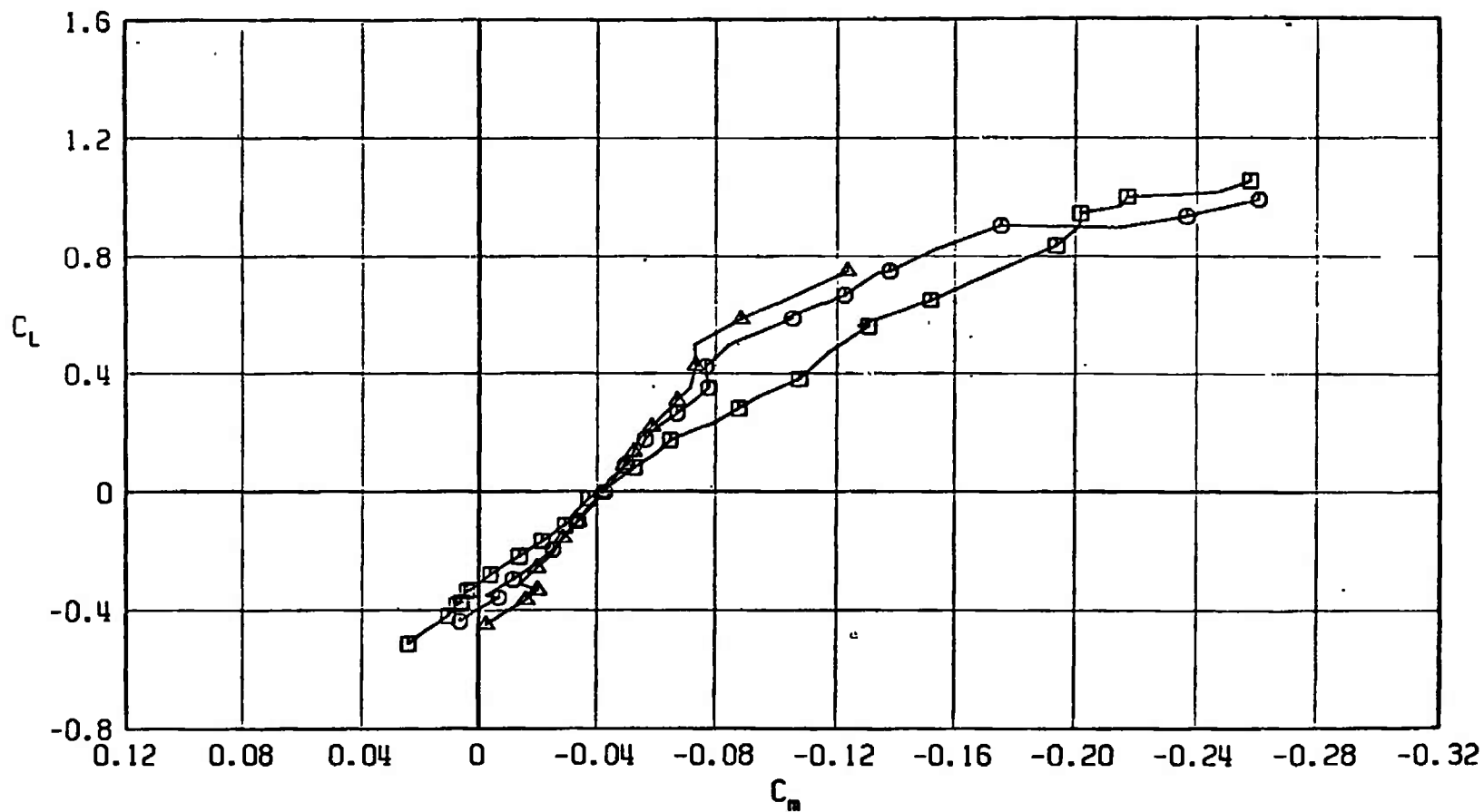
○

A710



b.  $M_\infty = 0.90$   
Fig. 17 Continued

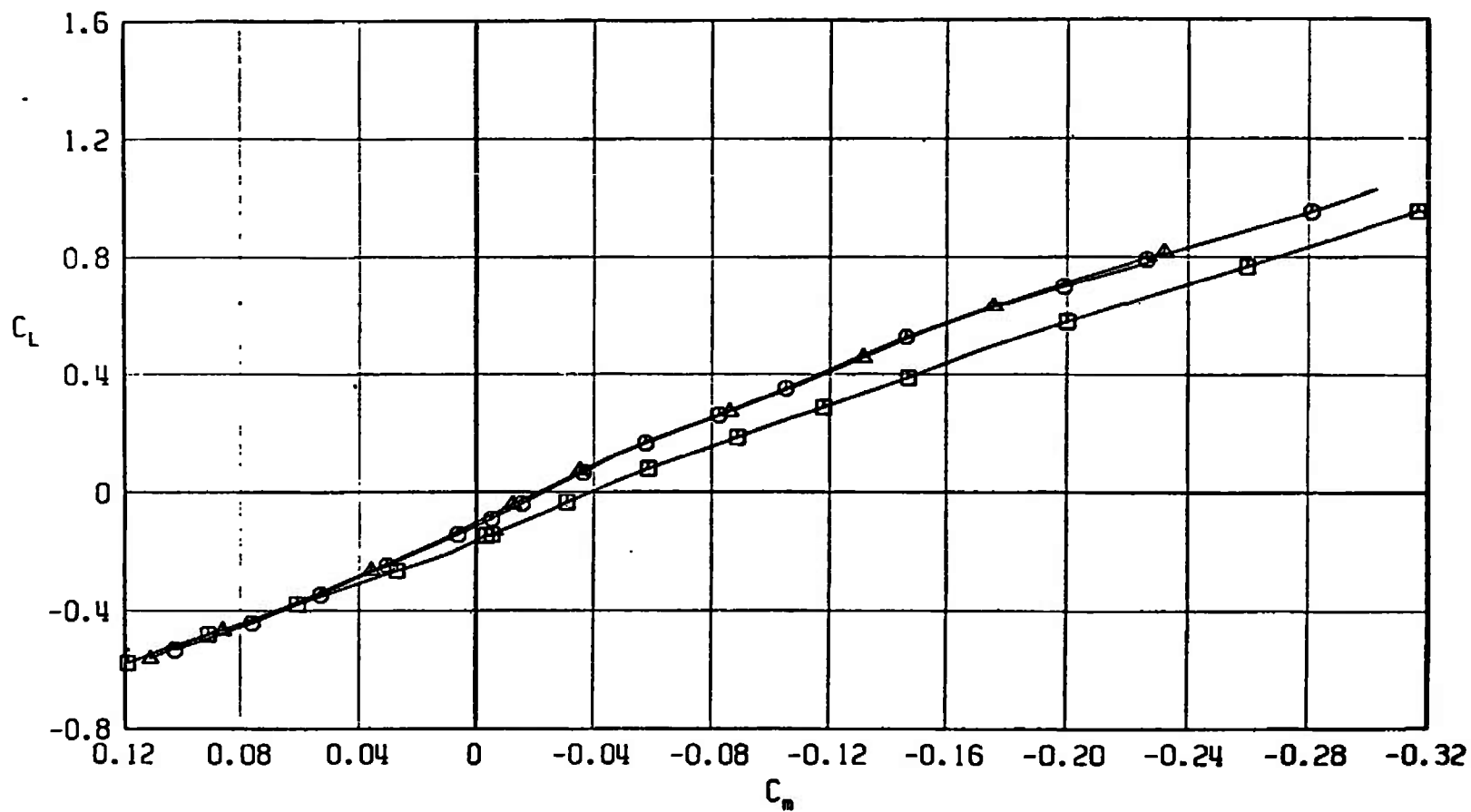
SYMBOL	CONFIGURATION
□	A701
○	A710
△	A707



c.  $M_\infty = 0.95$   
Fig. 17 Continued



SYMBOL	CONFIGURATION
□	A701
○	A710
△	A707



d.  $M_\infty = 1.05$   
Fig. 17 Concluded

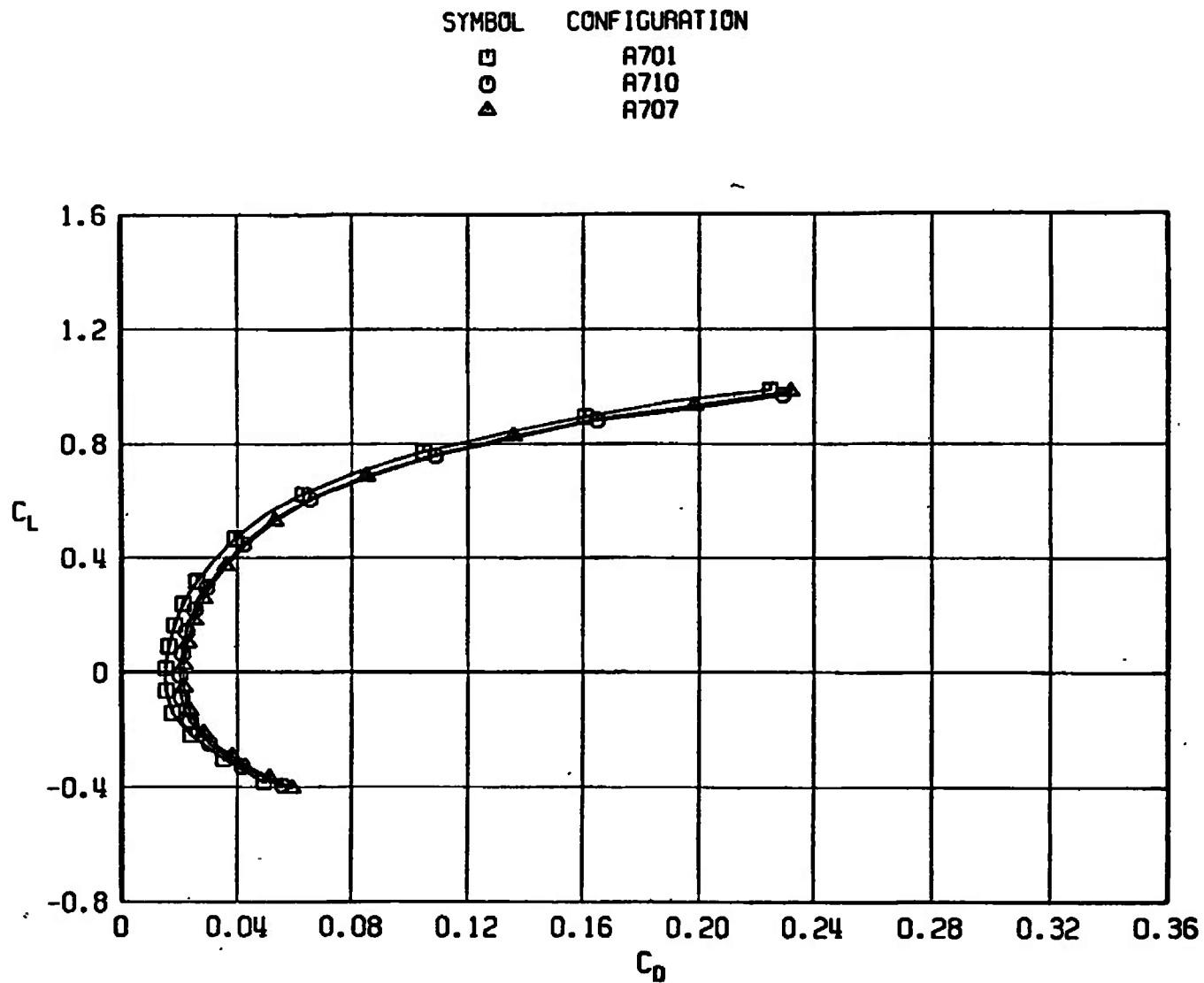
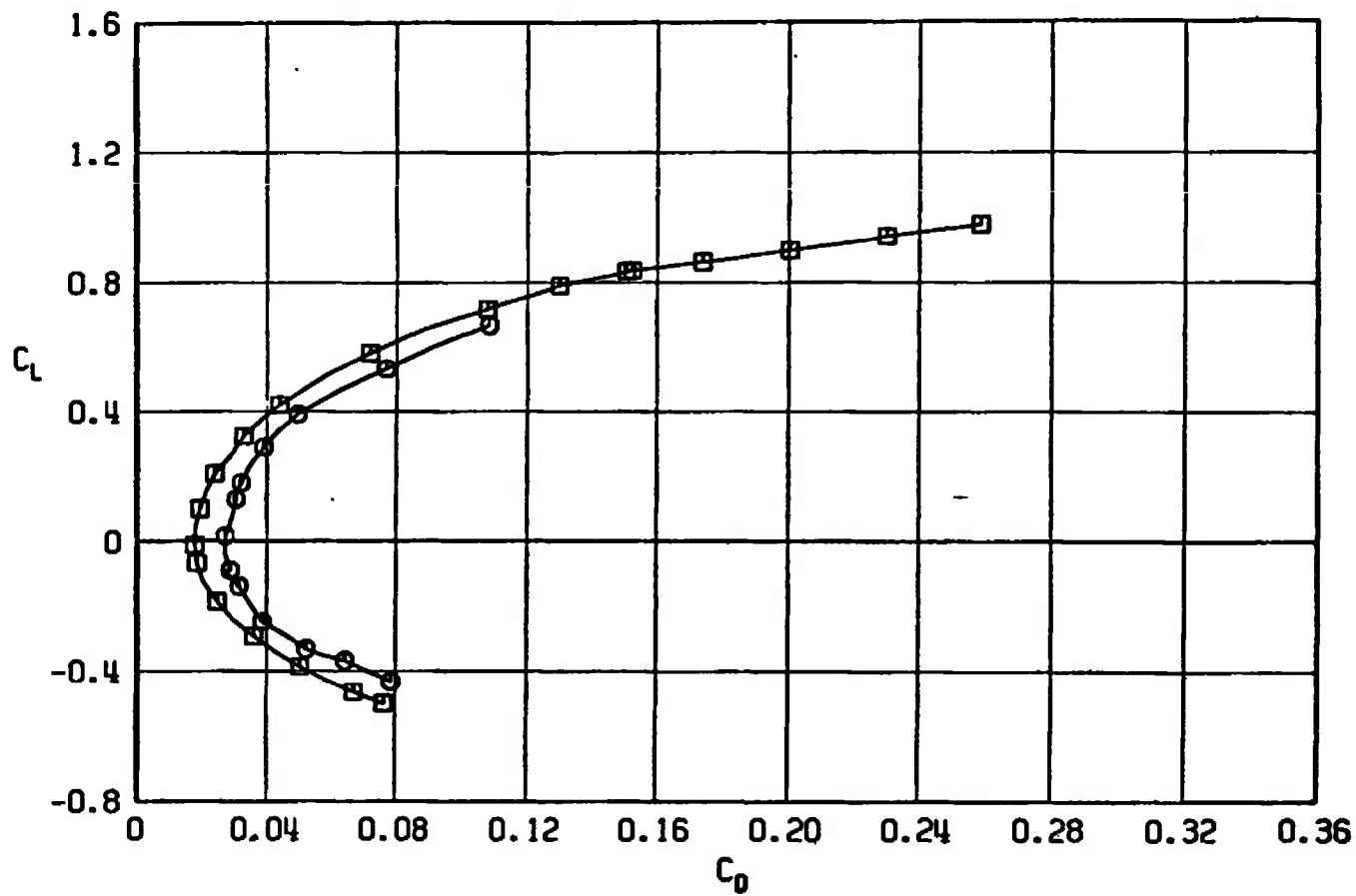
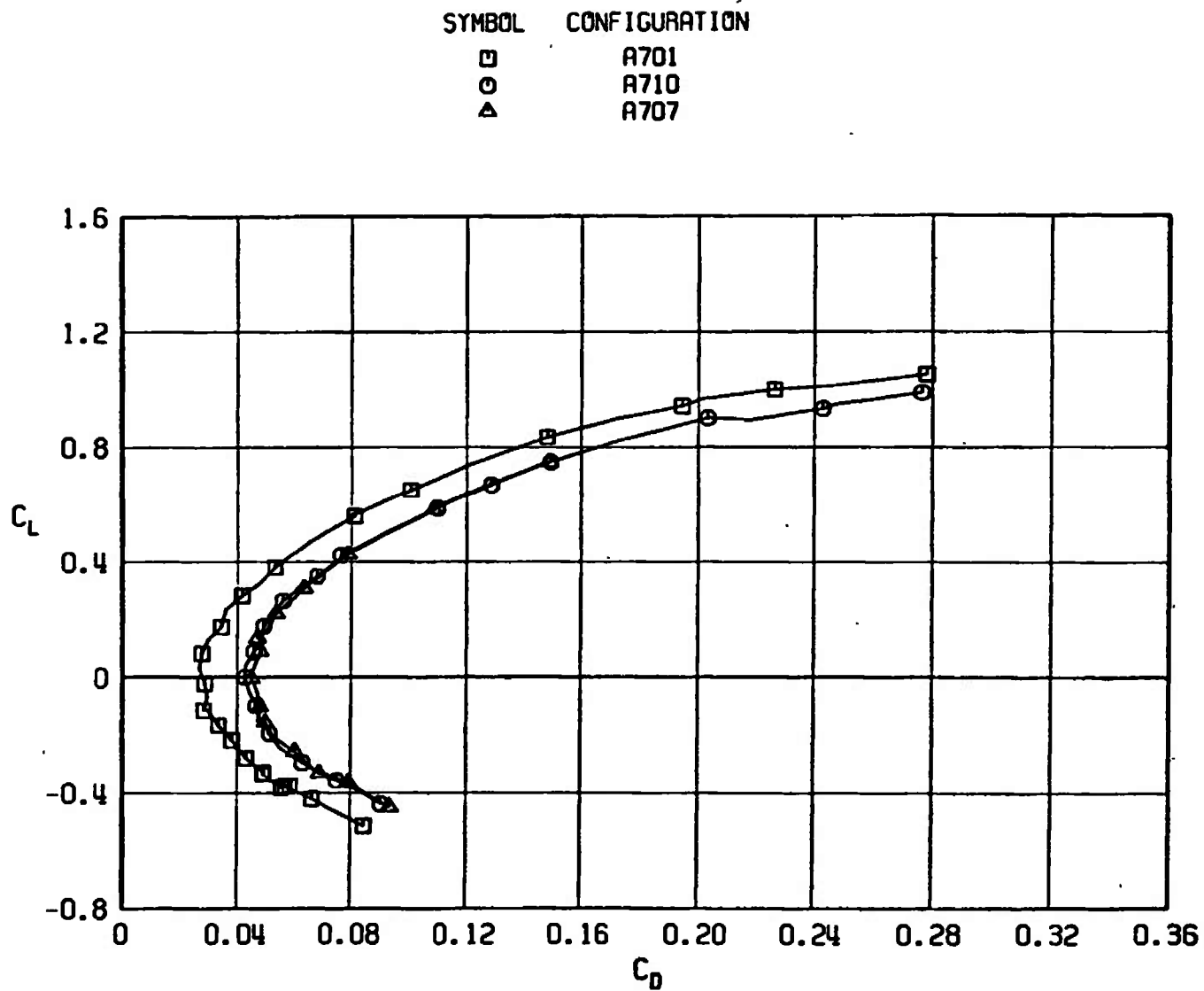
a.  $M_\infty = 0.50$ 

Fig. 18 Drag Coefficient Variation with Lift Coefficient for Configurations A701, A707, and A710

SYMBOL	CONFIGURATION
□	A701
○	A710

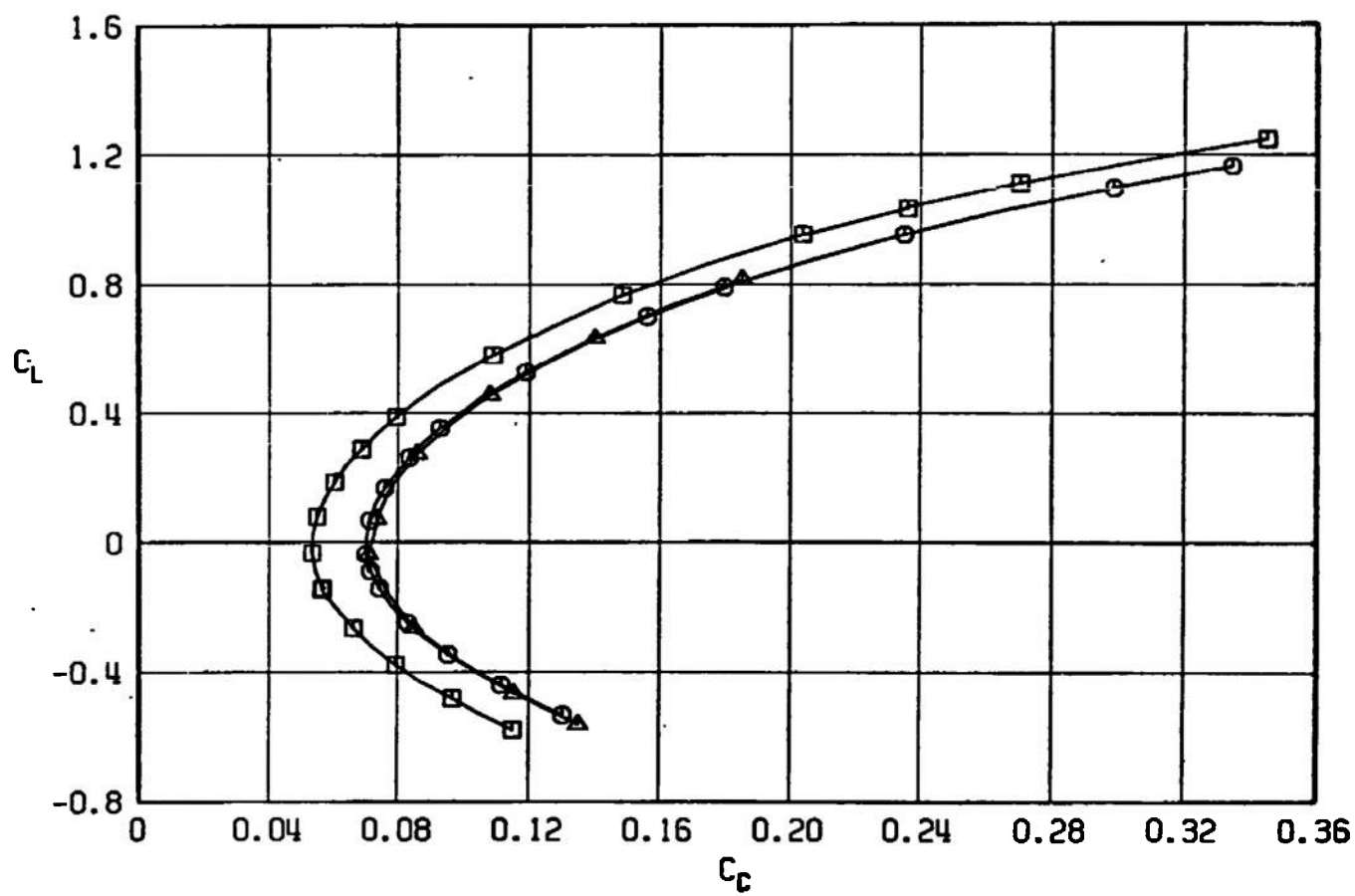


b.  $M_\infty = 0.90$   
Fig. 18 Continued



c.  $M_\infty = 0.95$   
Fig. 18 Continued

SYMBOL	CONFIGURATION
□	A701
○	A710
△	A707



d.  $M_\infty = 1.05$   
Fig. 18 Concluded

SYMBOL	CONFIGURATION
□	A701
○	A710
△	A707

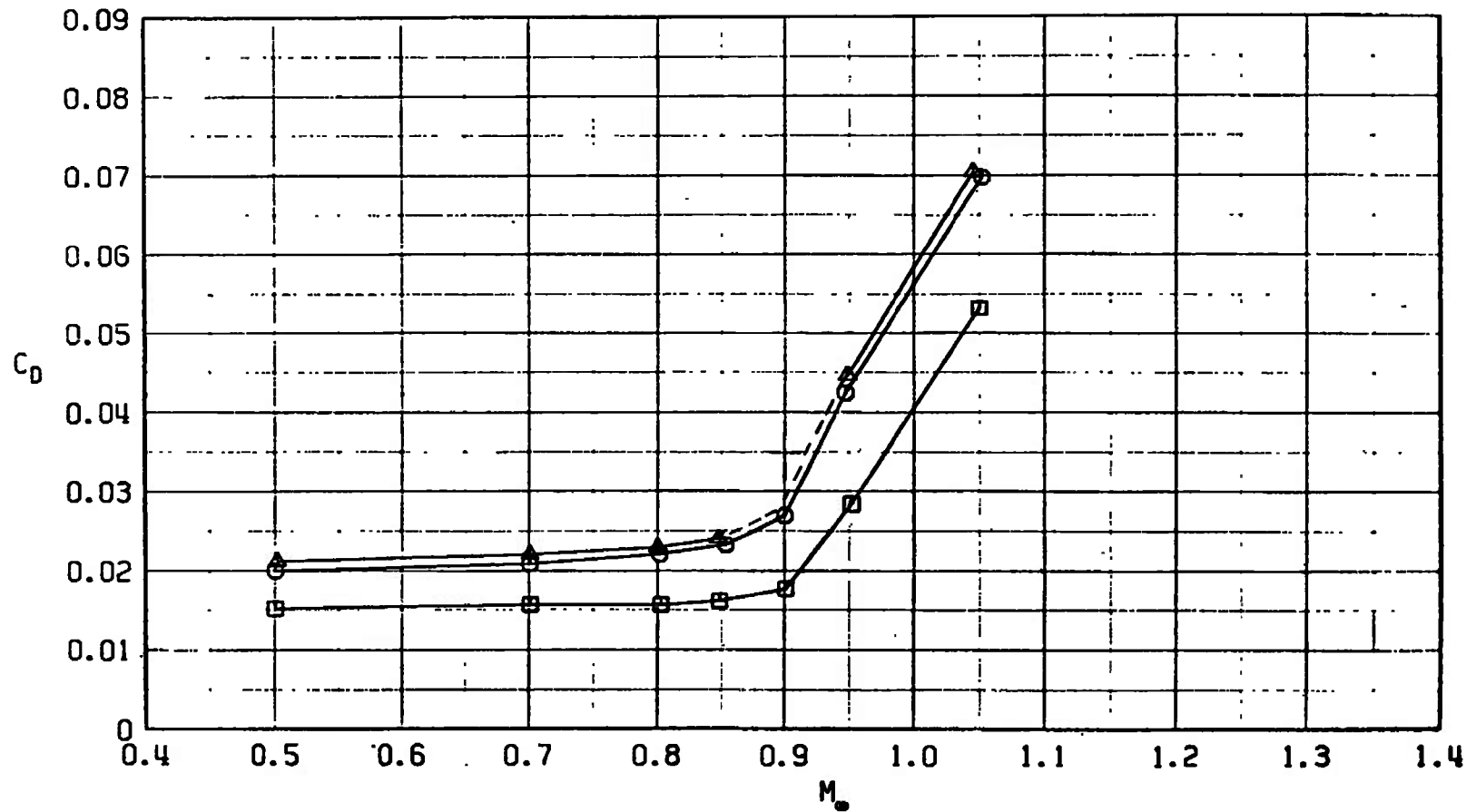
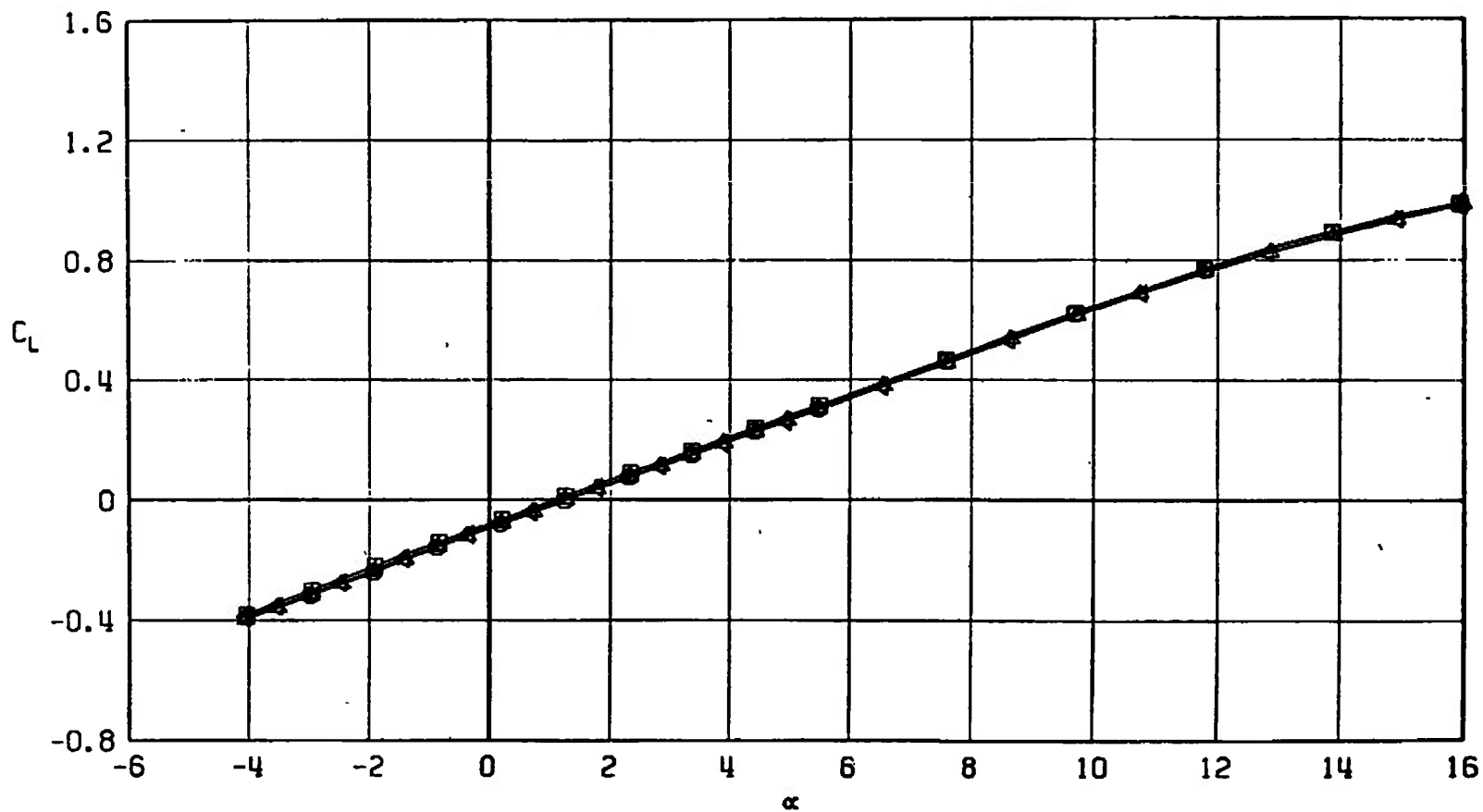


Fig. 19 Drag Coefficient Variation with Mach Number at  $C_L = 0$  for Configurations A701, A707, and A710

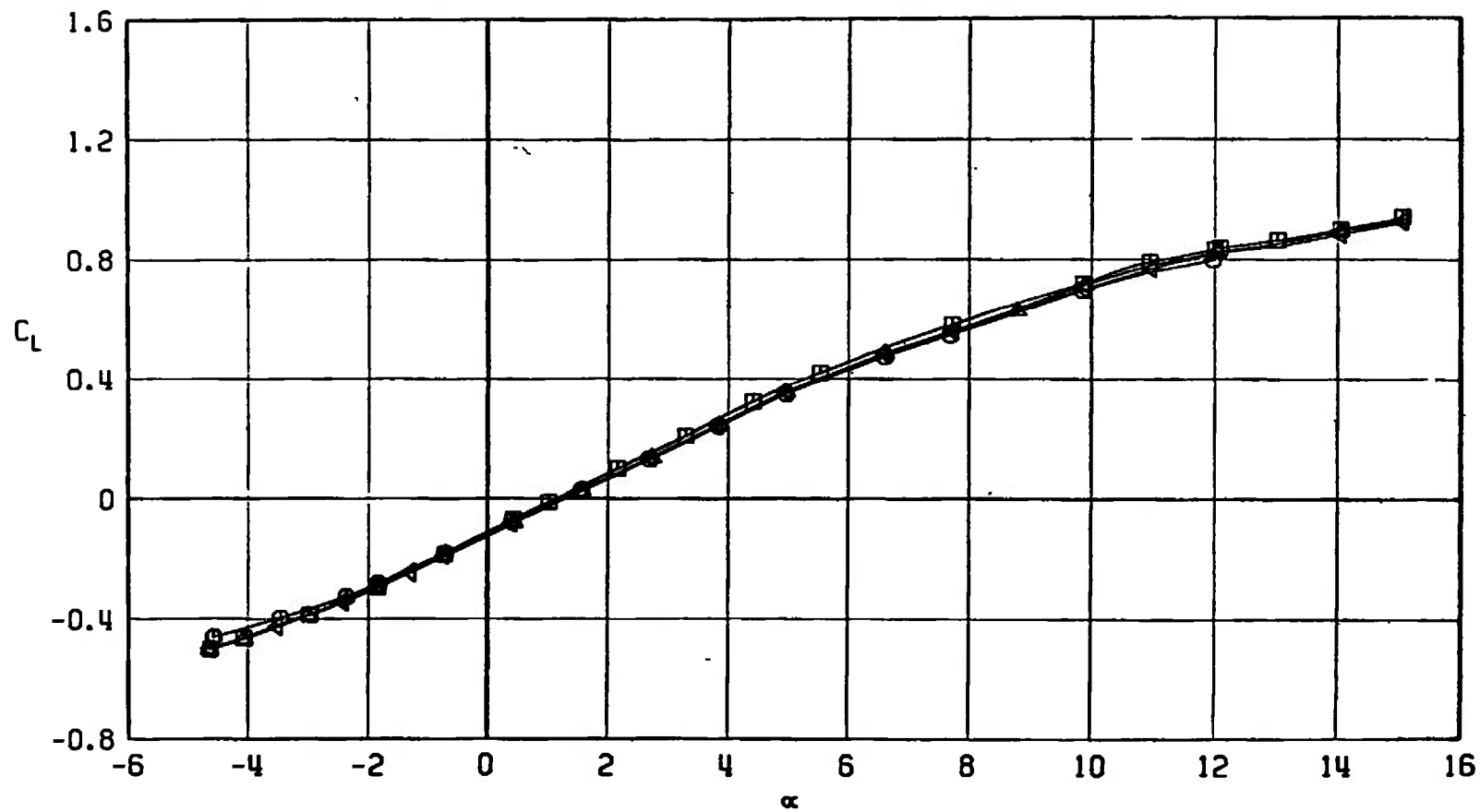
SYMBOL	CONFIGURATION
□	A701
○	A713
△	A712
◀	A711



a.  $M_\infty = 0.50$

Fig. 20 Lift Coefficient Variation with Angle of Attack for Configurations A701, A711, A712, and A713

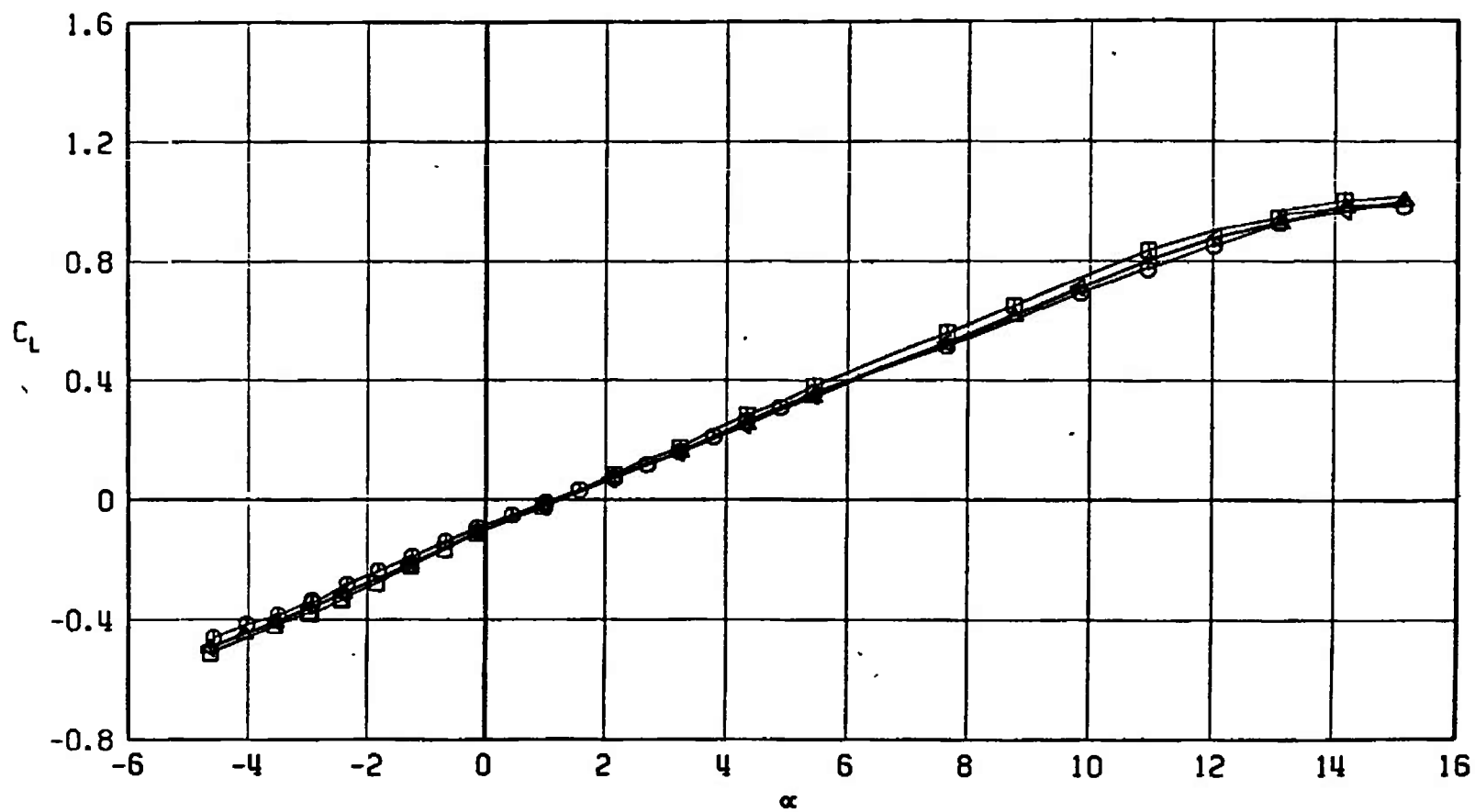
SYMBOL	CONFIGURATION
□	A701
○	A713
△	A712
◁	A711



b.  $M_\infty = 0.90$   
Fig. 20 Continued

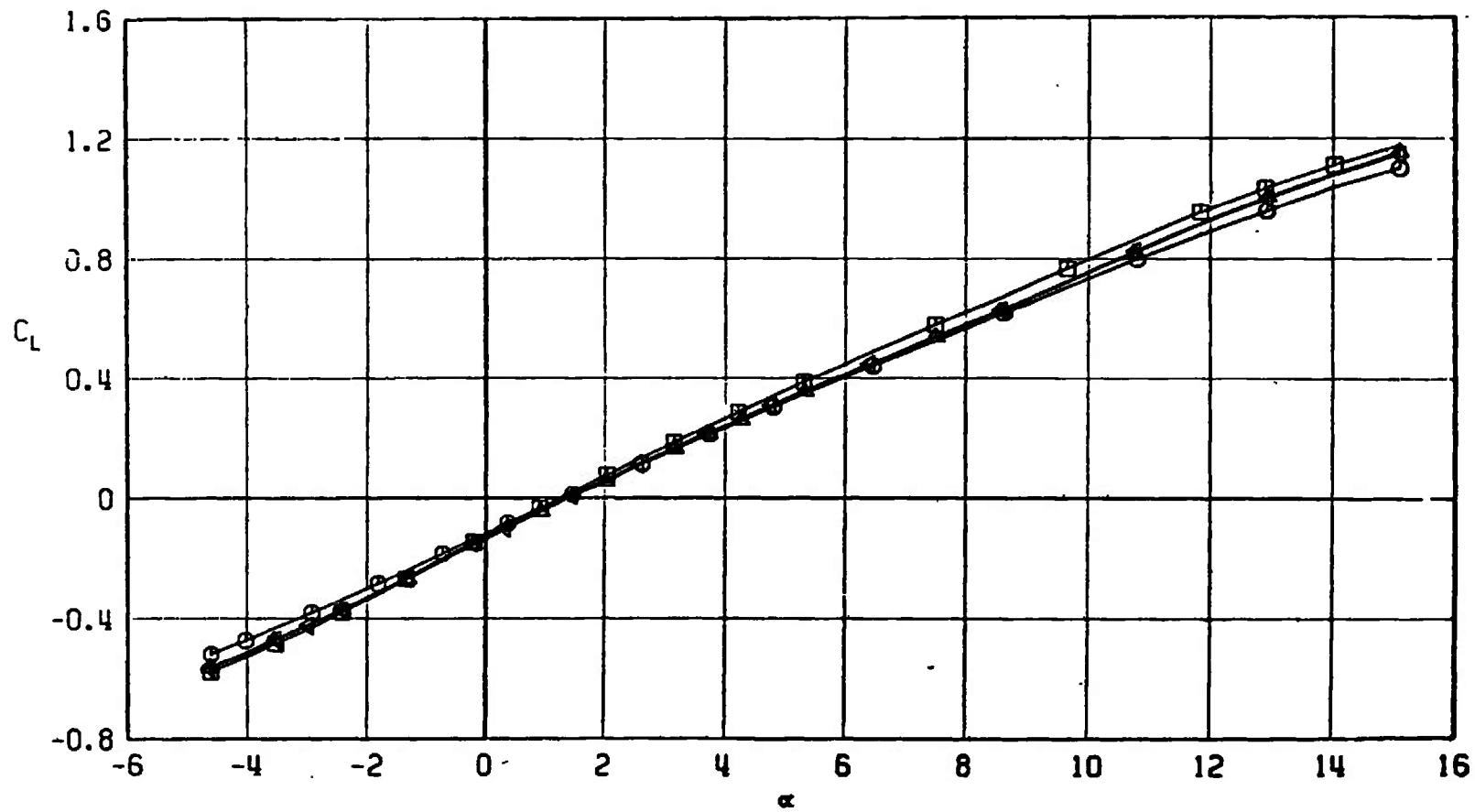


SYMBOL	CONFIGURATION
□	A701
○	A713
△	A712
▽	A711



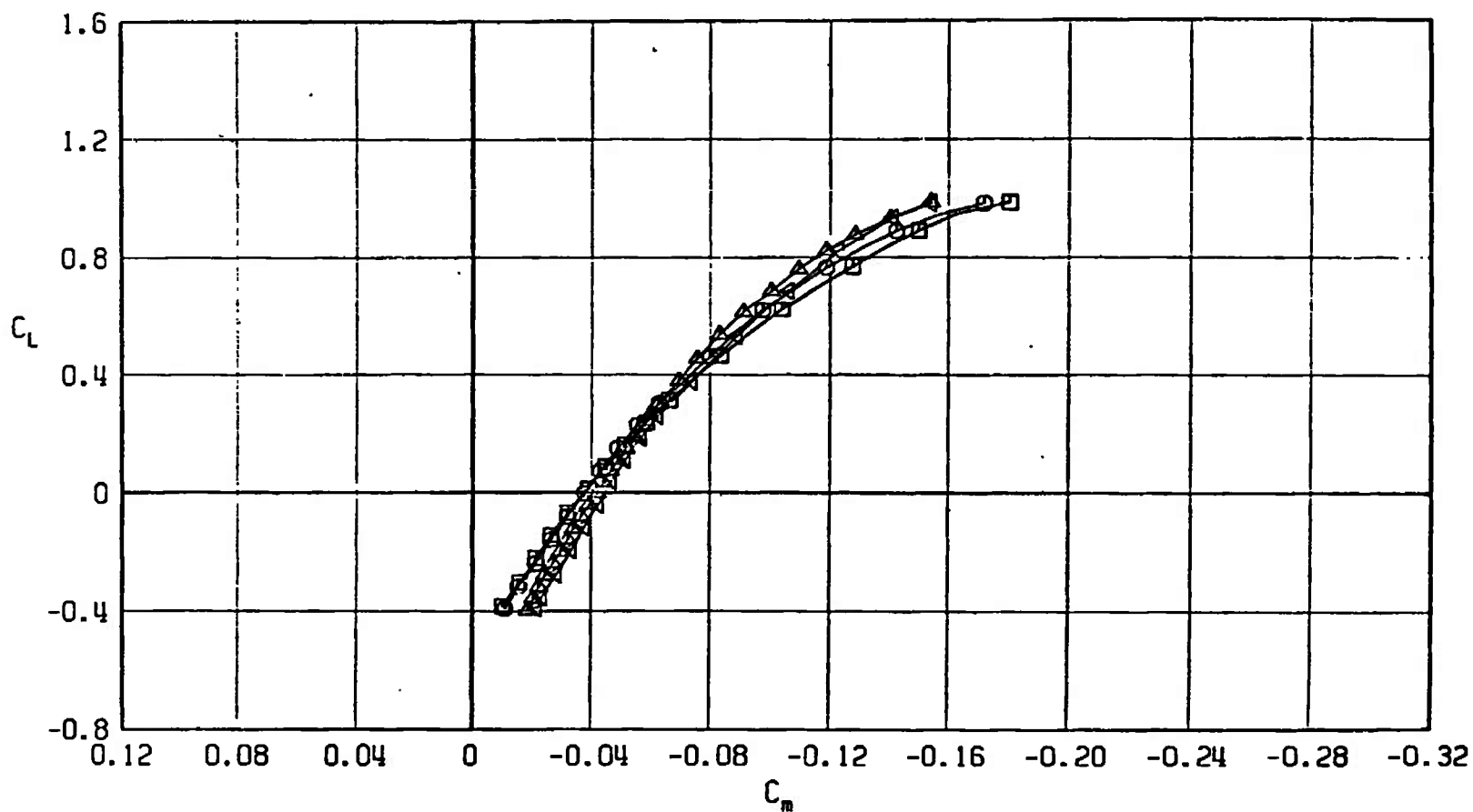
c.  $M_\infty = 0.95$   
Fig. 20 Continued

SYMBOL	CONFIGURATION
□	A701
○	A713
△	A712
◀	A711



d.  $M_\infty = 1.05$   
Fig. 20 Concluded

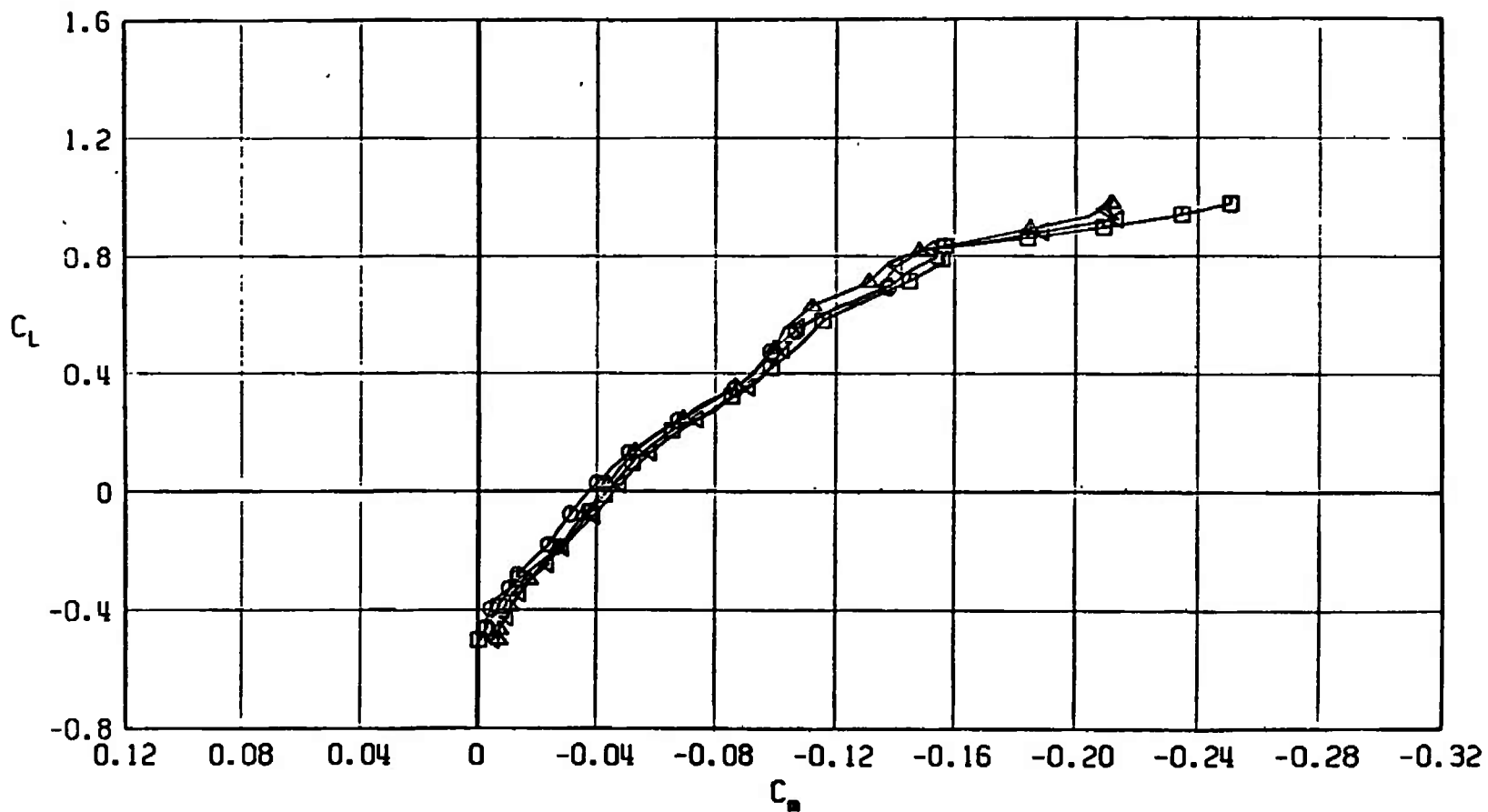
SYMBOL	CONFIGURATION
□	A701
○	A713
△	A712
▽	A711



a.  $M_\infty = 0.50$

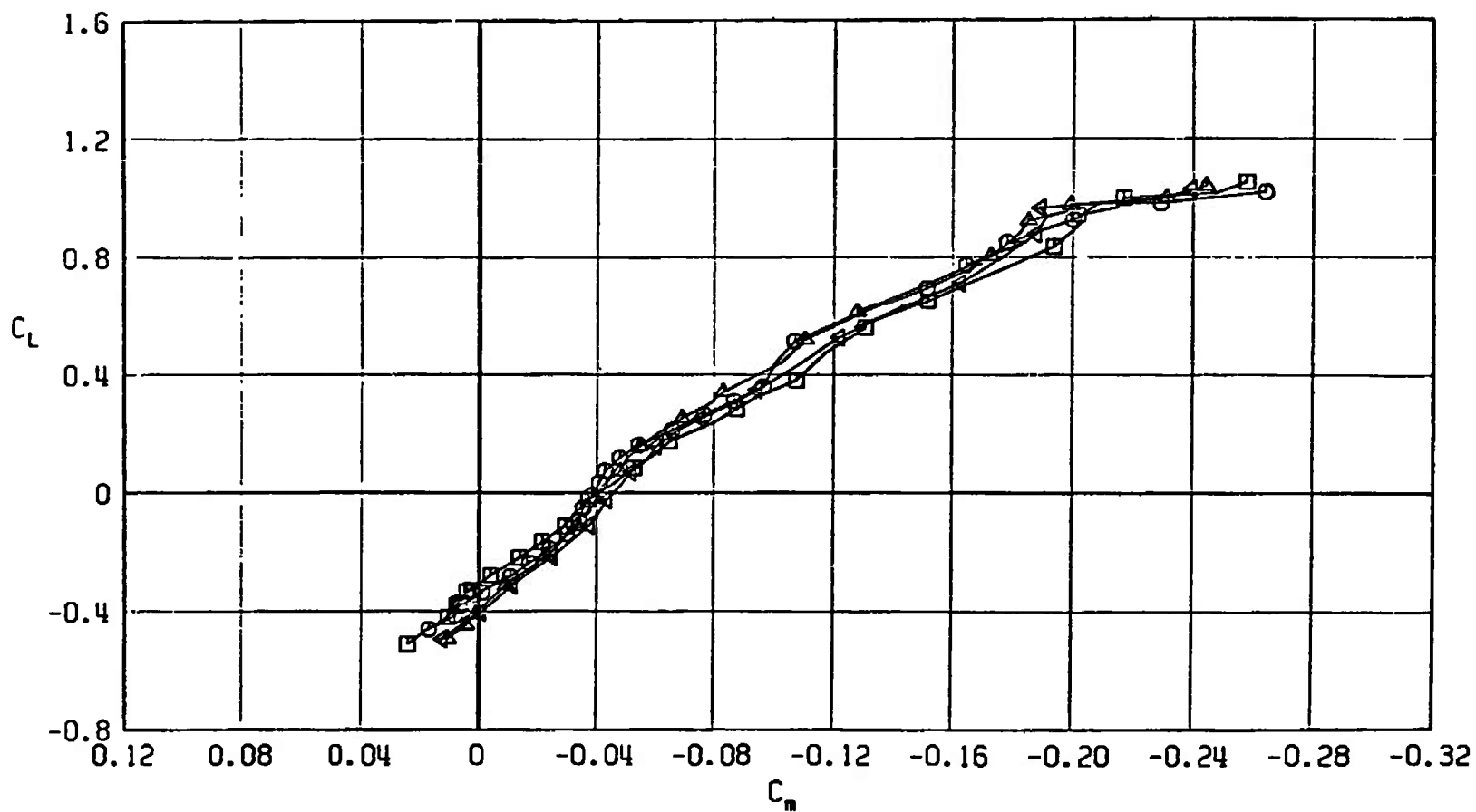
Fig. 21 Pitching-Moment Coefficient Variation with Lift Coefficient for Configurations A701, A711, A712, and A713

SYMBOL	CONFIGURATION
□	A701
○	A713
△	A712
◁	A711



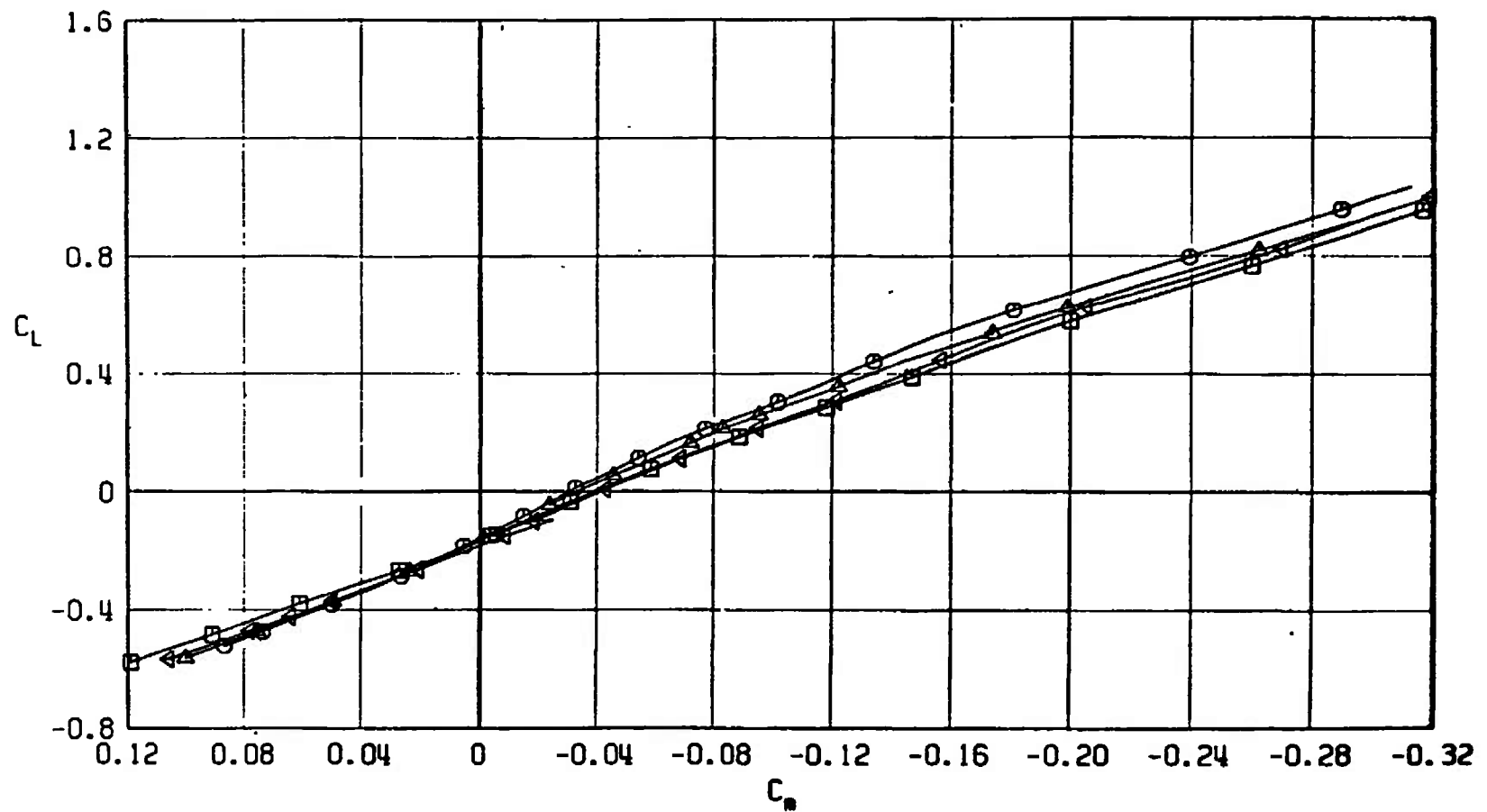
b.  $M_\infty = 0.90$   
Fig. 21 Continued

SYMBOL	CONFIGURATION
□	A701
○	A713
△	A712
▽	A711



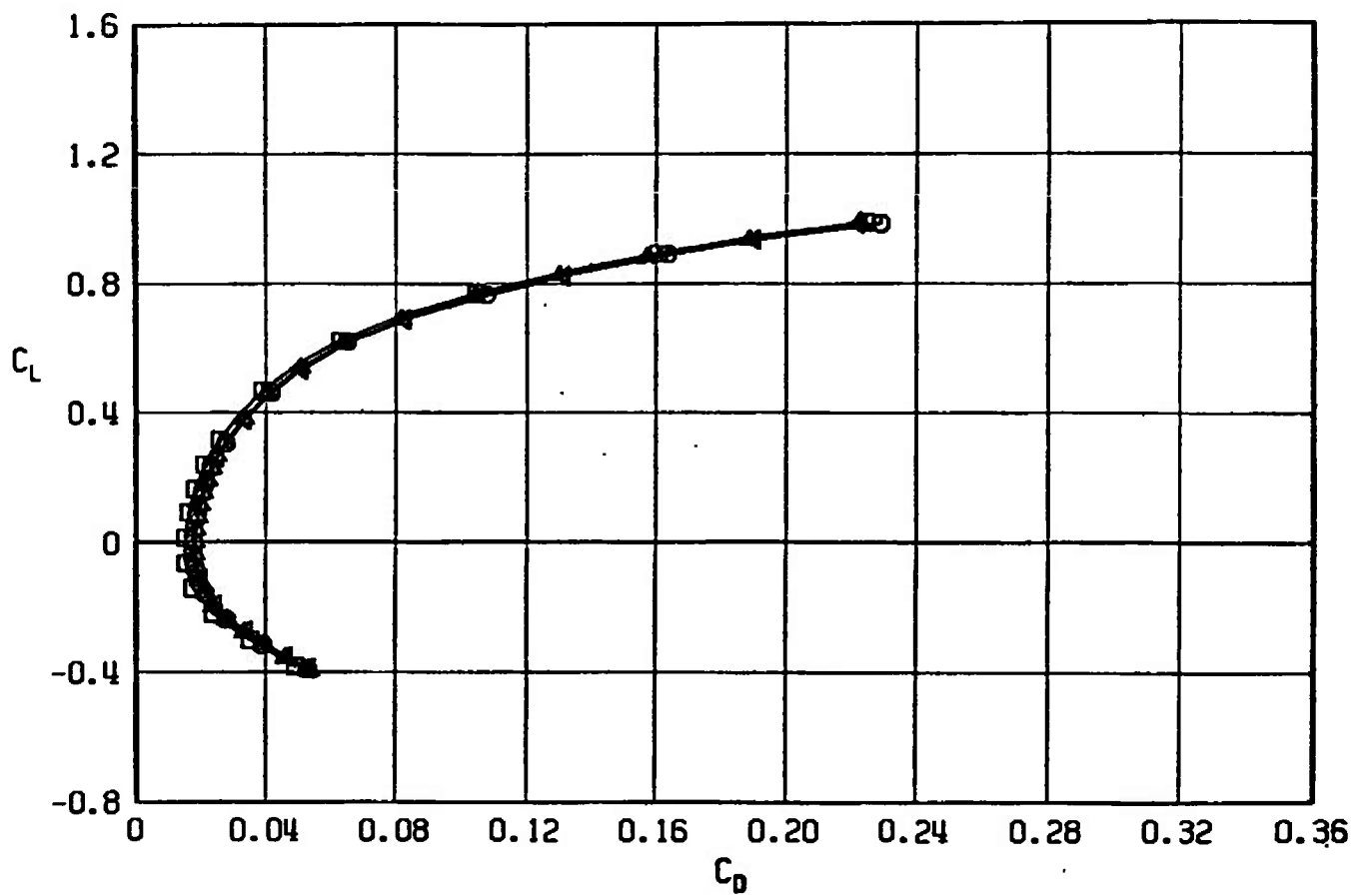
c.  $M_\infty = 0.95$   
Fig. 21 Continued

SYMBOL	CONFIGURATION
□	A701
○	A713
△	A712
◀	A711



d.  $M_\infty = 1.05$   
Fig. 21 Concluded

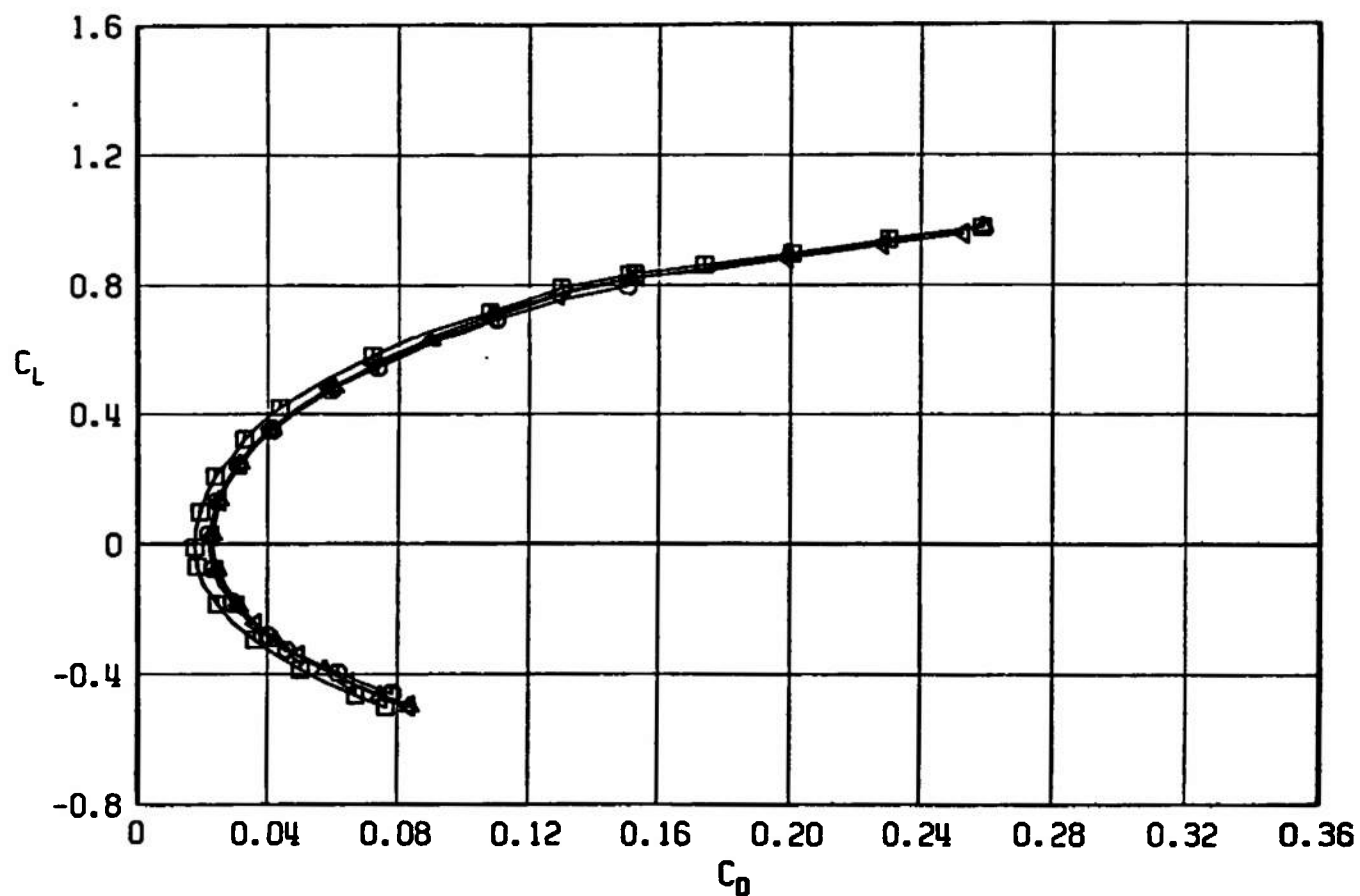
SYMBOL	CONFIGURATION
□	A701
○	A713
△	A712
▽	A711



a.  $M_\infty = 0.50$

Fig. 22 Drag Coefficient Variation with Lift Coefficient for Configurations A701, A711, A712, and A713

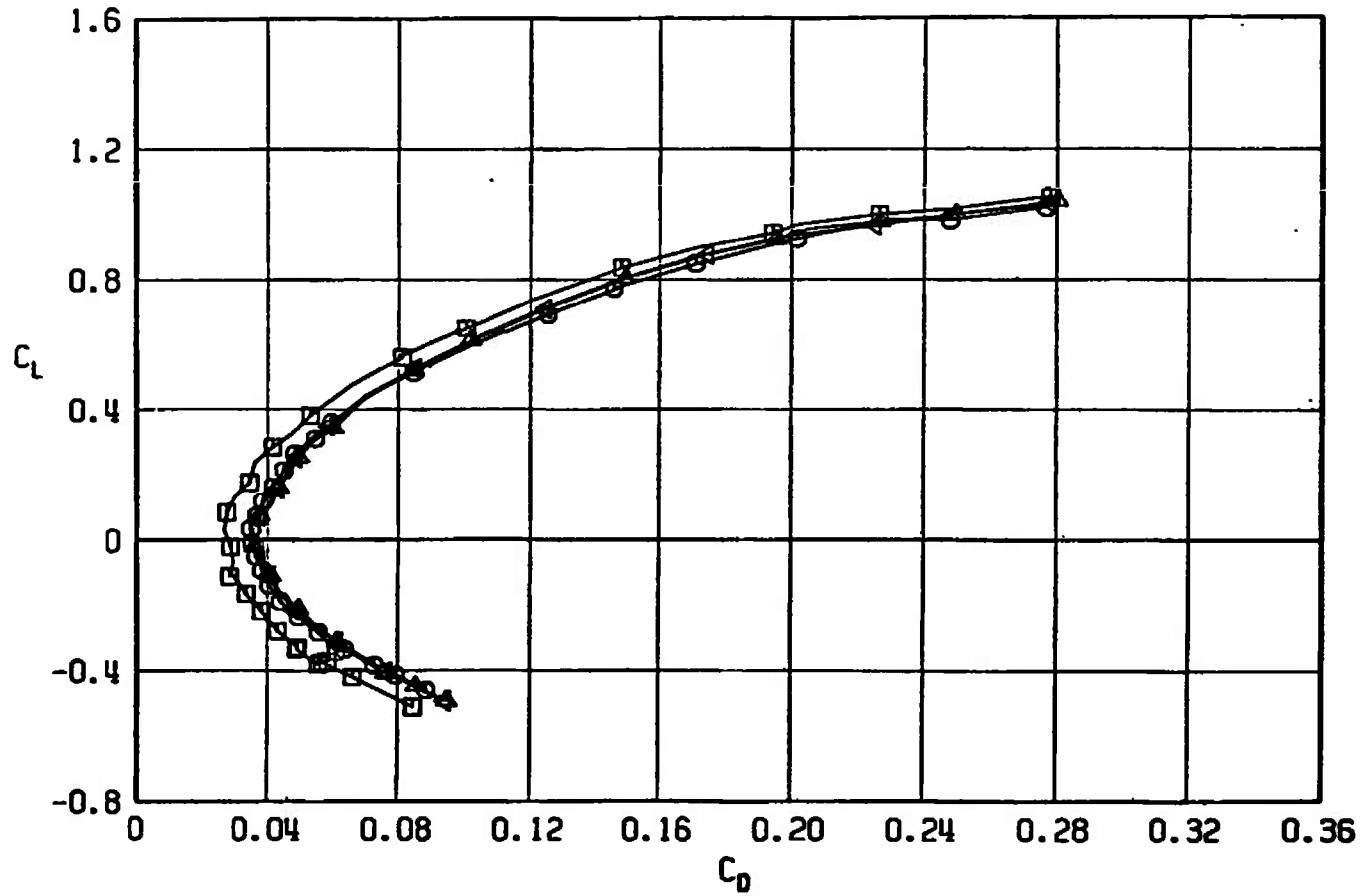
SYMBOL	CONFIGURATION
□	A701
○	A713
△	A712
◄	A711



b.  $M_\infty = 0.90$   
Fig. 22 Continued



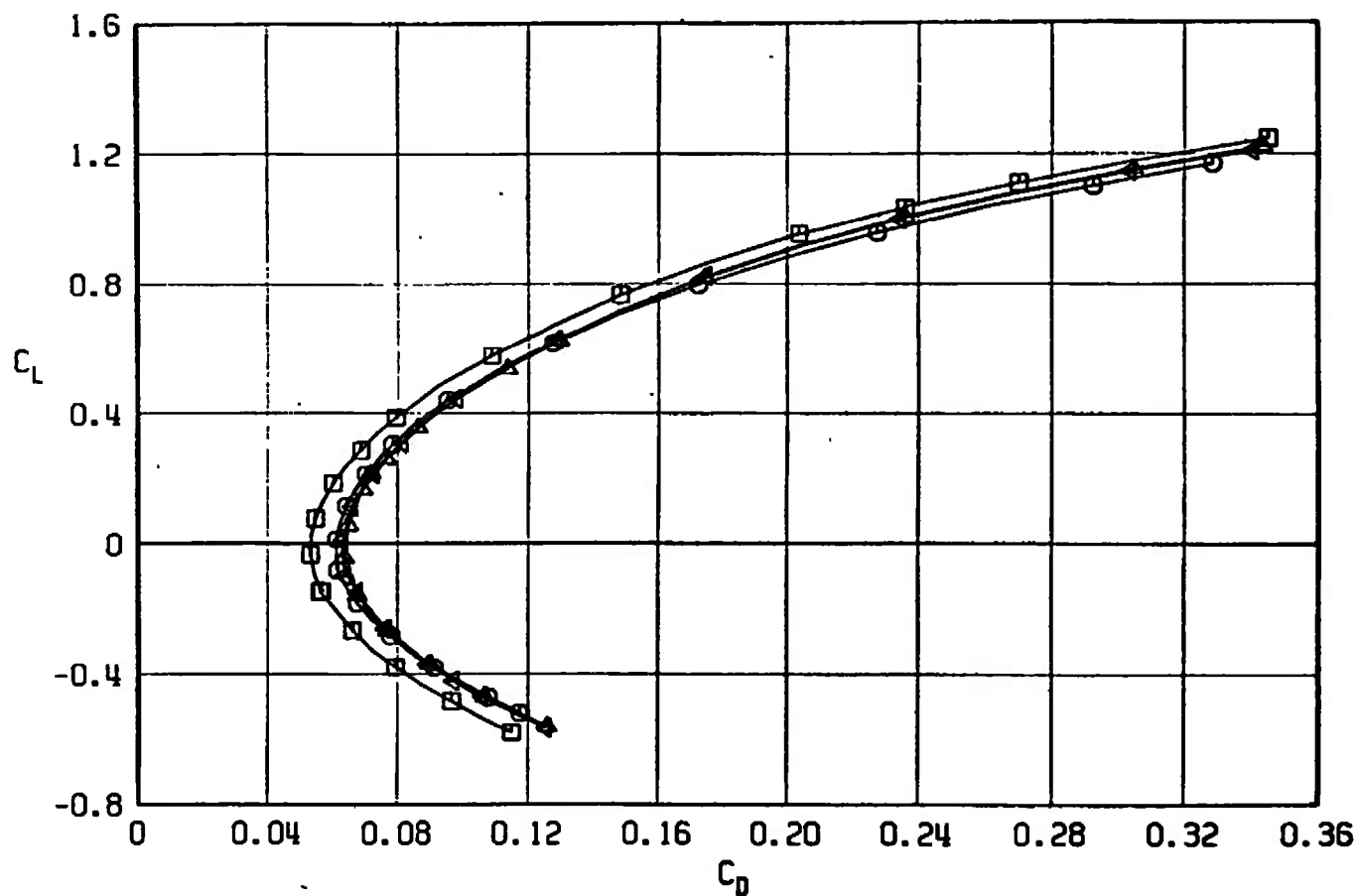
SYMBOL	CONFIGURATION
□	A701
○	A713
△	A712
▽	A711



c.  $M_\infty = 0.95$   
Fig. 22 Continued

SYMBOL	CONFIGURATION
--------	---------------

□	A701
○	A713
△	A712
◄	A711



d.  $M_\infty = 1.05$   
Fig. 22 Concluded

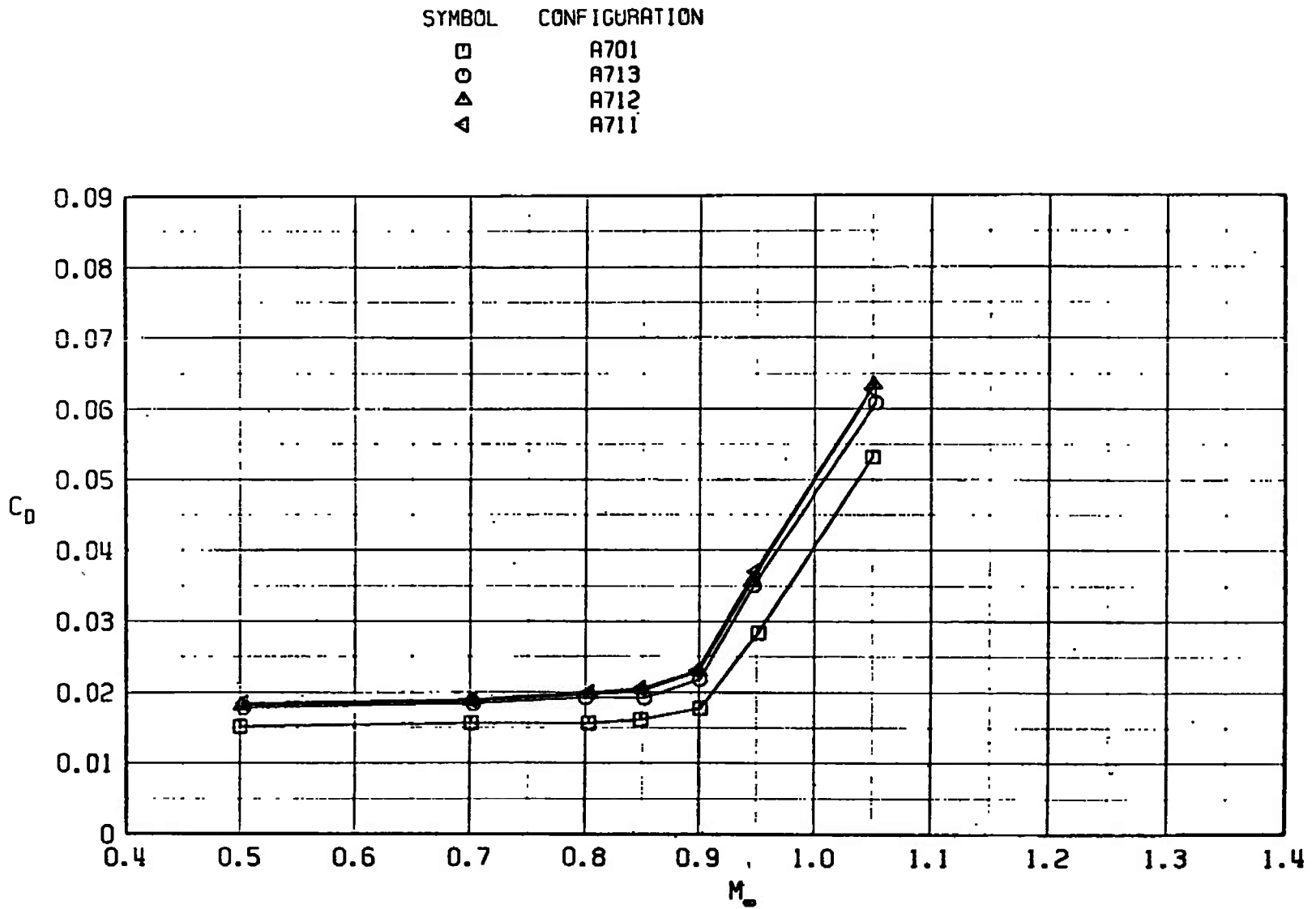
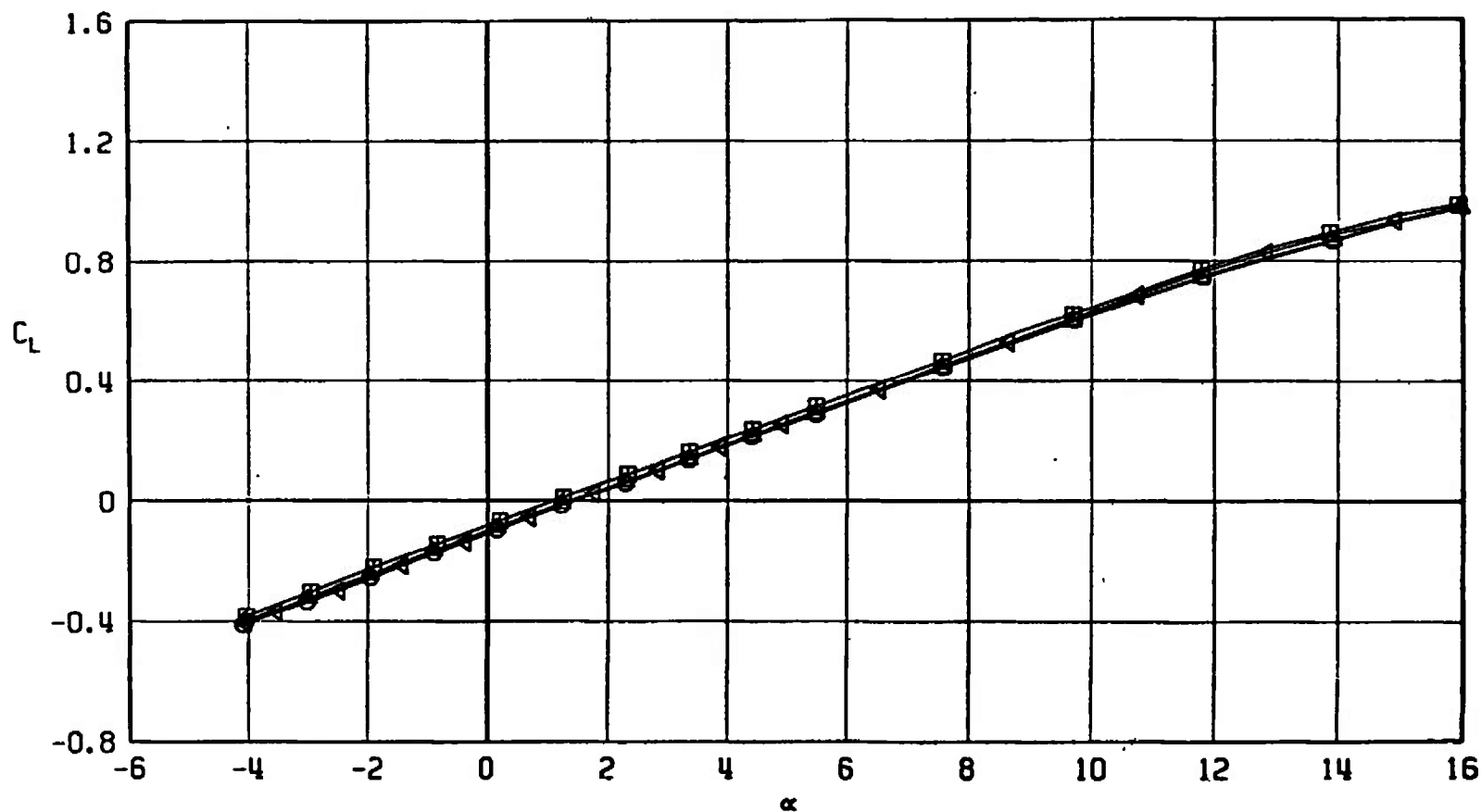


Fig. 23 Drag Coefficient Variation with Mach Number at  $C_L = 0$  for Configurations A701, A711, A712, and A713

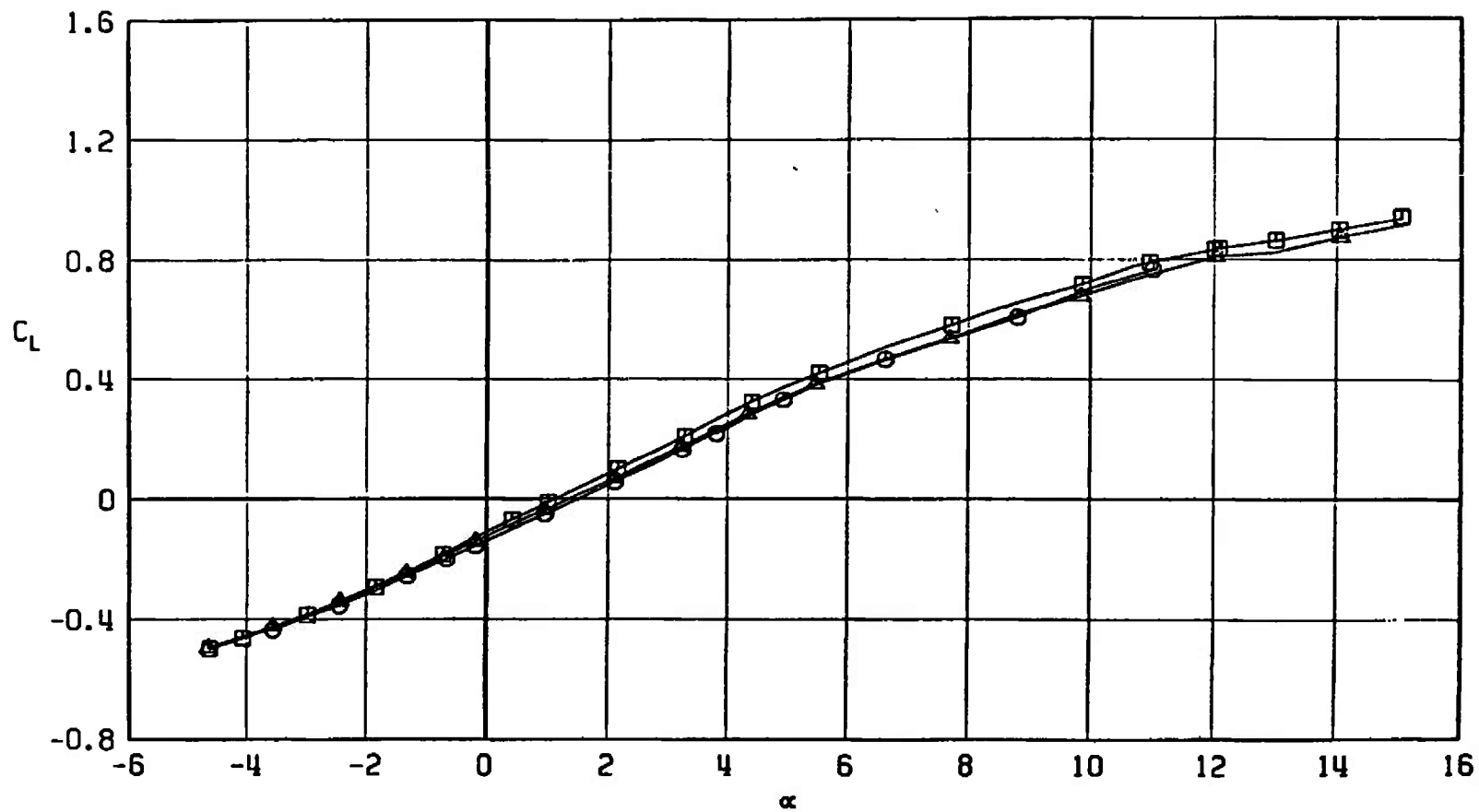
SYMBOL	CONFIGURATION
□	A701
○	A706
△	A705
◀	A707



a.  $M_\infty = 0.50$

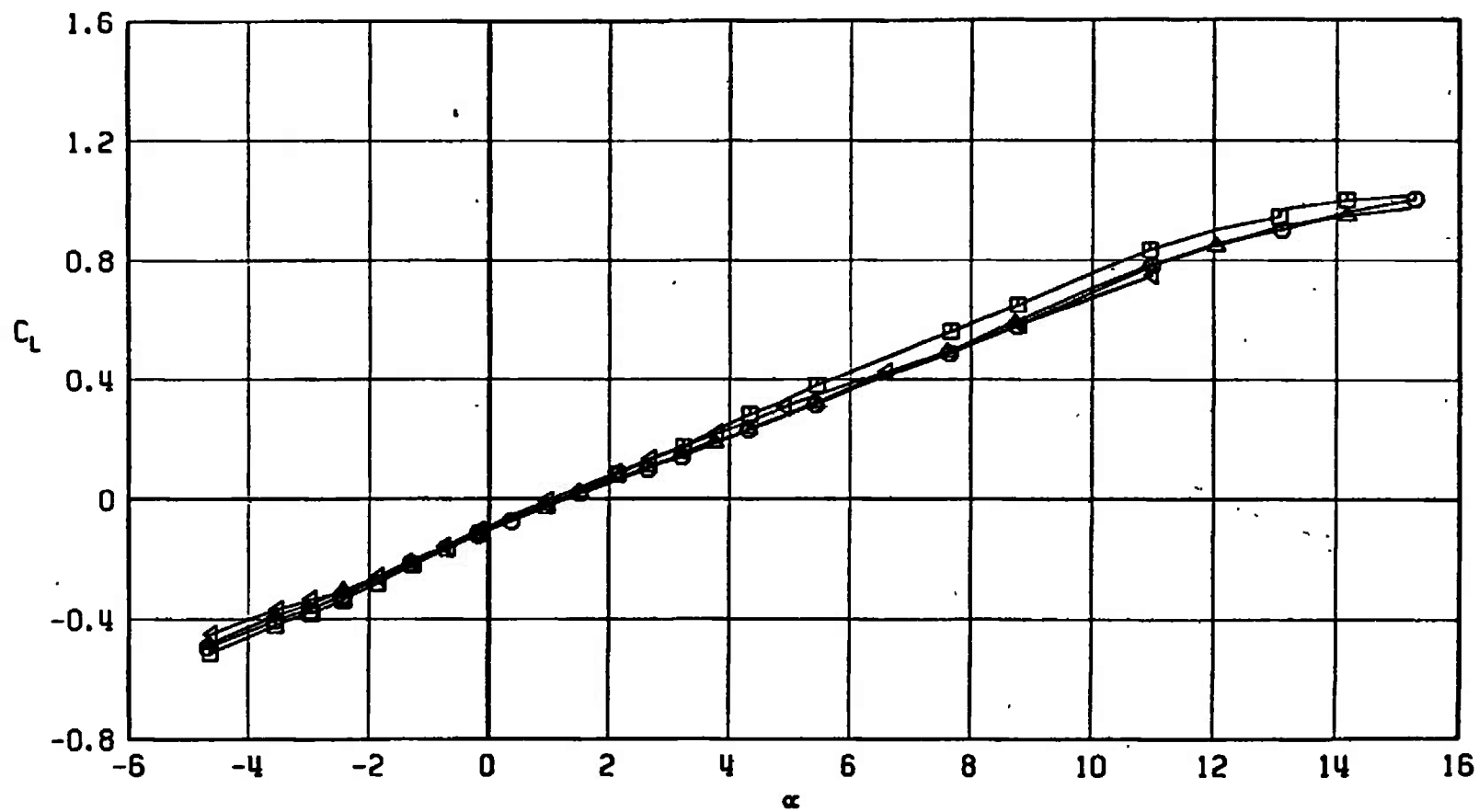
Fig. 24 Lift Coefficient Variation with Angle of Attack for Configurations A701, A705, A706, and A707

SYMBOL	CONFIGURATION
□	A701
○	A706
△	A705



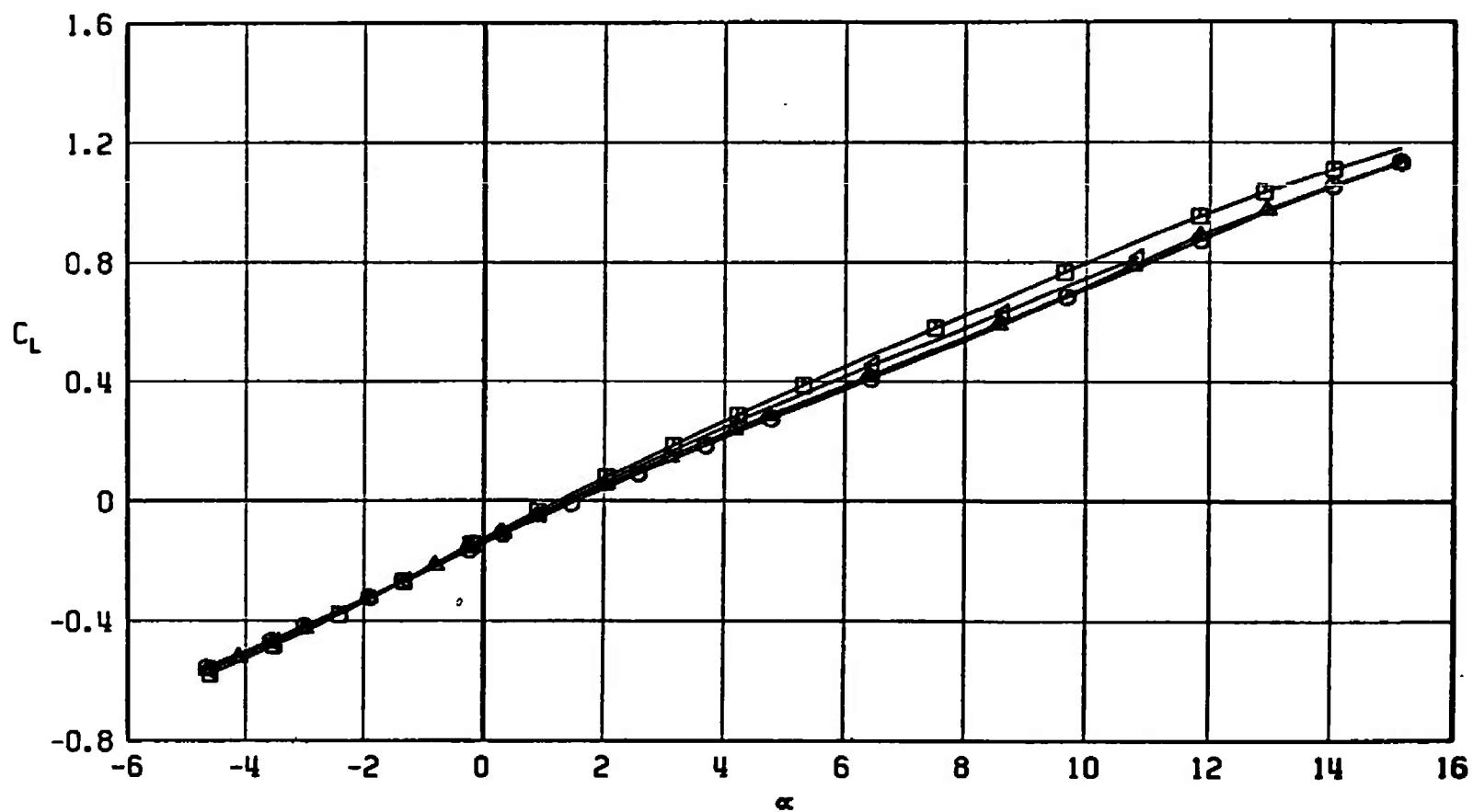
b.  $M_\infty = 0.90$   
Fig. 24 Continued

SYMBOL	CONFIGURATION
□	A701
○	A706
△	A705
◀	A707



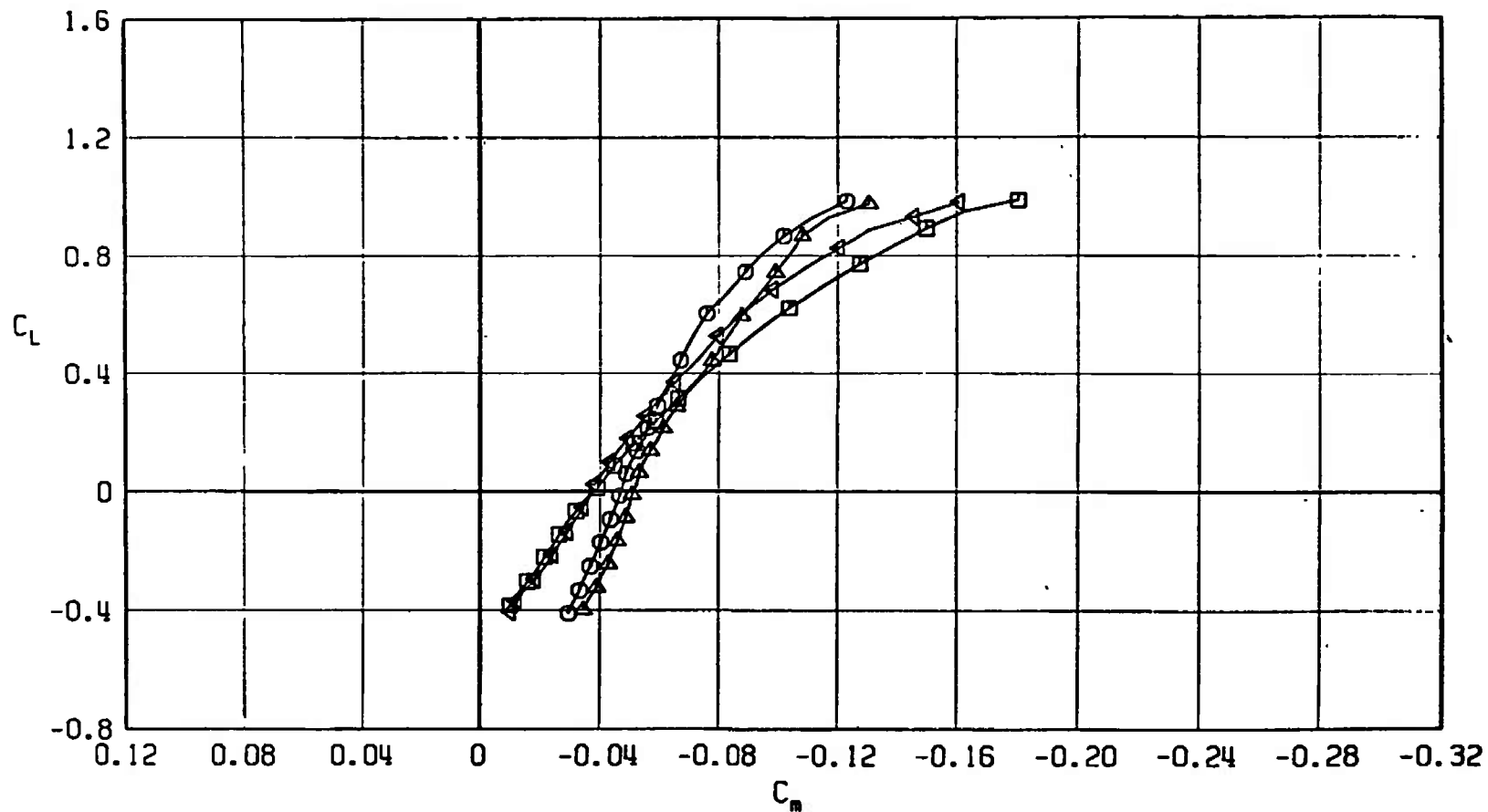
c.  $M_\infty = 0.95$   
Fig. 24 Continued

SYMBOL	CONFIGURATION
□	A701
○	A706
△	A705
▽	A707



d.  $M_\infty = 1.05$   
Fig. 24 Concluded

SYMBOL	CONFIGURATION
□	A701
○	A706
△	A705
◀	A707

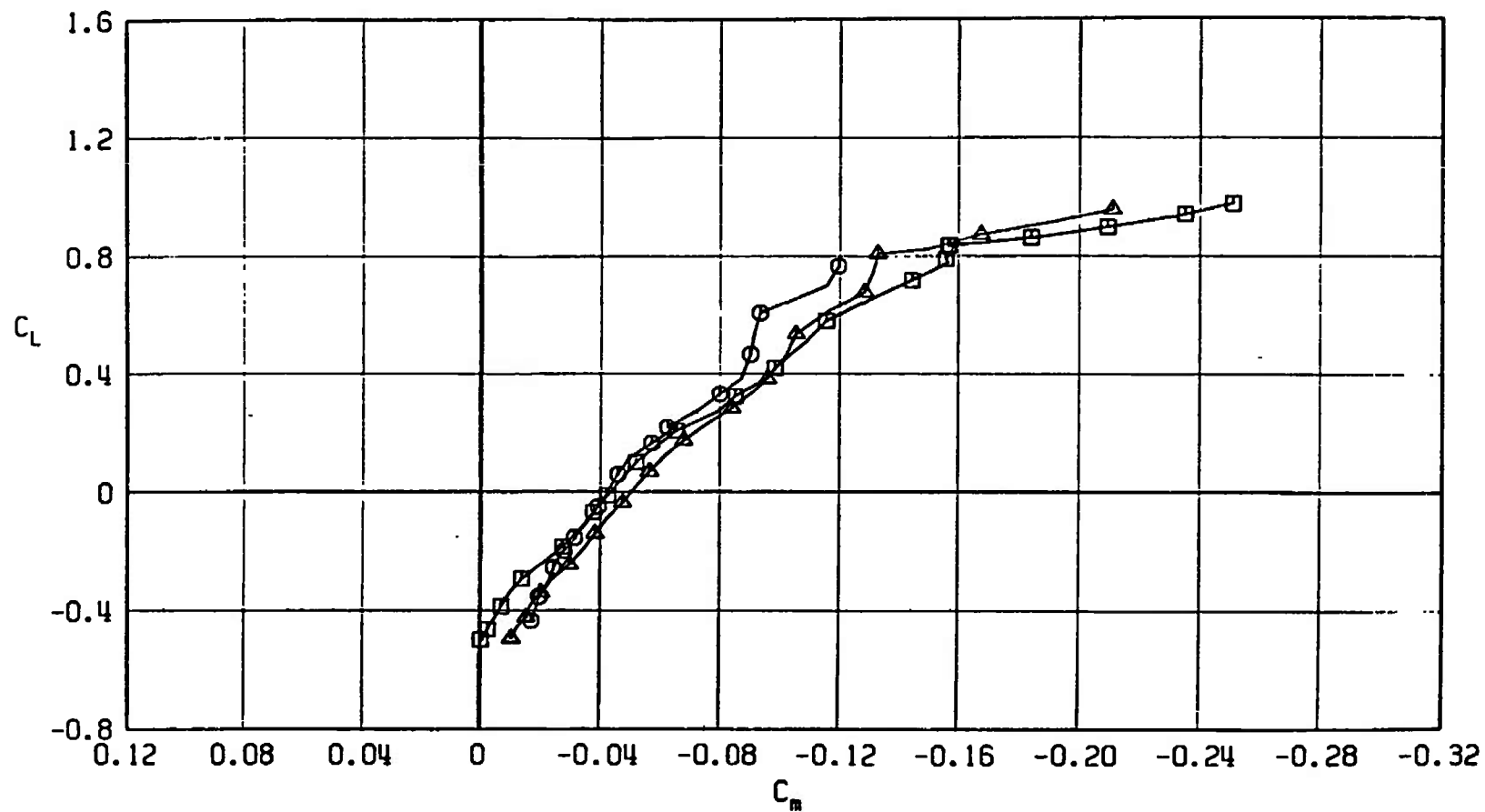


a.  $M_\infty = 0.50$

Fig. 25 Pitching-Moment Coefficient Variation with Lift Coefficient for Configurations A701, A705, A706, and A707

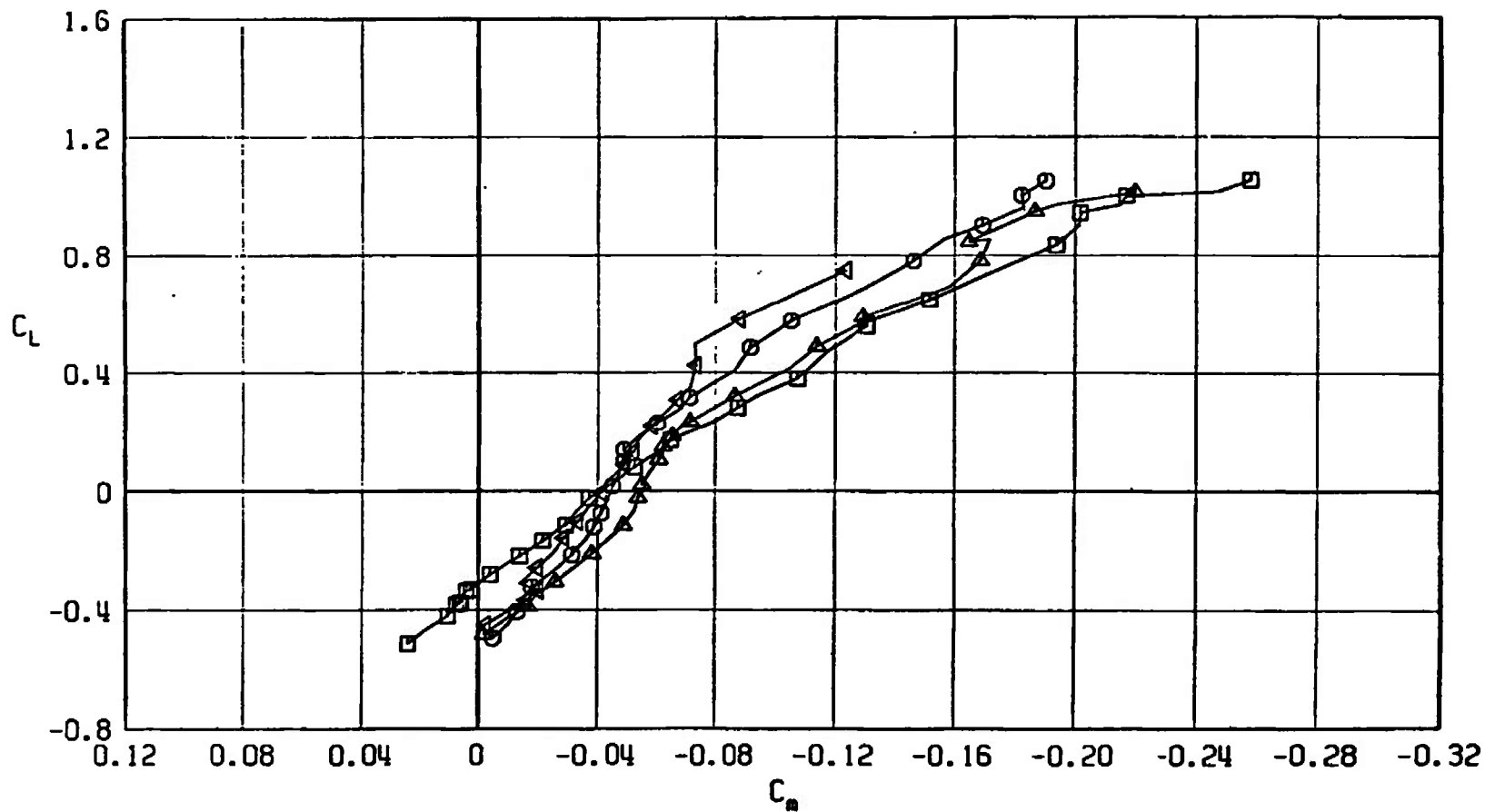


SYMBOL	CONFIGURATION
□	A701
○	A706
△	A705



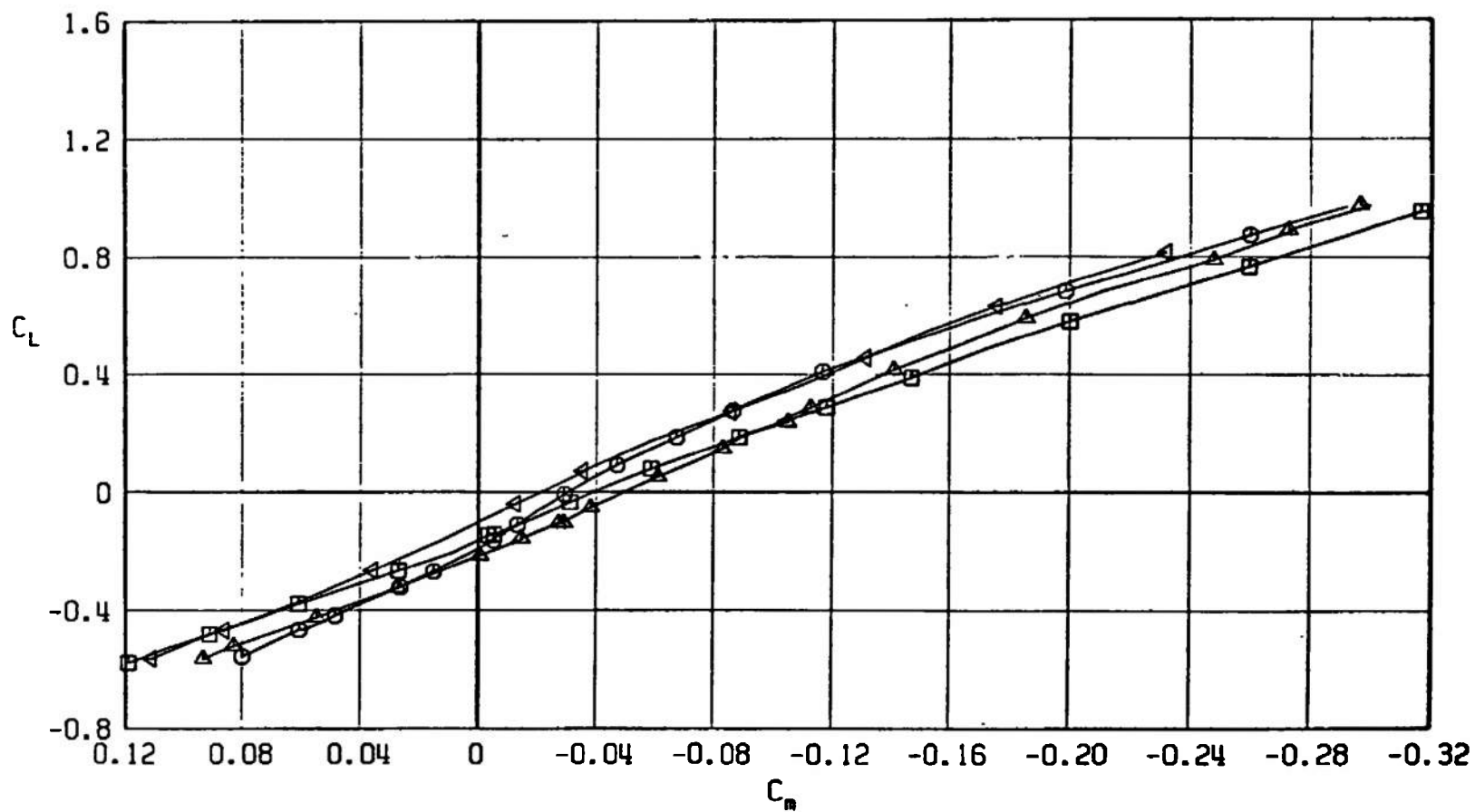
b.  $M_\infty = 0.90$   
Fig. 25 Continued

SYMBOL	CONFIGURATION
□	A701
○	A706
△	A705
◀	A707

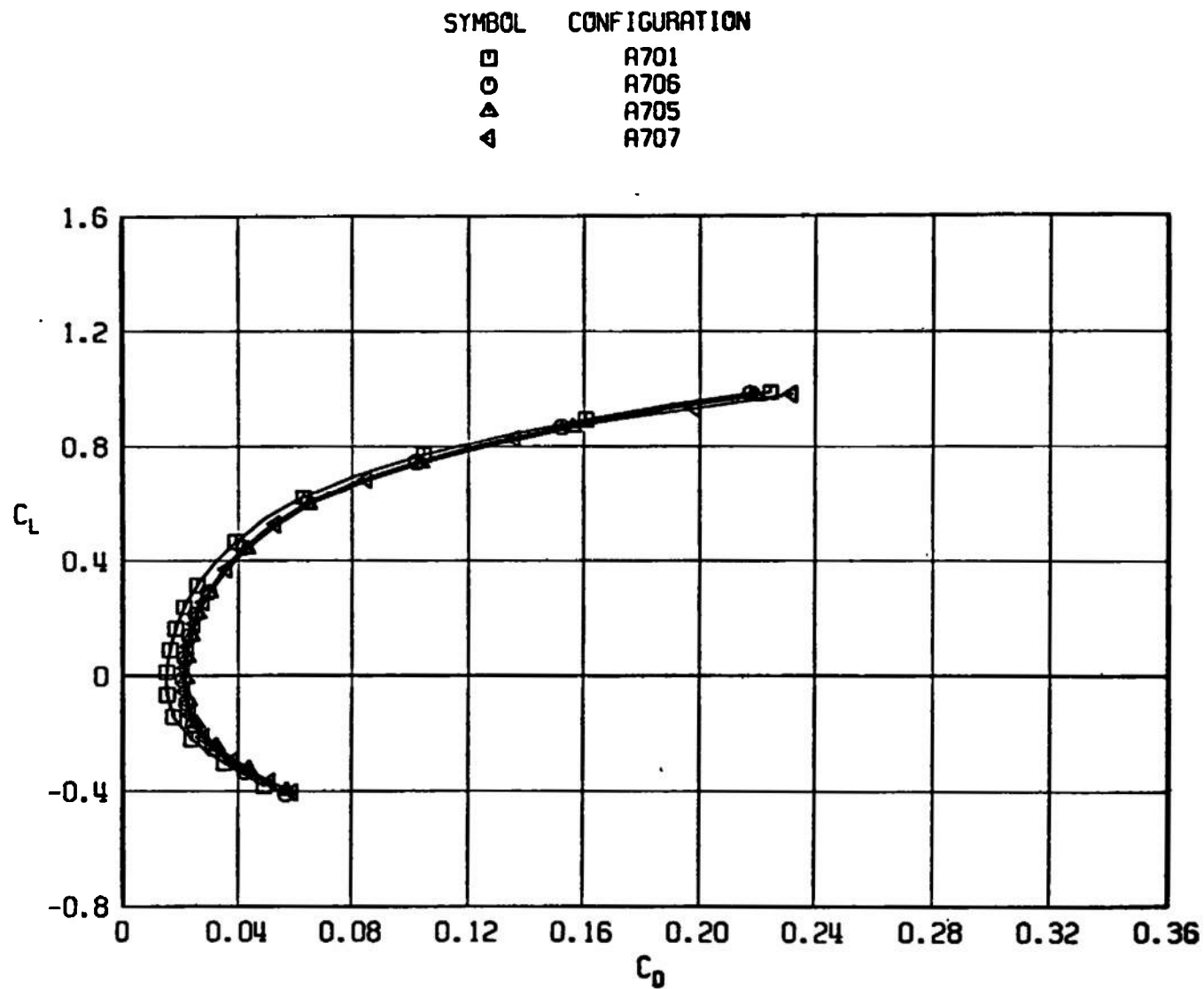


c.  $M_\infty = 0.95$   
Fig. 25 Continued

SYMBOL	CONFIGURATION
□	A701
○	A706
△	A705
▽	A707



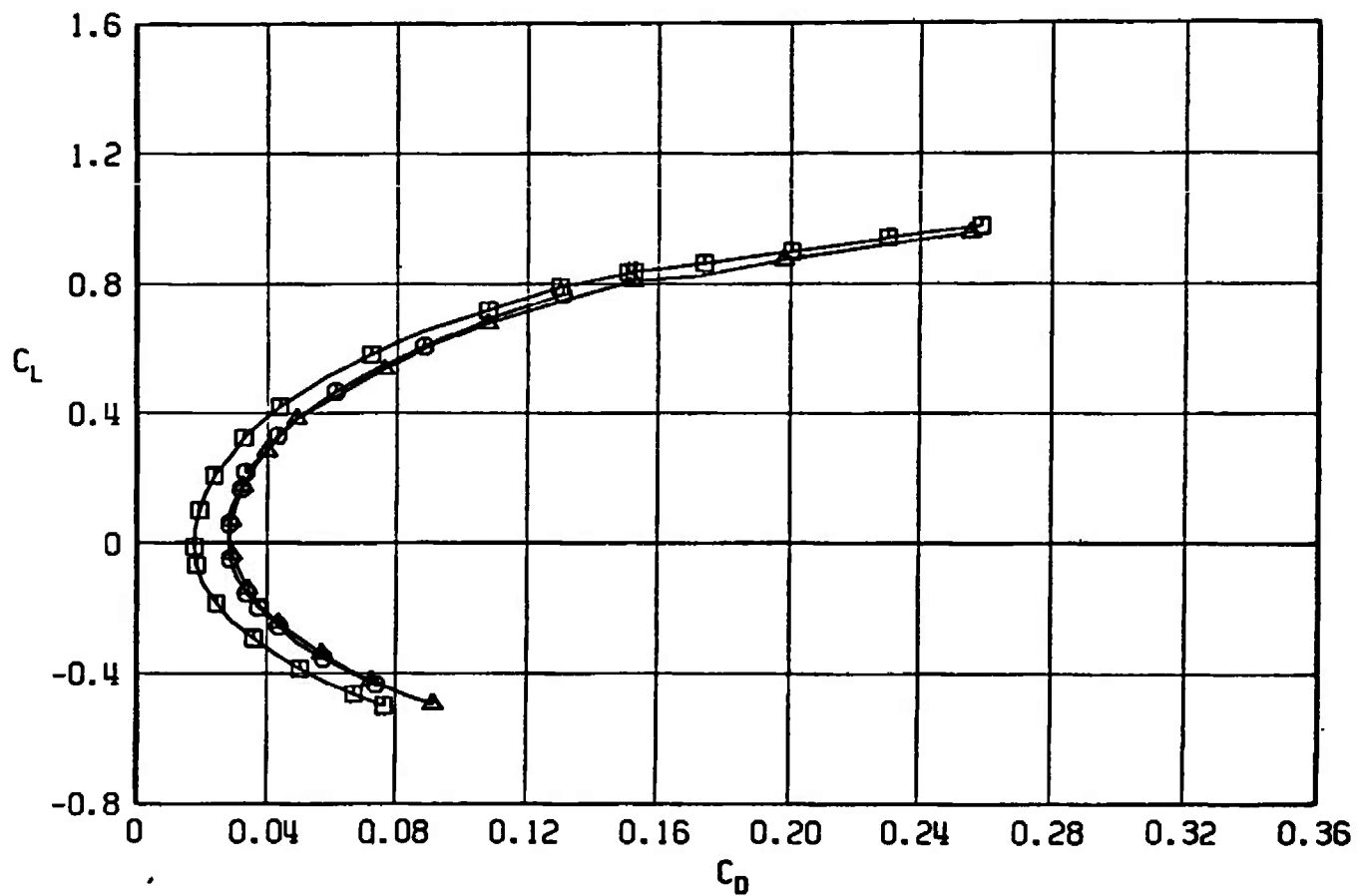
d.  $M_\infty = 1.05$   
Fig. 25 Concluded



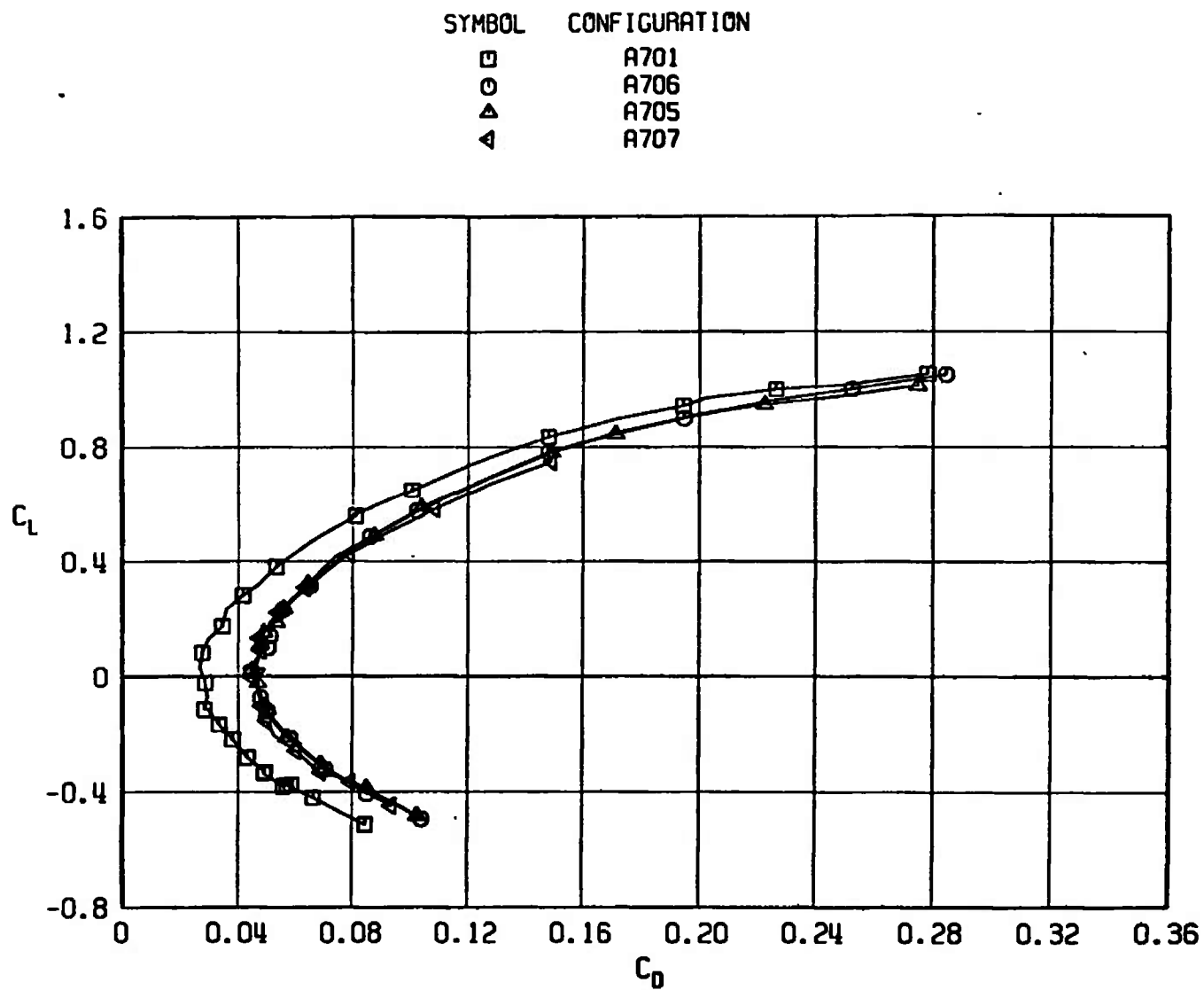
a.  $M_\infty = 0.50$

Fig. 26 Drag Coefficient Variation with Lift Coefficient for Configurations A701, A705, A706, and A707

SYMBOL	CONFIGURATION
□	A701
○	A706
△	A705

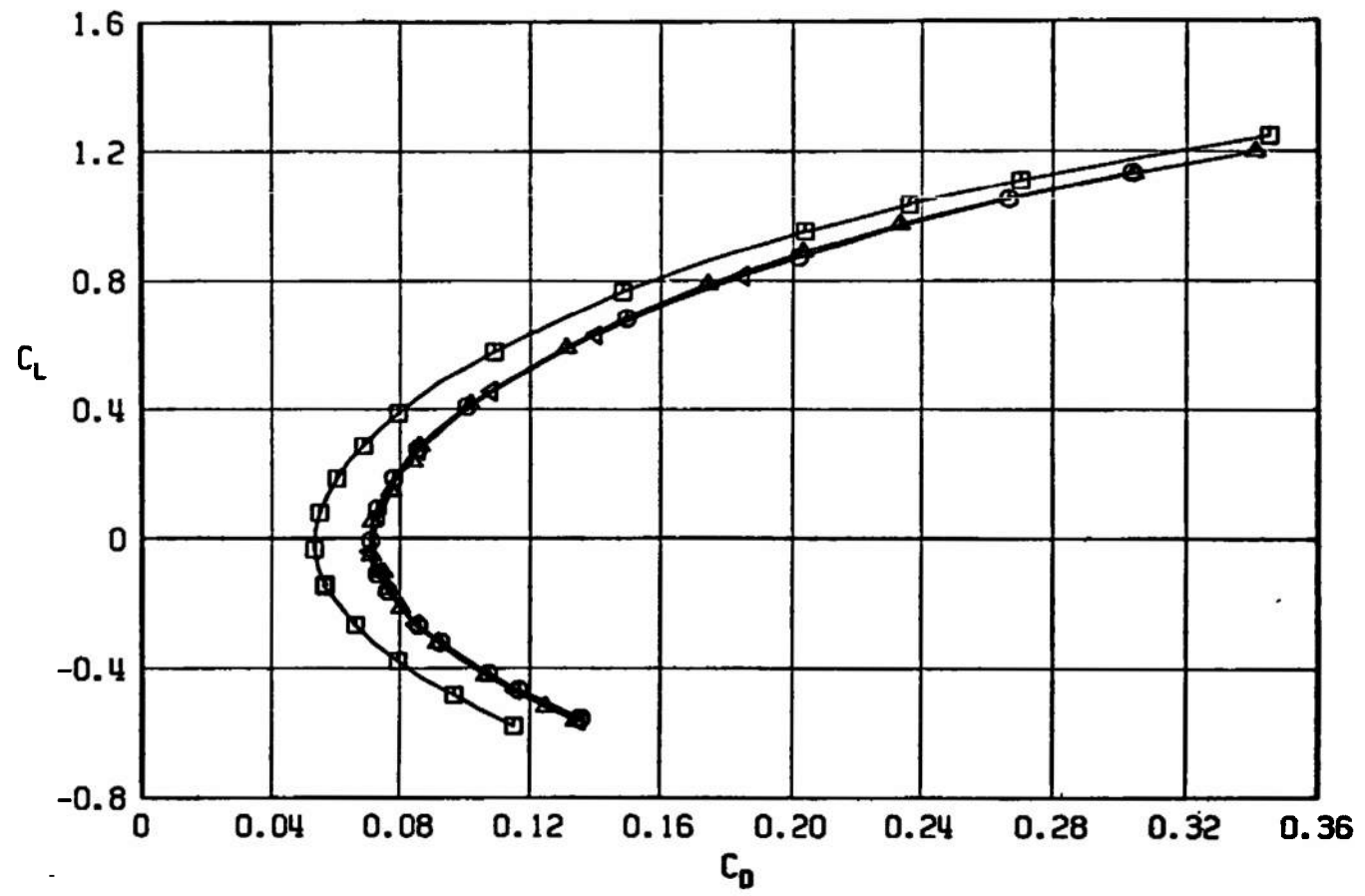


b.  $M_\infty = 0.90$   
Fig. 26 Continued



c.  $M_\infty = 0.95$   
Fig. 26 Continued

SYMBOL	CONFIGURATION
□	A701
○	A706
△	A705
◀	A707



d.  $M_\infty = 1.05$   
Fig. 26 Concluded

SYMBOL	CONFIGURATION
□	A701
○	A706
△	A705
▽	A707

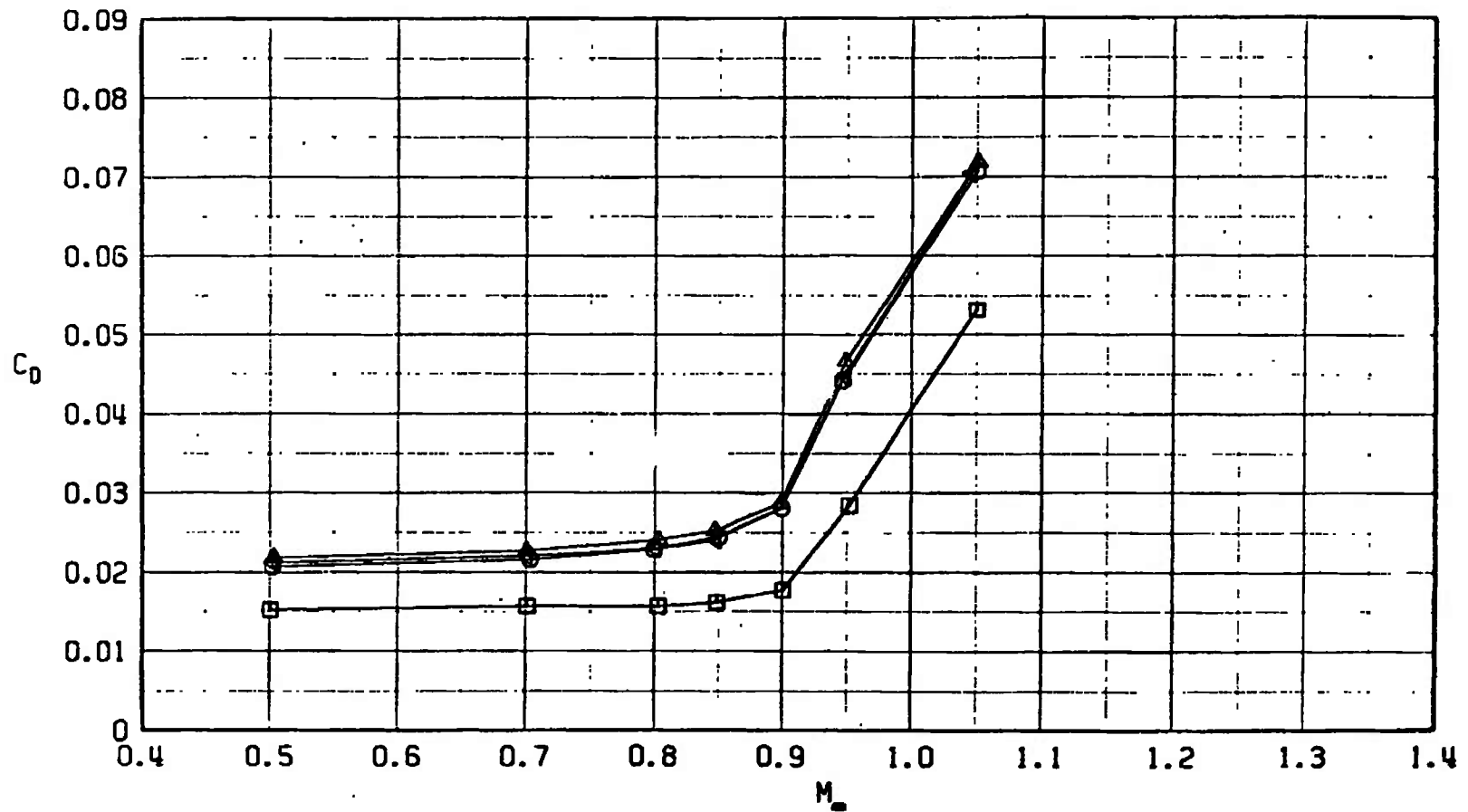


Fig. 27 Drag Coefficient Variation with Mach Number at  $C_L = 0$  for Configurations A701, A705, A706, and A707



SYMBOL	CONFIGURATION
□	A701
○	A713
△	A707

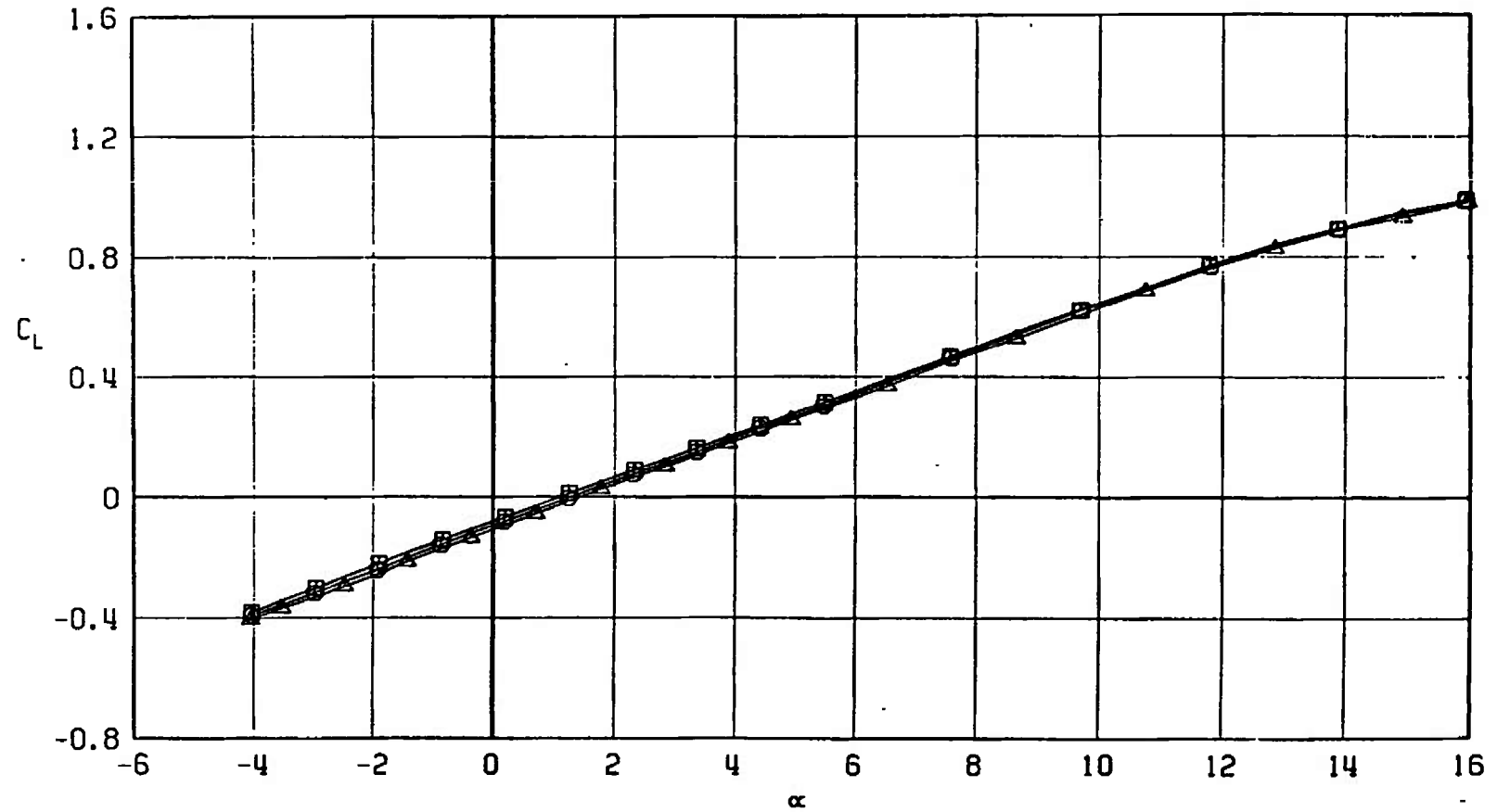
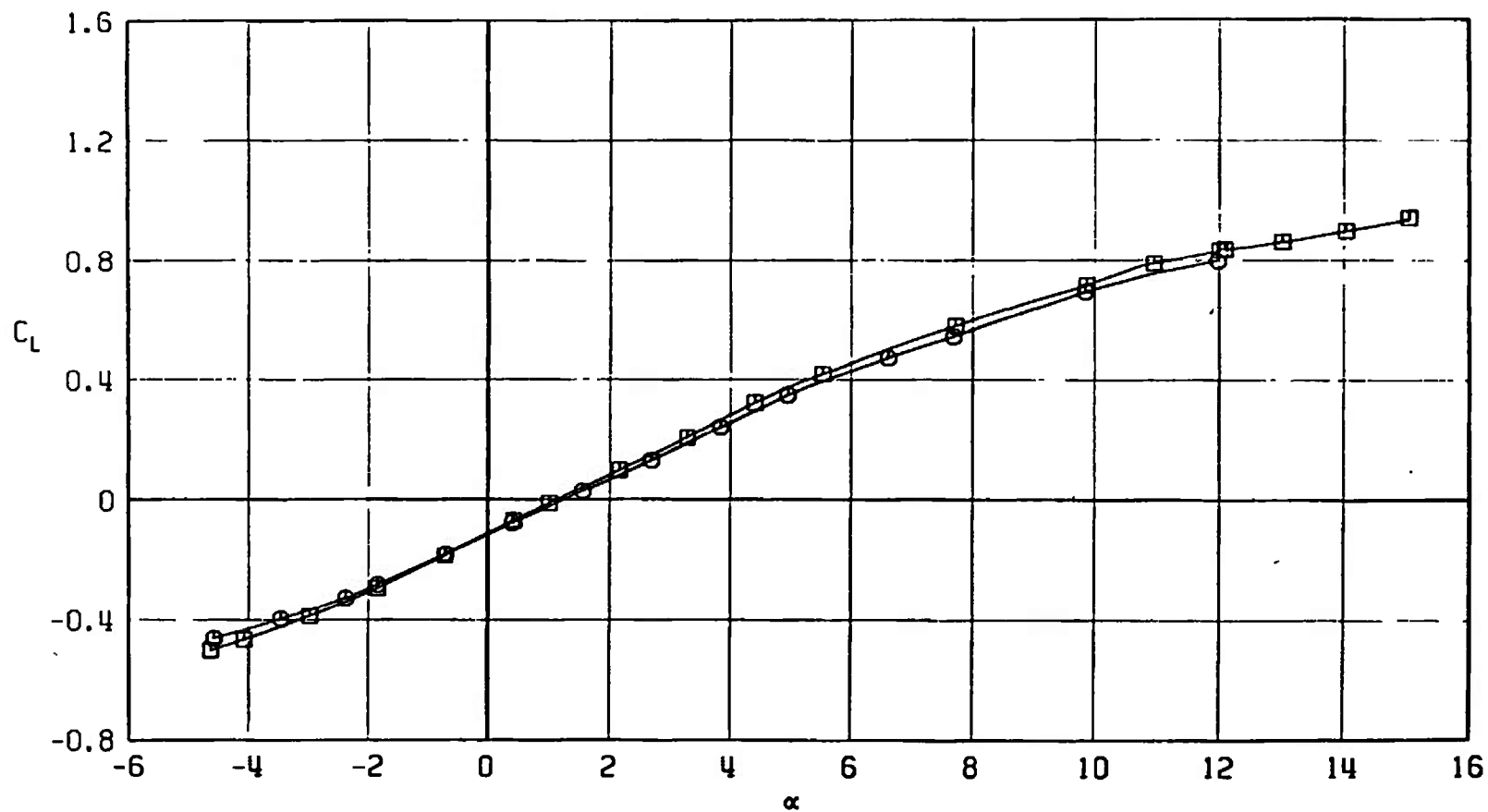
a.  $M_\infty = 0.50$ 

Fig. 28 Lift Coefficient Variation with Angle of Attack for Configurations A701, A707, and A713

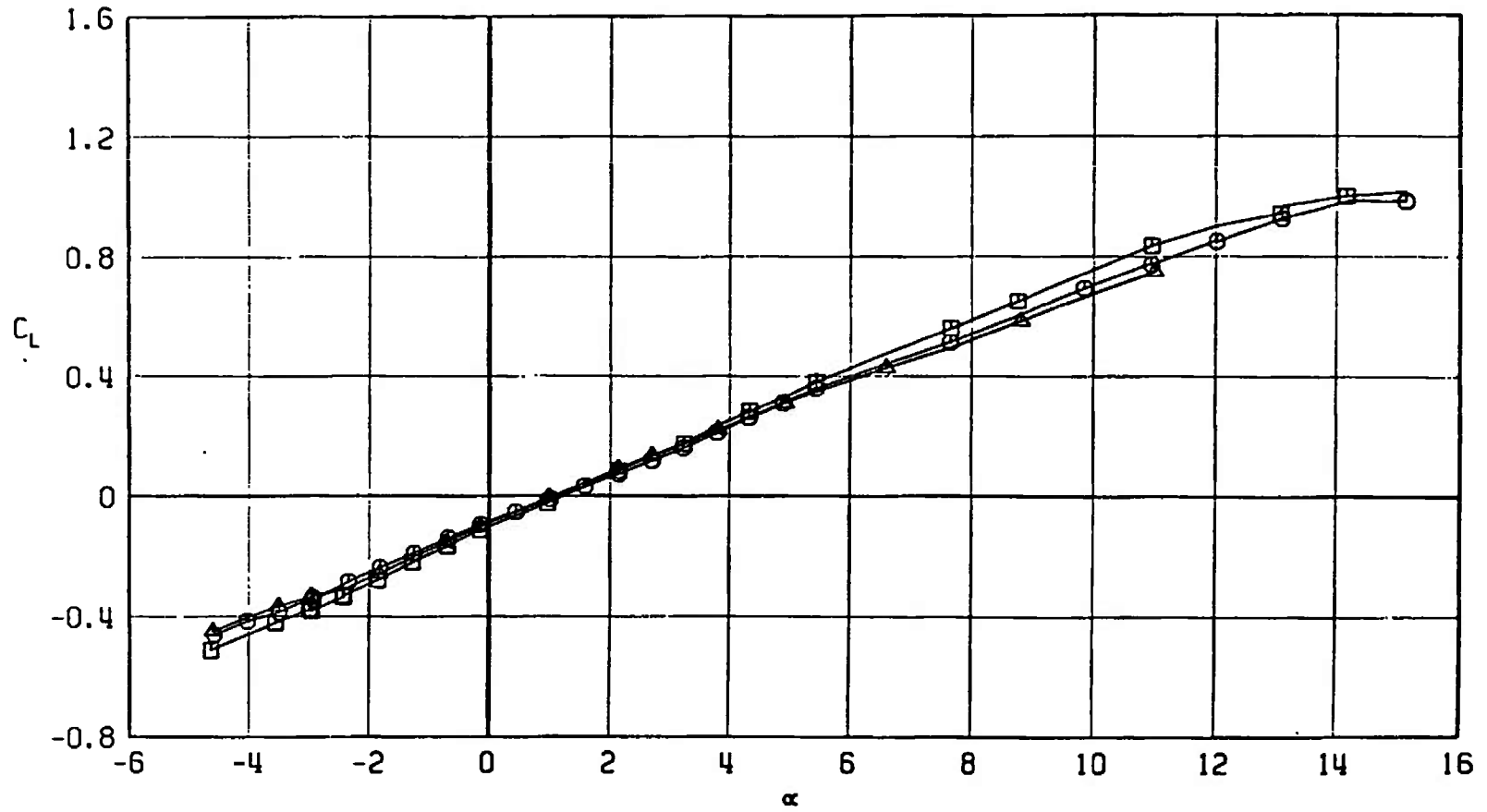
SYMBOL CONFIGURATION

□	A701
○	A713



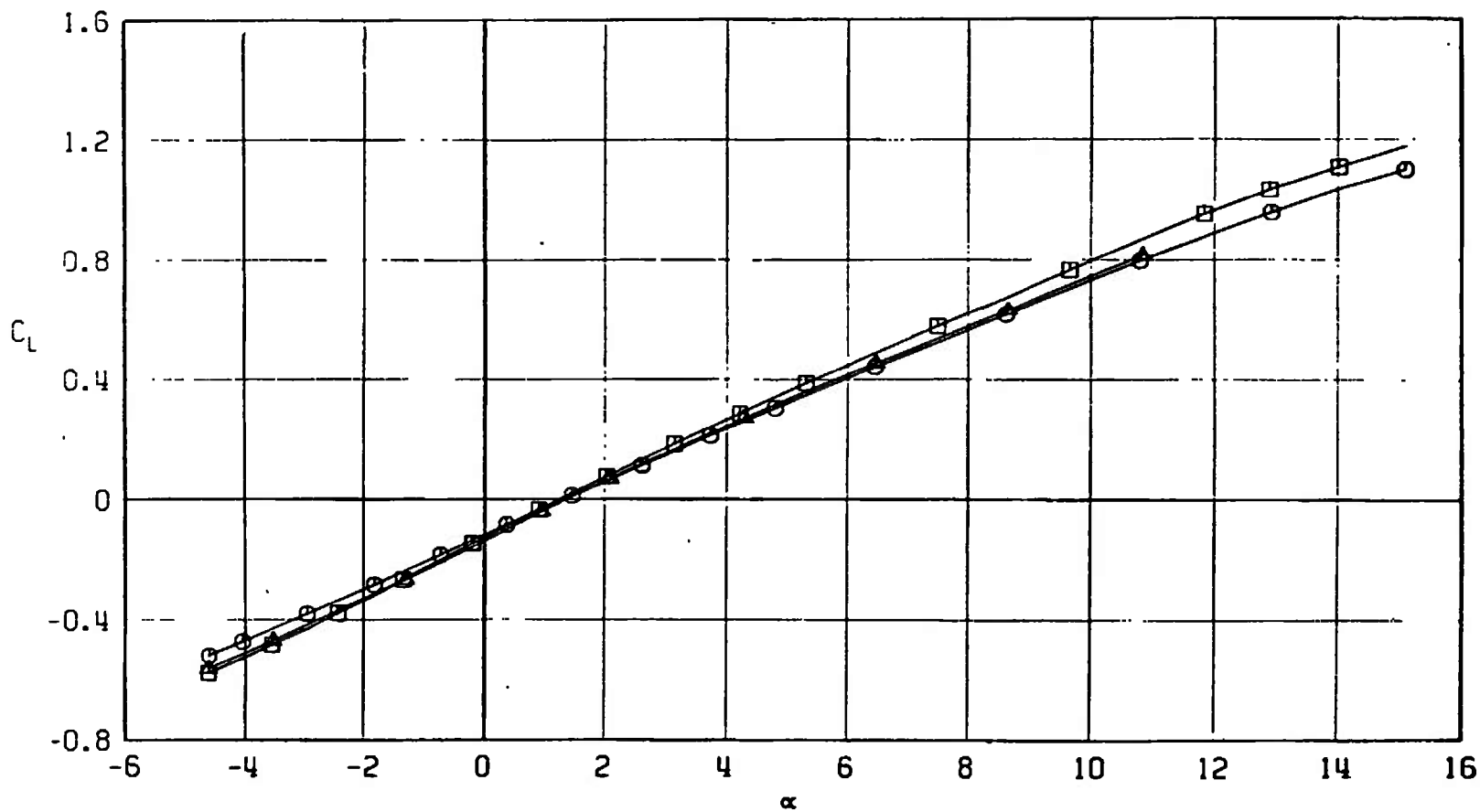
b.  $M_\infty = 0.90$   
Fig. 28 Continued

SYMBOL	CONFIGURATION
□	A701
○	A713
△	A707



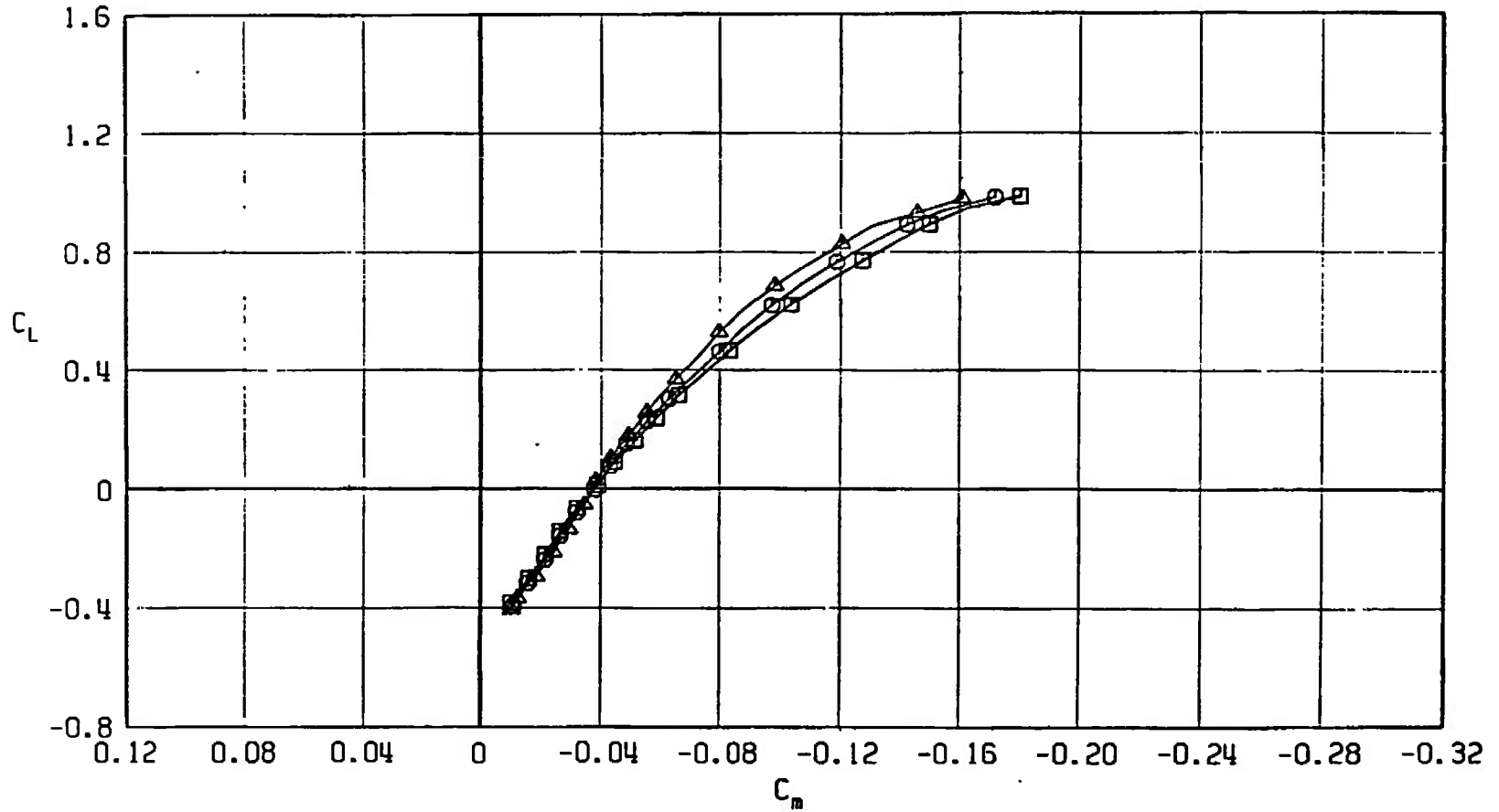
c.  $M_\infty = 0.95$   
Fig. 28 Continued

SYMBOL	CONFIGURATION
□	A701
○	A713
△	A707



d.  $M_\infty = 1.05$   
Fig. 28 Concluded

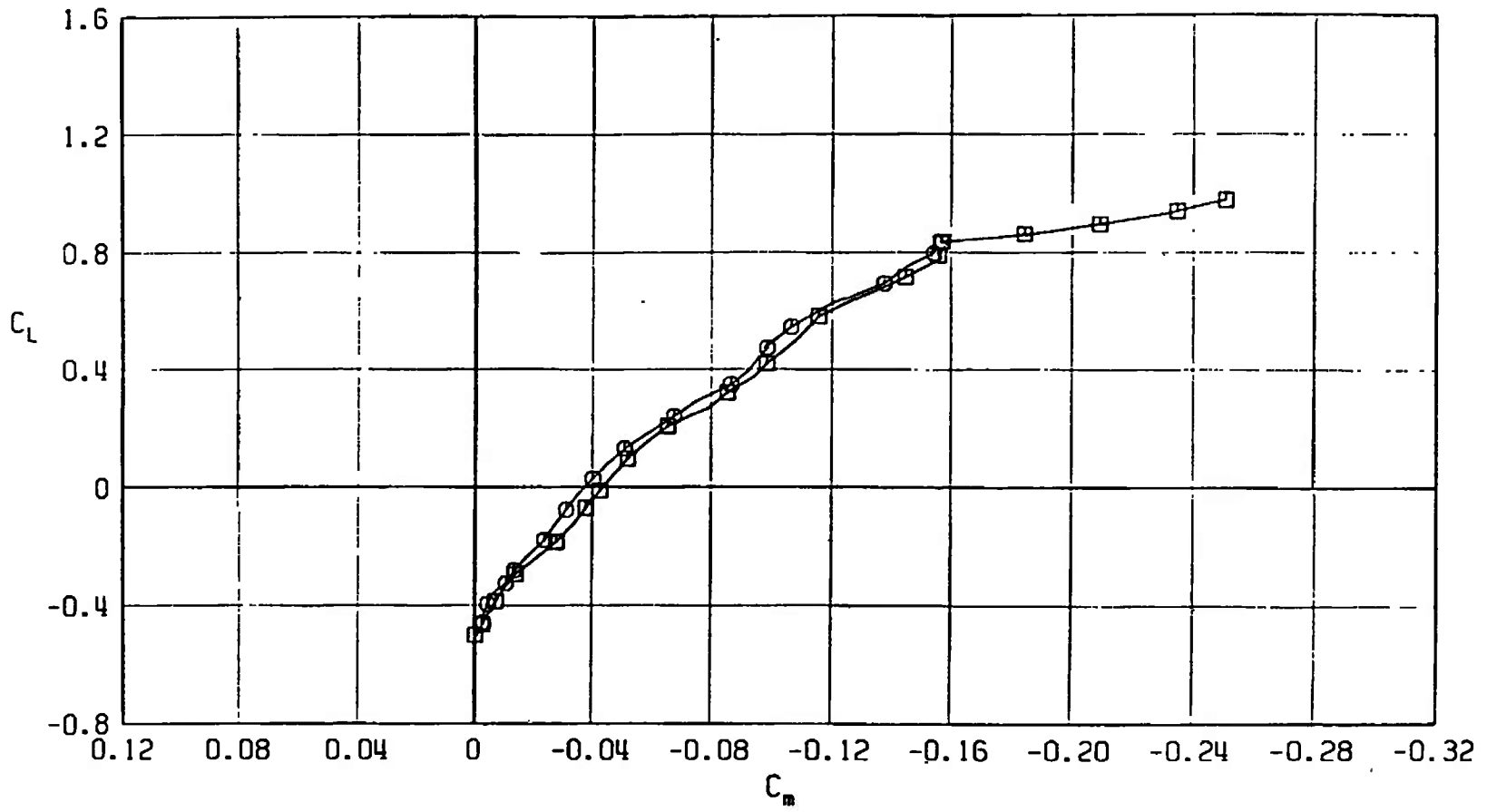
SYMBOL	CONFIGURATION
□	A701
○	A713
△	A707



a.  $M_\infty = 0.50$

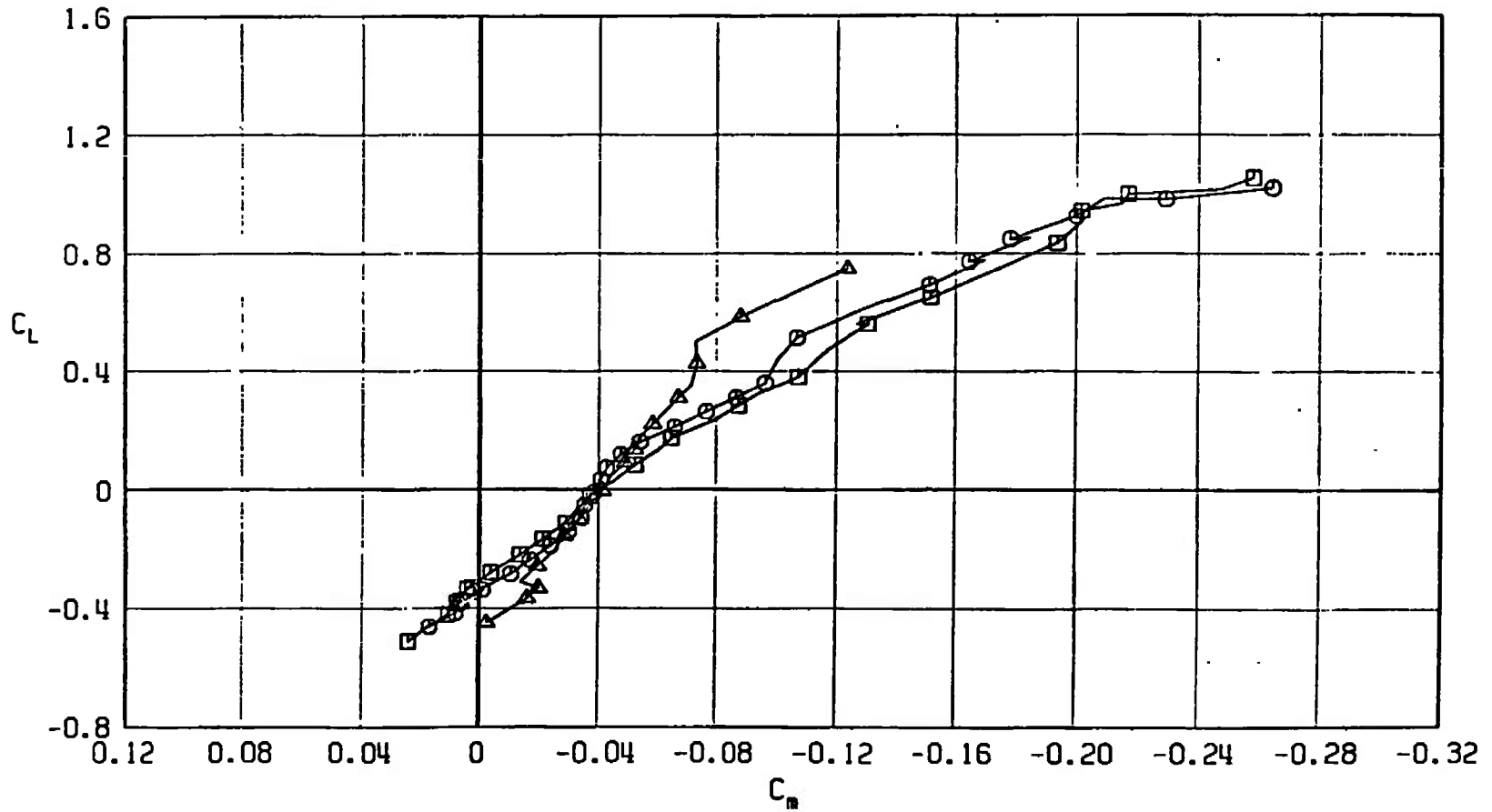
Fig. 29 Pitching-Moment Coefficient Variation with Lift Coefficient for Configurations A701, A707, and A713

SYMBOL	CONFIGURATION
□	A701
○	A713



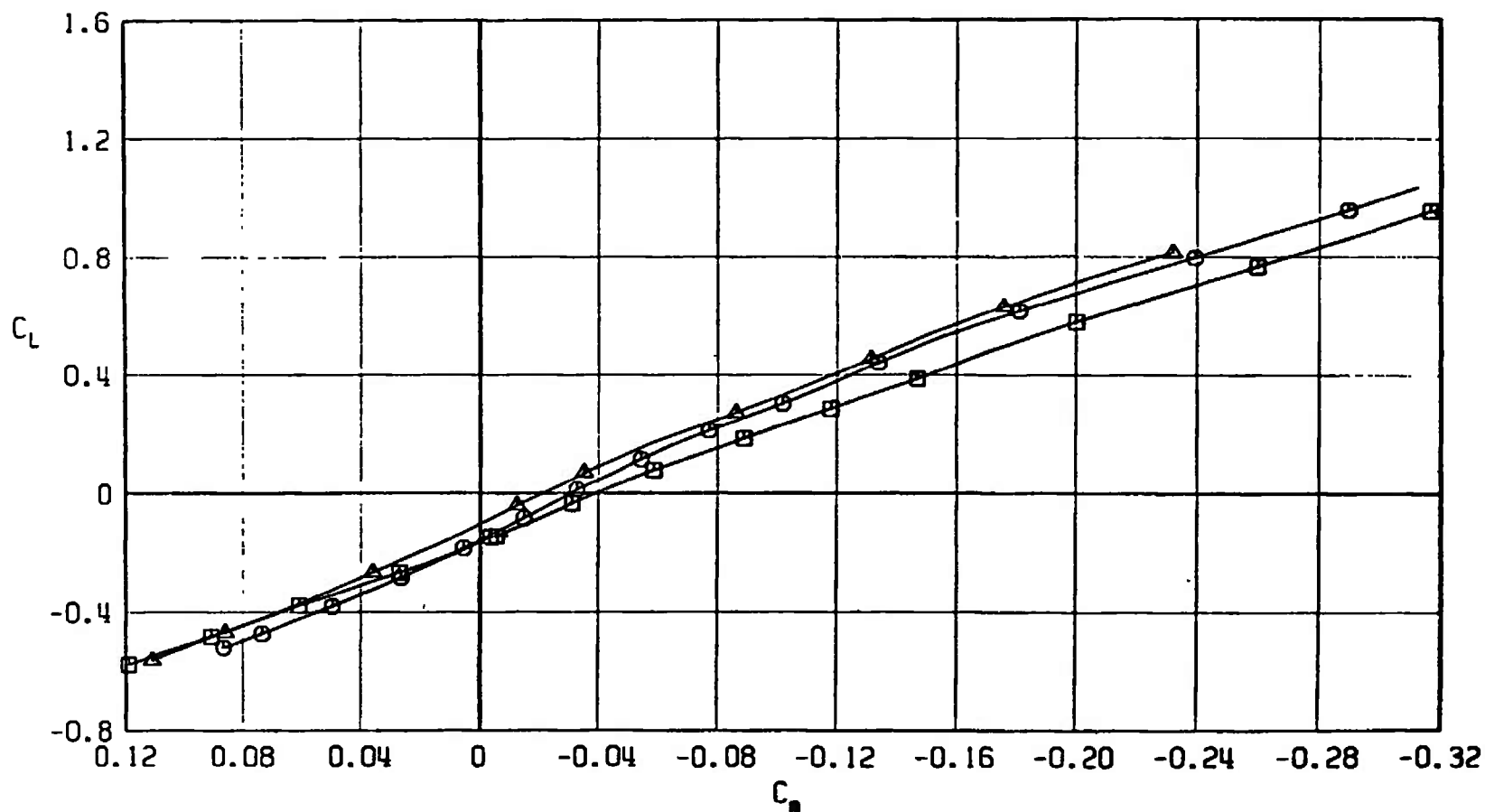
b.  $M_\infty = 0.90$   
Fig. 29 Continued

SYMBOL	CONFIGURATION
□	A701
○	A713
△	A707



c.  $M_\infty = 0.95$   
Fig. 29 Continued

SYMBOL	CONFIGURATION
□	A701
○	A713
△	A707



d.  $M_\infty = 1.05$   
Fig. 29 Concluded



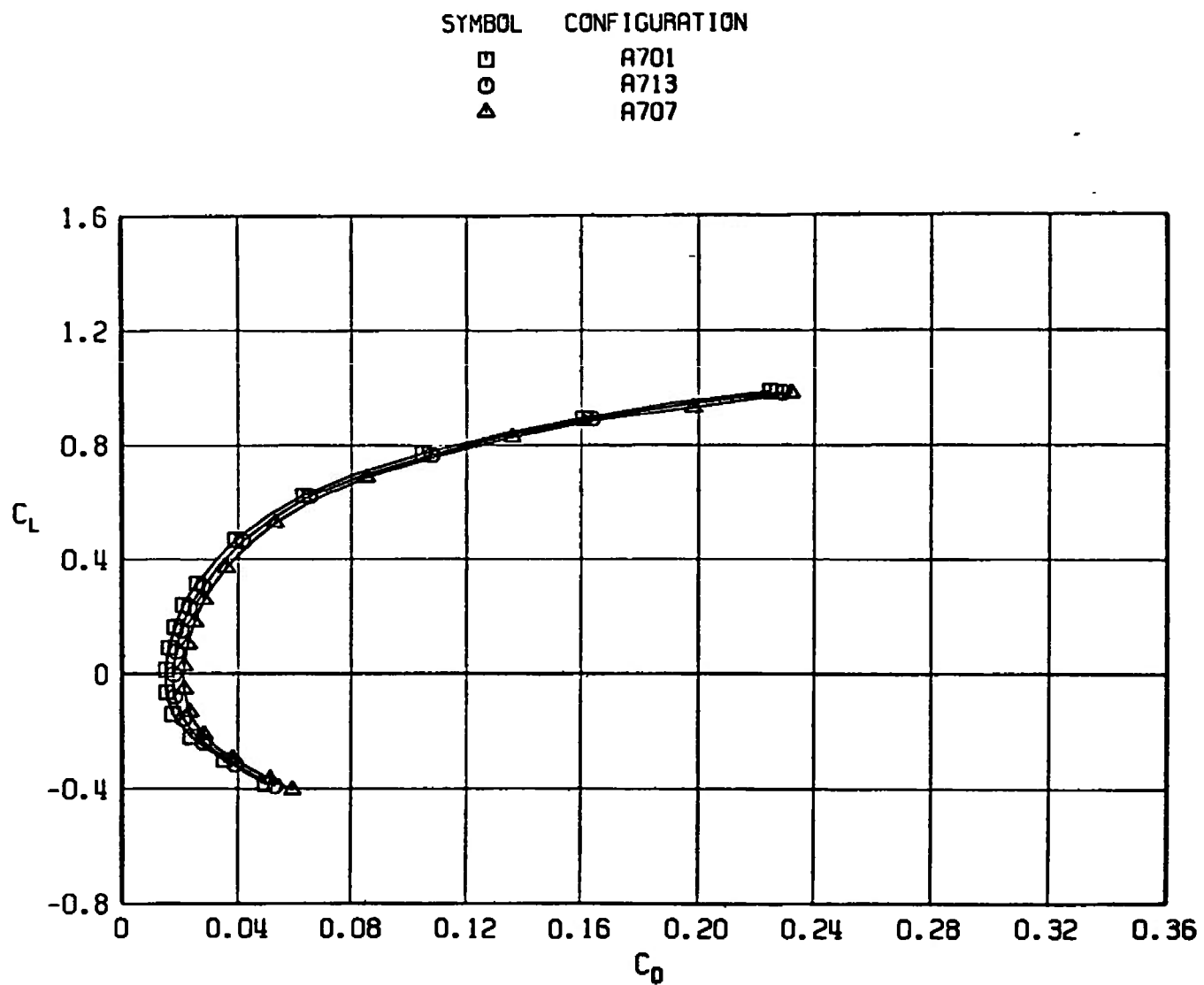
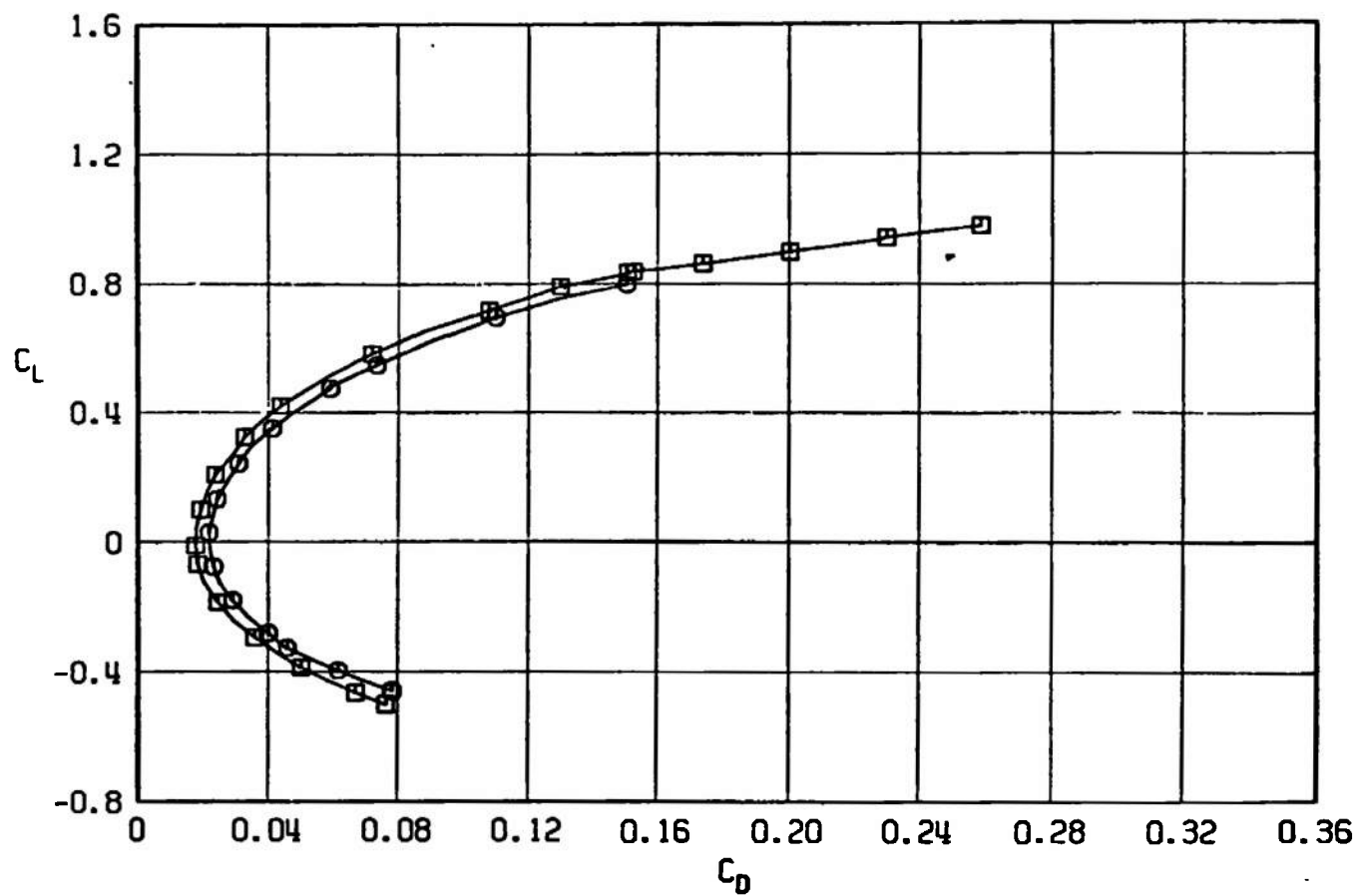
a.  $M_\infty = 0.50$ 

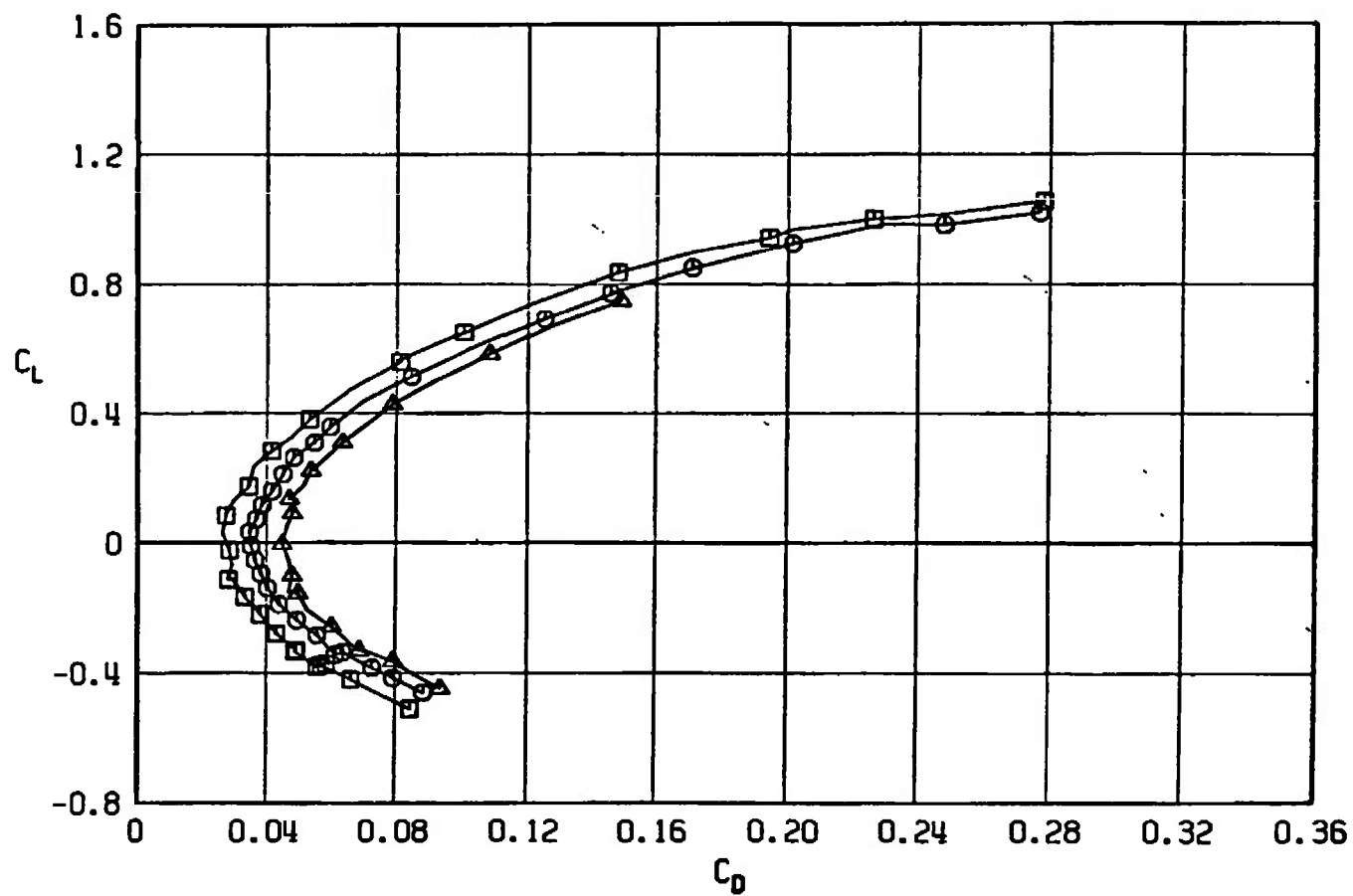
Fig. 30 Drag Coefficient Variation with Lift Coefficient for Configurations A701, A707, and A713

SYMBOL	CONFIGURATION
□	A701
○	A713

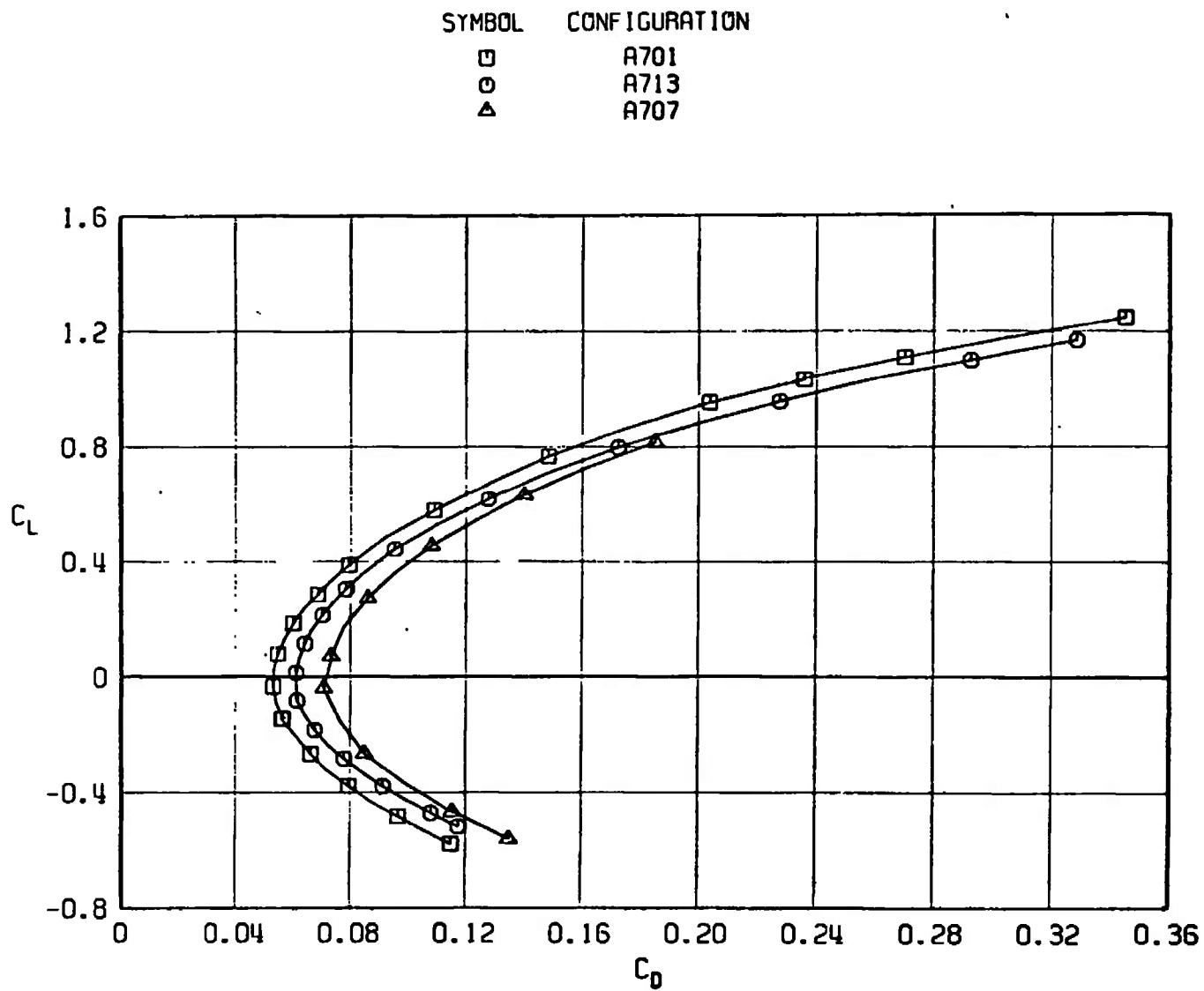


b.  $M_\infty = 0.90$   
Fig. 30 Continued

SYMBOL	CONFIGURATION
□	A701
○	A713
△	A707



c.  $M_\infty = 0.95$   
Fig. 30 Continued



d.  $M_\infty = 1.05$   
Fig. 30 Concluded

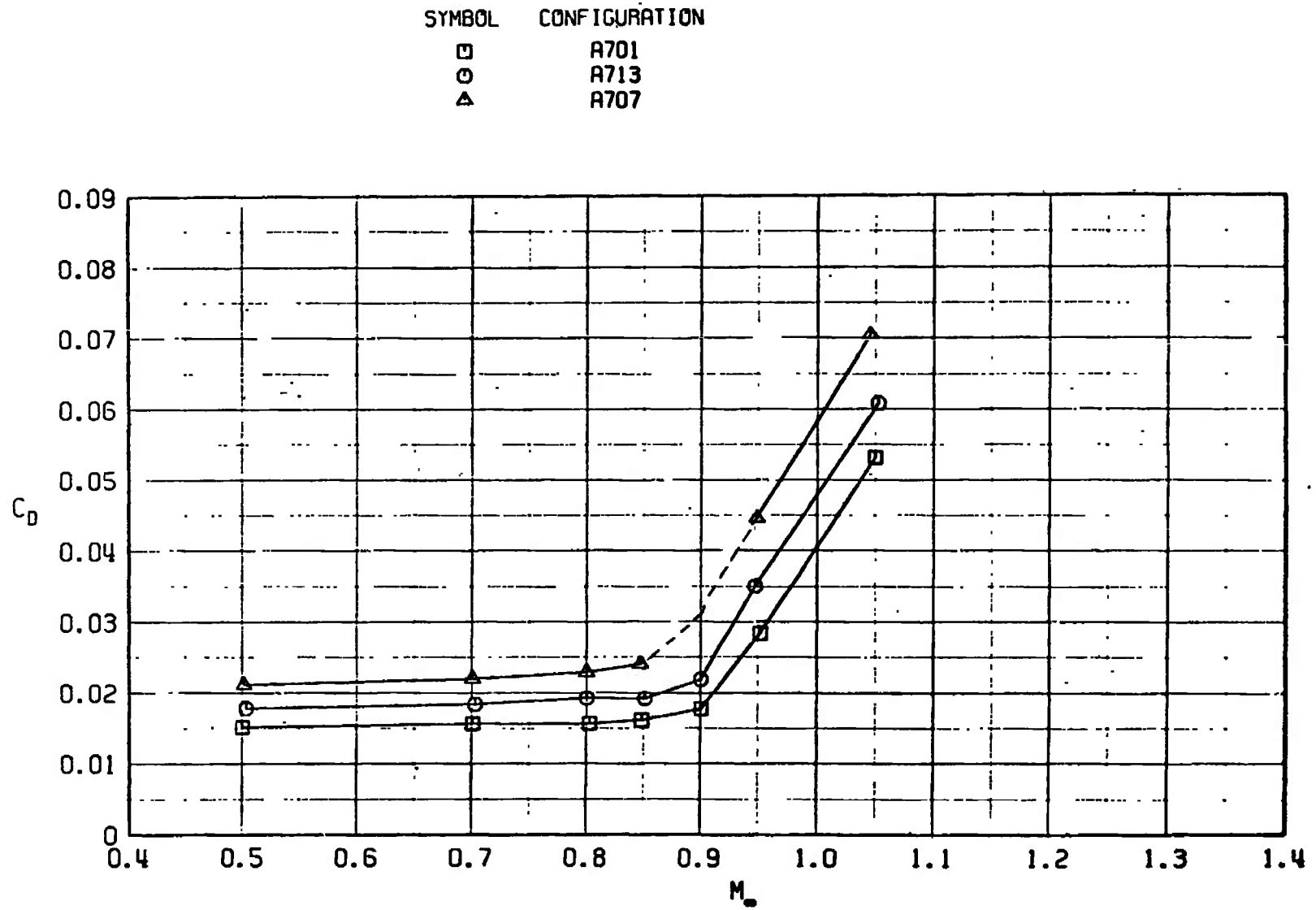
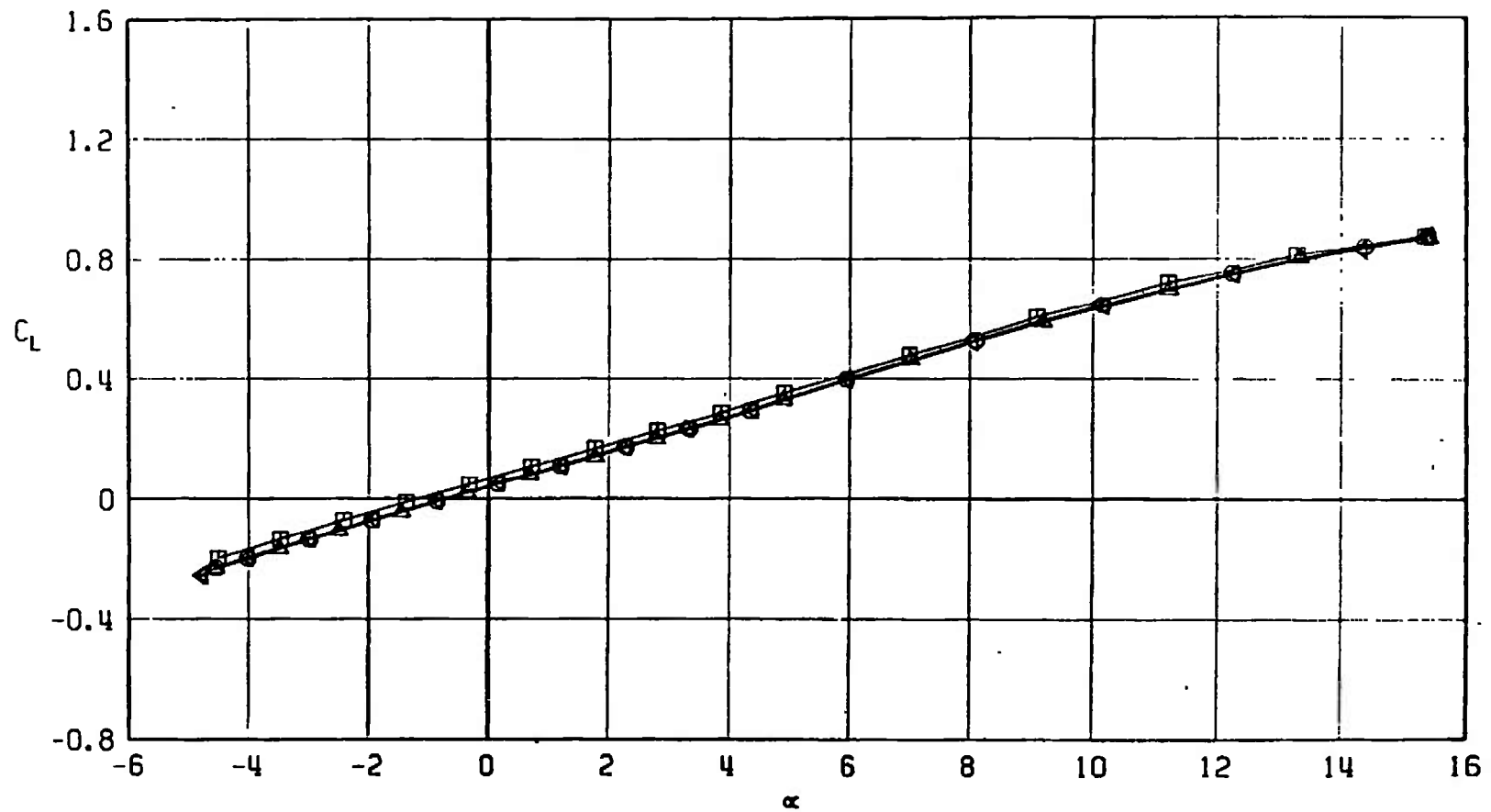


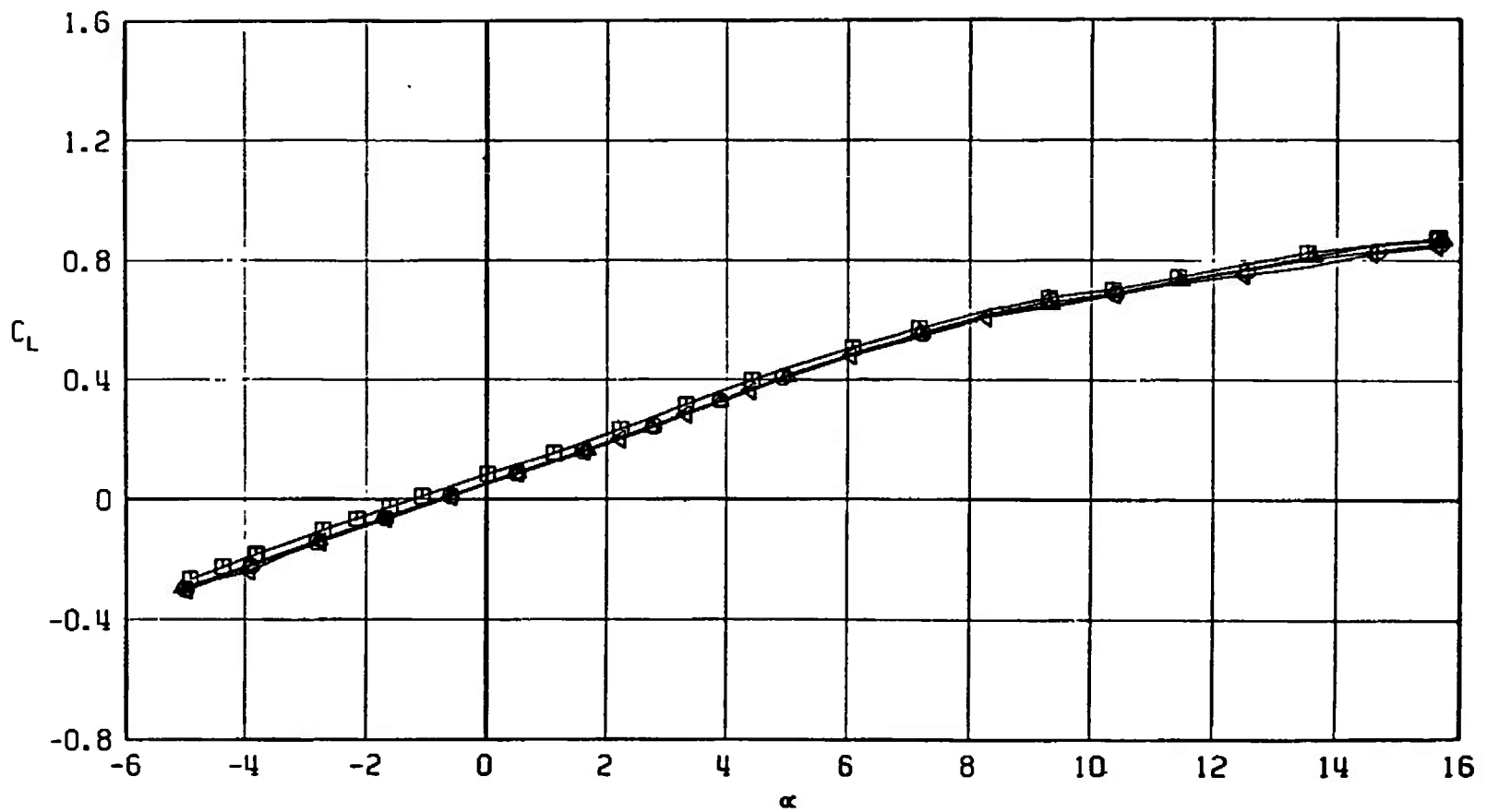
Fig. 31 Drag Coefficient Variation with Mach Number at  $C_L = 0$  for Configurations A701, A707, and A713

SYMBOL	CONFIGURATION
□	F401
○	F403
△	F404
◄	F402



a.  $M_\infty = 0.50$   
 Fig. 32 Lift Coefficient Variation with Angle of Attack for Configurations F401, F402, F403, and F404.

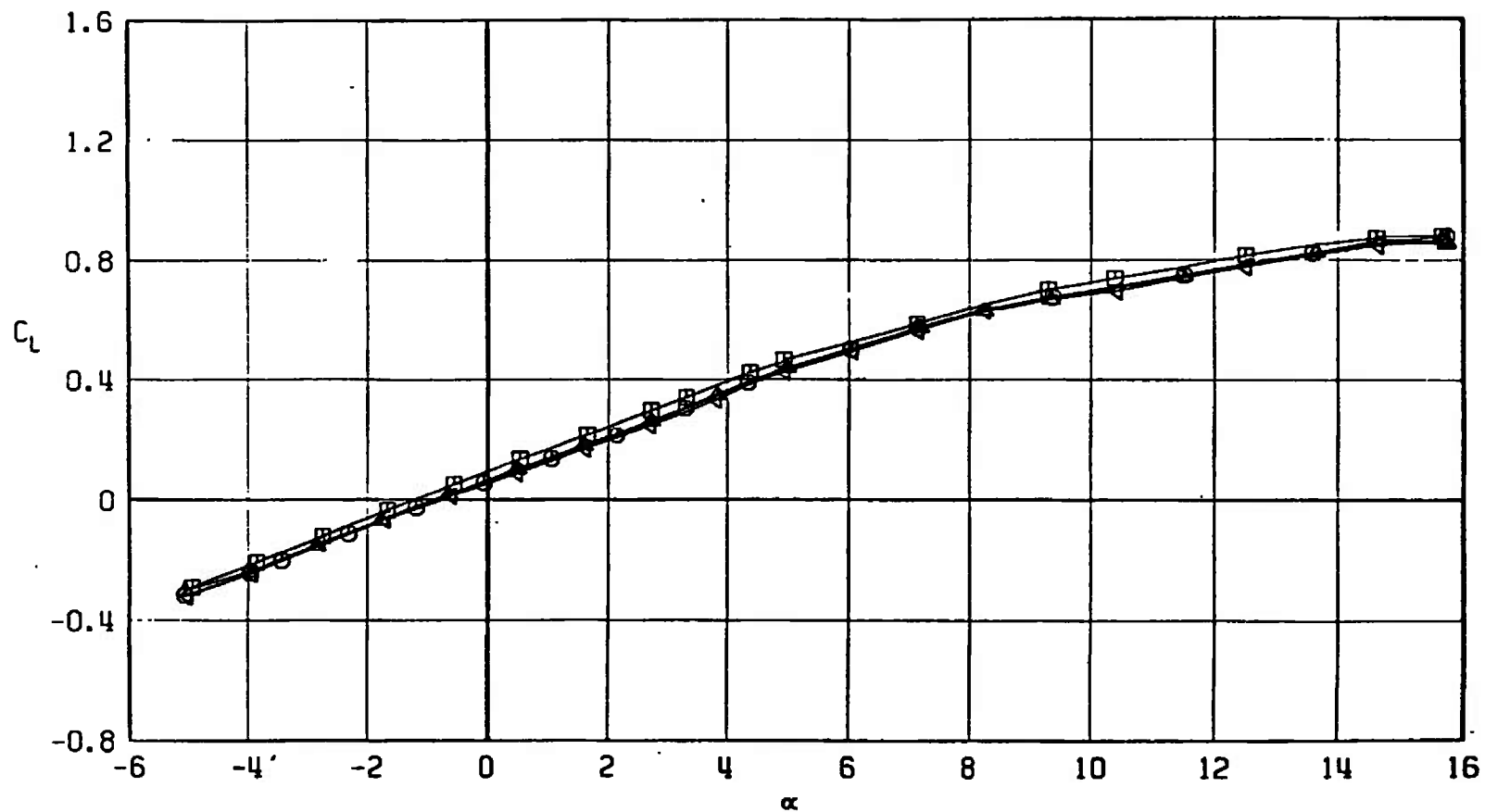
SYMBOL	CONFIGURATION
□	F401
○	F403
△	F404
◀	F402



b.  $M_\infty = 0.90$   
Fig. 32 Continued

SYMBOL CONFIGURATION

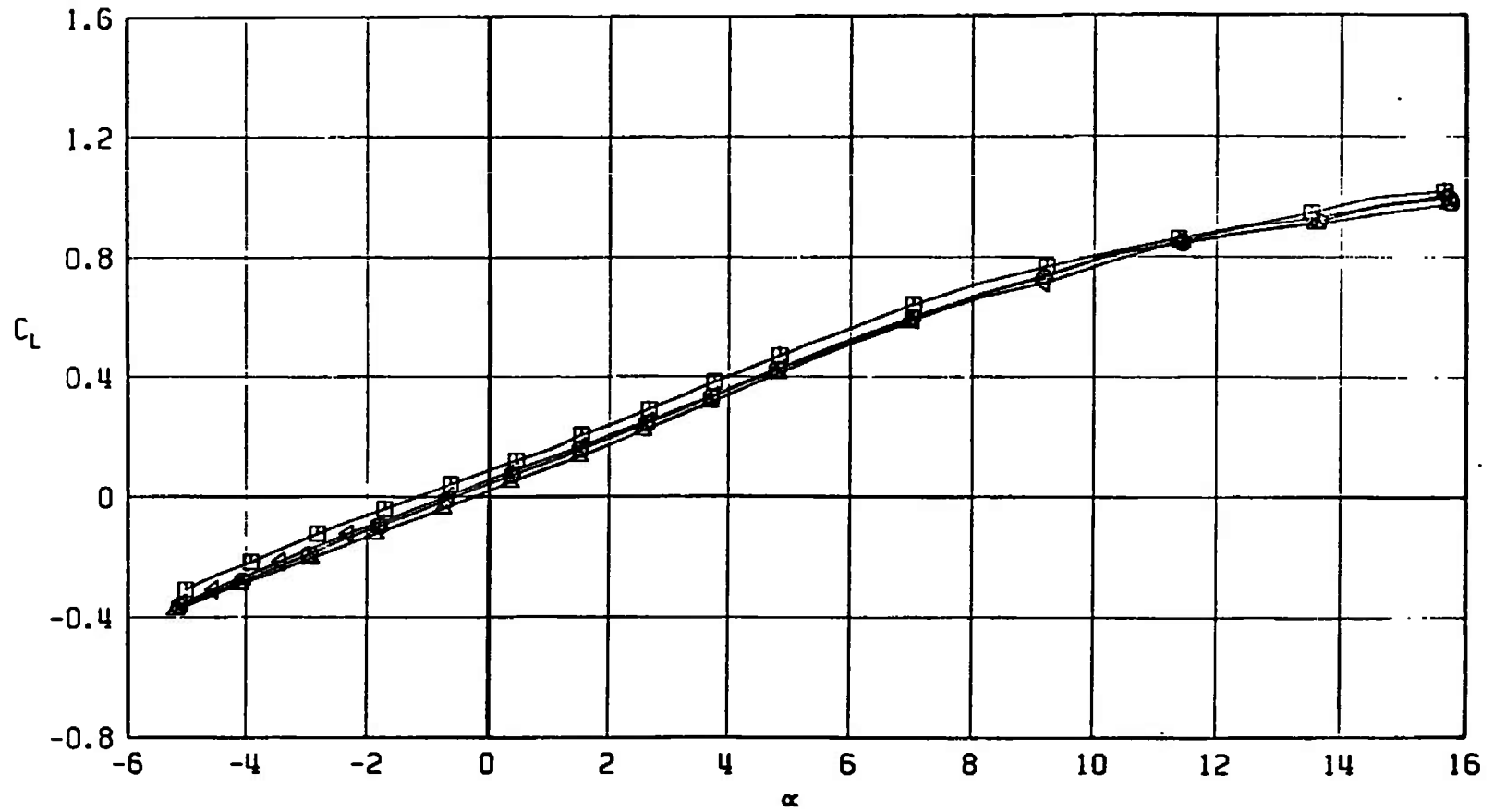
□	F401
○	F403
△	F404
◀	F402*



c.  $M_\infty = 0.95$   
Fig. 32 Continued

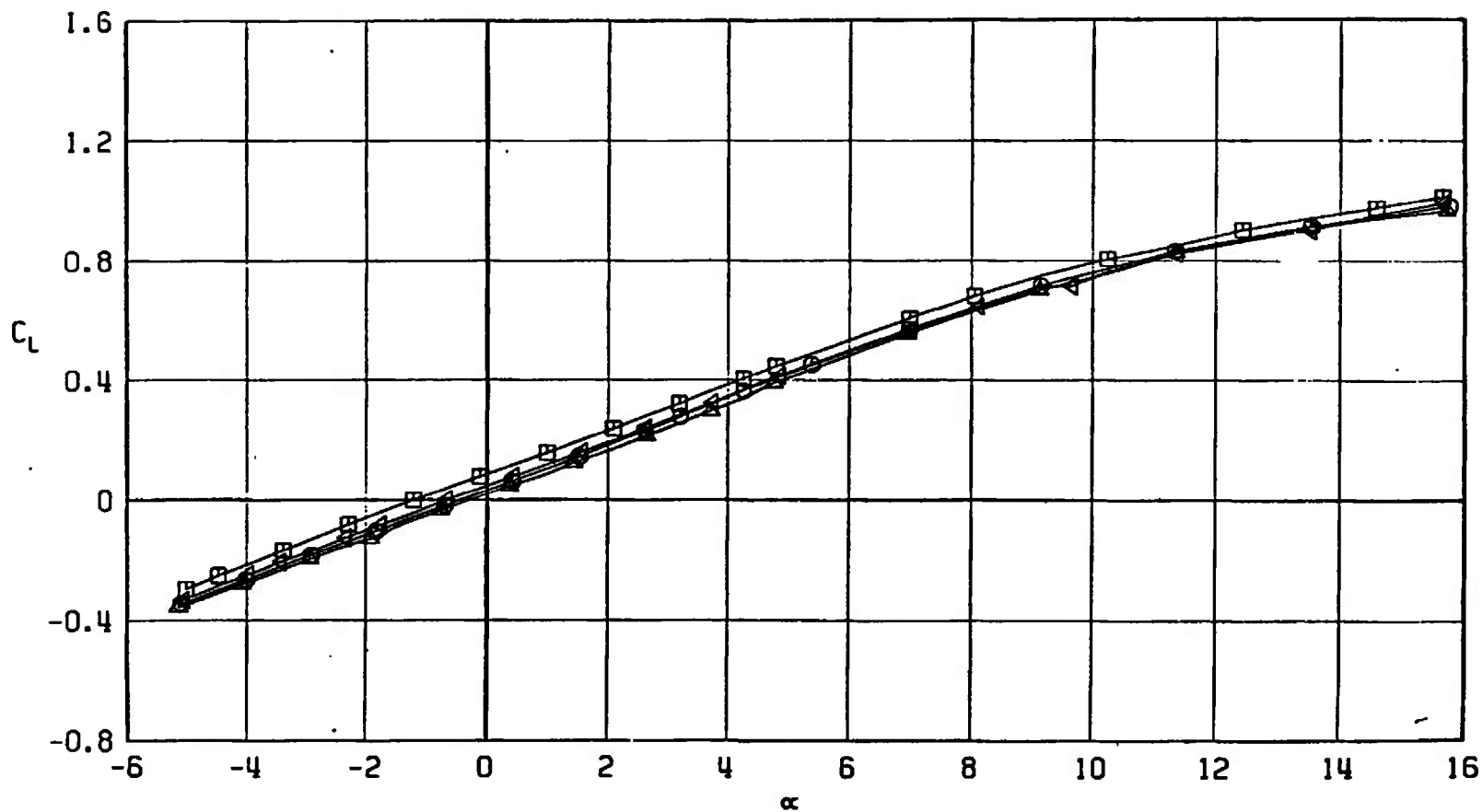


SYMBOL	CONFIGURATION
□	F401
○	F403
△	F404
◀	F402



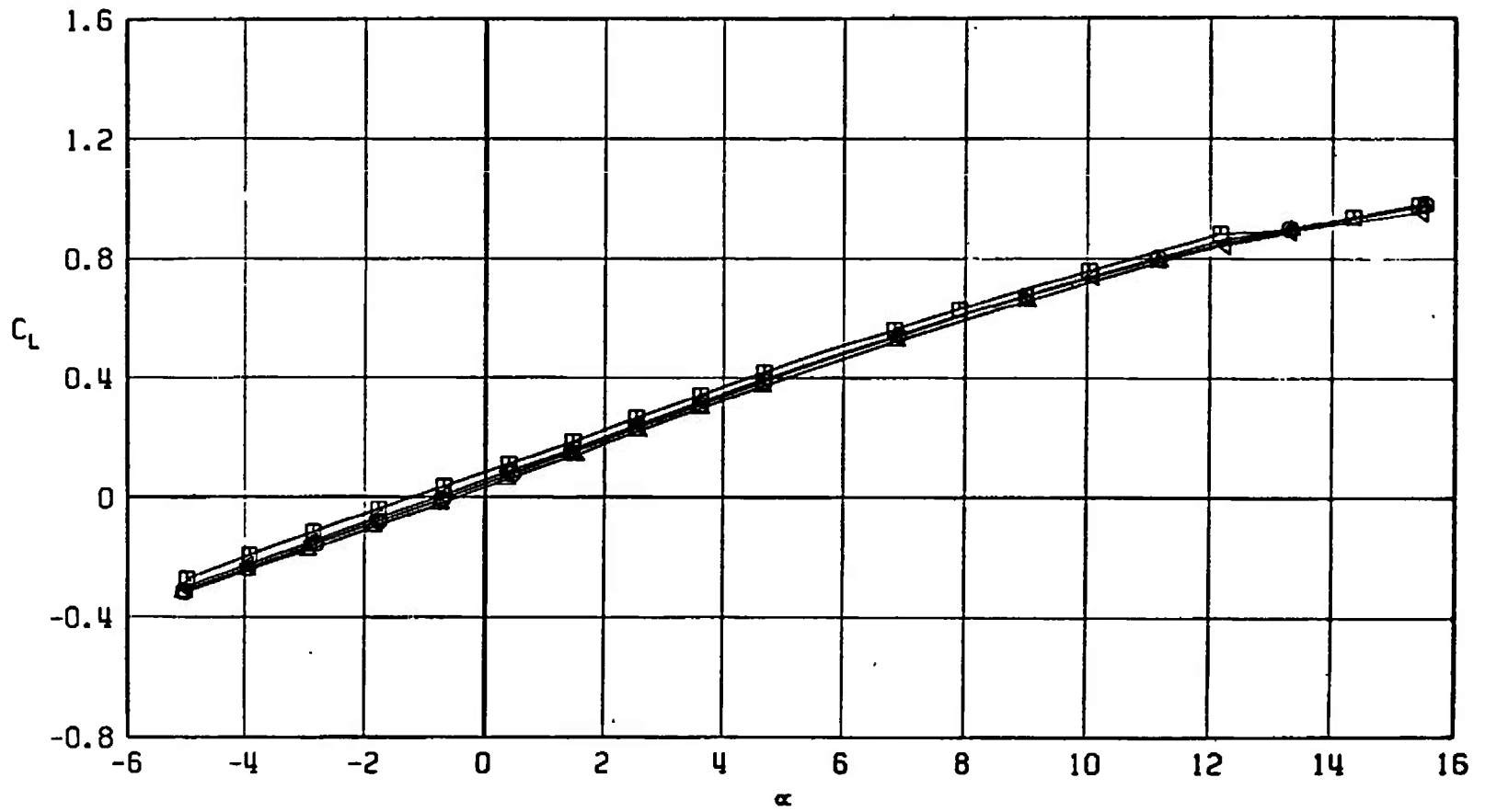
d.  $M_\infty = 1.05$   
Fig. 32 Continued

SYMBOL	CONFIGURATION
□	F401
○	F403
△	F404
◄	F402



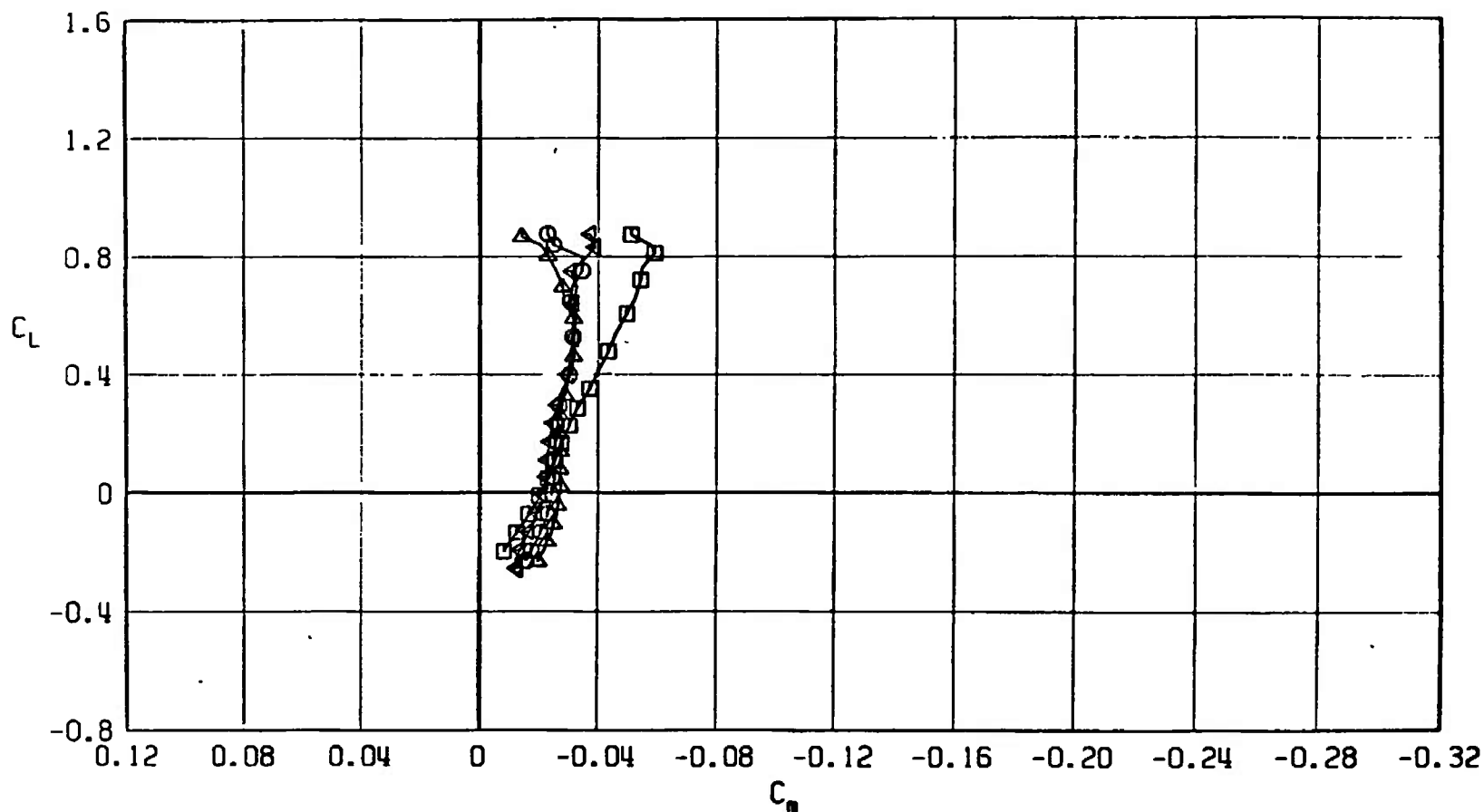
e.  $M_\infty = 1.10$   
Fig. 32 Continued

SYMBOL	CONFIGURATION
□	F401
○	F403
△	F404
▽	F402



f.  $M_\infty = 1.20$   
Fig. 32 Concluded

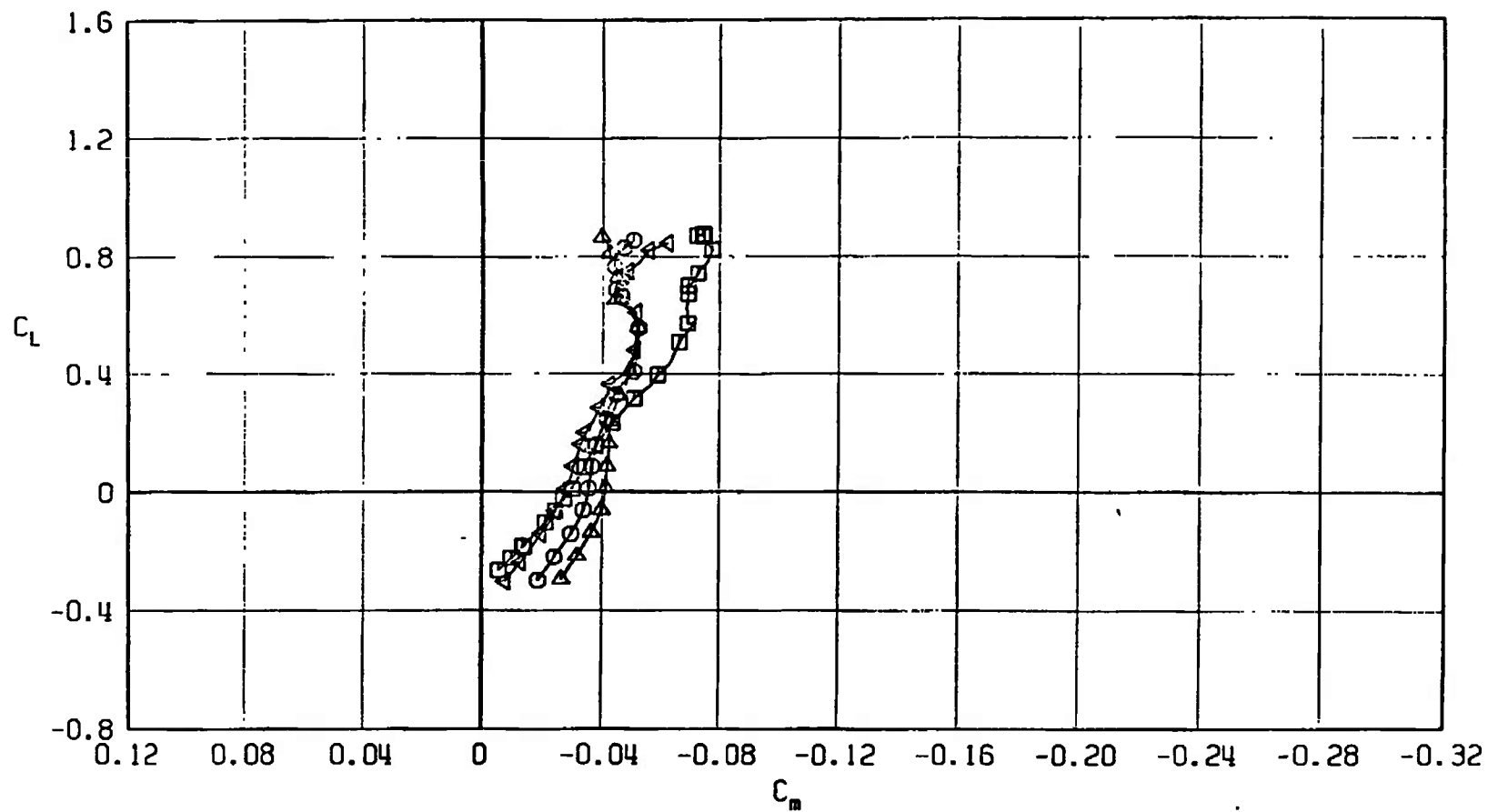
SYMBOL	CONFIGURATION
□	F401
○	F403
△	F404
◀	F402



a.  $M_\infty = 0.50$

Fig. 33 Pitching-Moment Coefficient Variation with Lift Coefficient for Configurations F401, F402, F403, and F404

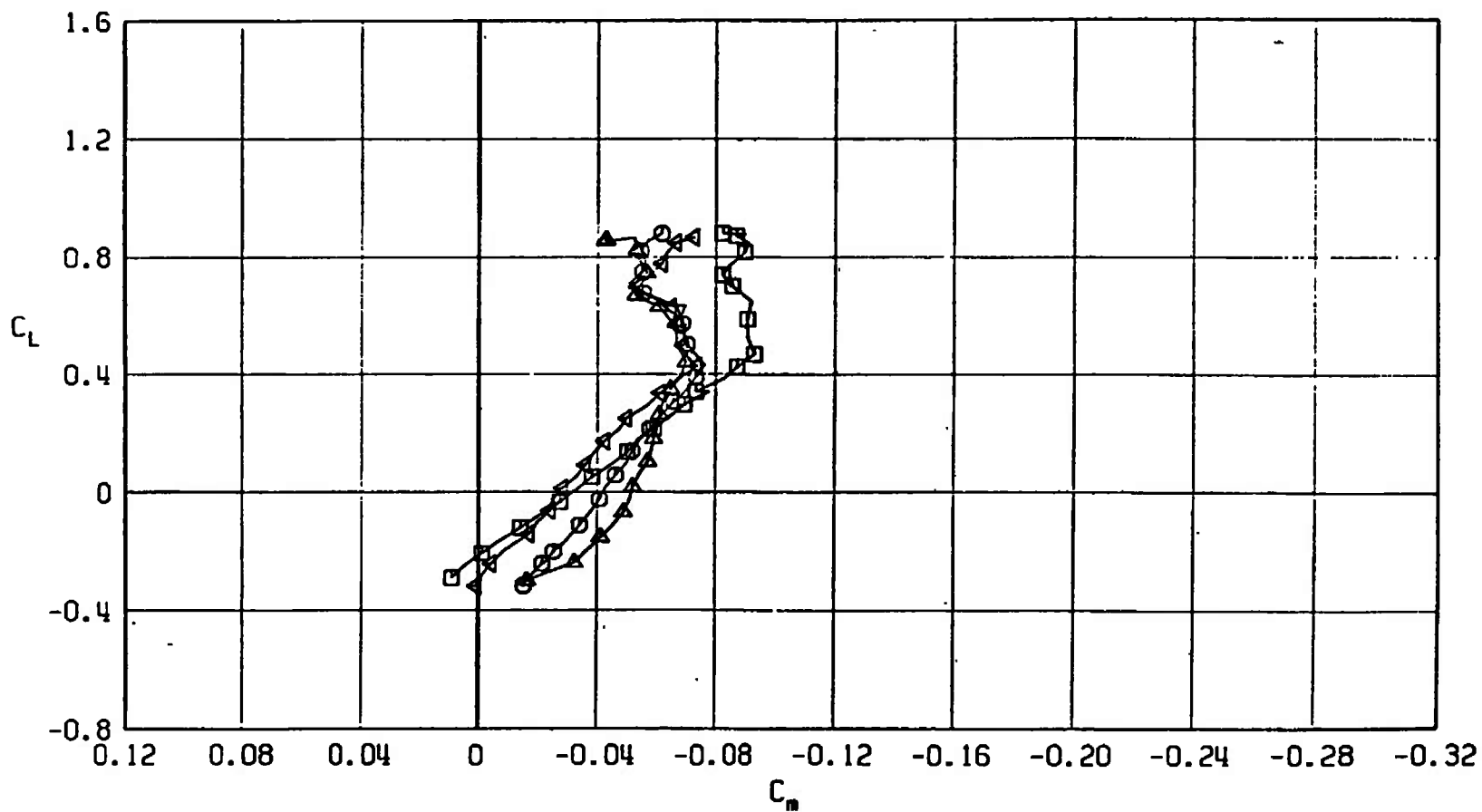
SYMBOL	CONFIGURATION
□	F401
○	F403
△	F404
▽	F402



b.  $M_\infty = 0.90$   
Fig. 33 Continued

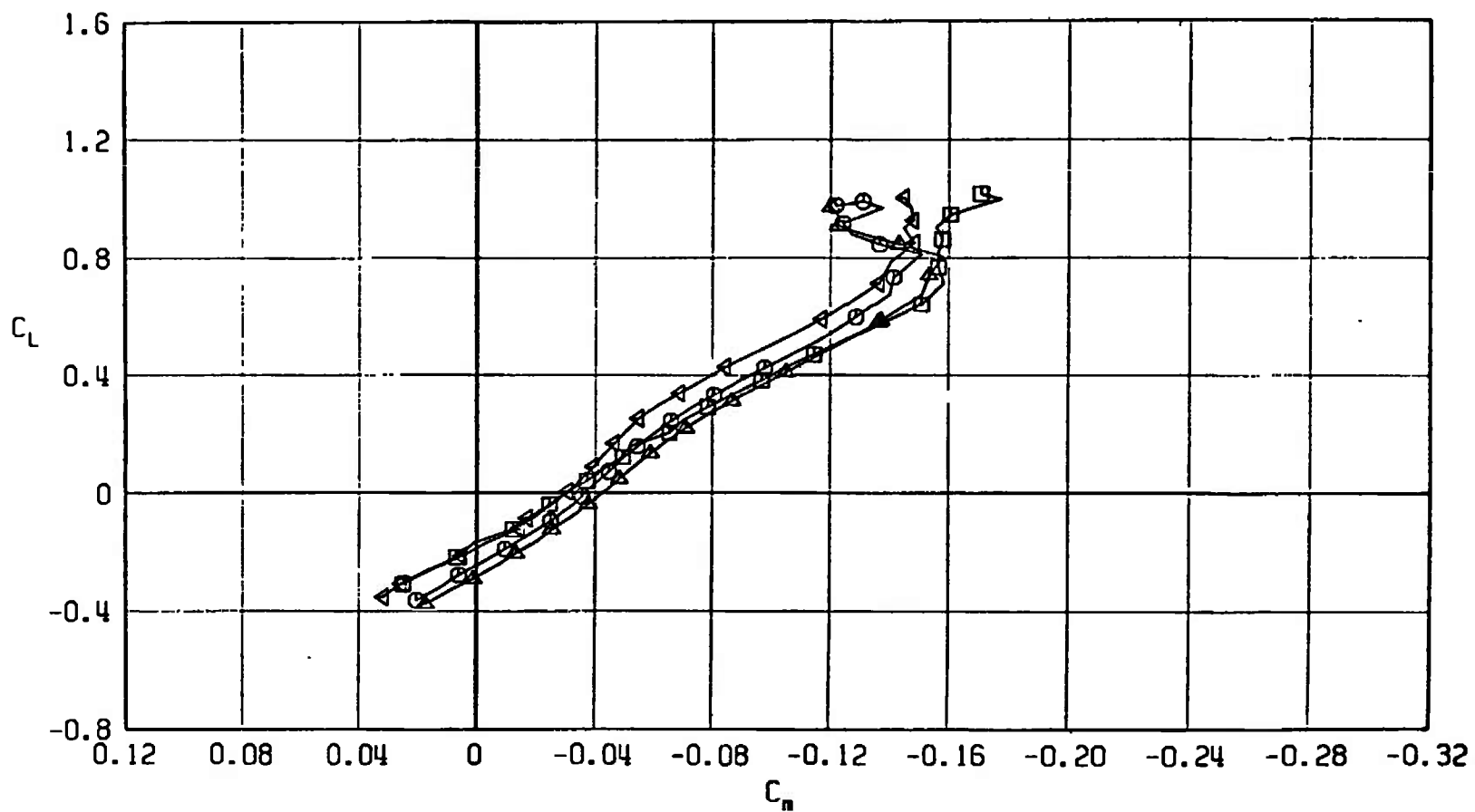
SYMBOL      CONFIGURATION

□	F401
○	F403
△	F404
◀	F402



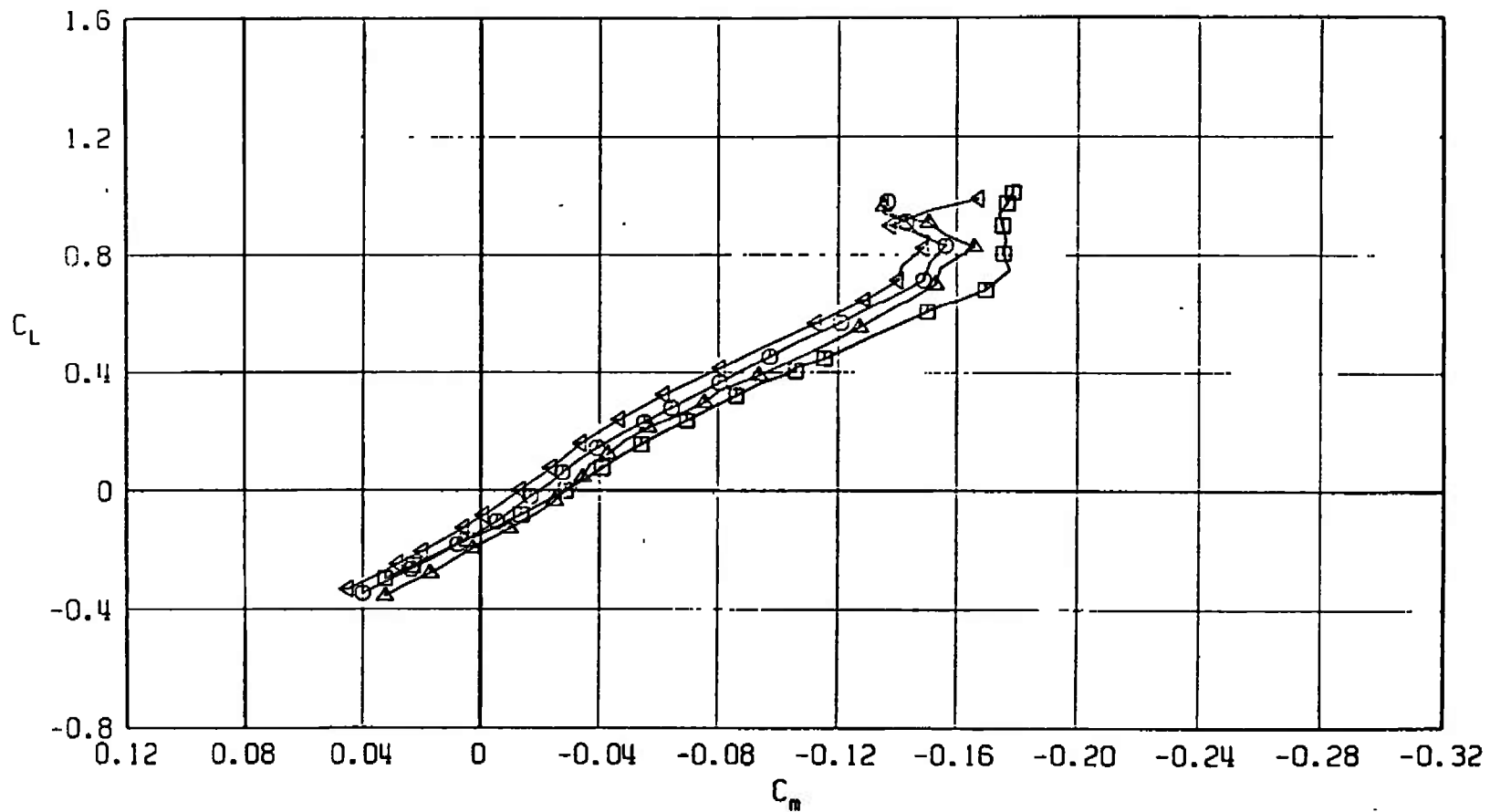
c.  $M_\infty = 0.95$   
Fig. 33 Continued

SYMBOL	CONFIGURATION
□	F401
○	F403
△	F404
▽	F402



d.  $M_\infty = 1.05$   
Fig. 33 Continued

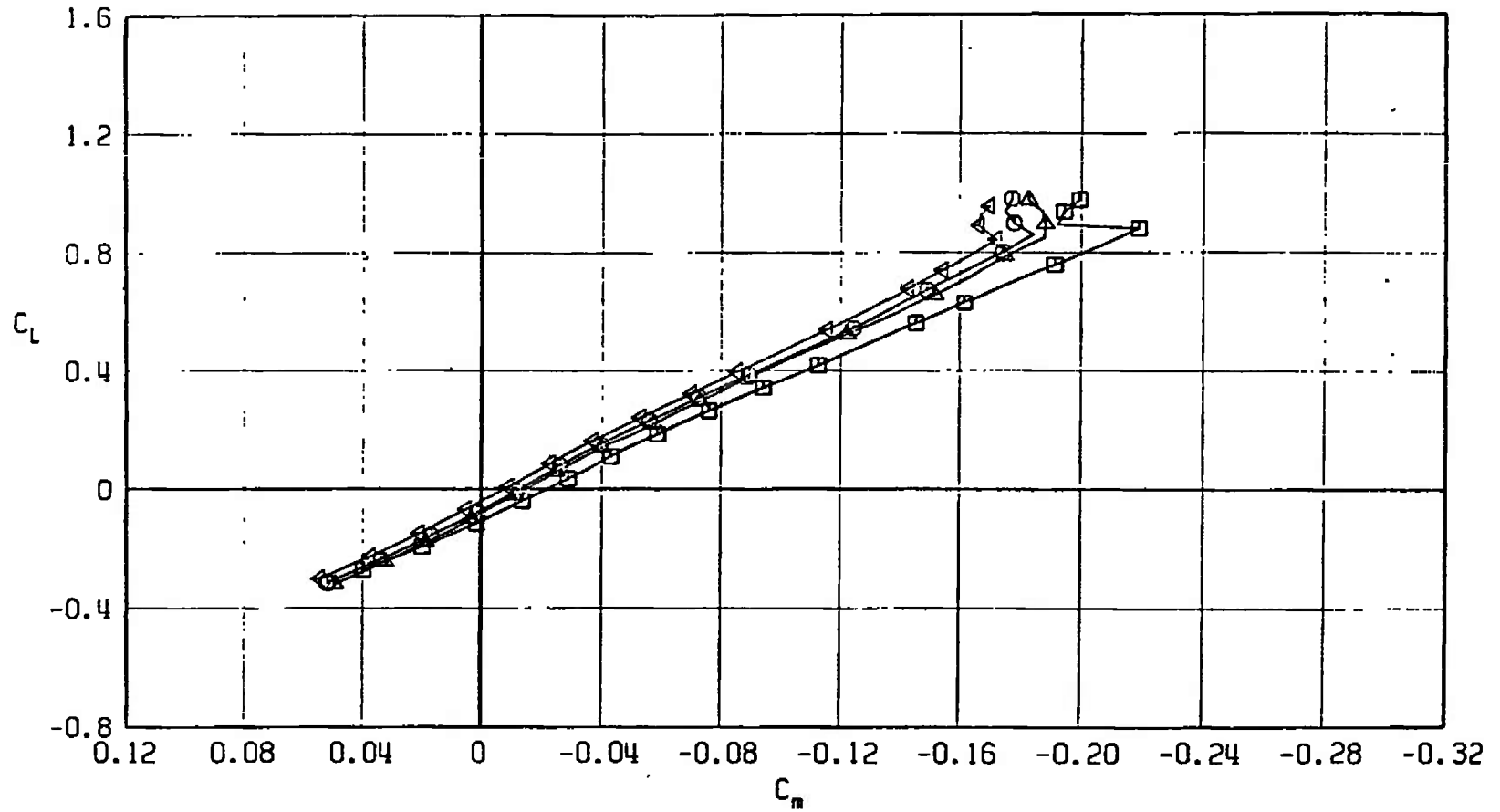
SYMBOL	CONFIGURATION
□	F401
○	F403
△	F404
◄	F402



e.  $M_\infty = 1.10$   
Fig. 33 Continued



SYMBOL	CONFIGURATION
□	F401
○	F403
△	F404
▽	F402



f.  $M_\infty = 1.20$   
Fig. 33 Concluded

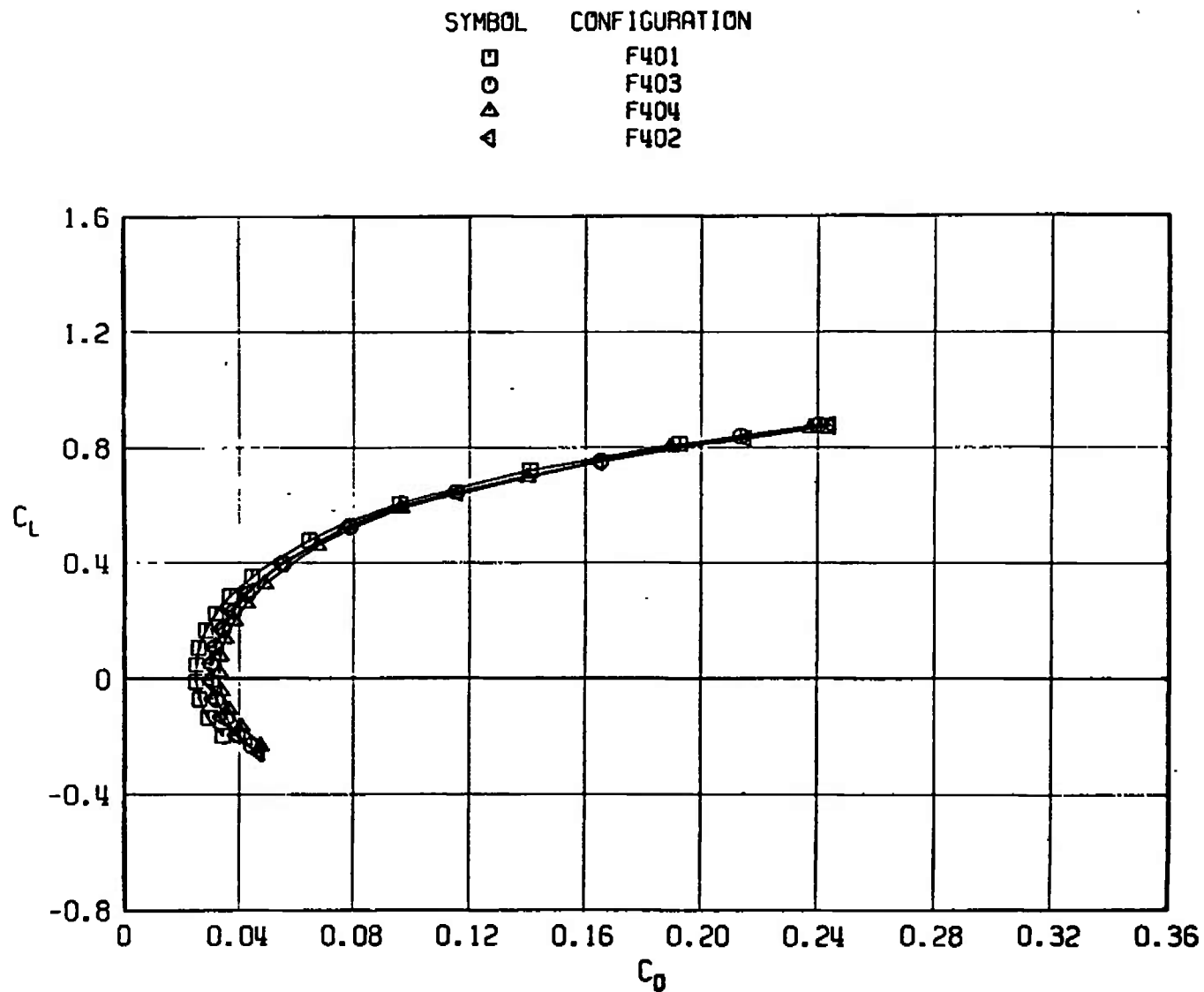
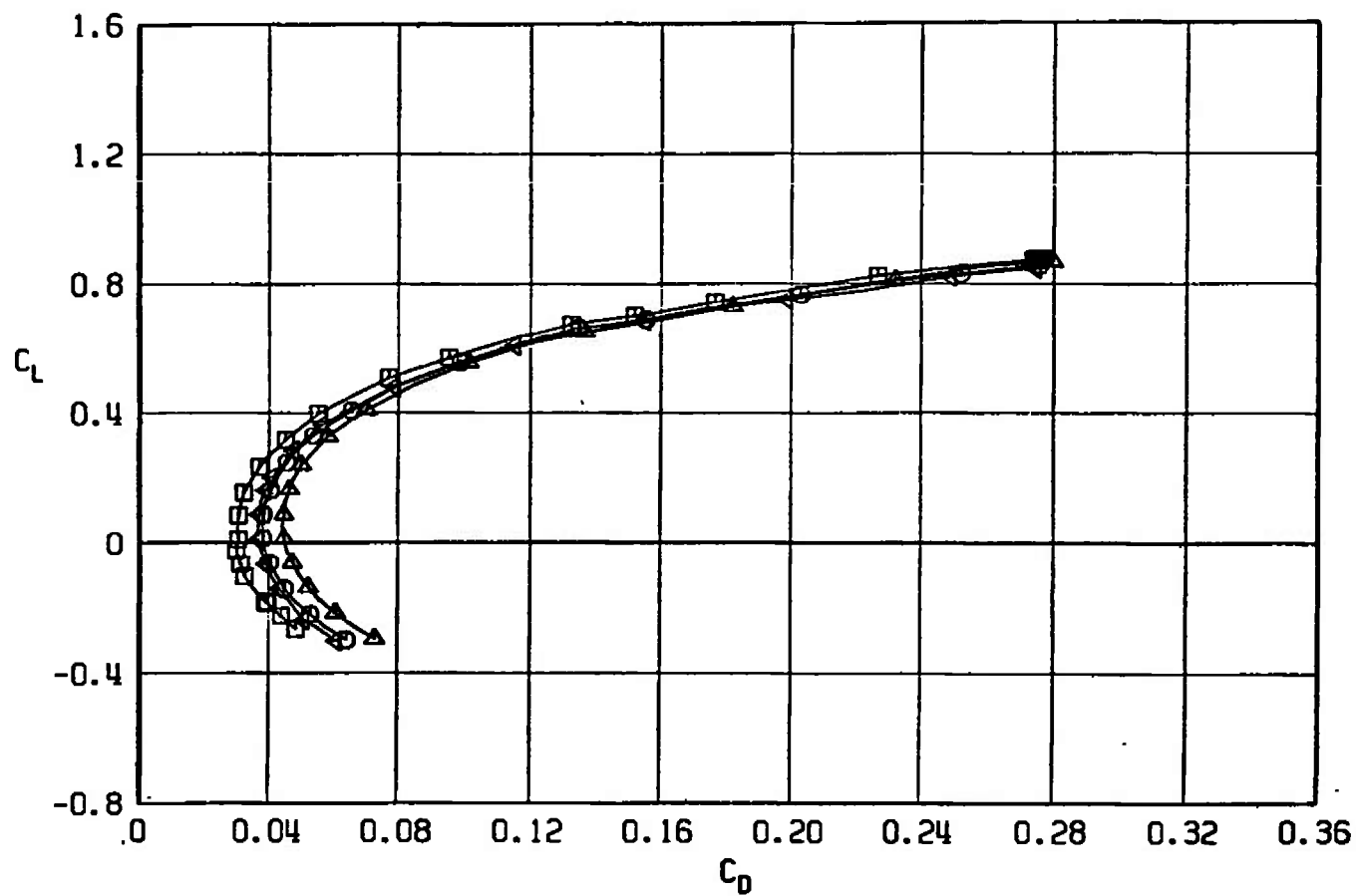
a.  $M_\infty = 0.50$ 

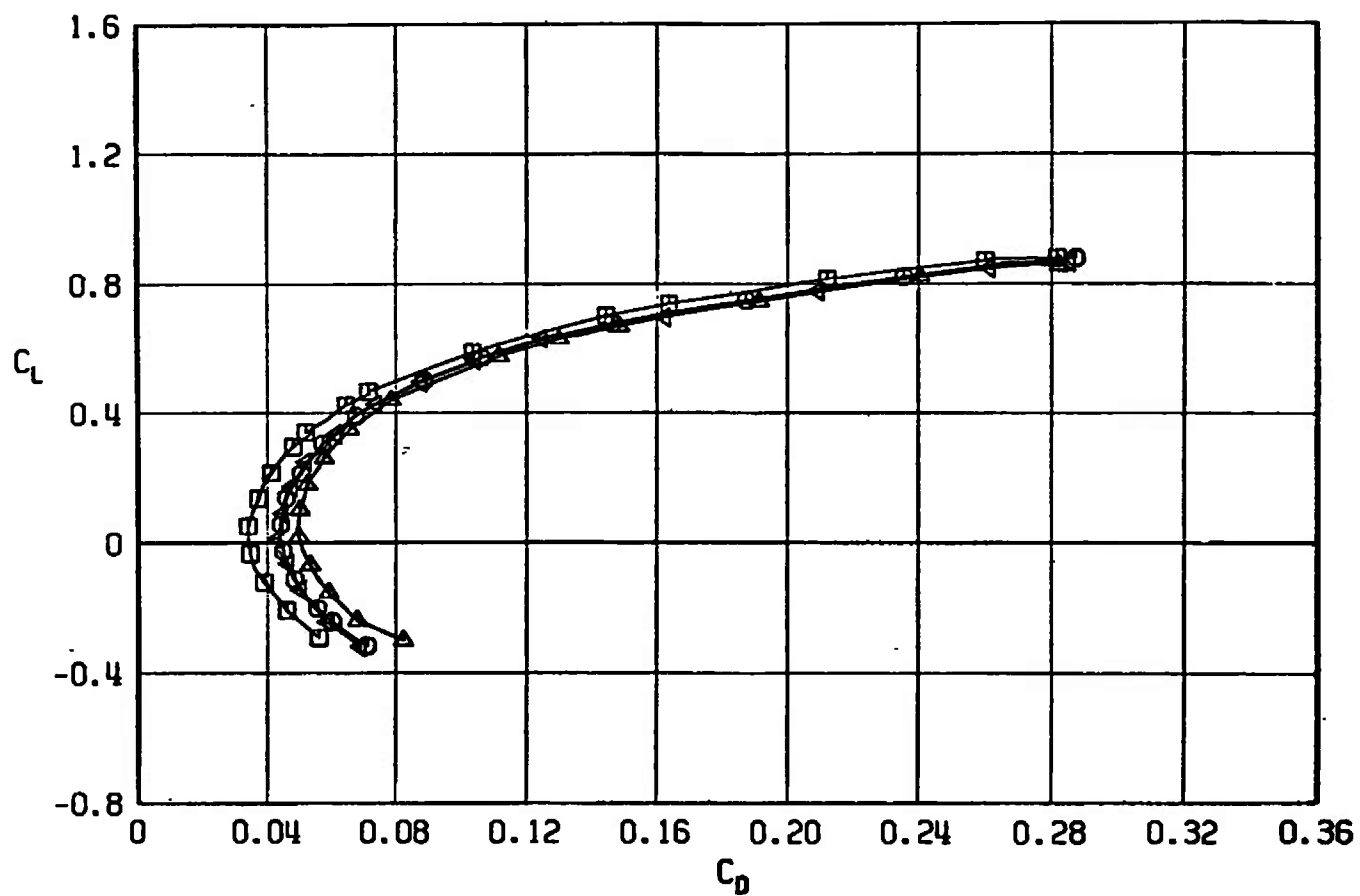
Fig. 34 Drag Coefficient Variation with Lift Coefficient for Configurations F401, F402, F403, and F404

SYMBOL	CONFIGURATION
□	F401
○	F403
△	F404
▽	F402



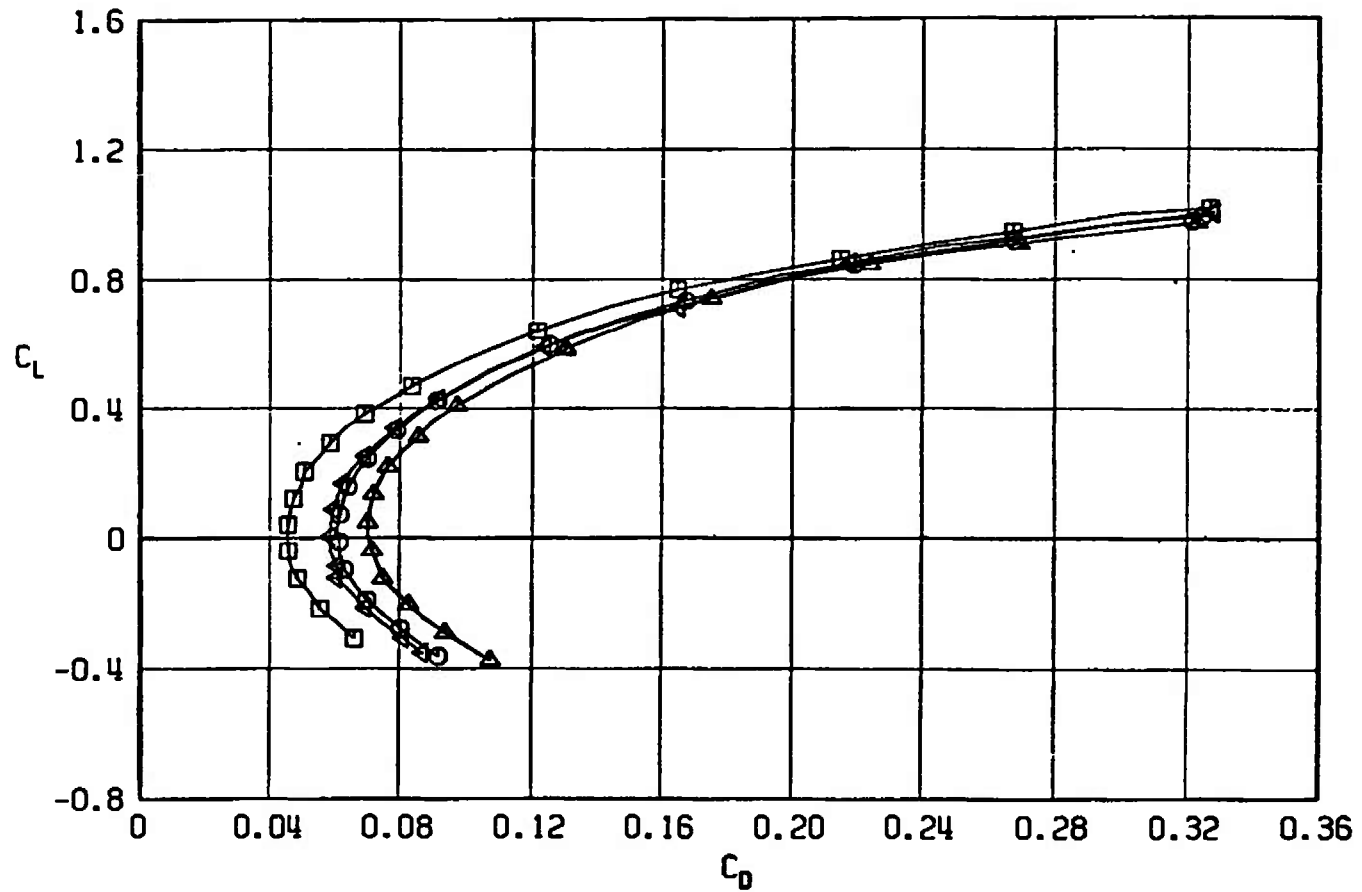
b.  $M_\infty = 0.90$   
Fig. 34 Continued

SYMBOL	CONFIGURATION
□	F401
○	F403
△	F404
◀	F402

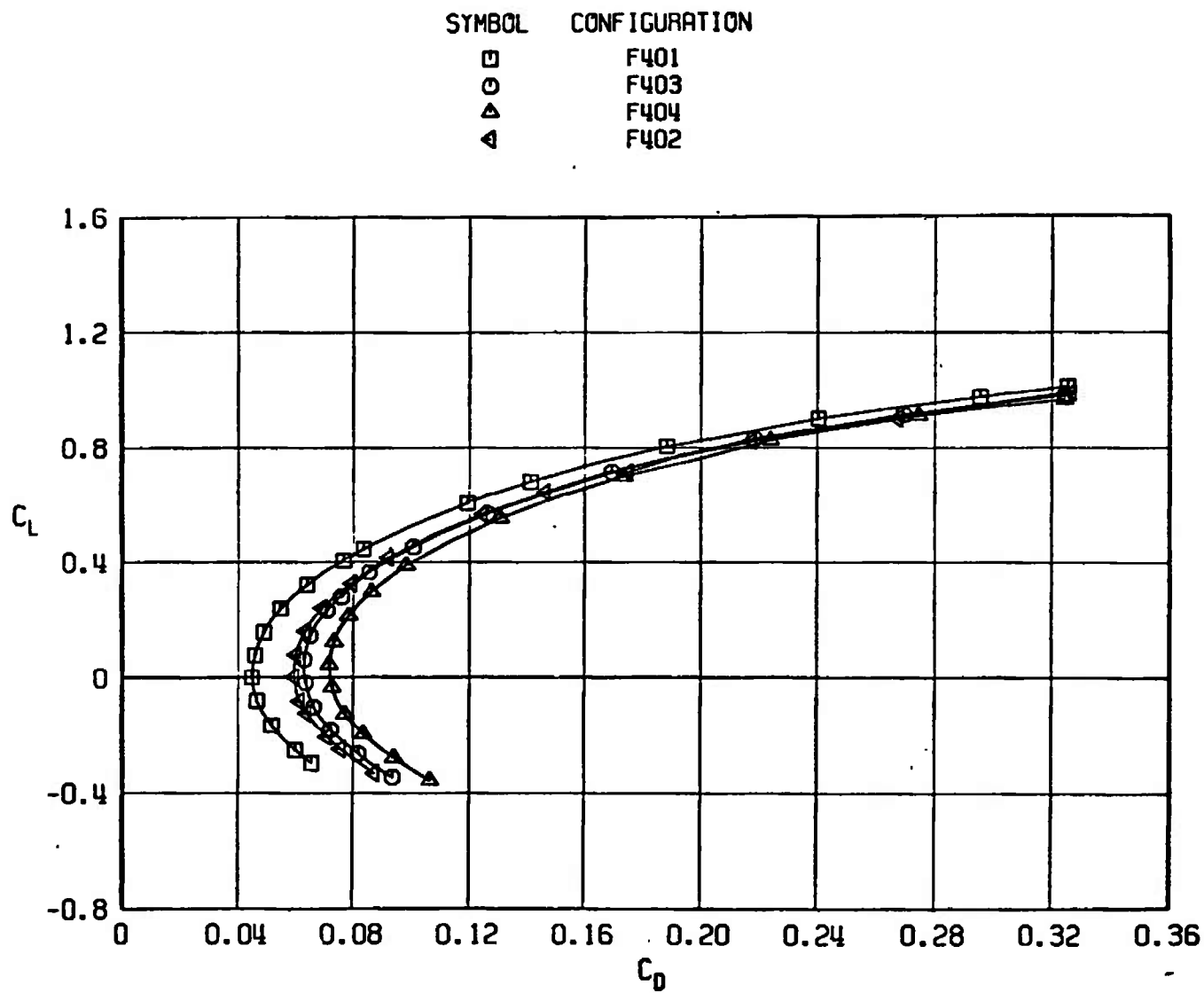


c.  $M_\infty = 0.95$   
Fig. 34 Continued

SYMBOL	CONFIGURATION
□	F401
○	F403
△	F404
◀	F402

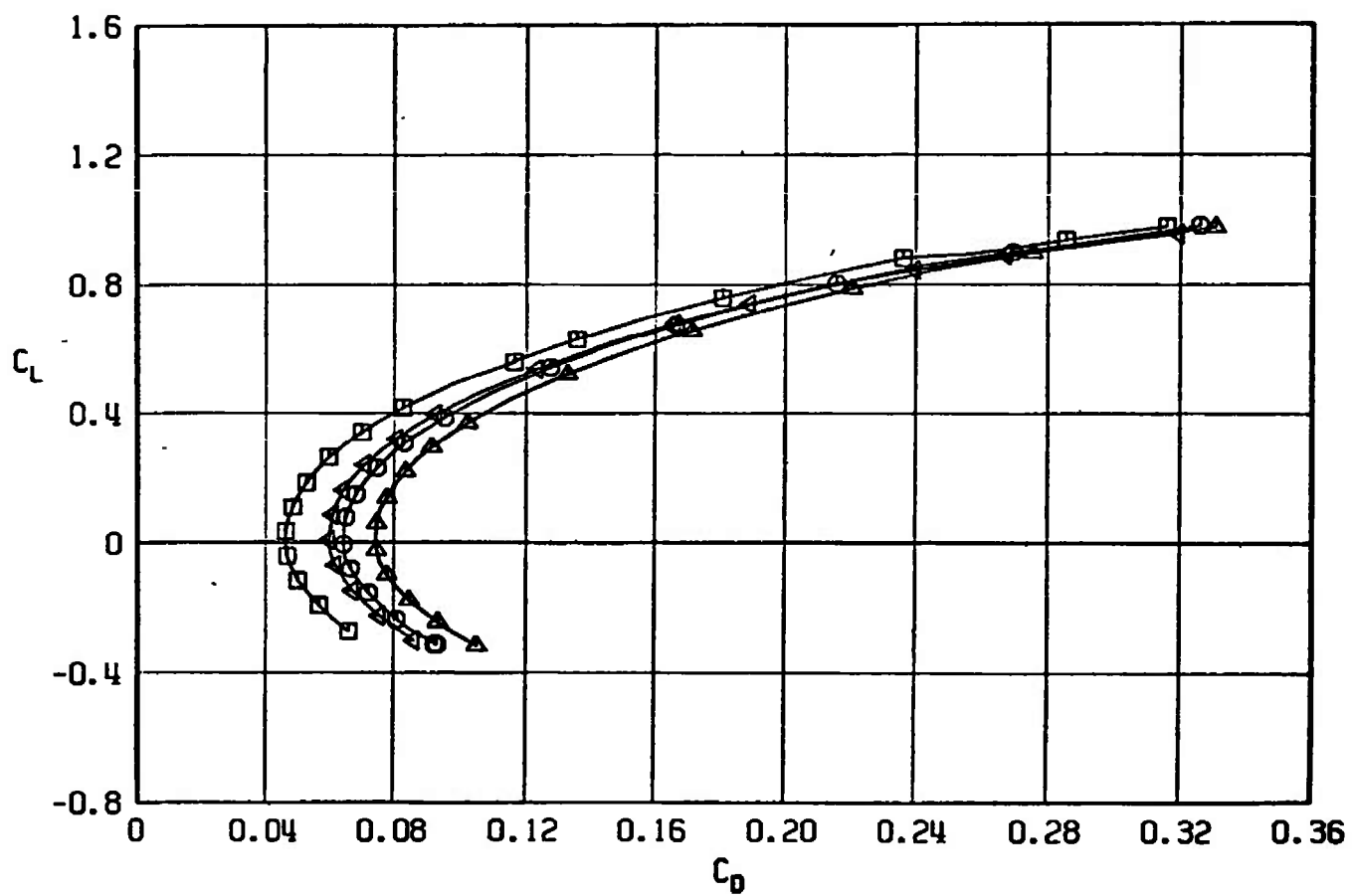


d.  $M_\infty = 1.05$   
Fig. 34 Continued



e.  $M_\infty = 1.10$   
Fig. 34 Continued

SYMBOL	CONFIGURATION
□	F401
○	F403
△	F404
▽	F402



f.  $M_\infty = 1.20$   
Fig. 34 Concluded

SYMBOL	CONFIGURATION
□	F401
○	F403
△	F404
◀	F402

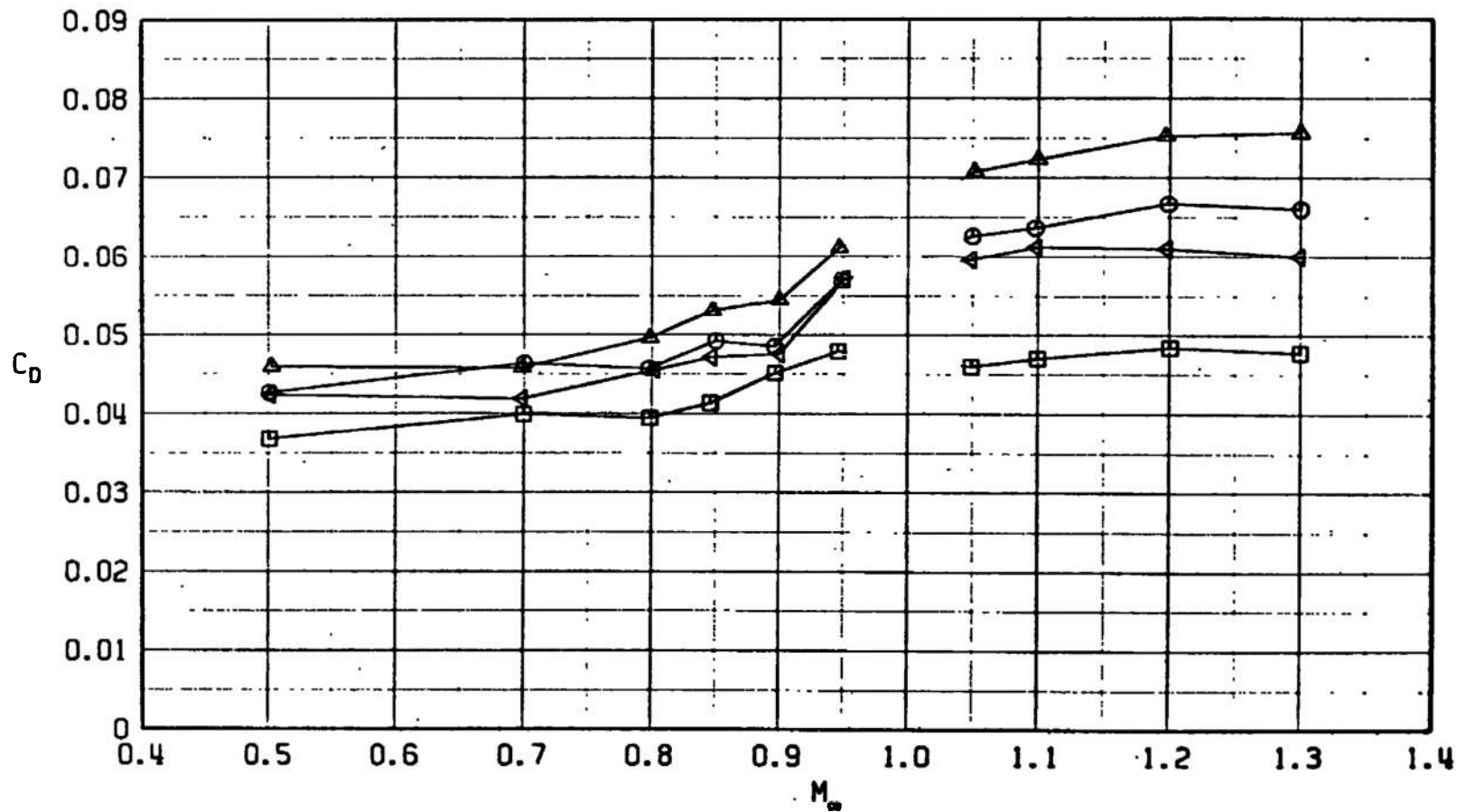
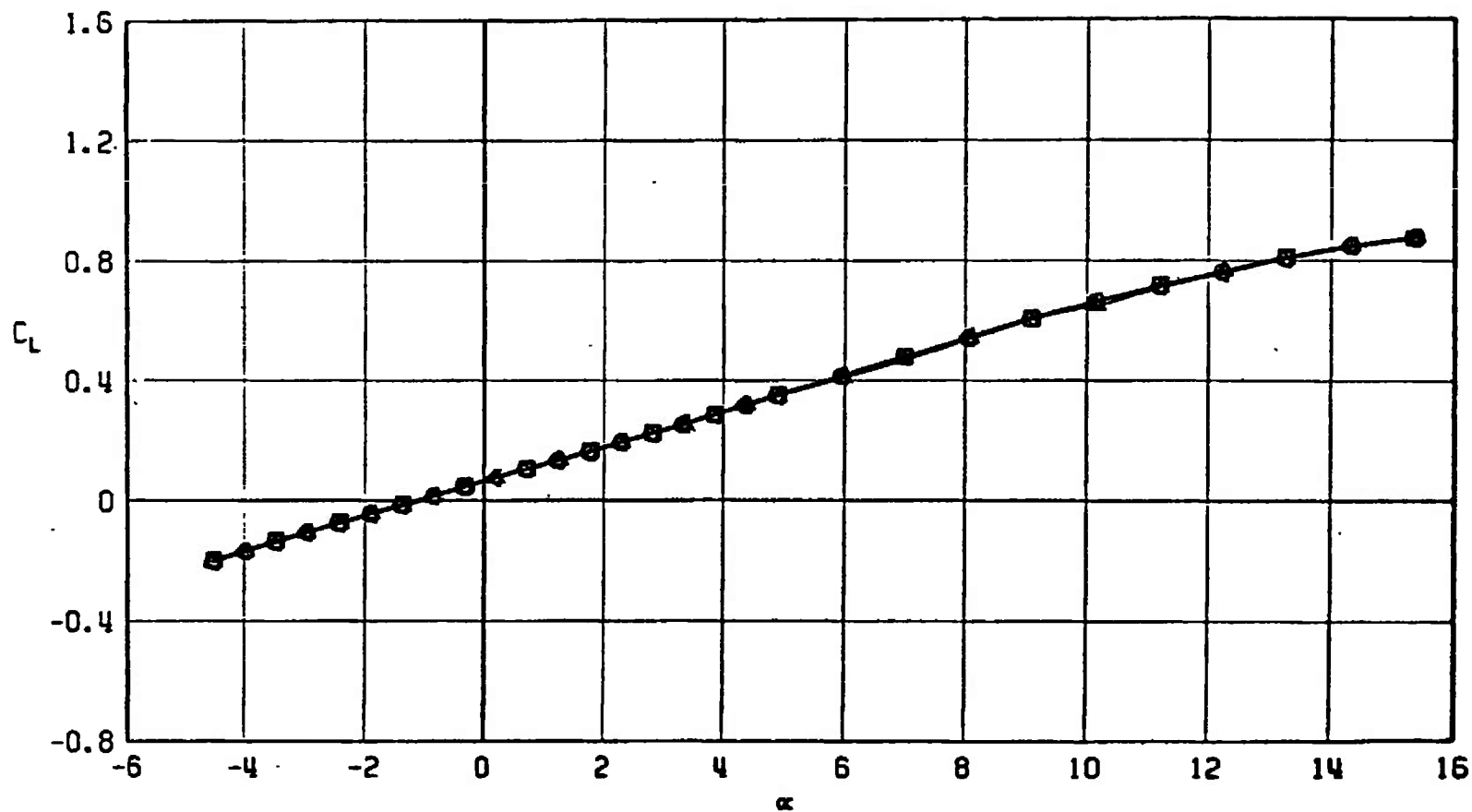


Fig. 35 Drag Coefficient Variation with Mach Number at  $C_L = 0.30$ ,  $M_\infty < 1.0$  and  $C_L = 0.1$ ,  $M_\infty > 1.0$  for Configurations F401, F402, F403, and F404



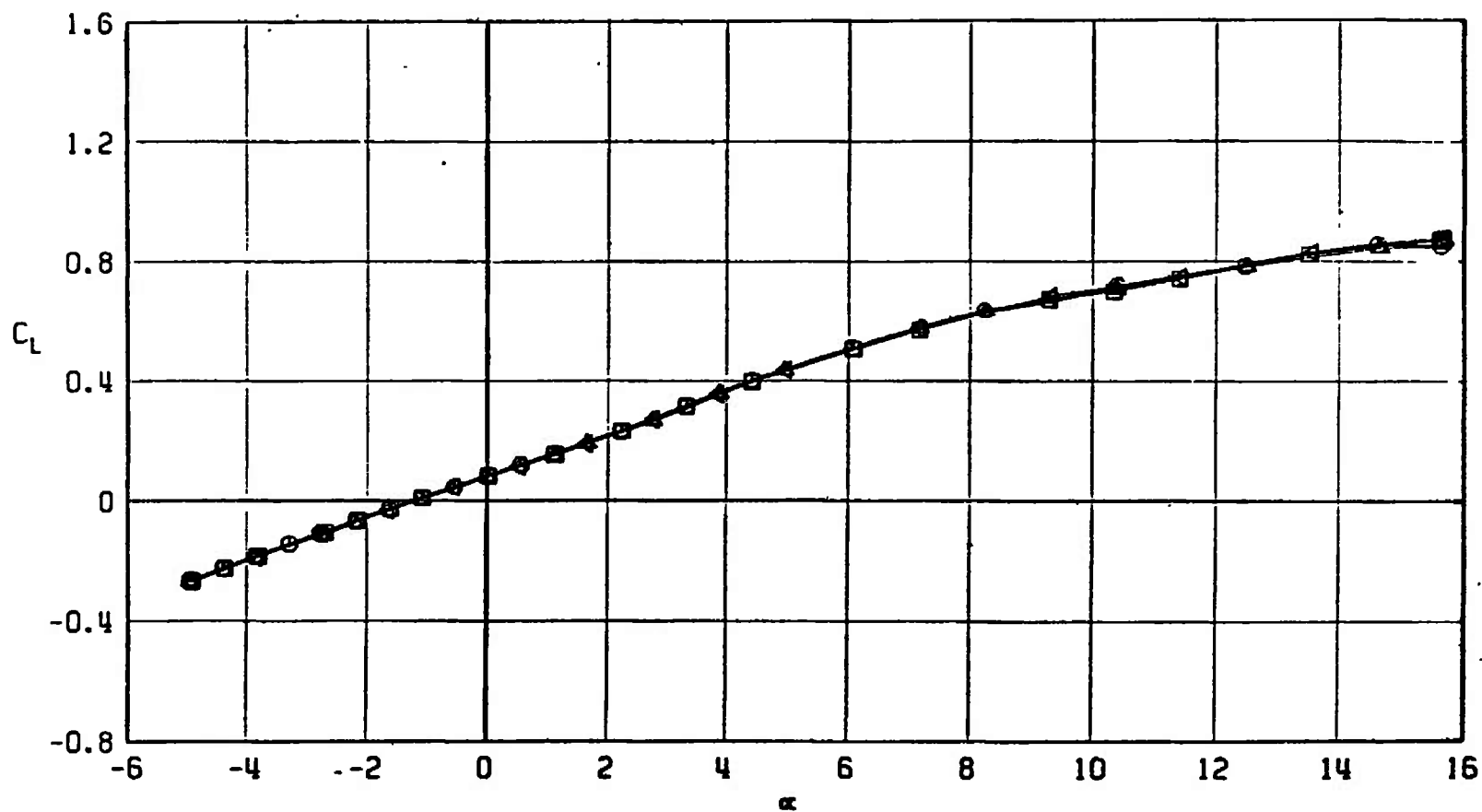
SYMBOL	CONFIGURATION
□	F401
○	F412
△	F418
▽	F415



a.  $M_\infty = 0.50$

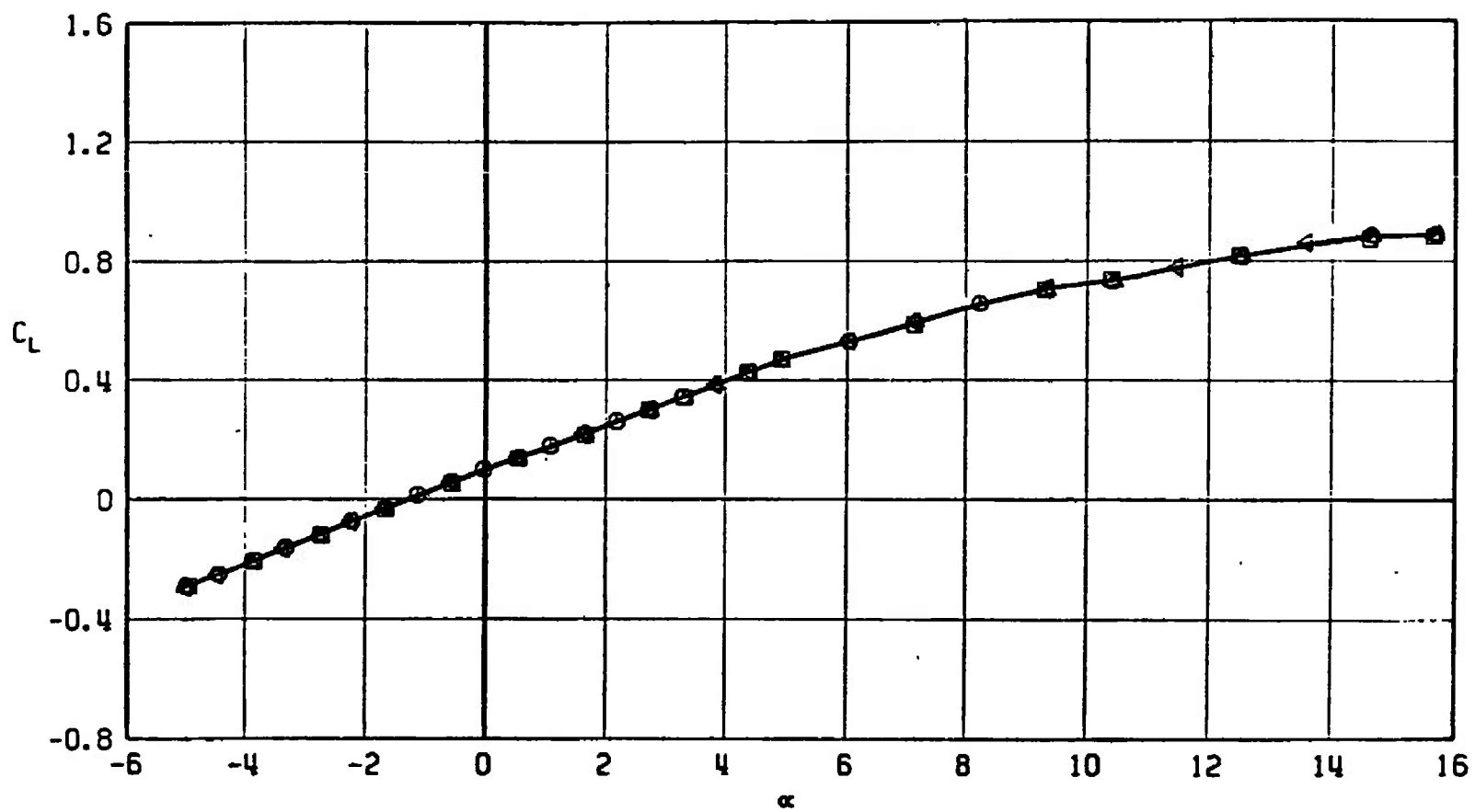
Fig. 36 Lift Coefficient Variation with Angle of Attack for Configurations F401, F412, F415, and F418

SYMBOL	CONFIGURATION
□	F401
○	F412
△	F418
◀	F415



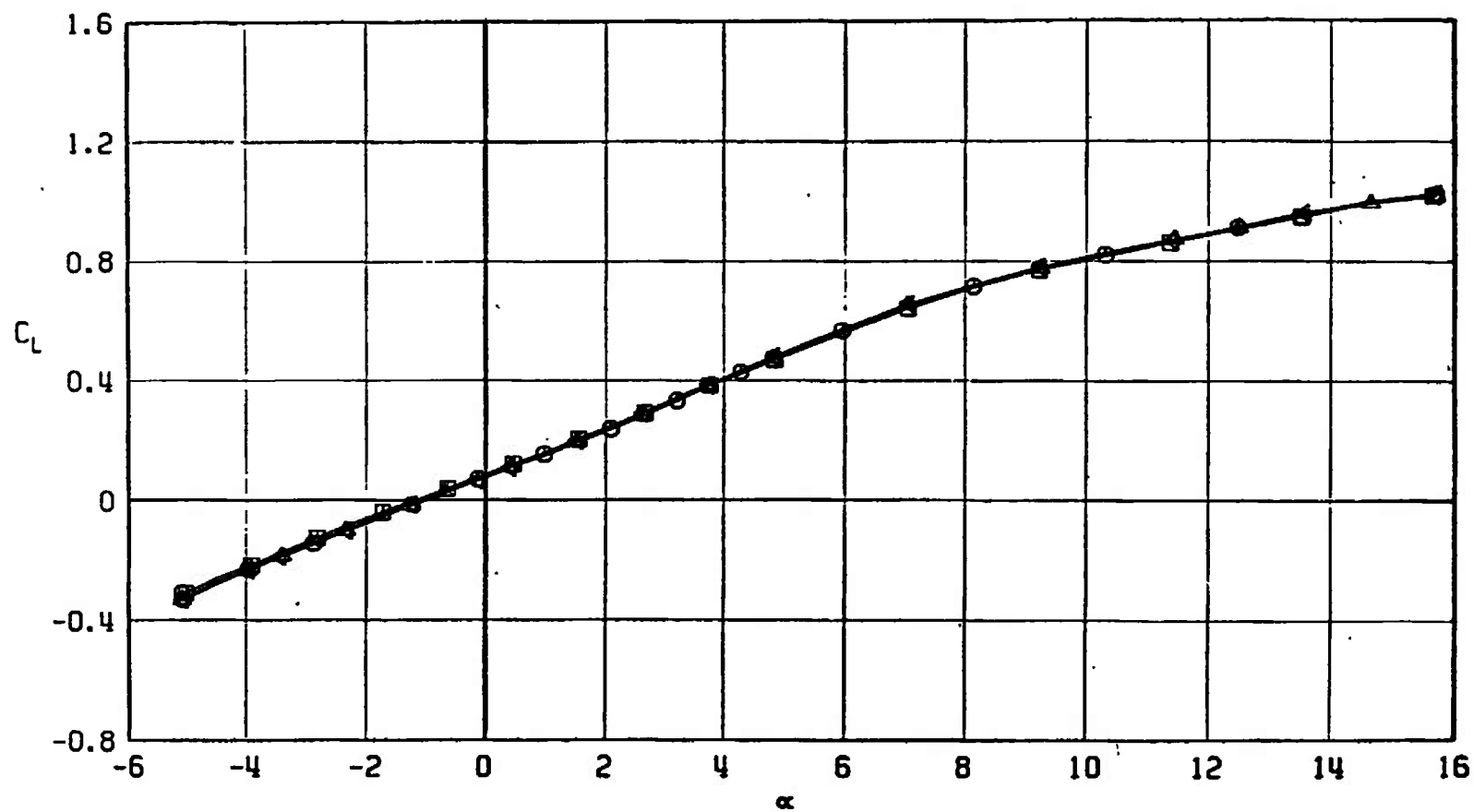
b.  $M_\infty = 0.90$   
Fig. 36 Continued

SYMBOL	CONFIGURATION
□	F401
○	F412
△	F418
▽	F415



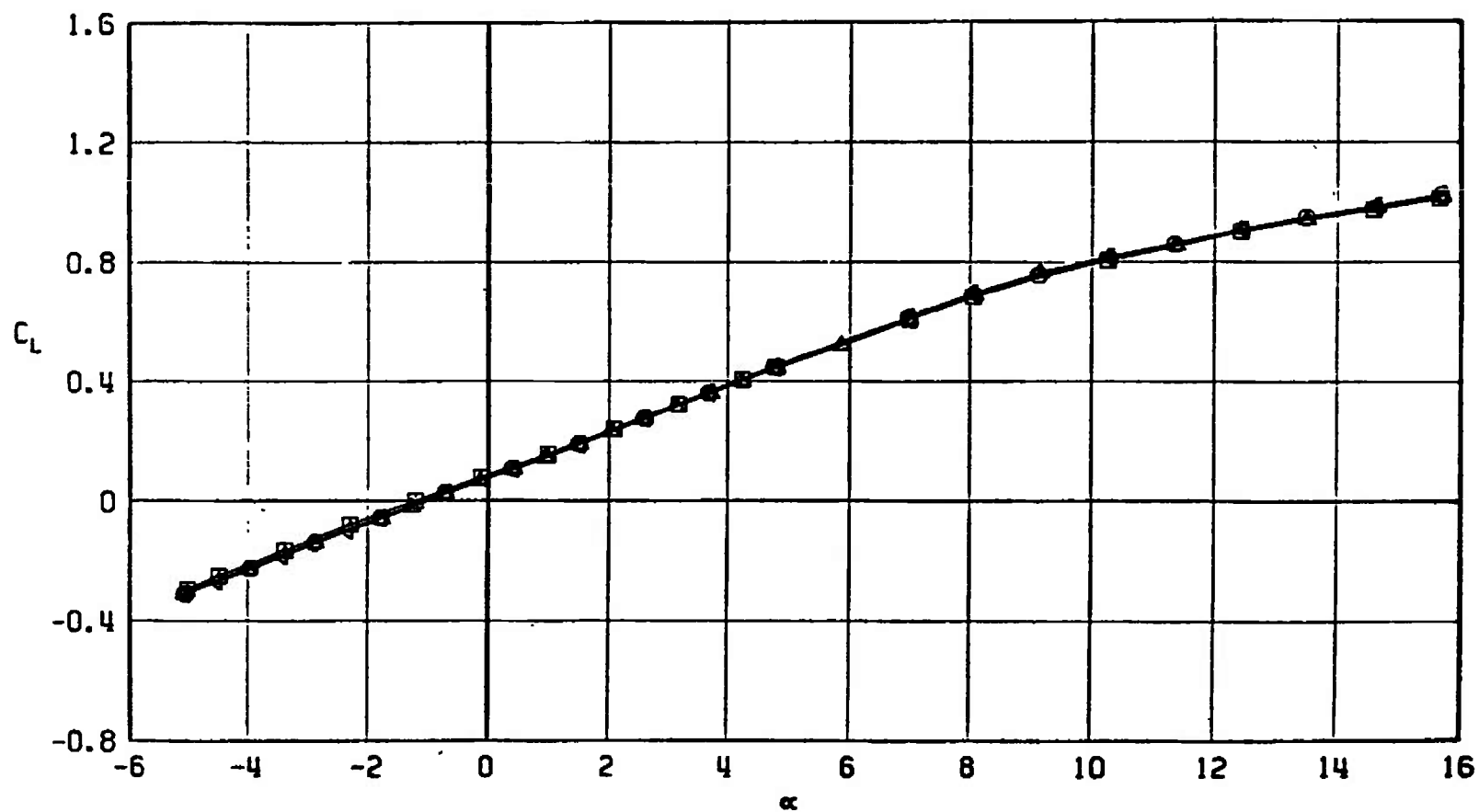
c.  $M_\infty = 0.95$   
Fig. 36 Continued

SYMBOL	CONFIGURATION
□	F401
○	F412
△	F418
◊	F415



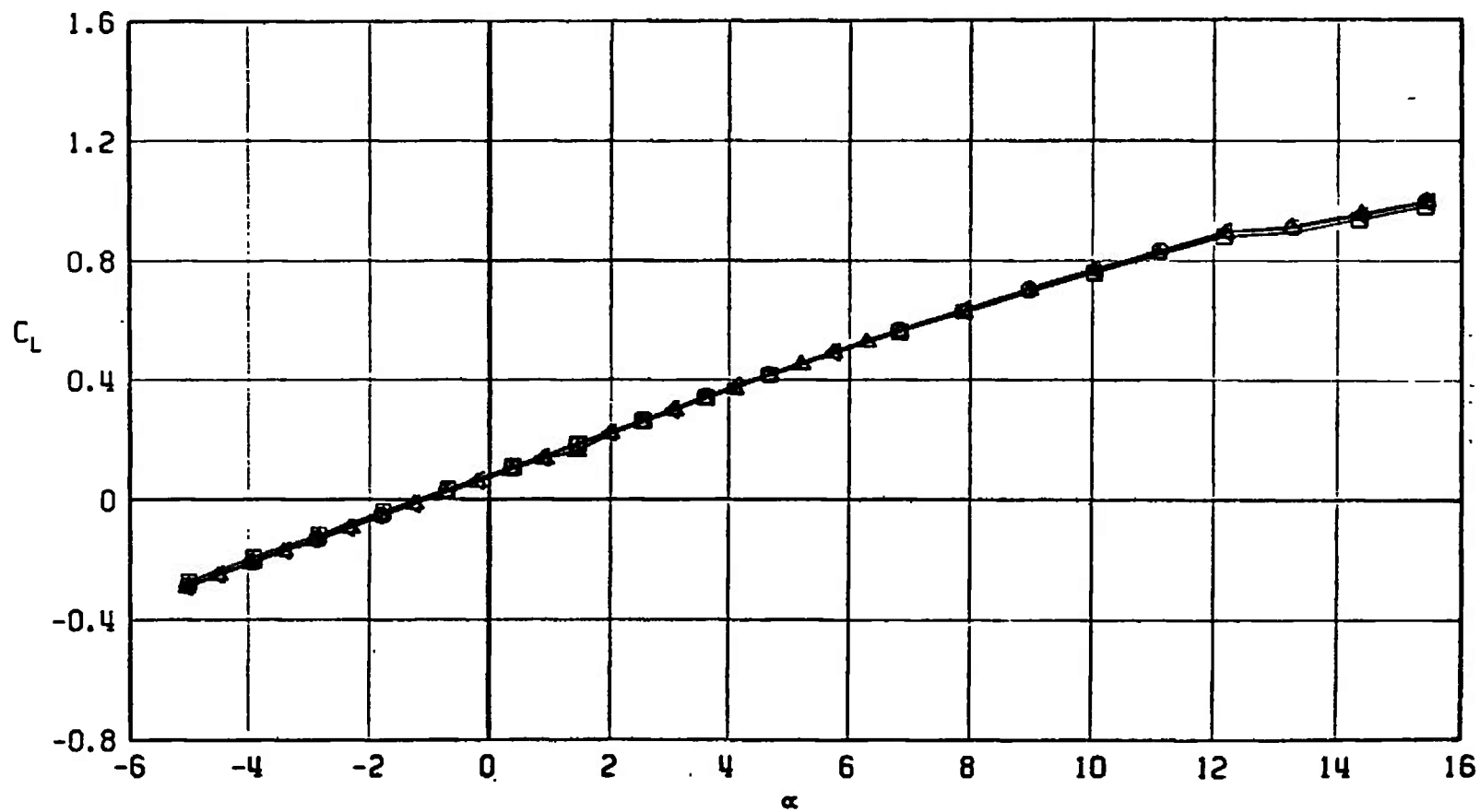
d.  $M_\infty = 1.05$   
Fig. 36 Continued

SYMBOL	CONFIGURATION
□	F401
△	F412
▽	F418
△	F415



e.  $M_\infty = 1.10$   
Fig. 36 Continued

SYMBOL	CONFIGURATION
□	F401
○	F412
△	F418
◊	F415



f.  $M_\infty = 1.20$   
Fig. 36 Concluded

SYMBOL CONFIGURATION

□	F401
○	F412
△	F418
▽	F415

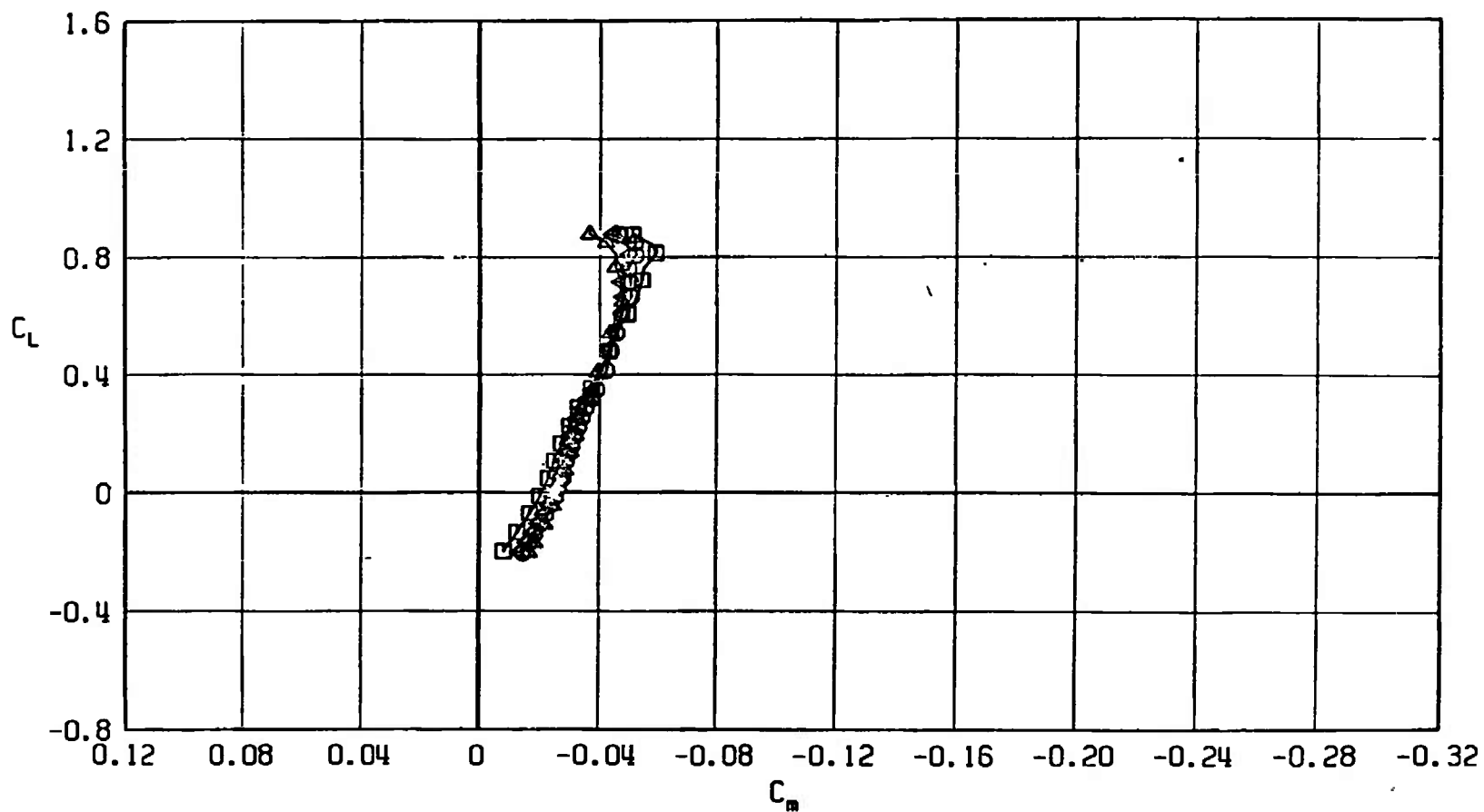
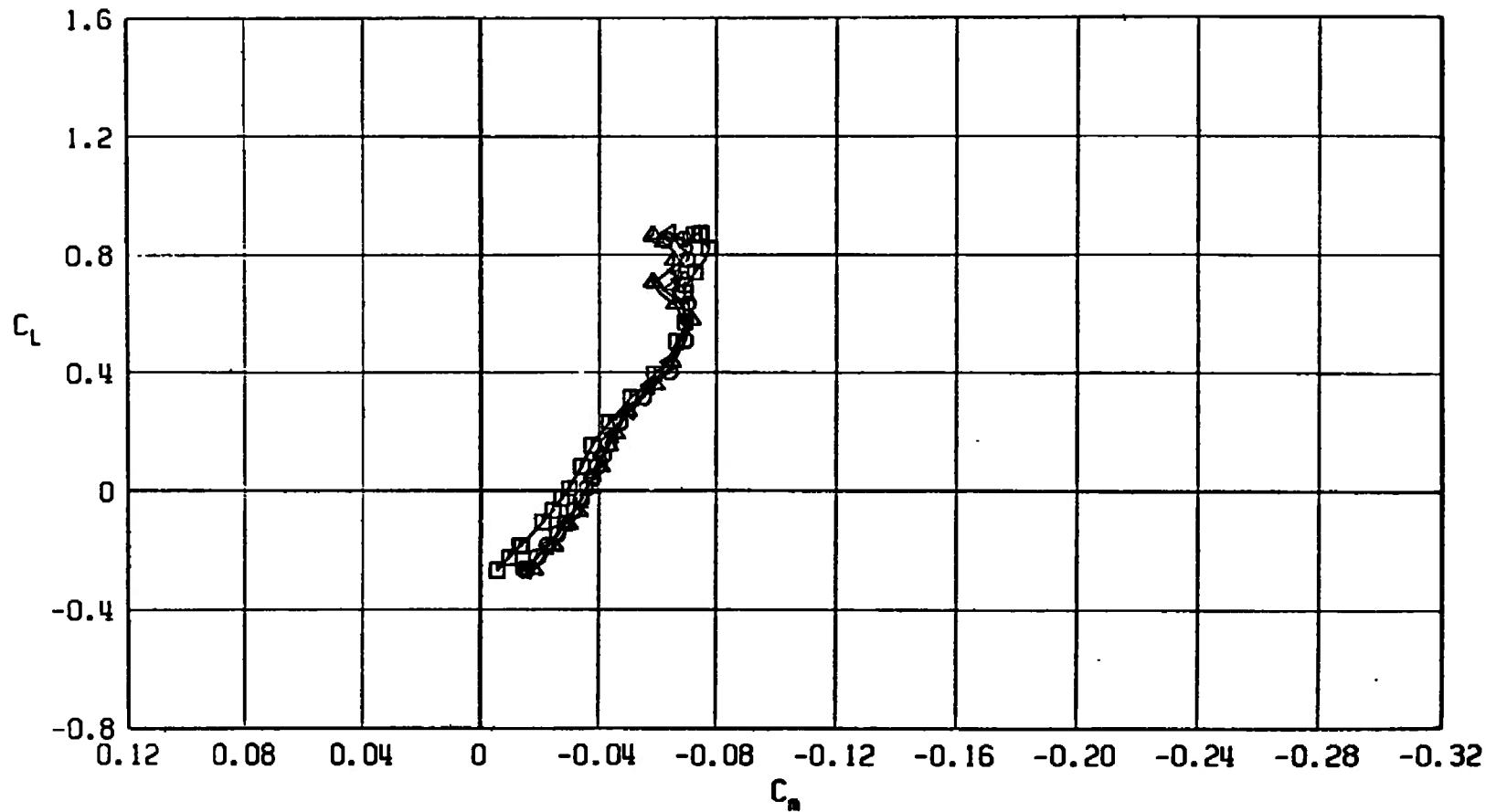
a.  $M_\infty = 0.50$ 

Fig. 37 Pitching-Moment Coefficient Variation with Lift Coefficient for Configurations F401, F412, F415, and F418.

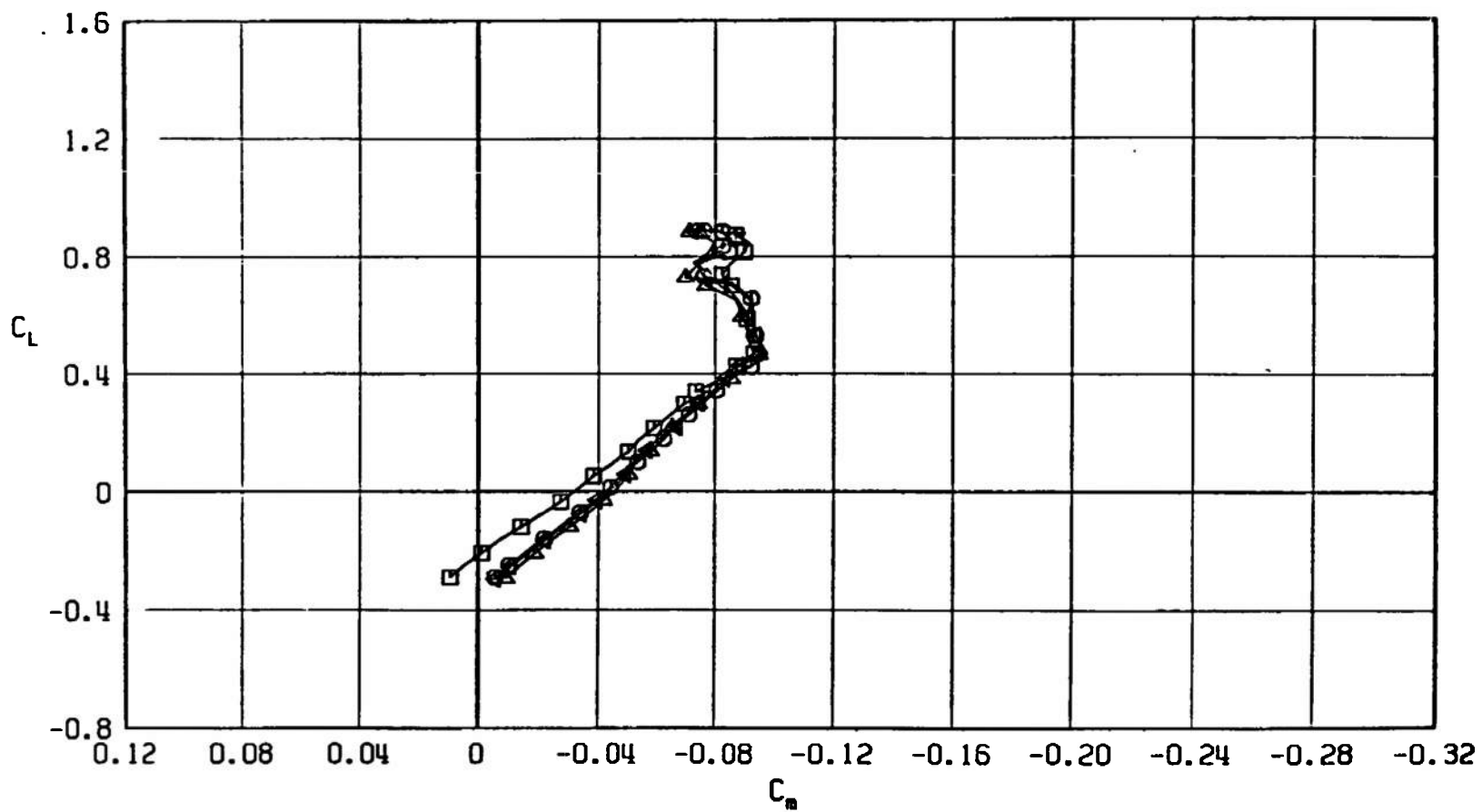
SYMBOL	CONFIGURATION
□	F401
○	F412
△	F418
◀	F415



b.  $M_\infty = 0.90$   
Fig. 37 Continued

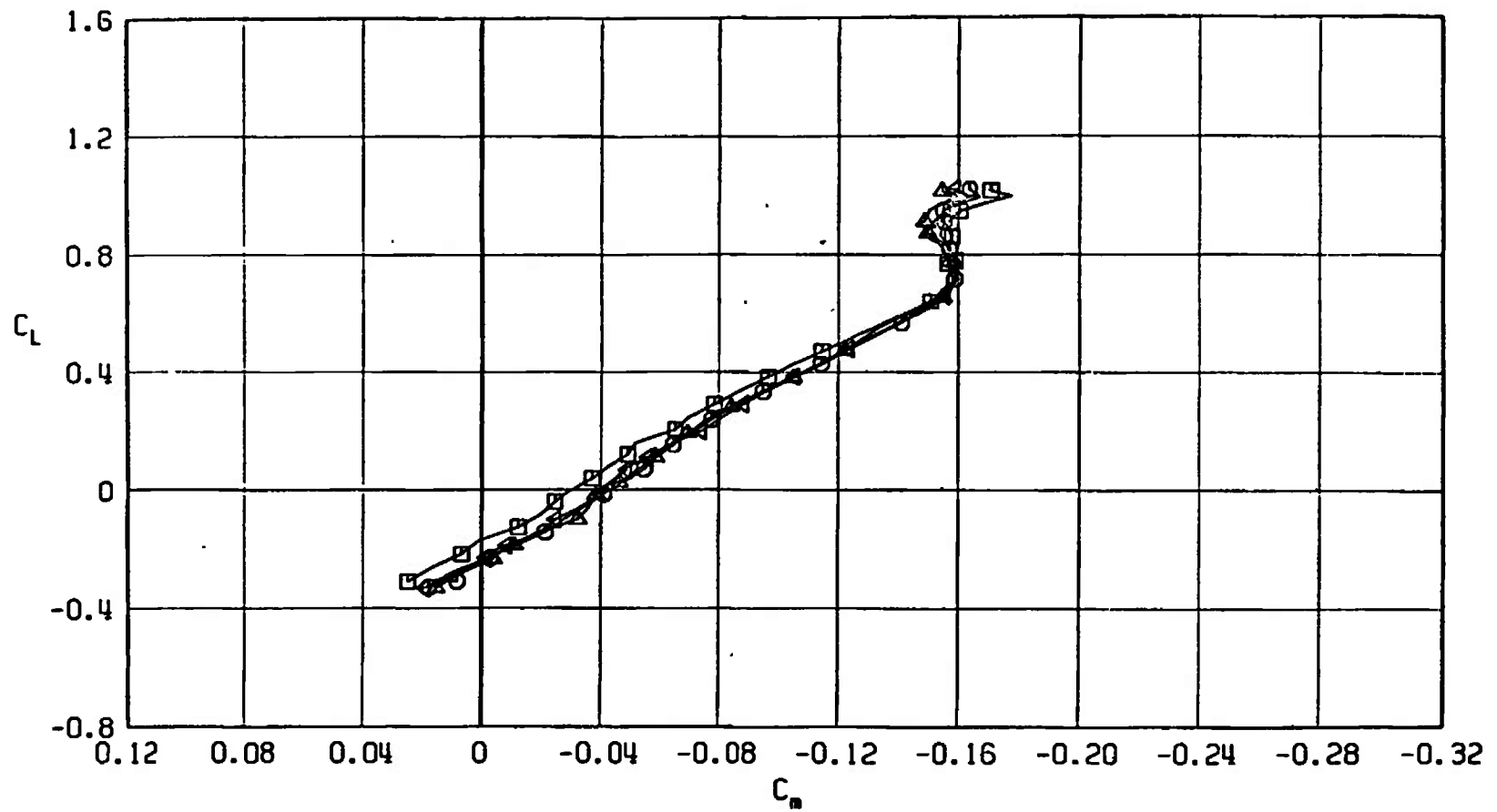


SYMBOL	CONFIGURATION
□	F401
○	F412
△	F418
▽	F415



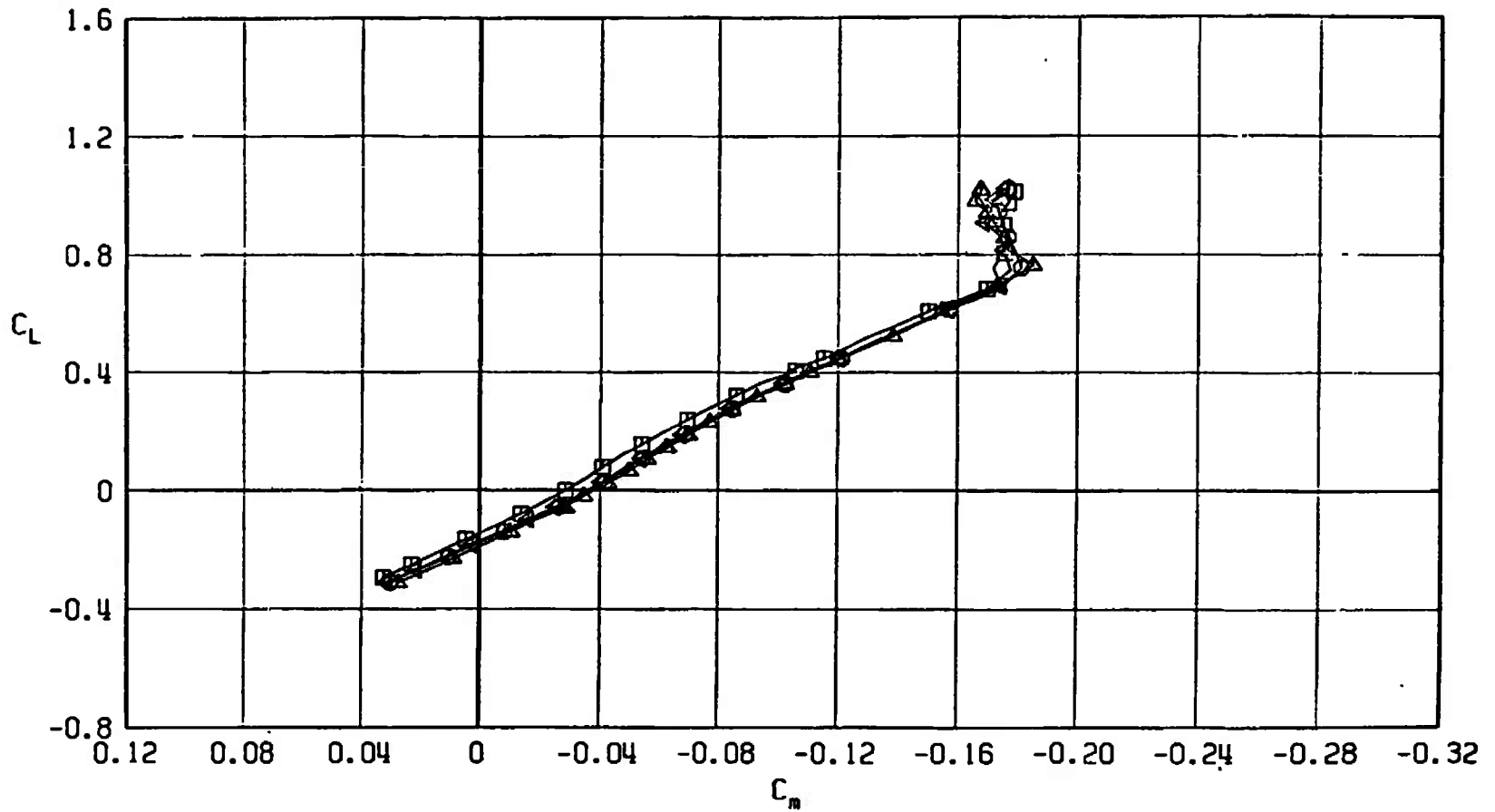
c.  $M_\infty = 0.95$   
Fig. 37 Continued

SYMBOL	CONFIGURATION
□	F401
○	F412
△	F418
▽	F415



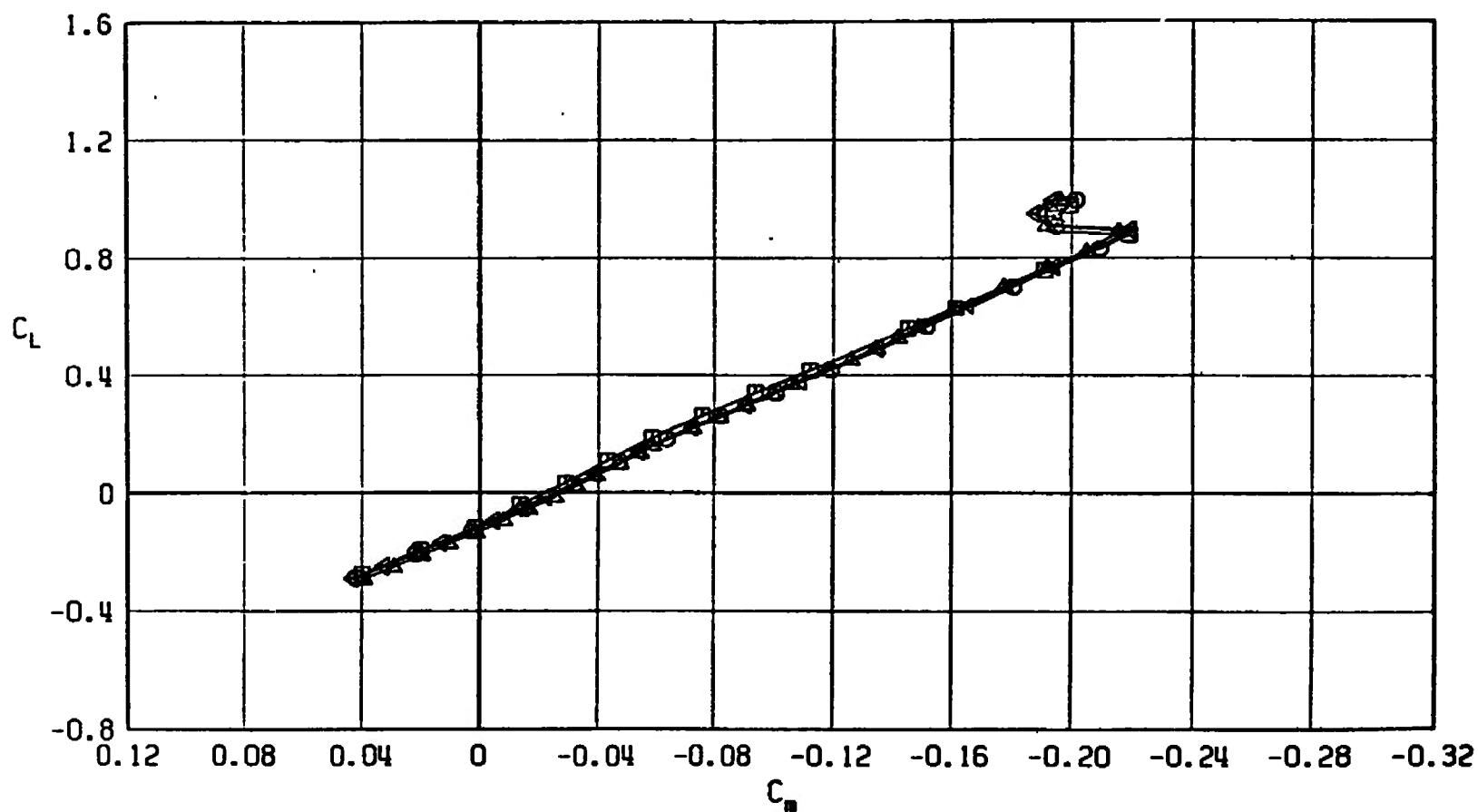
d.  $M_\infty = 1.05$   
Fig. 37 Continued

SYMBOL	CONFIGURATION
□	F401
○	F412
△	F418
▽	F415



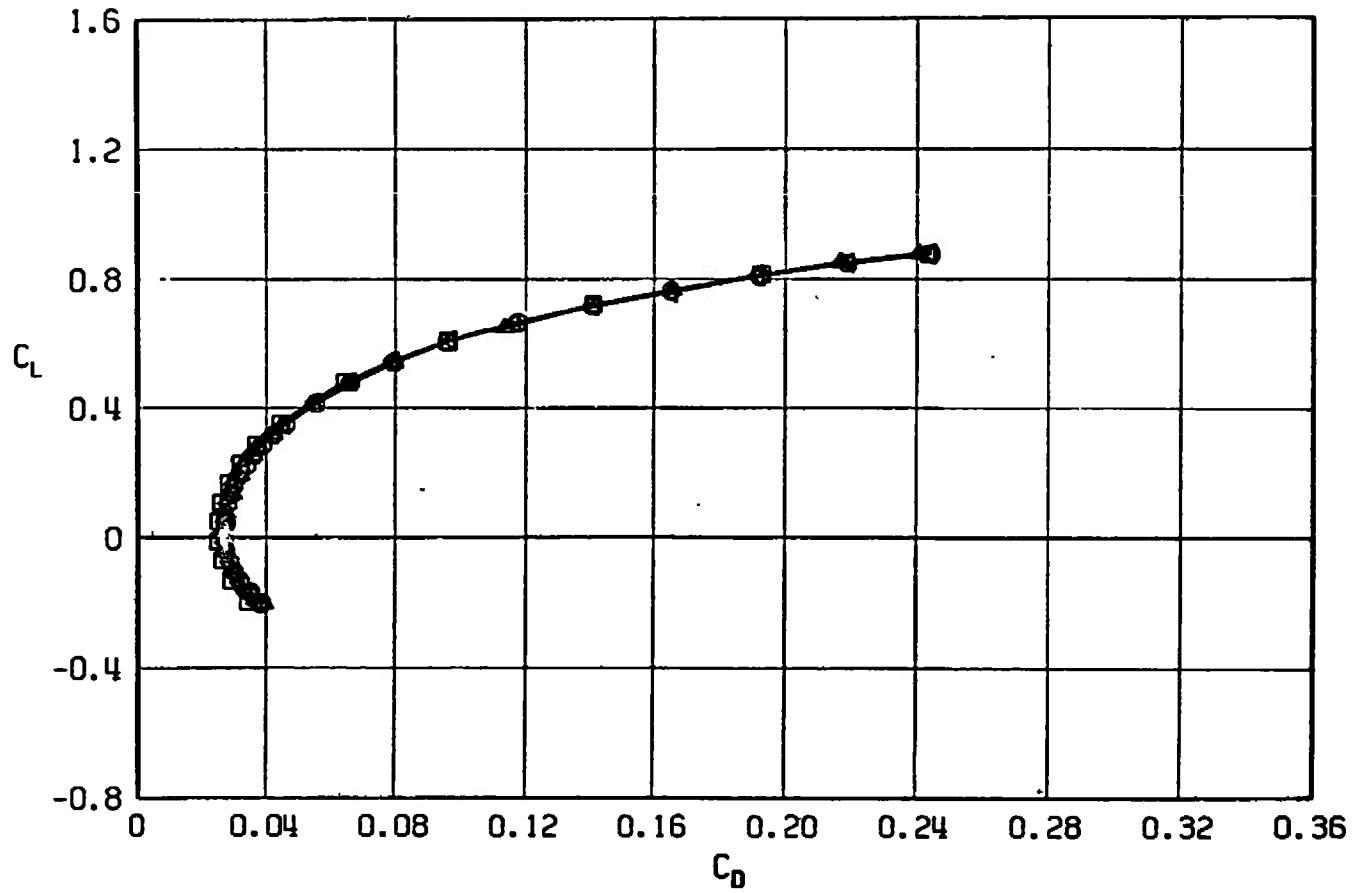
e.  $M_\infty = 1.10$   
Fig. 37 Continued

SYMBOL	CONFIGURATION
□	F401
○	F412
△	F418
▽	F415



f.  $M_\infty = 1.20$   
Fig. 37 Concluded

SYMBOL	CONFIGURATION
□	F401
○	F412
△	F418
▽	F415

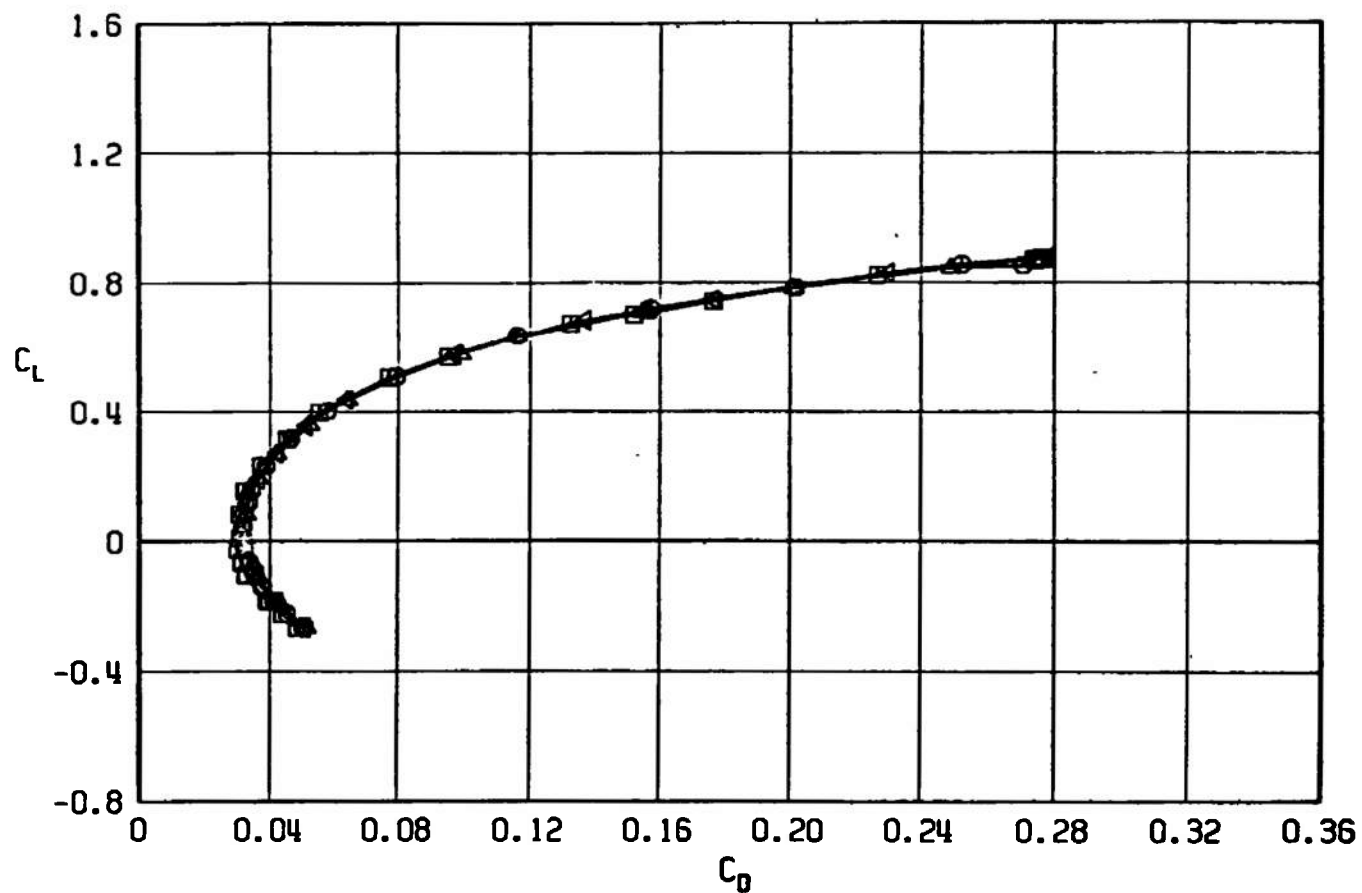


a.  $M_\infty = 0.50$

Fig. 38 Drag Coefficient Variation with Lift Coefficient for Configurations F401, F412, F415, and F418

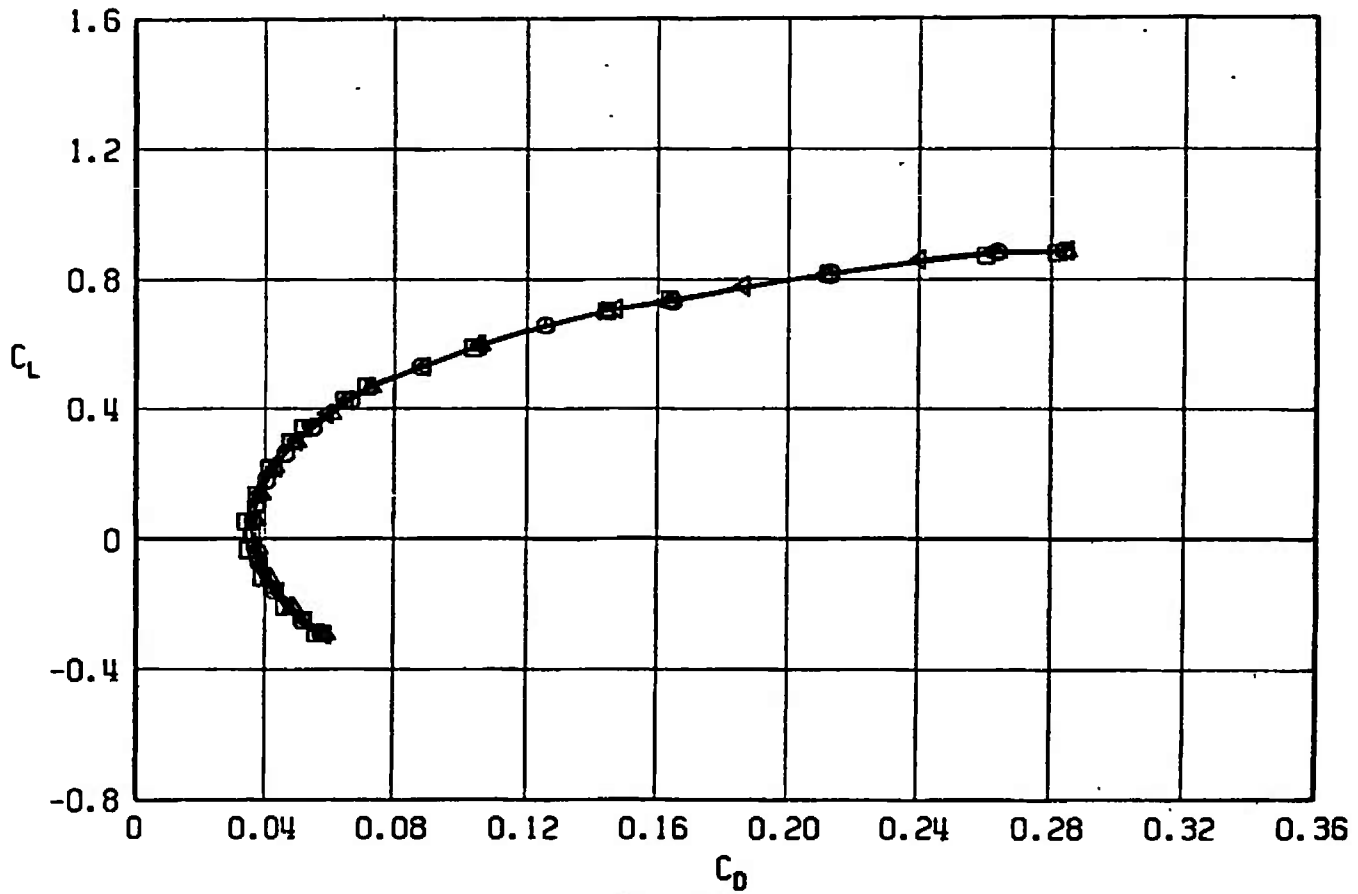
SYMBOL	CONFIGURATION
--------	---------------

□	F401
○	F412
△	F418
▽	F415



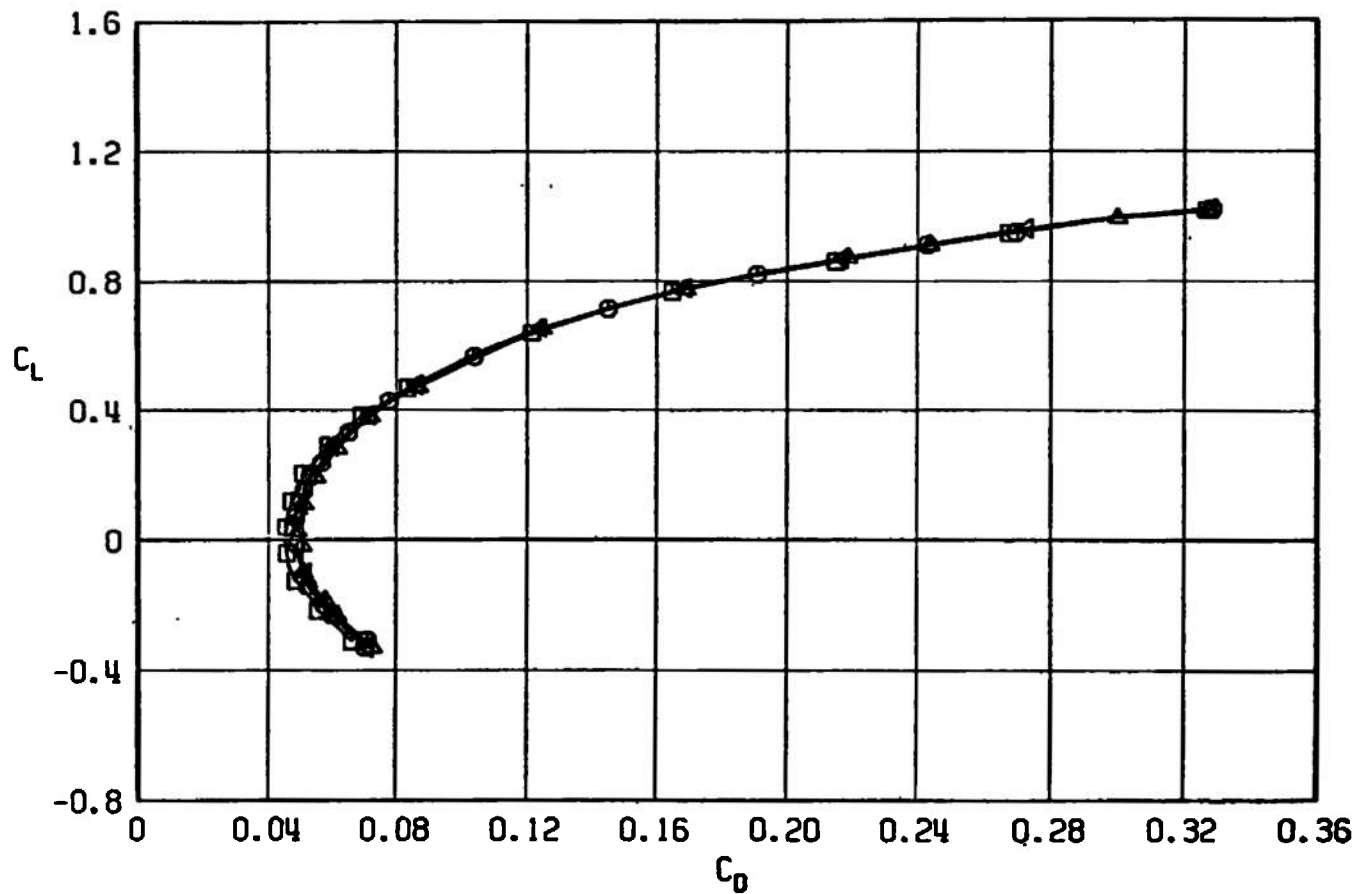
b.  $M_\infty = 0.90$   
Fig. 38 Continued

SYMBOL	CONFIGURATION
□	F401
○	F412
△	F418
▽	F415



c.  $M_\infty = 0.95$   
Fig. 38 Continued

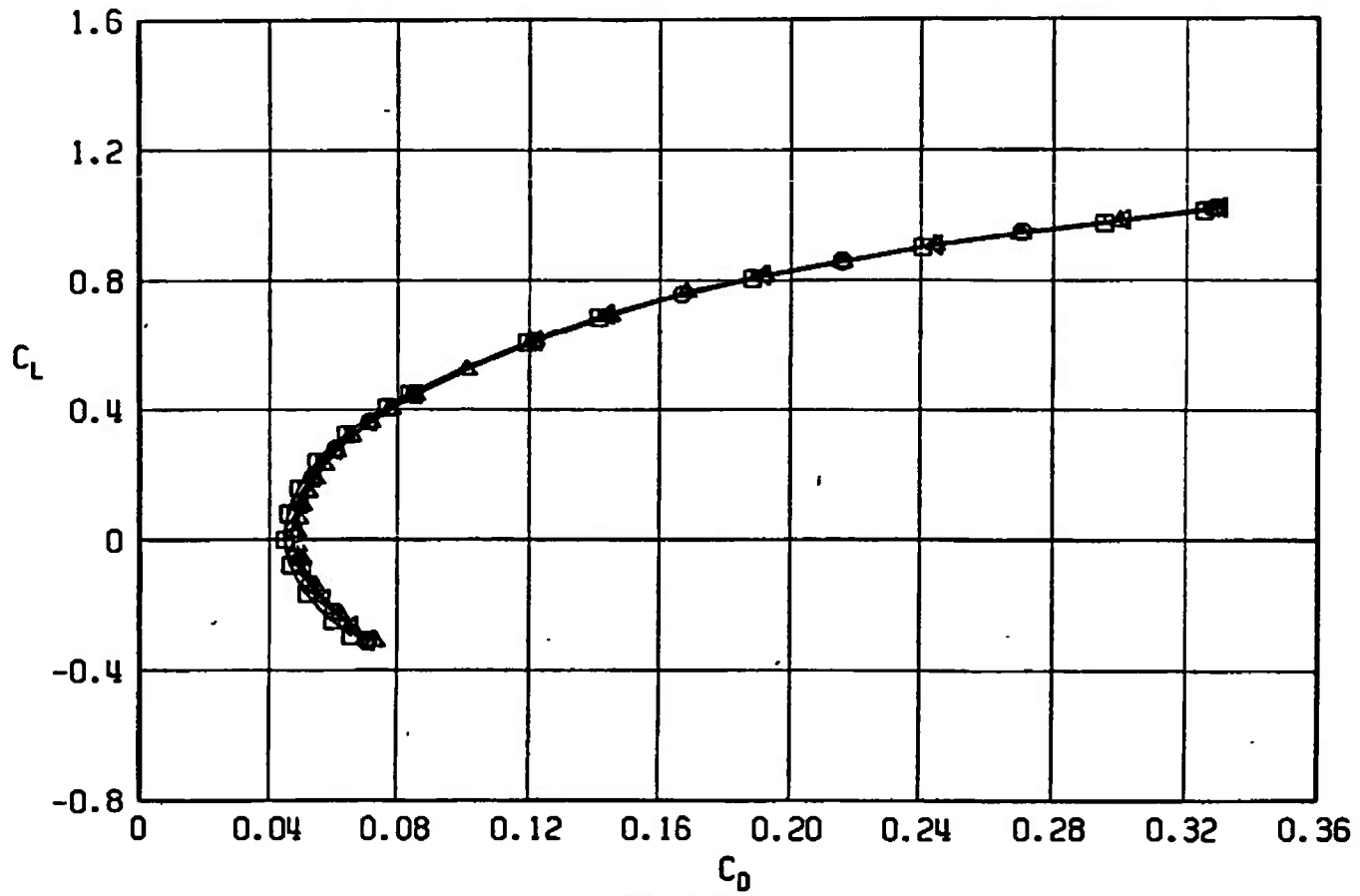
SYMBOL	CONFIGURATION
□	F401
○	F412
△	F418
▽	F415



d.  $M_\infty = 1.05$   
Fig. 38 Continued

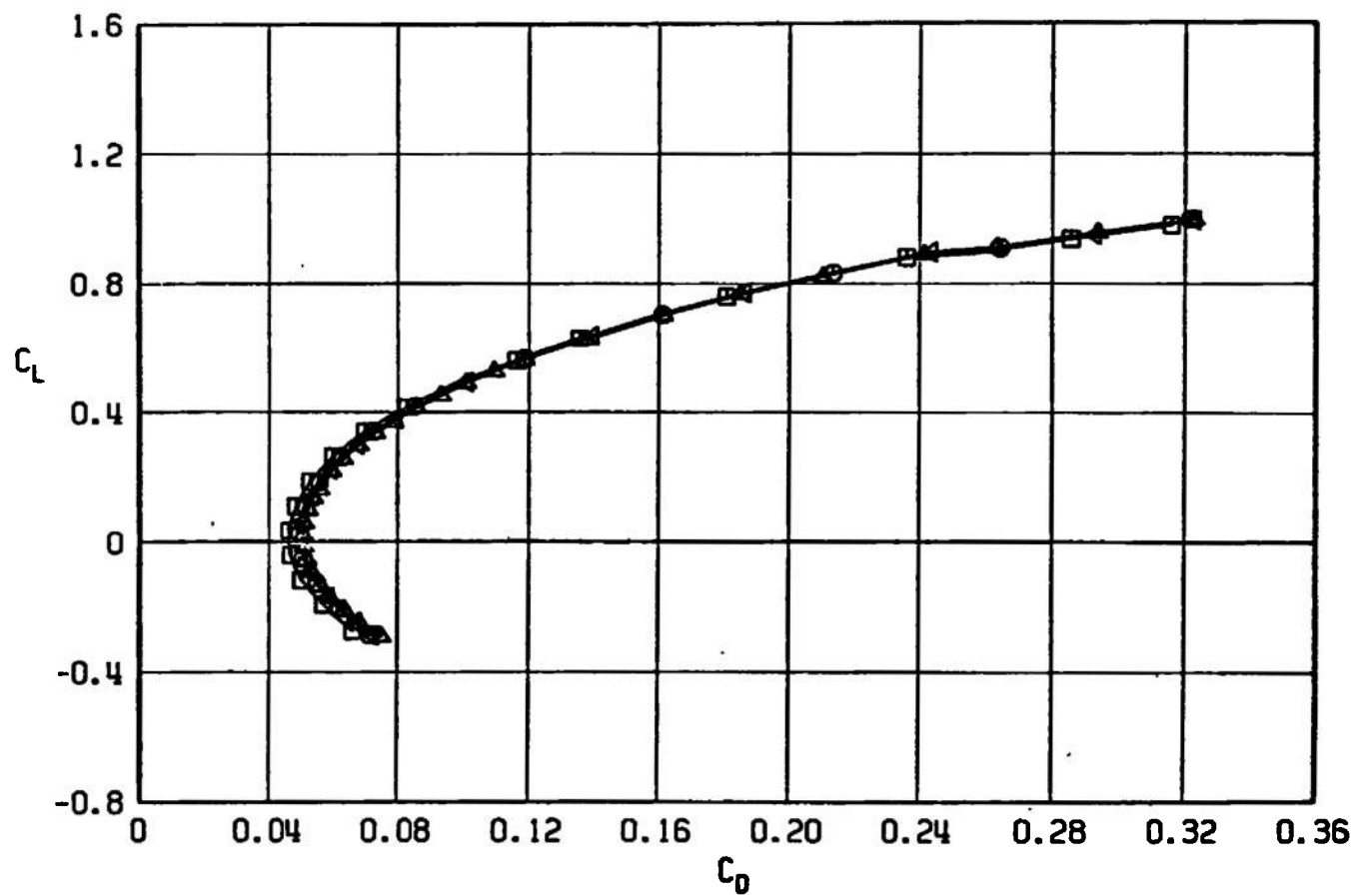


SYMBOL	CONFIGURATION
□	F401
○	F412
△	F418
▽	F415



e.  $M_\infty = 1.10$   
Fig. 38 Continued

SYMBOL	CONFIGURATION
□	F401
○	F412
△	F418
◀	F415



f.  $M_\infty = 1.20$   
Fig. 38 Concluded

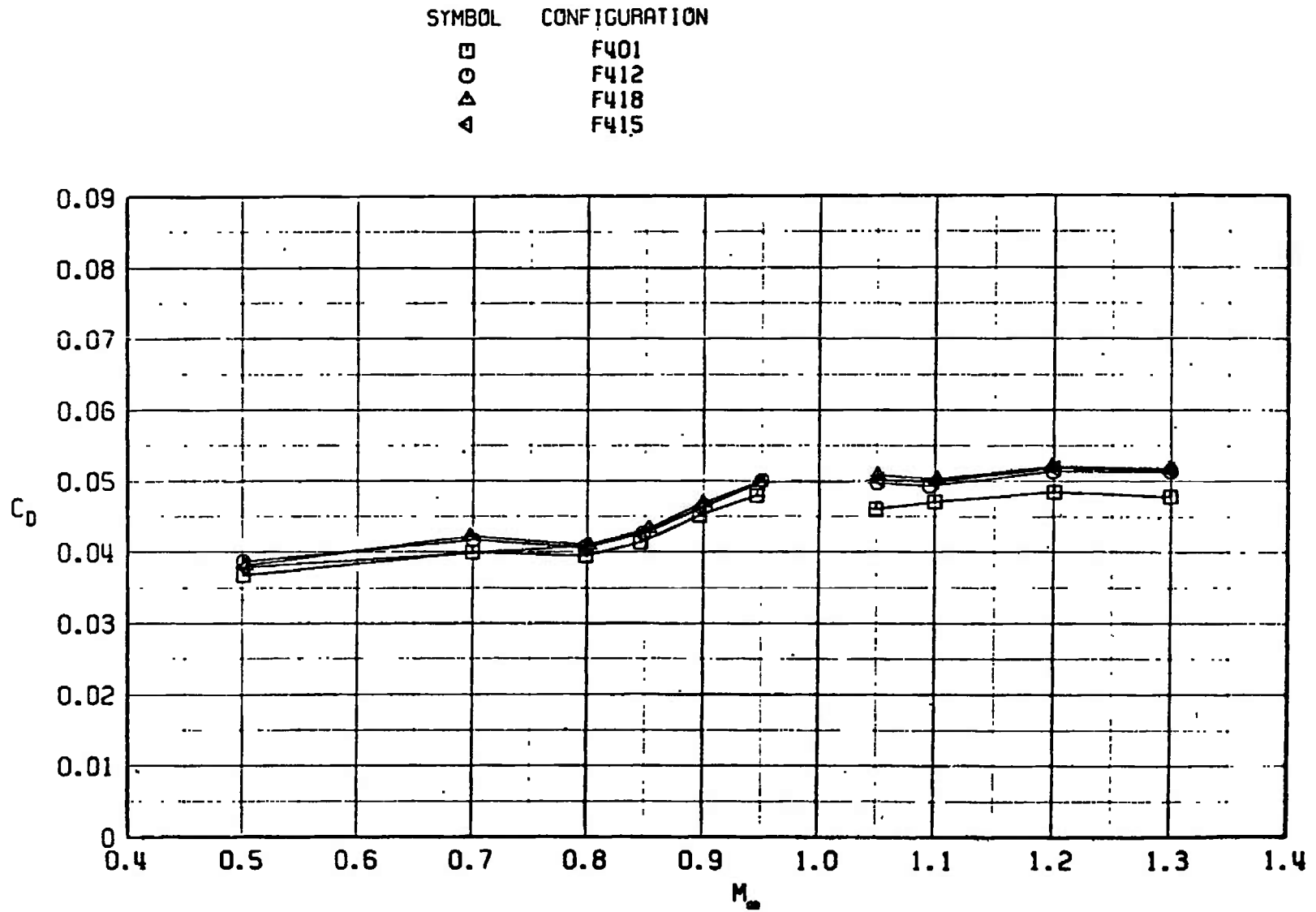
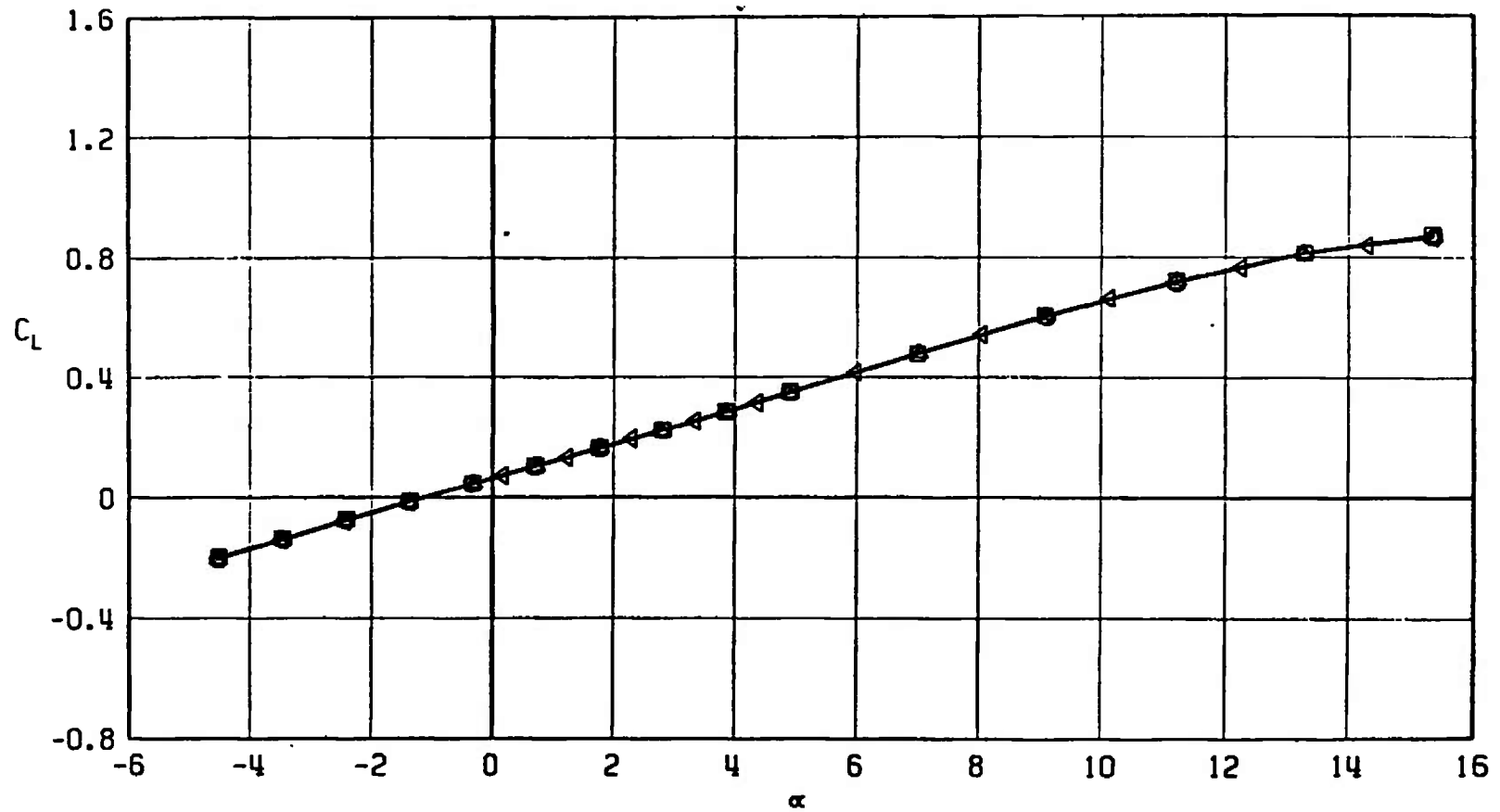


Fig. 39 Drag Coefficient Variation with Mach Number at  $C_L = 0.30$ ,  $M_\infty < 1.0$  and  $C_L = 0.1$ ,  $M_\infty > 1.0$  for Configurations F401, F412, F415, and F418

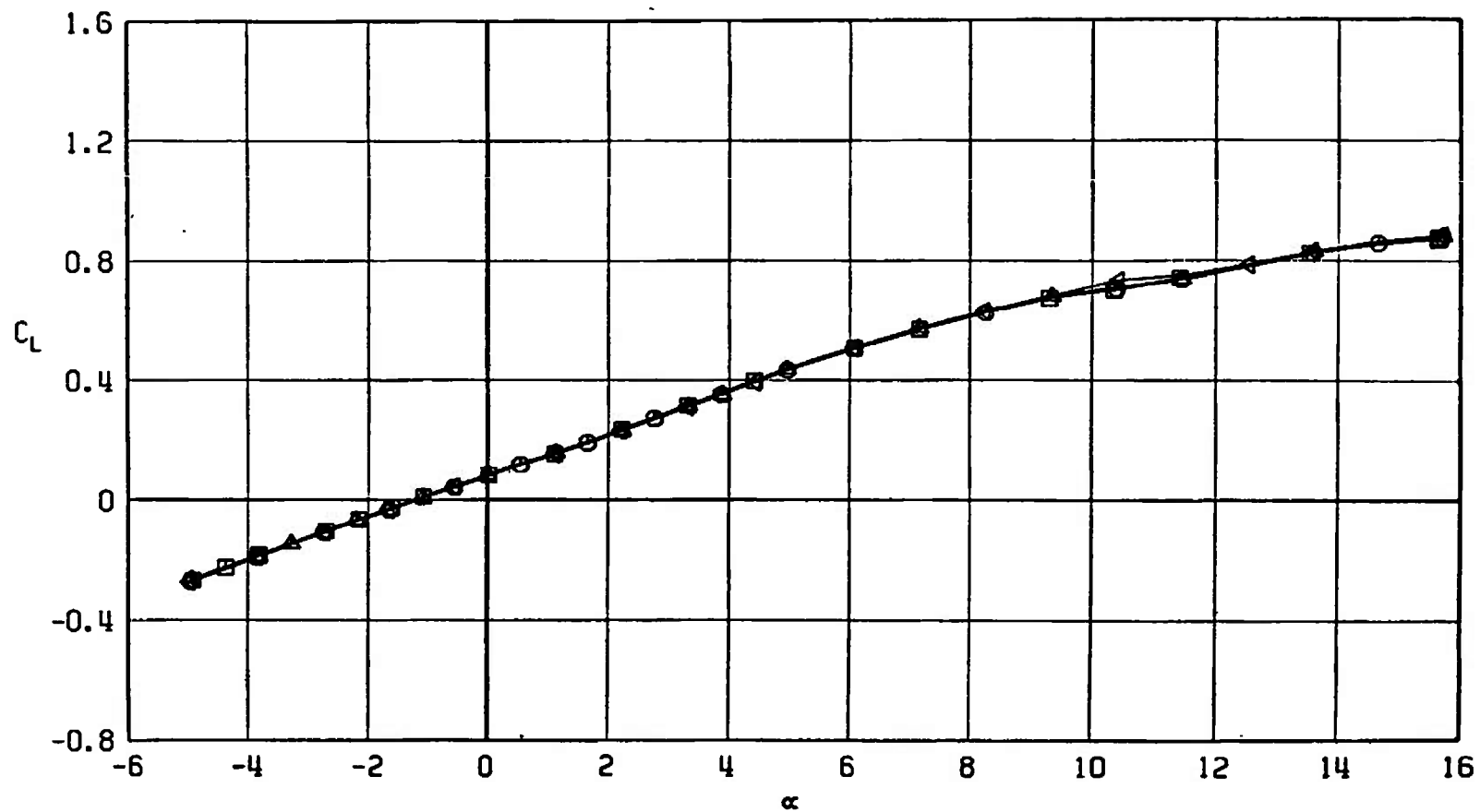
SYMBOL	CONFIGURATION
□	F401
○	F406
△	F407
◁	F405



a.  $M_\infty = 0.50$

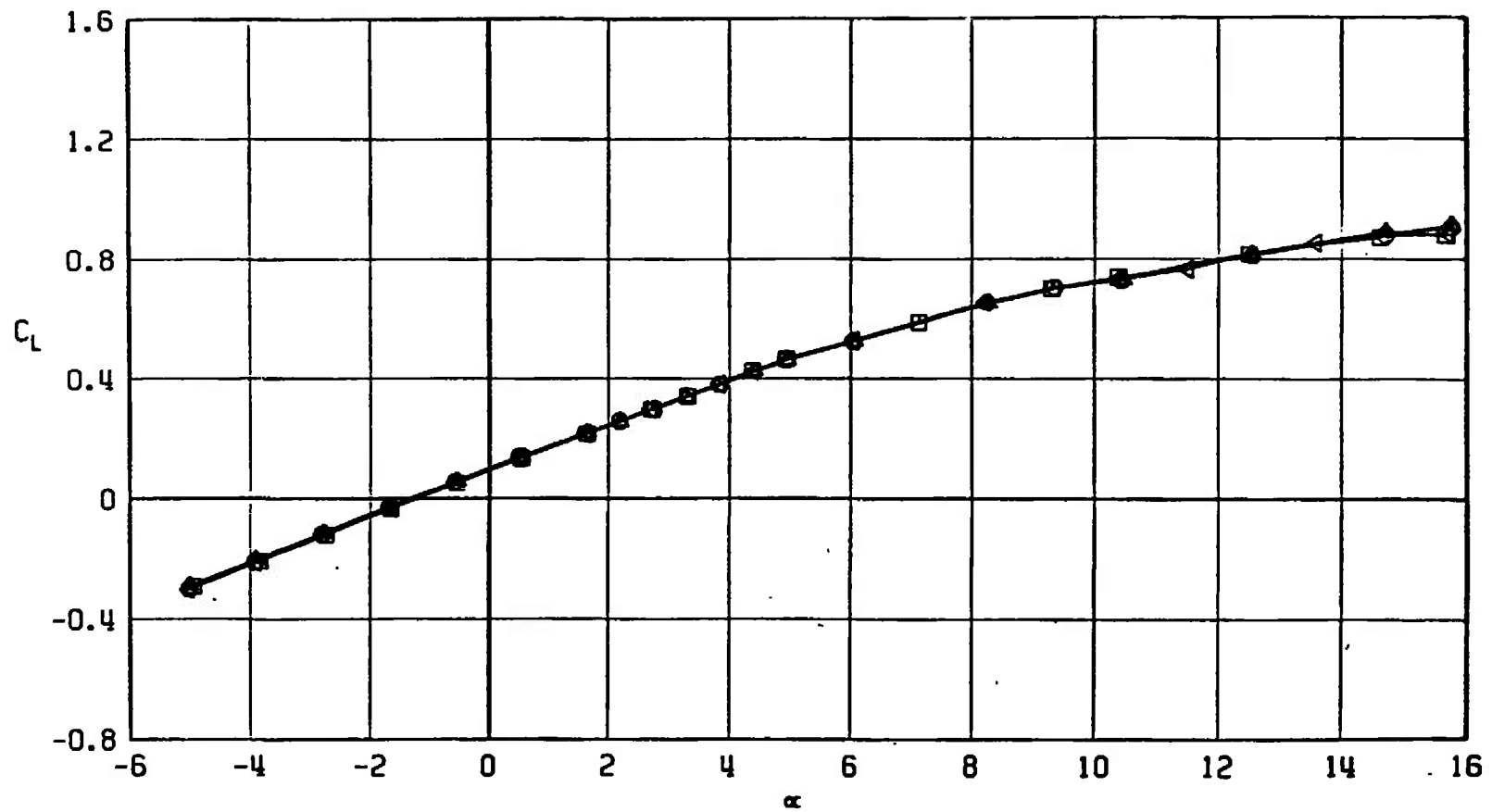
Fig. 40 Lift Coefficient Variation with Angle of Attack for Configurations F401, F405, F406, and F407

SYMBOL	CONFIGURATION
□	F401
○	F406
△	F407
◀	F405



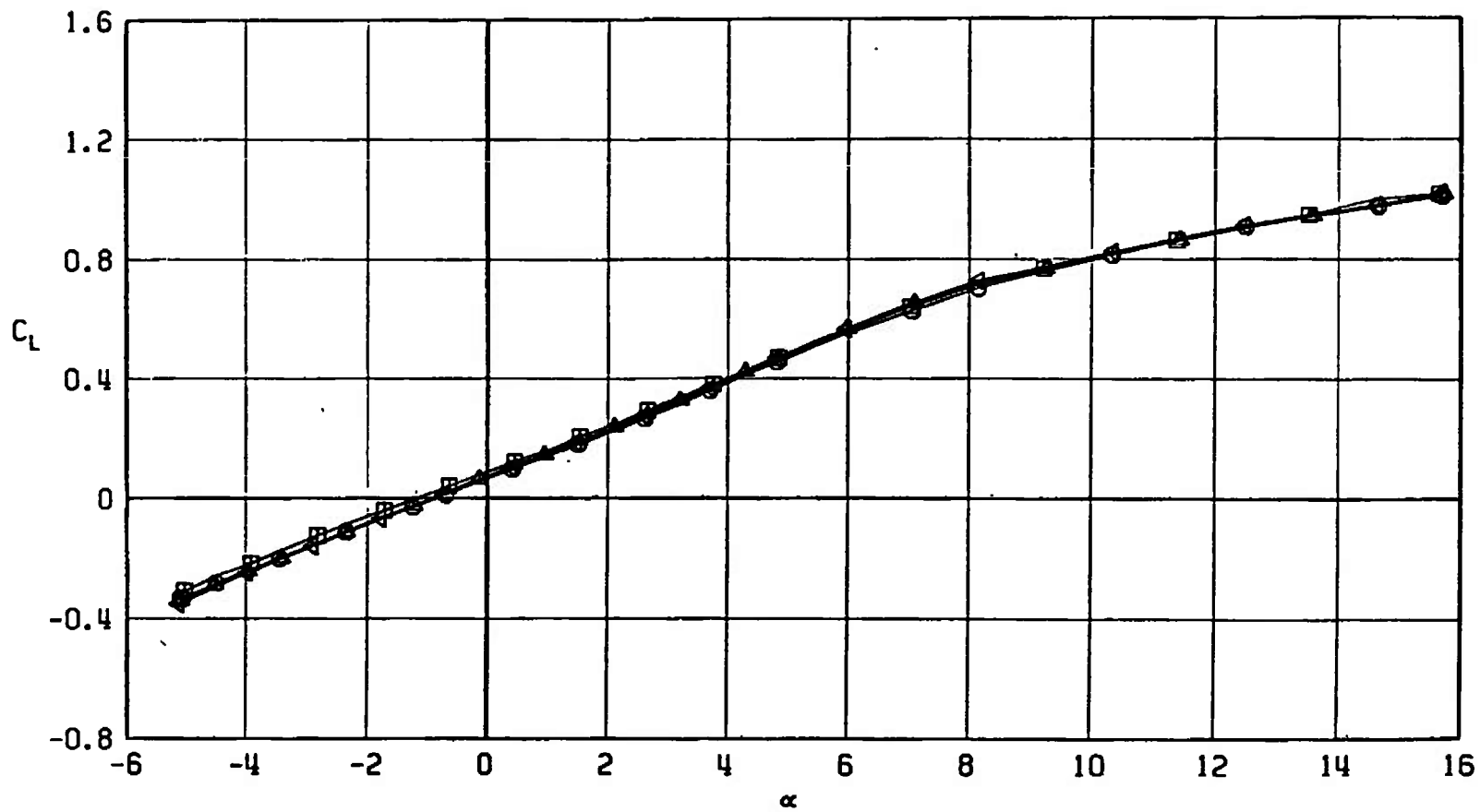
b.  $M_\infty = 0.90$   
Fig. 40 Continued

SYMBOL	CONFIGURATION
□	F401
○	F406
△	F407
▽	F405



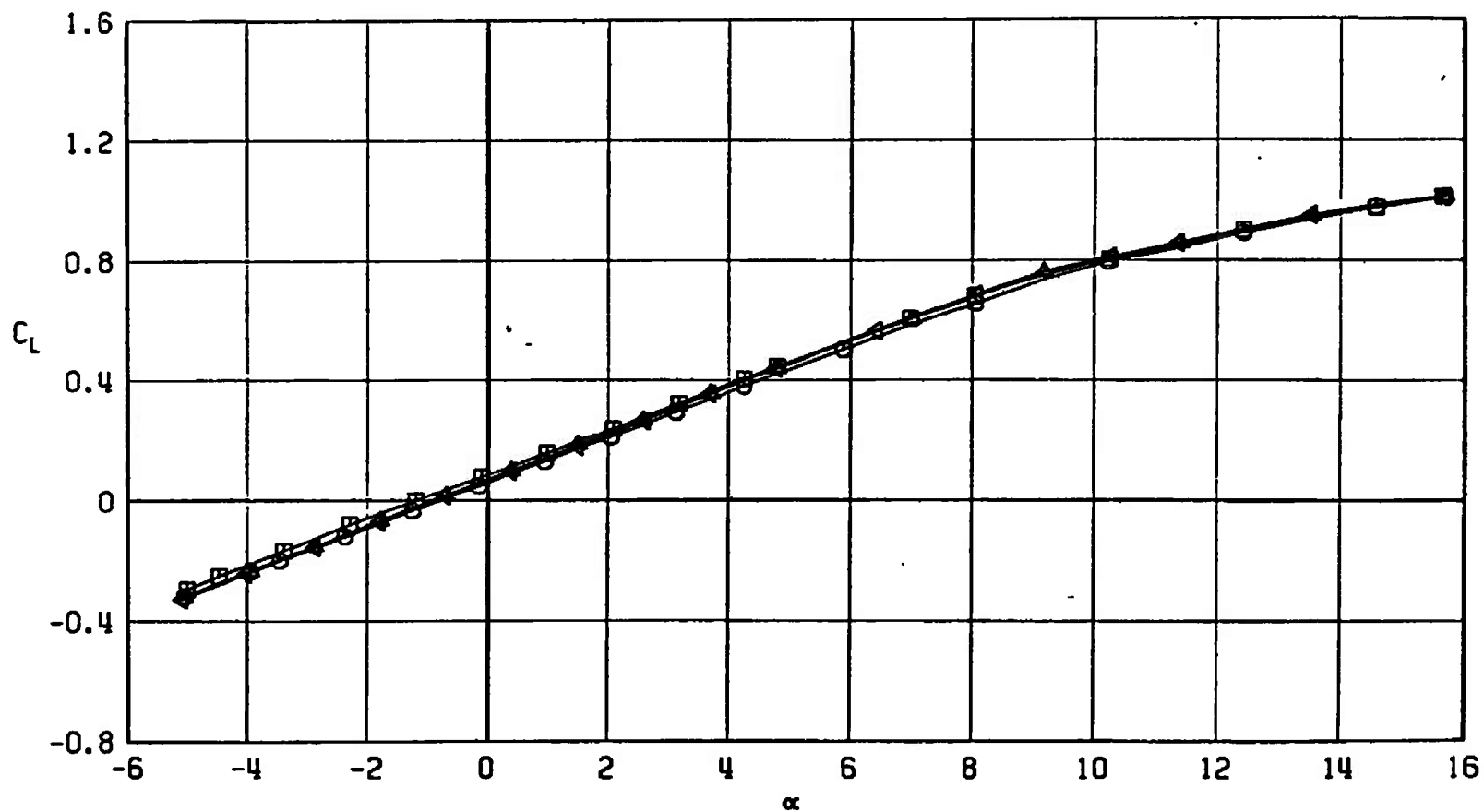
c.  $M_\infty = 0.95$   
Fig. 40 Continued

SYMBOL	CONFIGURATION
□	F401
○	F406
△	F407
▽	F405



d.  $M_\infty = 1.05$   
Fig. 40 Continued

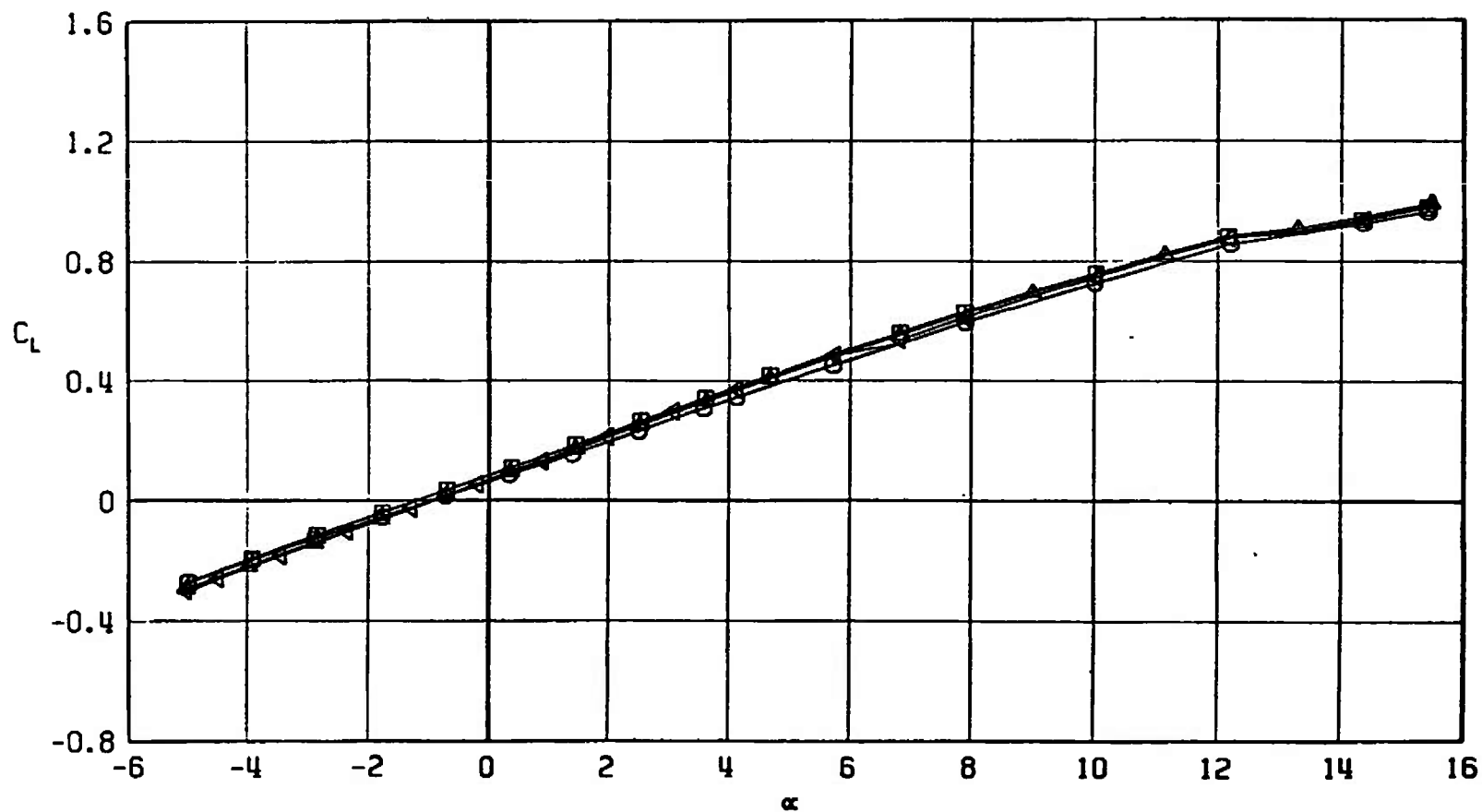
SYMBOL	CONFIGURATION
□	F401
○	F406
△	F407
◀	F405



e.  $M_\infty = 1.10$   
Fig. 40 Continued

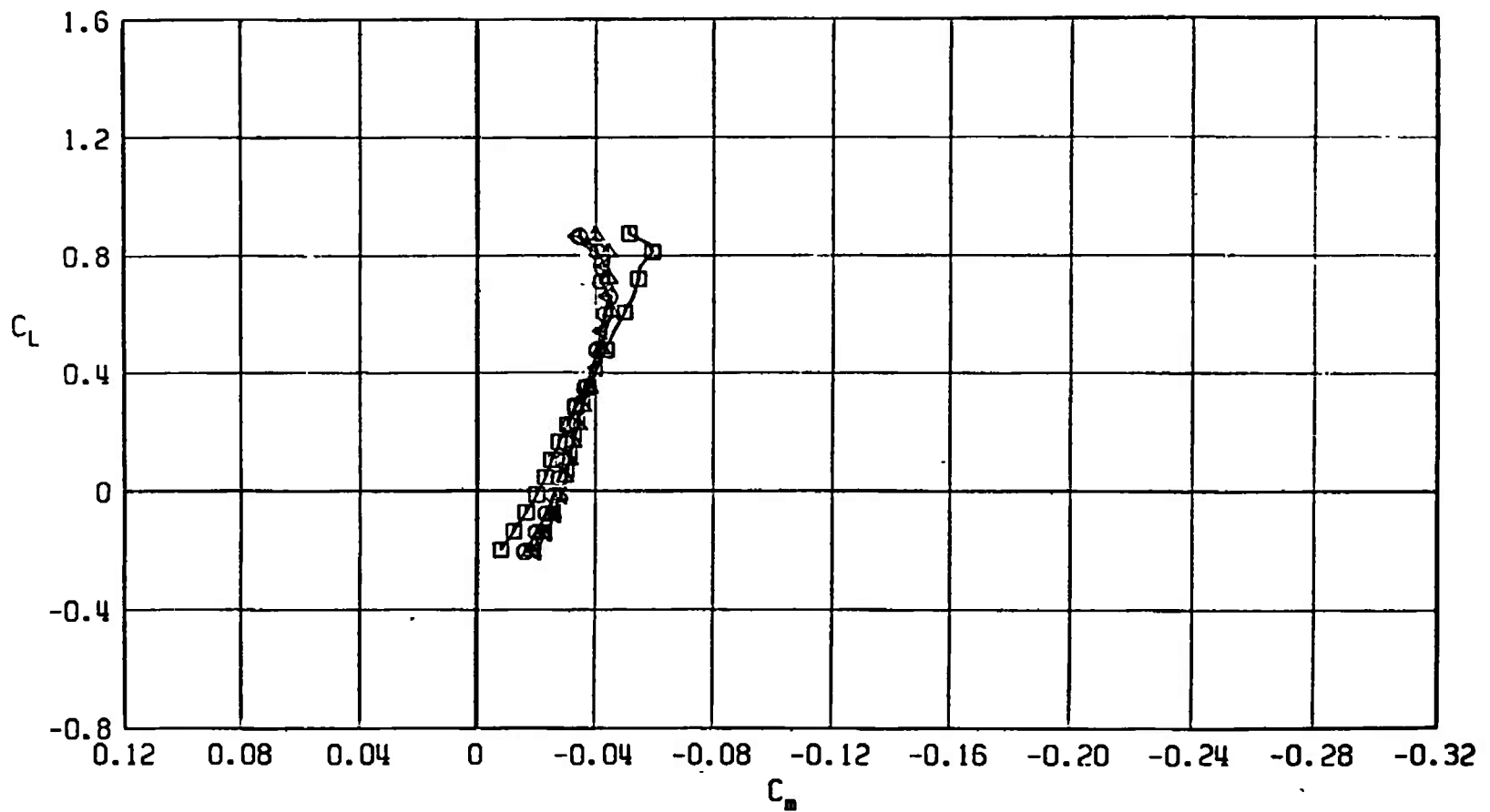


SYMBOL	CONFIGURATION
□	F401
○	F406
△	F407
▽	F405



f.  $M_\infty = 1.20$   
Fig. 40 Concluded

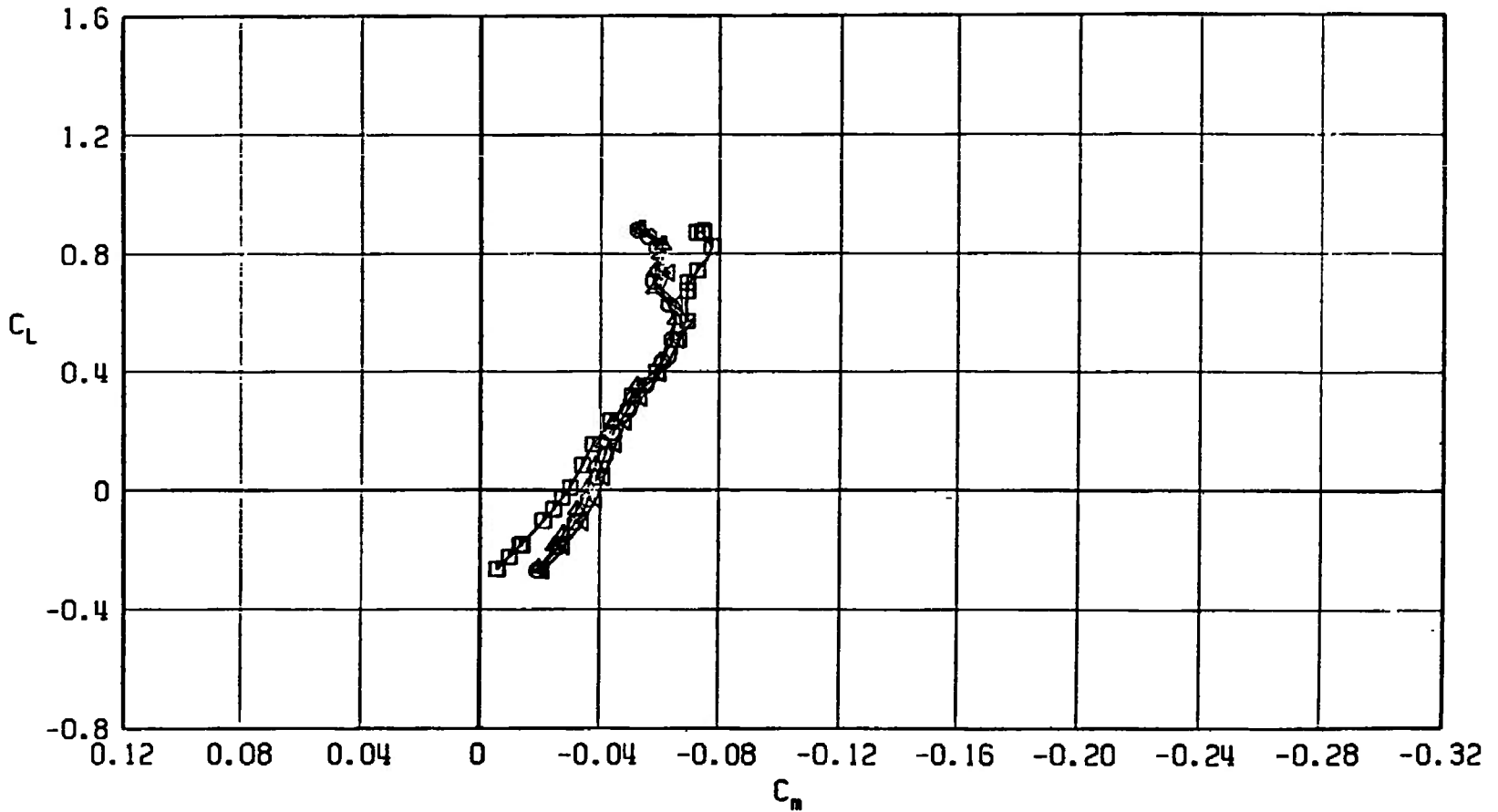
SYMBOL	CONFIGURATION
□	F401
○	F406
△	F407
◀	F405



a.  $M_\infty = 0.50$

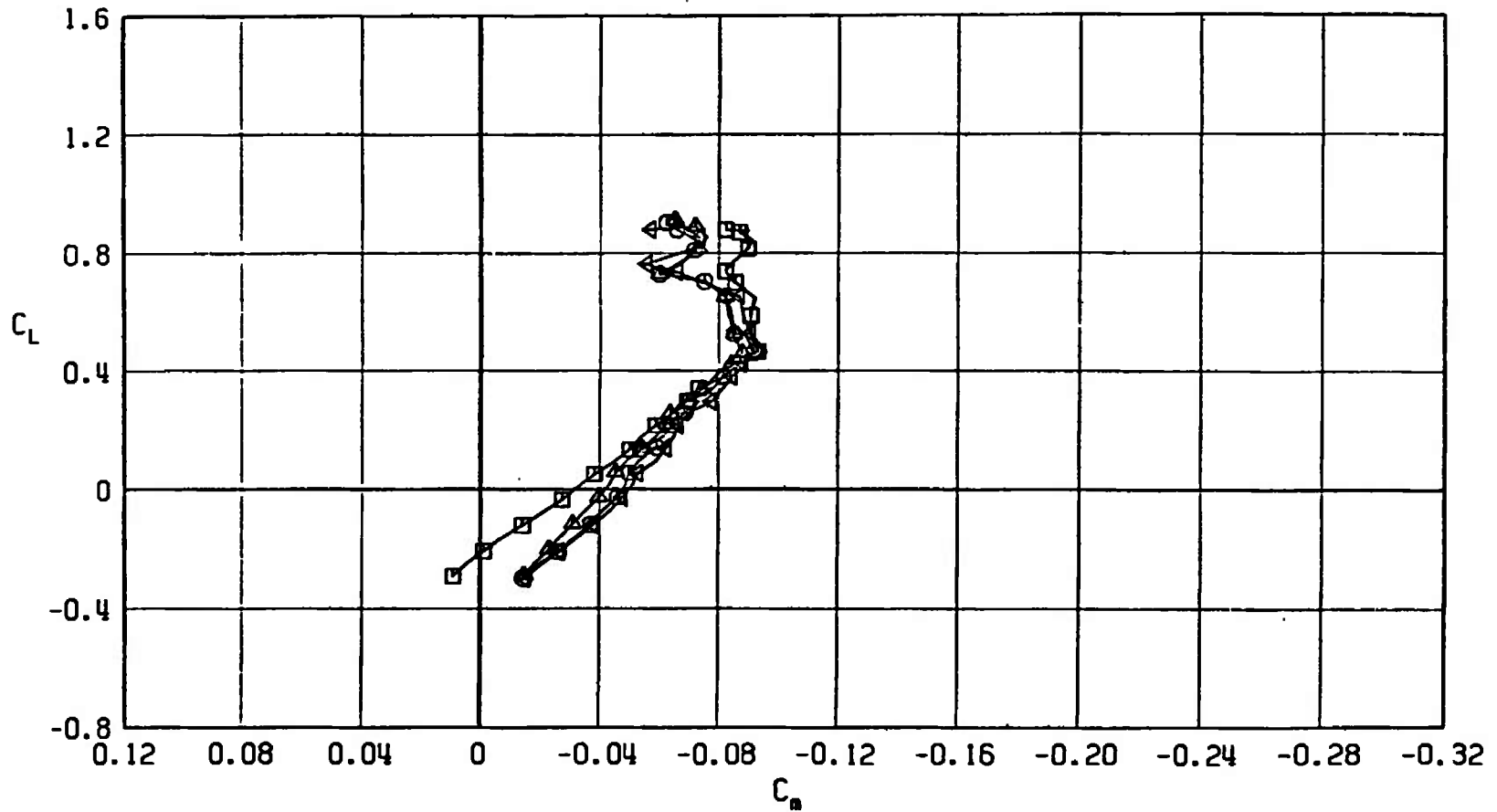
Fig. 41 Pitching-Moment Coefficient Variation with Lift Coefficient for Configurations F401, F405, F406, and F407

SYMBOL	CONFIGURATION
□	F401
○	F406
△	F407
◀	F405



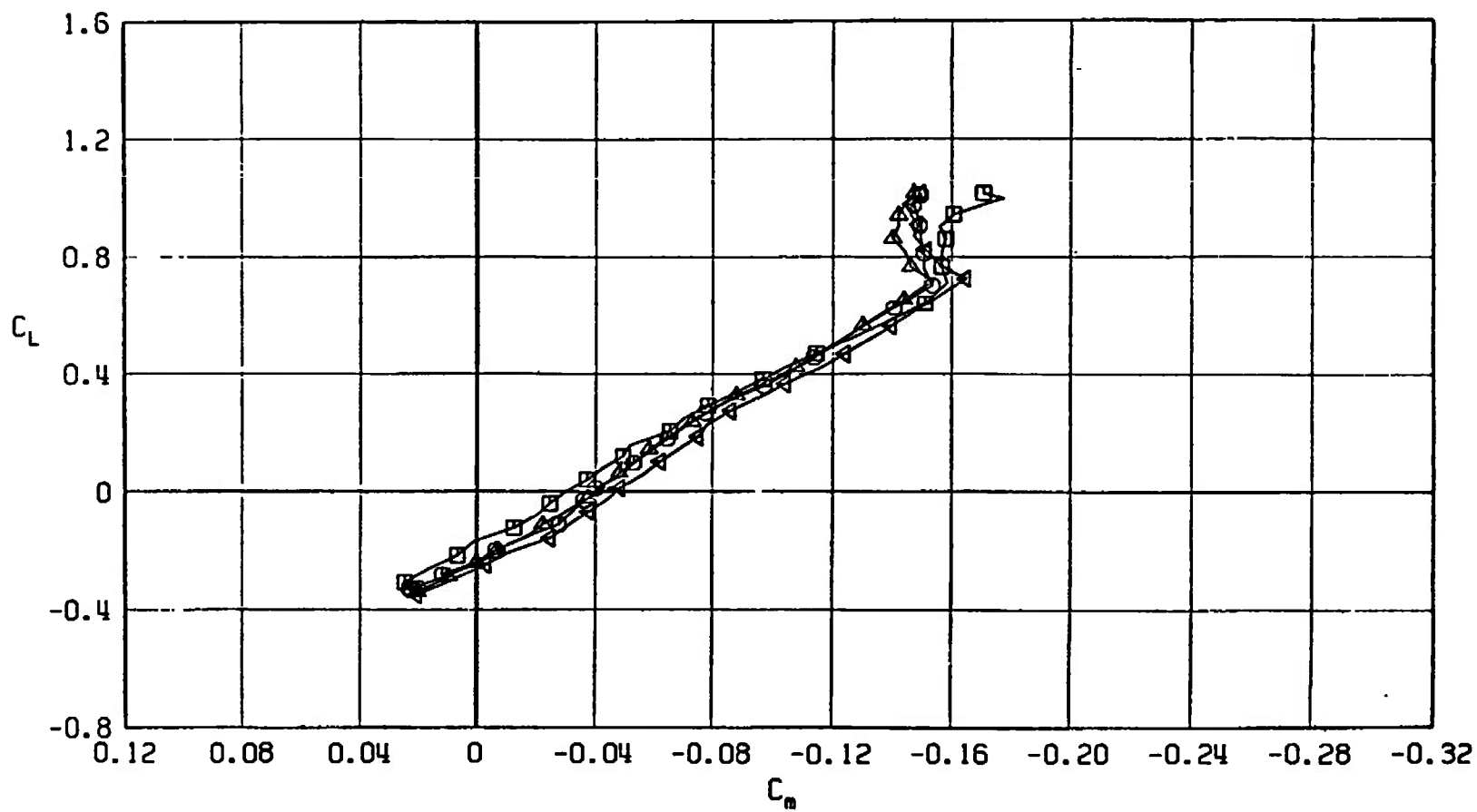
b.  $M_\infty = 0.90$   
Fig. 41 Continued

SYMBOL	CONFIGURATION
□	F401
○	F406
△	F407
◀	F405



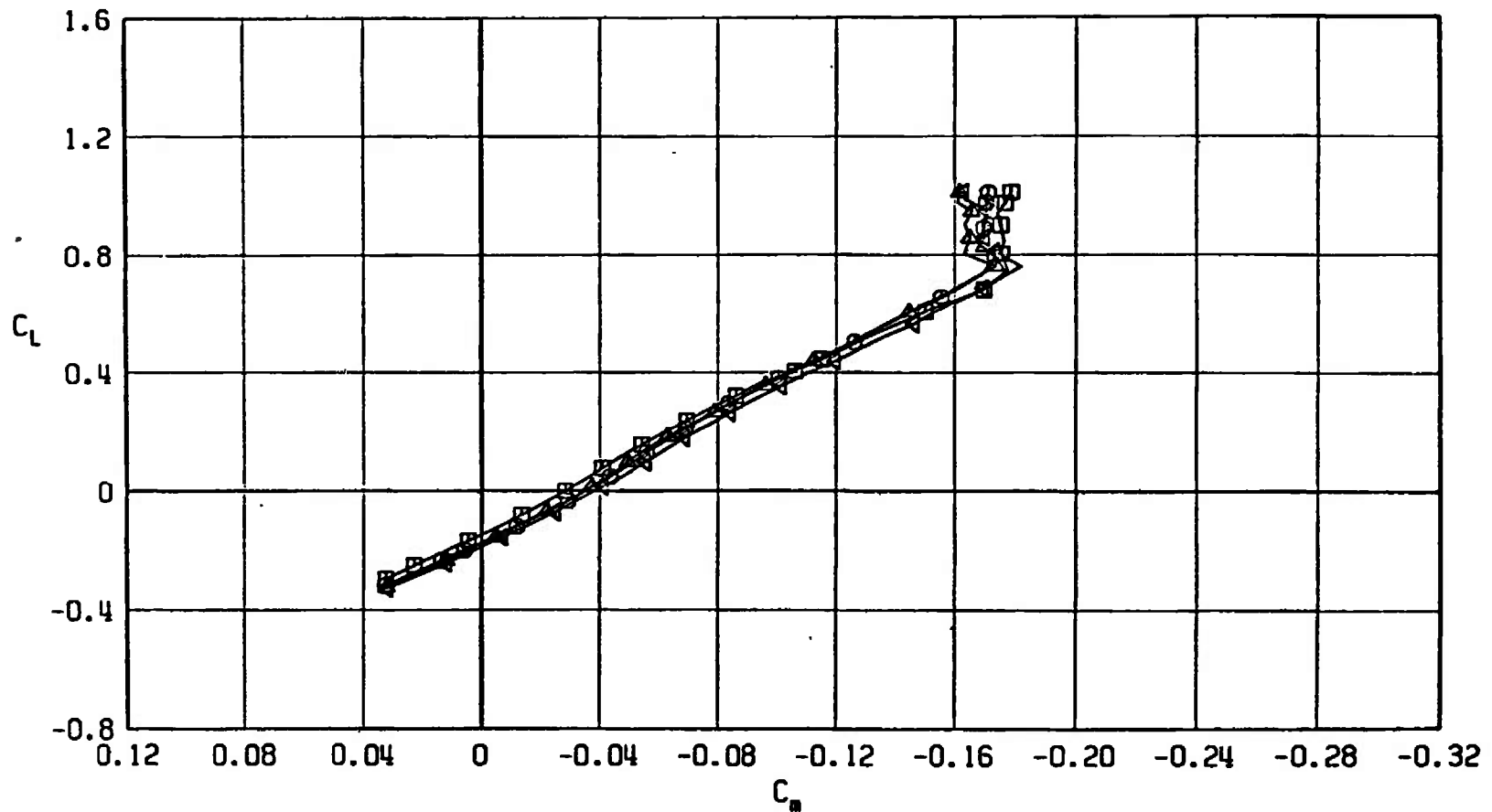
c.  $M_\infty = 0.95$   
Fig. 41 Continued

SYMBOL	CONFIGURATION
□	F401
○	F406
△	F407
▽	F405



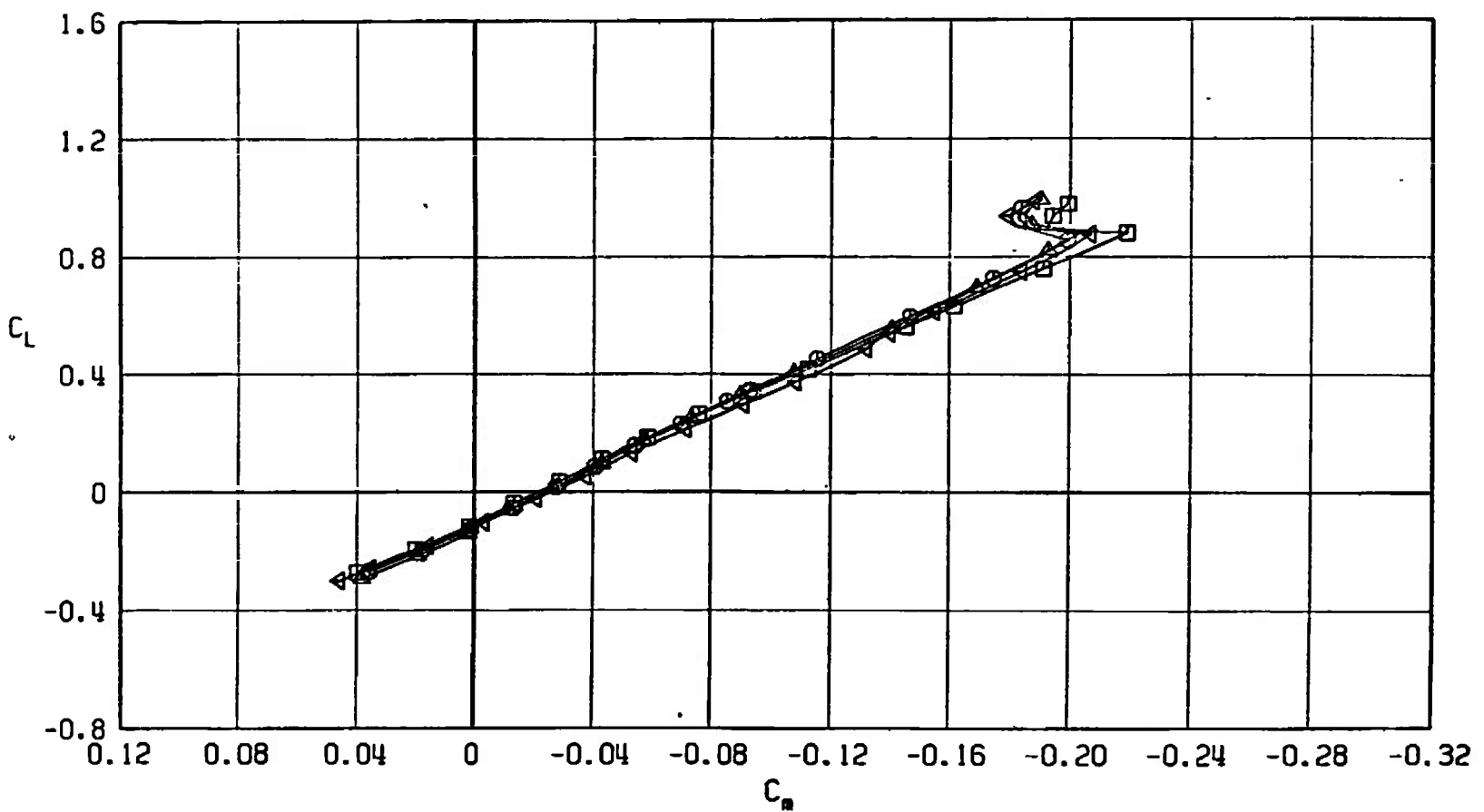
d.  $M_\infty = 1.05$   
Fig. 41 Continued

SYMBOL	CONFIGURATION
□	F401
○	F406
△	F407
▽	F405



e.  $M_\infty = 1.10$   
Fig. 41 Continued

SYMBOL	CONFIGURATION
□	F401
○	F406
△	F407
▽	F405



f.  $M_\infty = 1.20$   
Fig. 41 Concluded

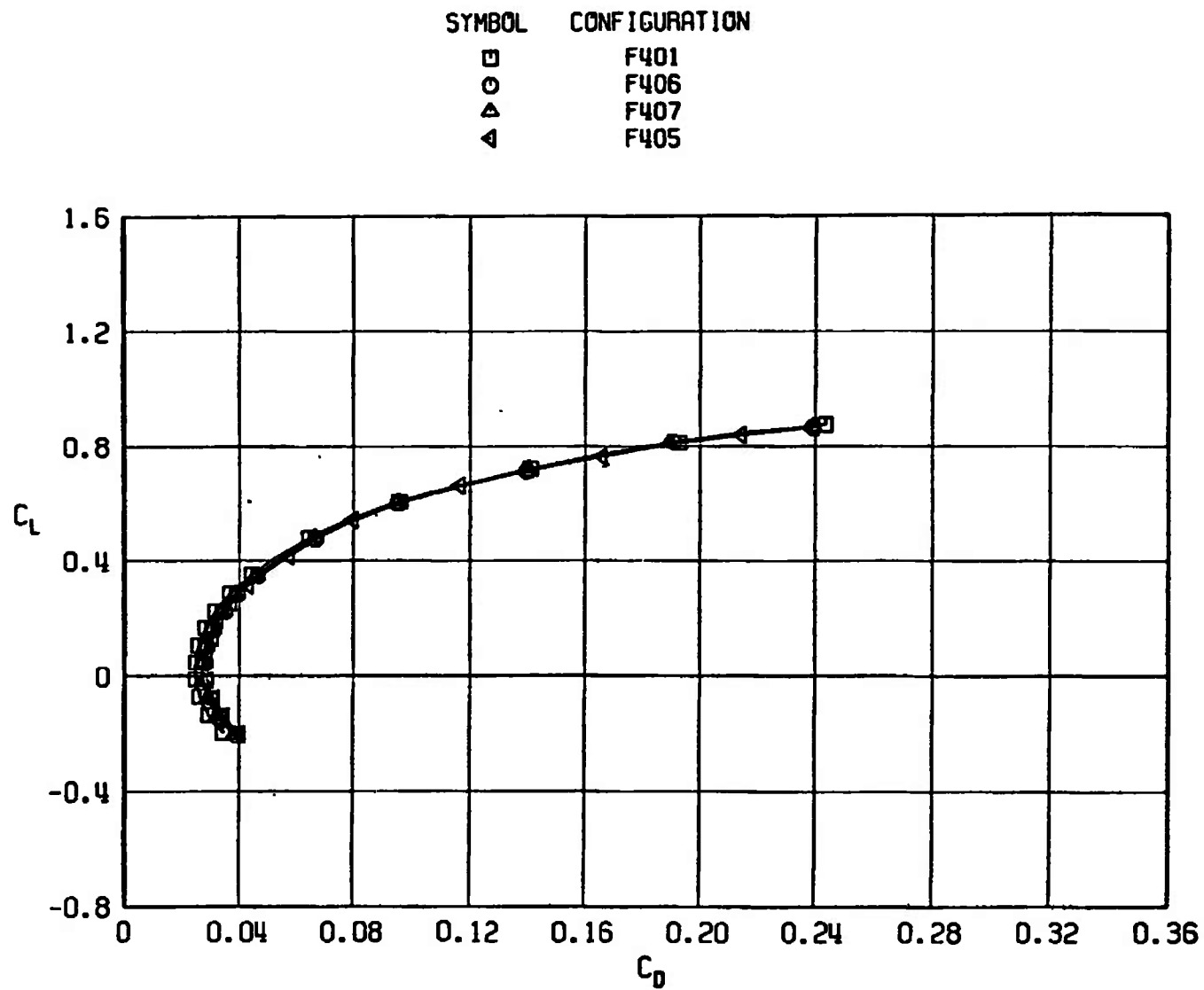
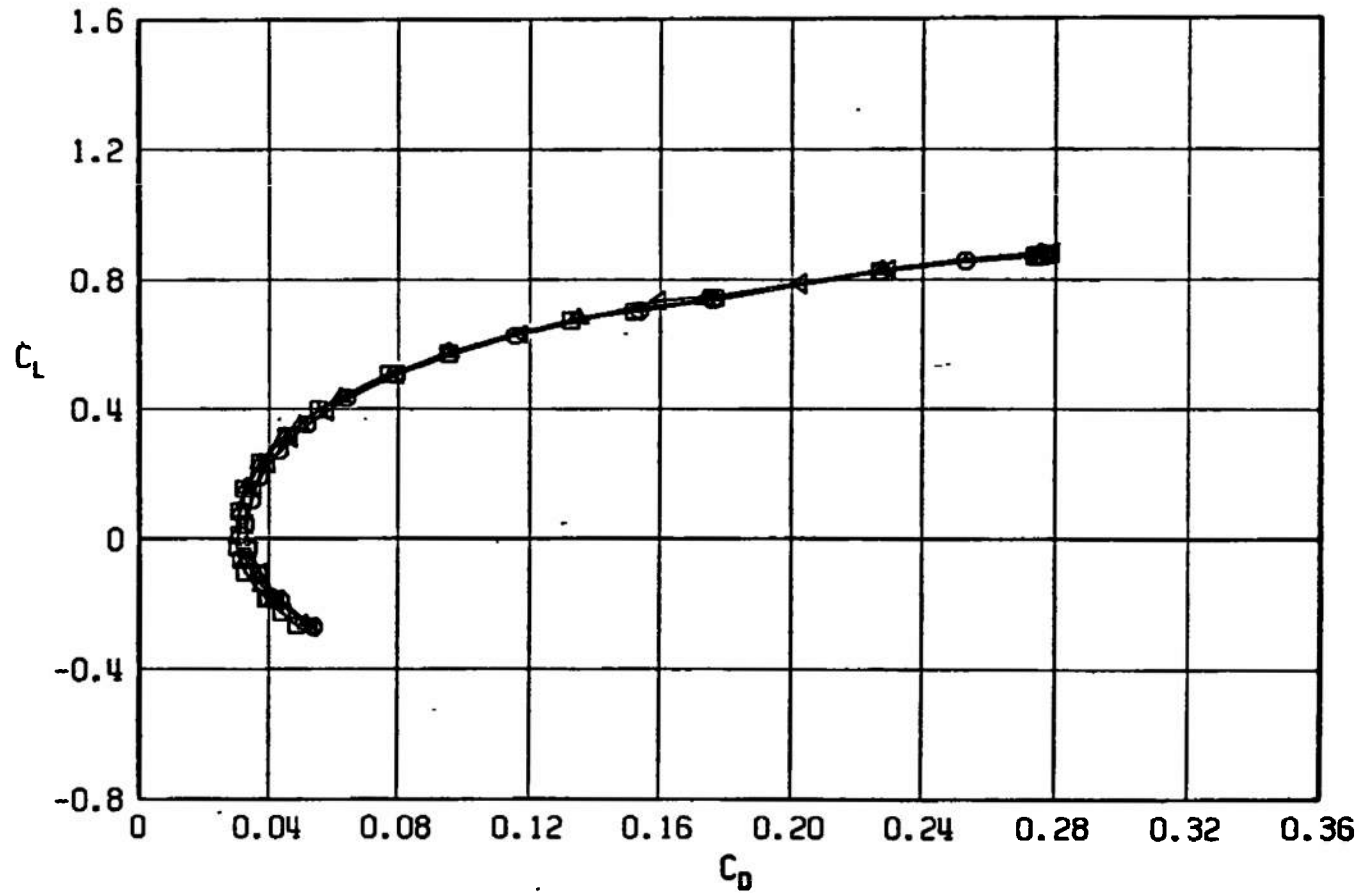
a.  $M_\infty = 0.50$ 

Fig. 42 Drag Coefficient Variation with Lift Coefficient for Configurations F401, F405, F406, and F407



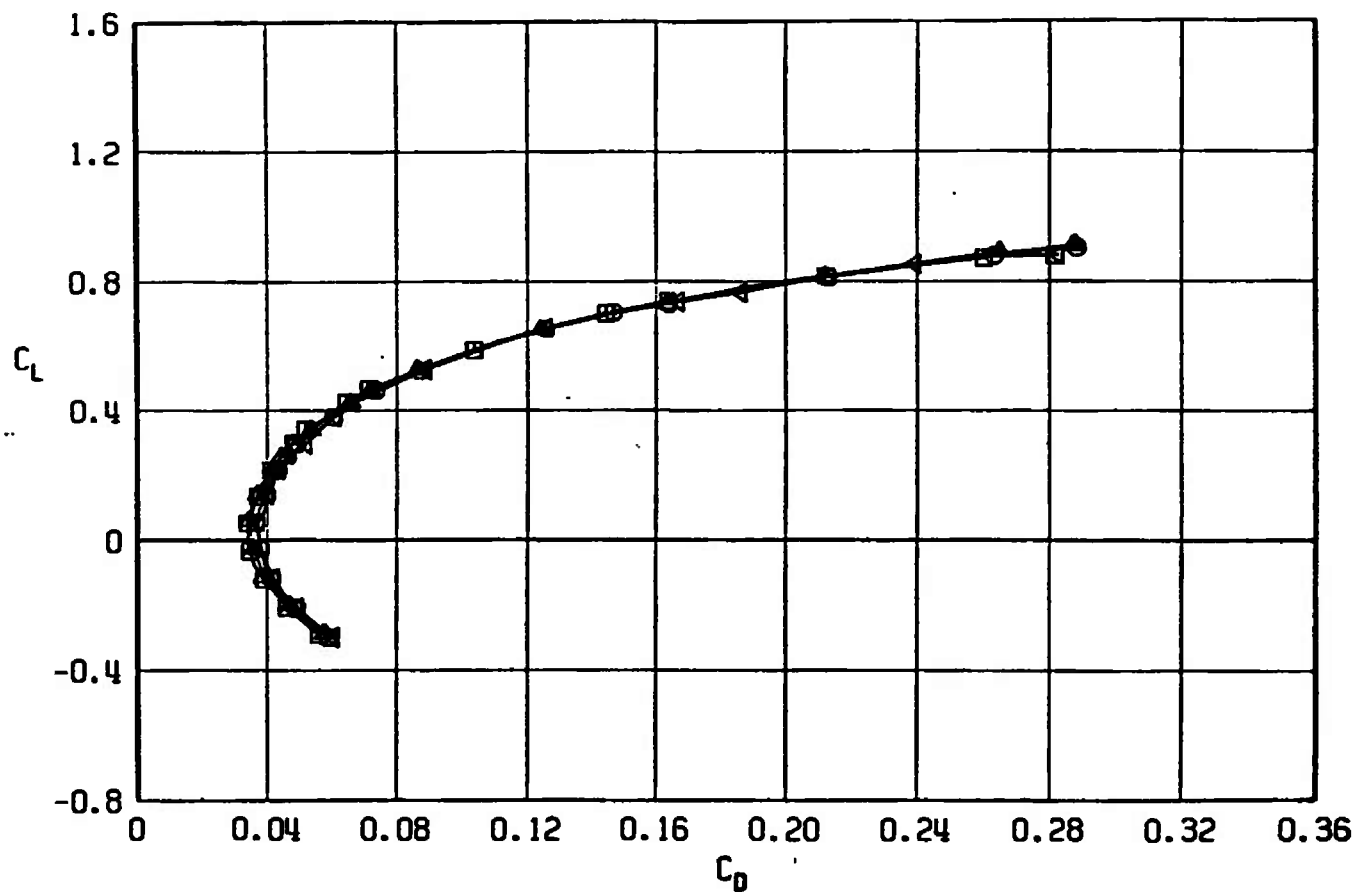
SYMBOL	CONFIGURATION
□	F401
○	F406
△	F407
▽	F405



b.  $M_\infty = 0.90$   
Fig. 42 Continued

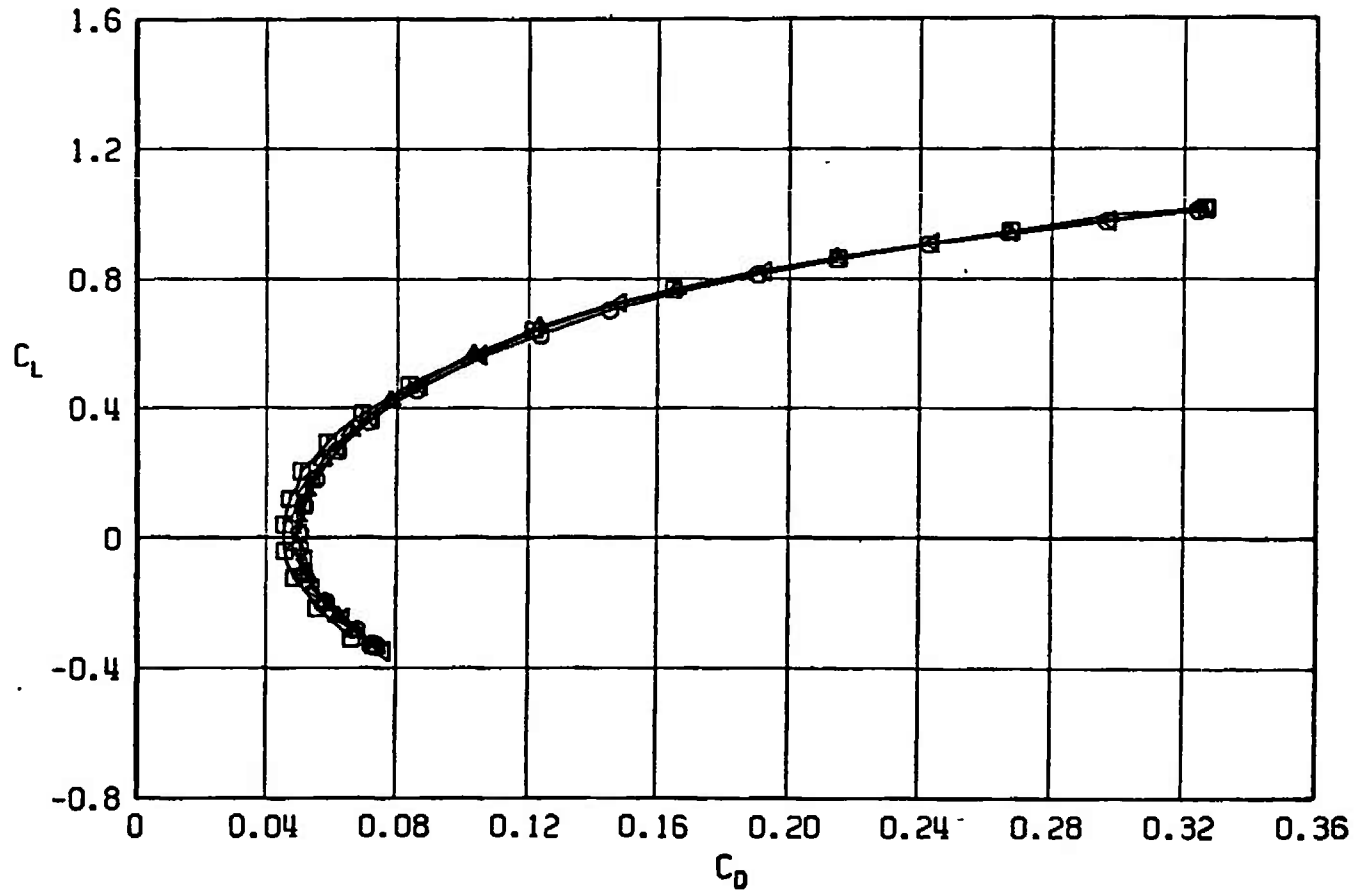
SYMBOL	CONFIGURATION
--------	---------------

□	F401
○	F406
△	F407
▽	F405



$c. M_\infty = 0.95$   
Fig. 42 Continued

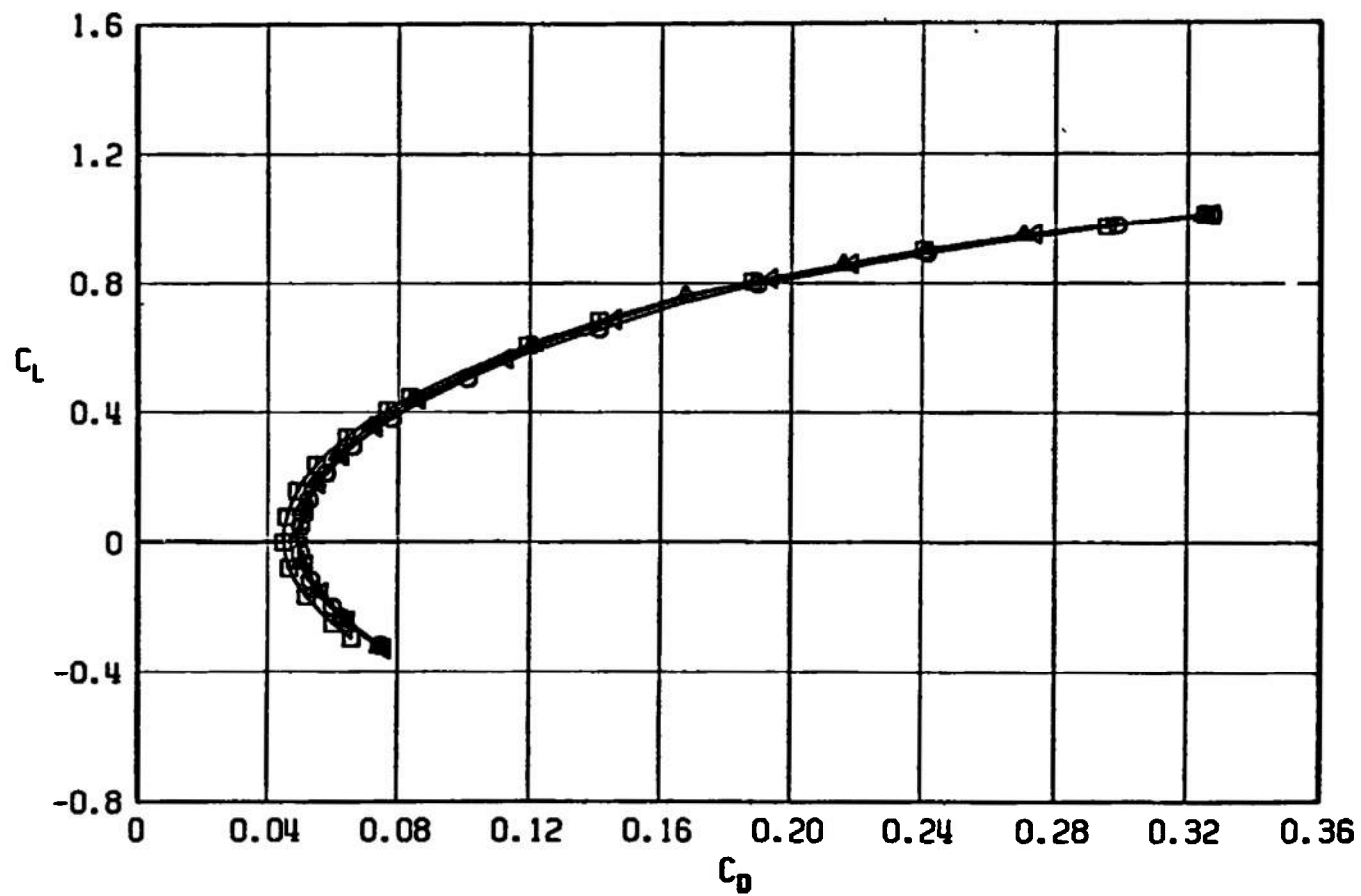
SYMBOL	CONFIGURATION
□	F401
○	F406
△	F407
▽	F405



d.  $M_\infty = 1.05$   
Fig. 42 Continued

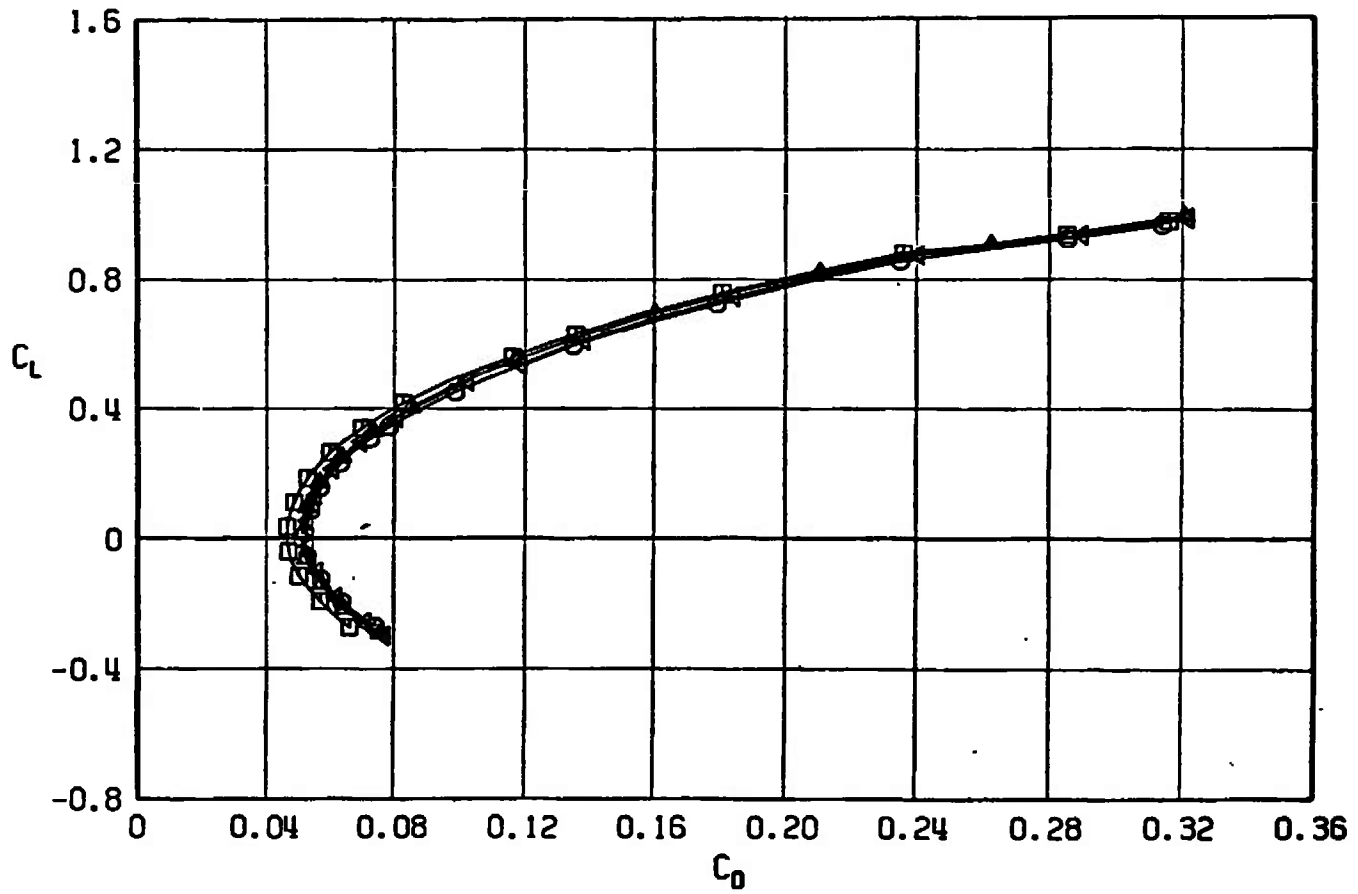
SYMBOL CONFIGURATION

□	F401
○	F406
△	F407
▲	F405



e.  $M_\infty = 1.10$   
Fig. 42 Continued

SYMBOL	CONFIGURATION
□	F401
○	F406
△	F407
▽	F405



f.  $M_\infty = 1.20$   
Fig. 42 Concluded

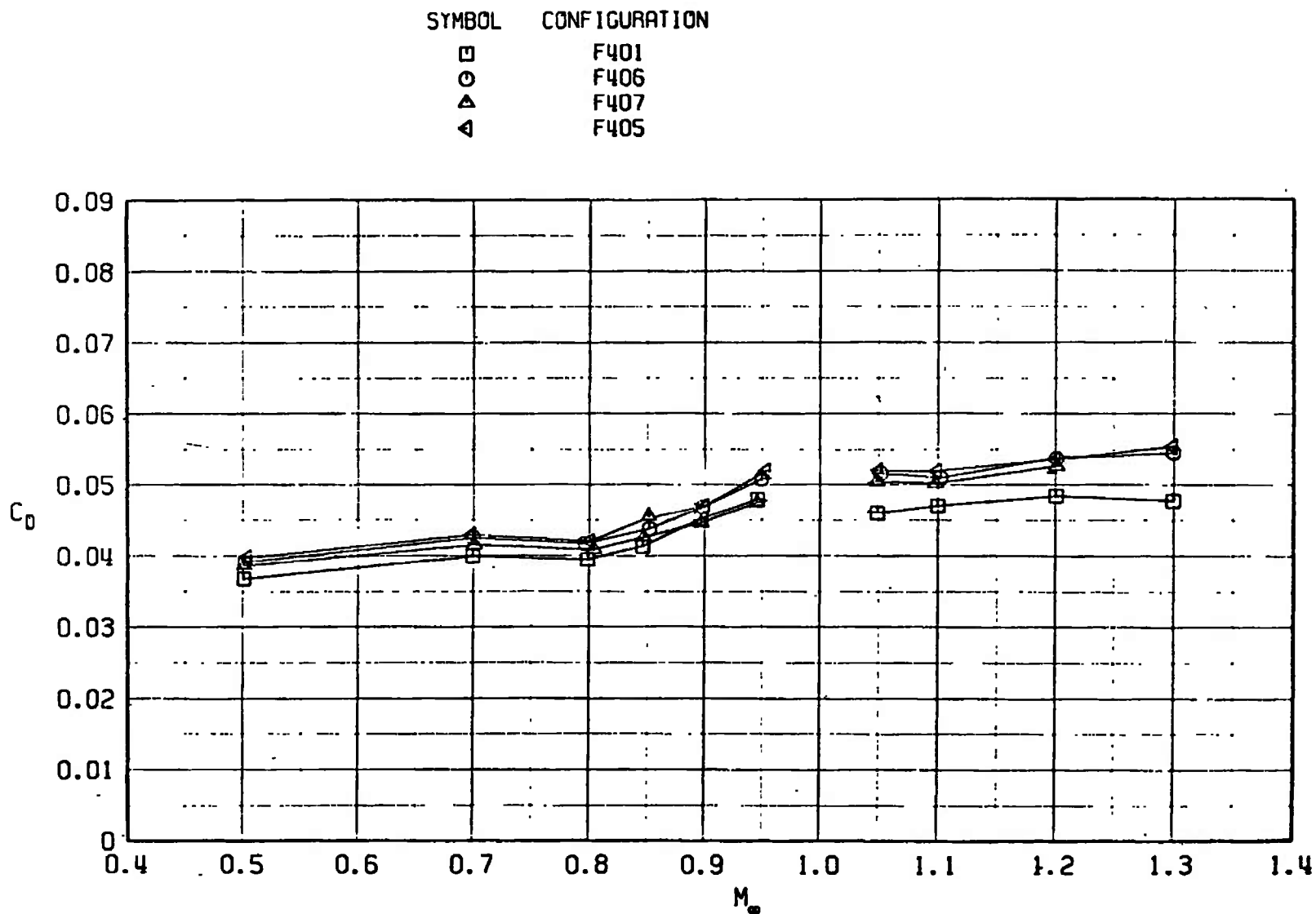
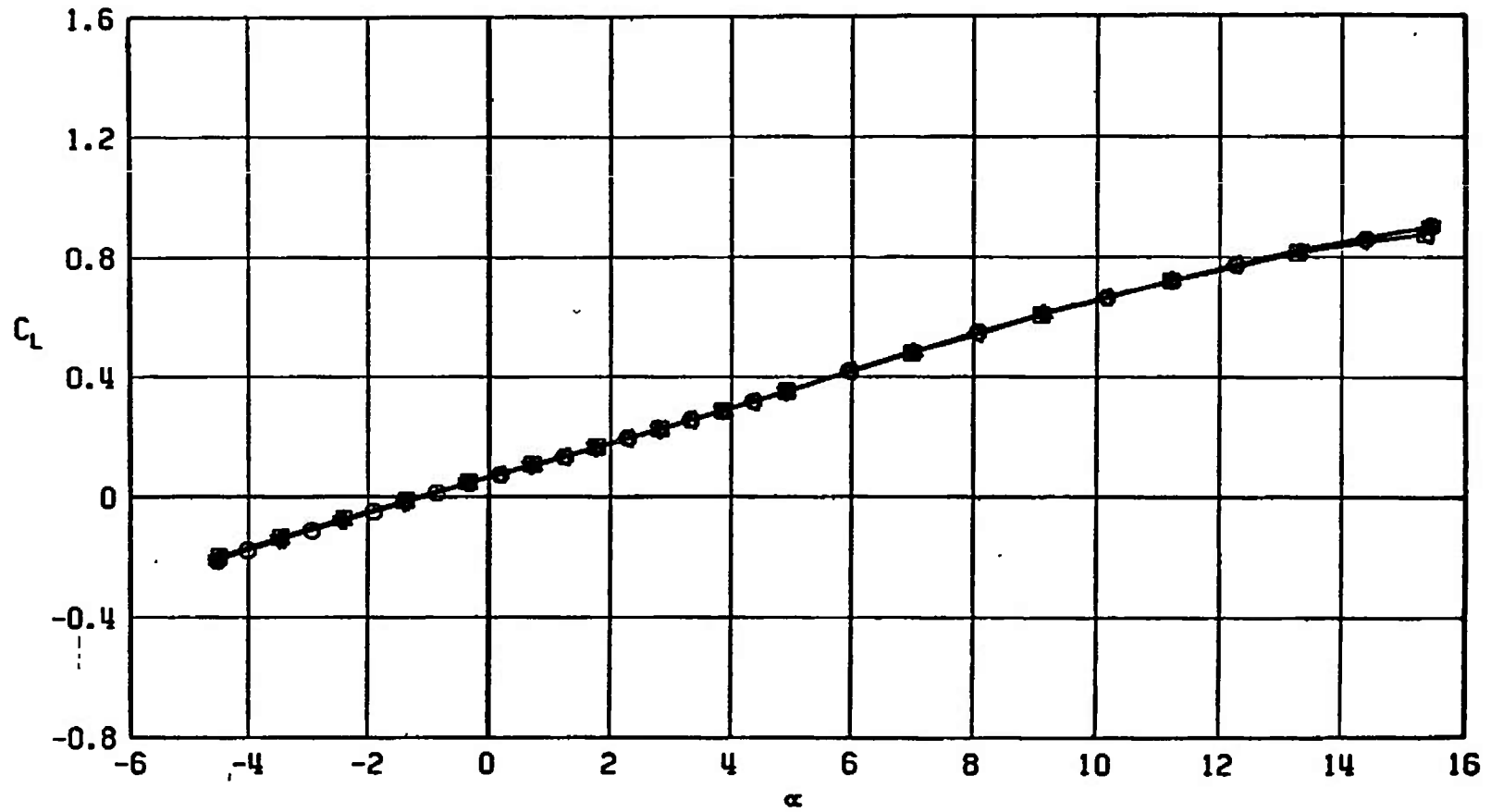


Fig. 43 Drag Coefficient Variation with Mach Number at  $C_L = 0.30$ ,  $M_\infty < 1.0$  and  $C_L = 0.1$ ,  $M_\infty > 1.0$  for Configurations F401, F405, F406, and F407

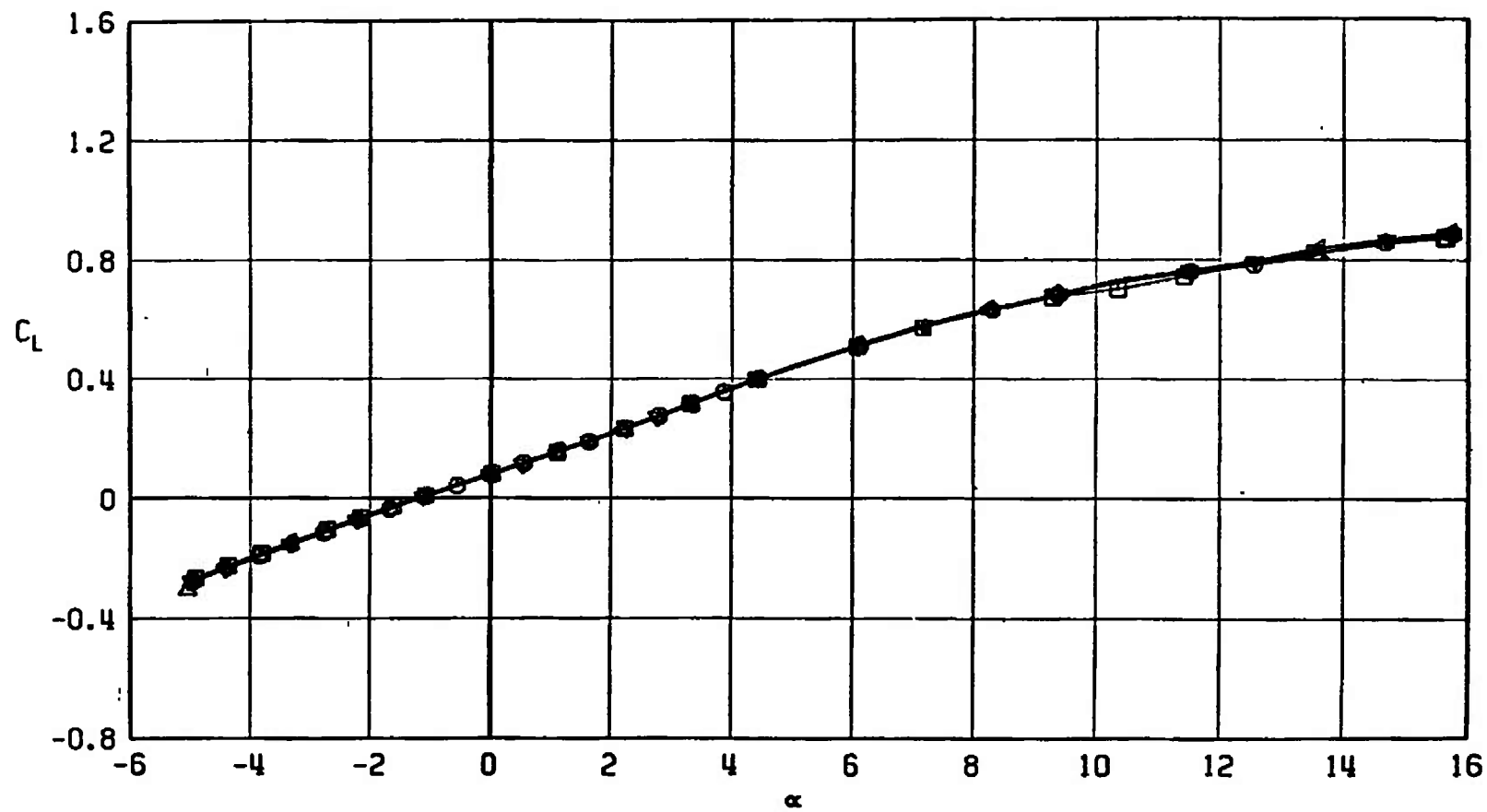
SYMBOL	CONFIGURATION
□	F401
○	F411
△	F410
▽	F408
◇	F409



a.  $M_\infty = 0.50$

Fig. 44 Lift Coefficient Variation with Angle of Attack for Configurations F401, F408, F407, F410, and F411

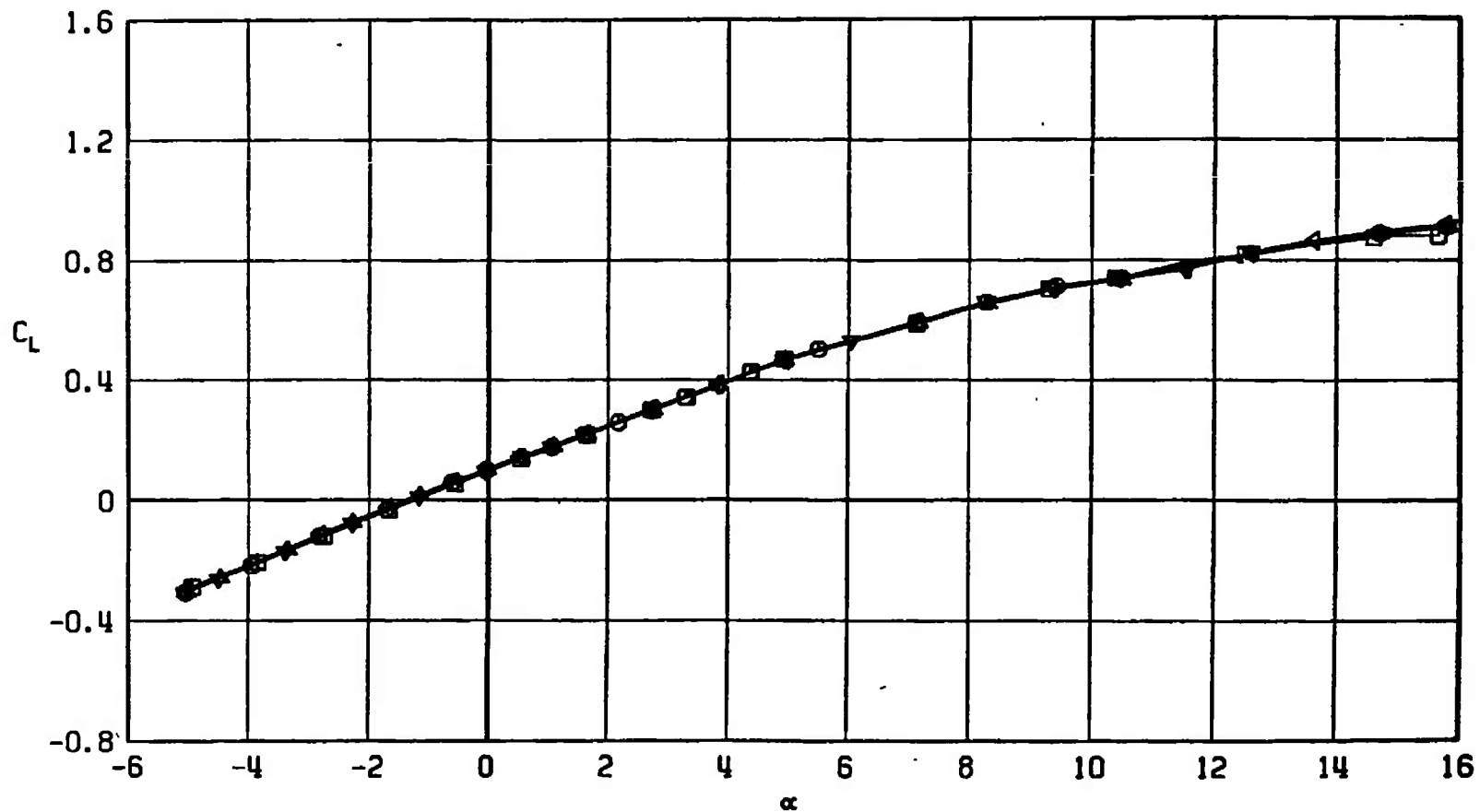
SYMBOL	CONFIGURATION
□	F401
○	F411
△	F410
◀	F408
▼	F409



b.  $M_\infty = 0.90$   
Fig. 44 Continued

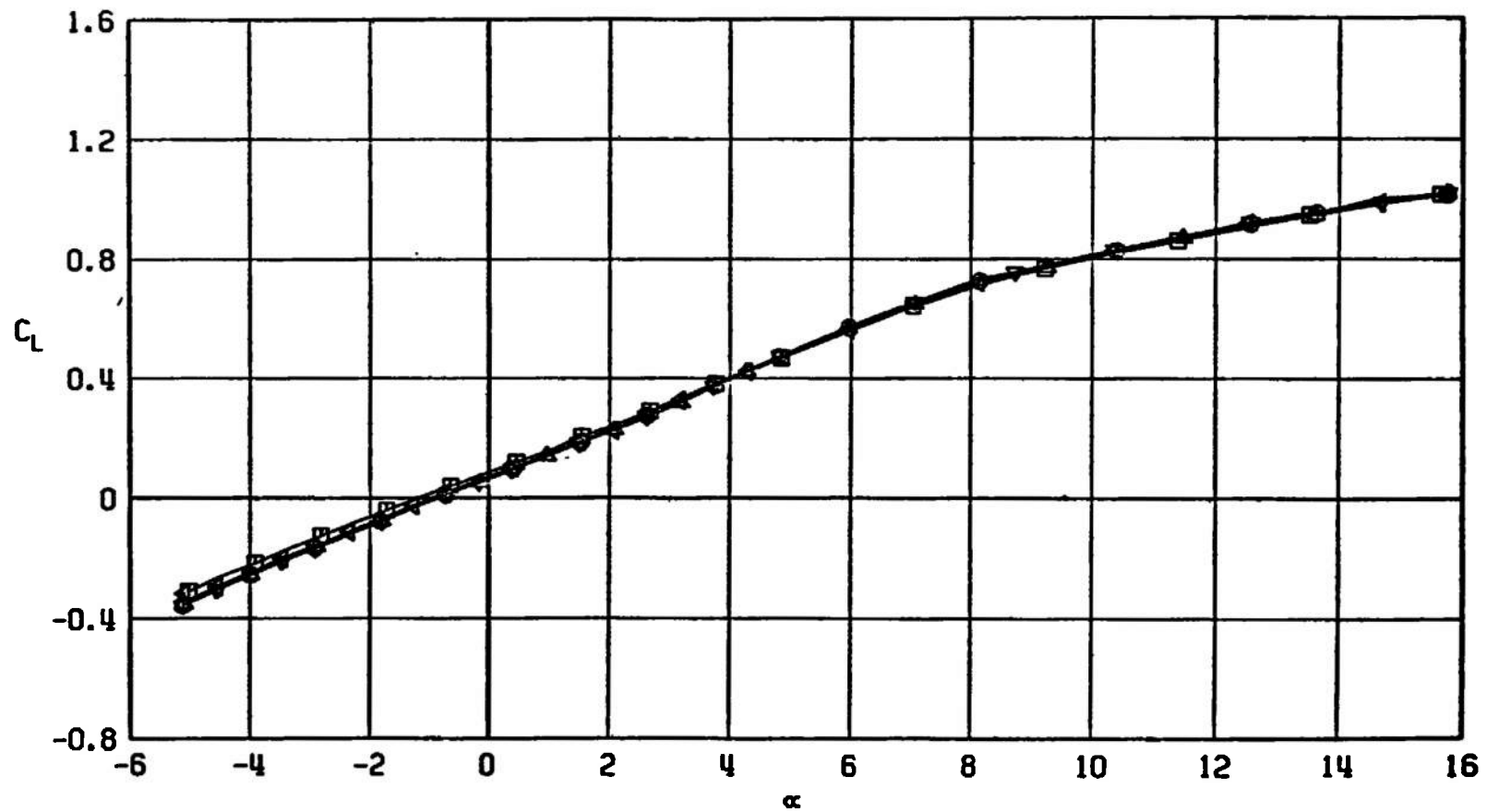


SYMBOL	CONFIGURATION
□	F401
○	F411
△	F410
▽	F408
▲	F409



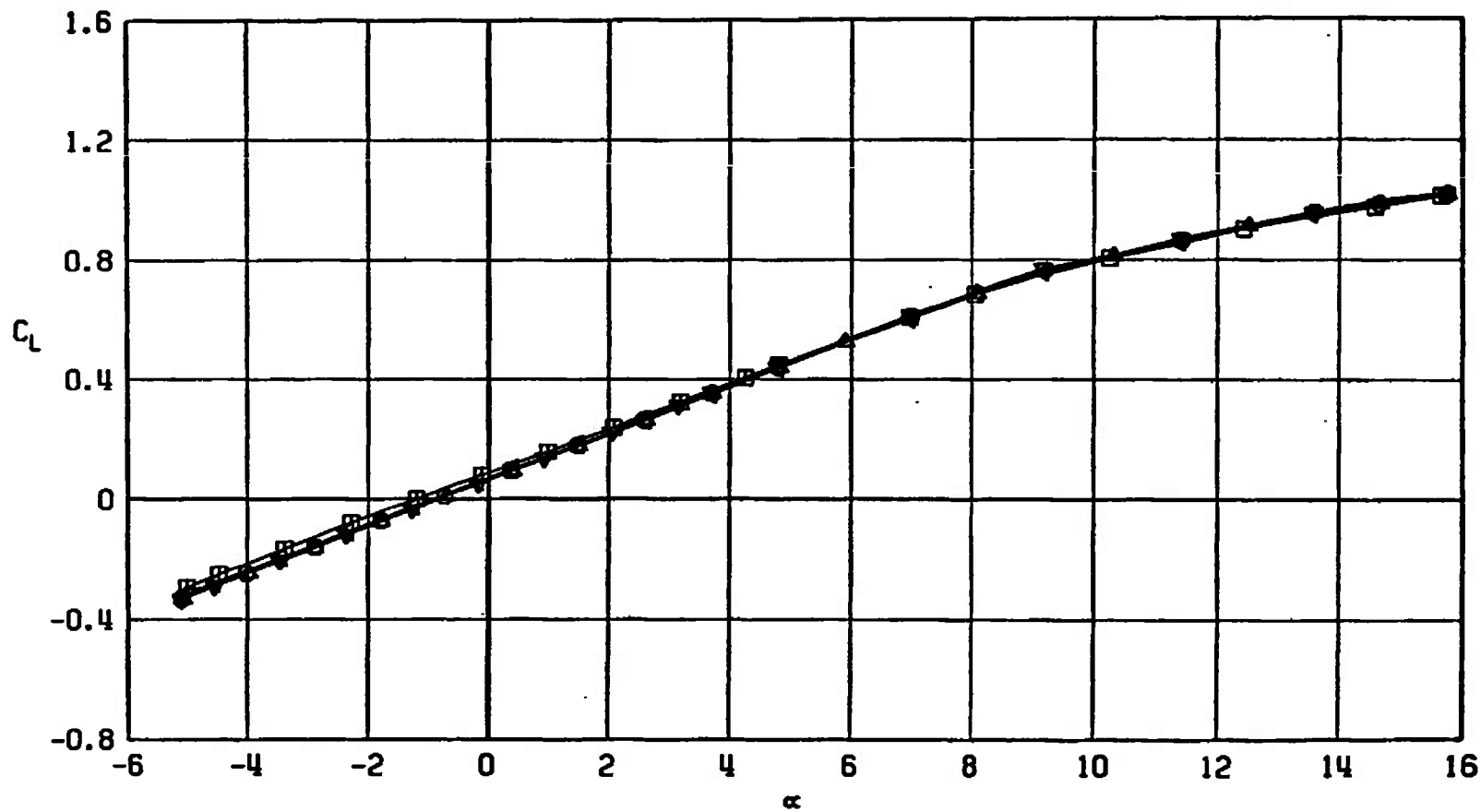
c.  $M_\infty = 0.95$   
Fig. 44 Continued

SYMBOL	CONFIGURATION
□	F401
○	F411
△	F410
▽	F408
▲	F409



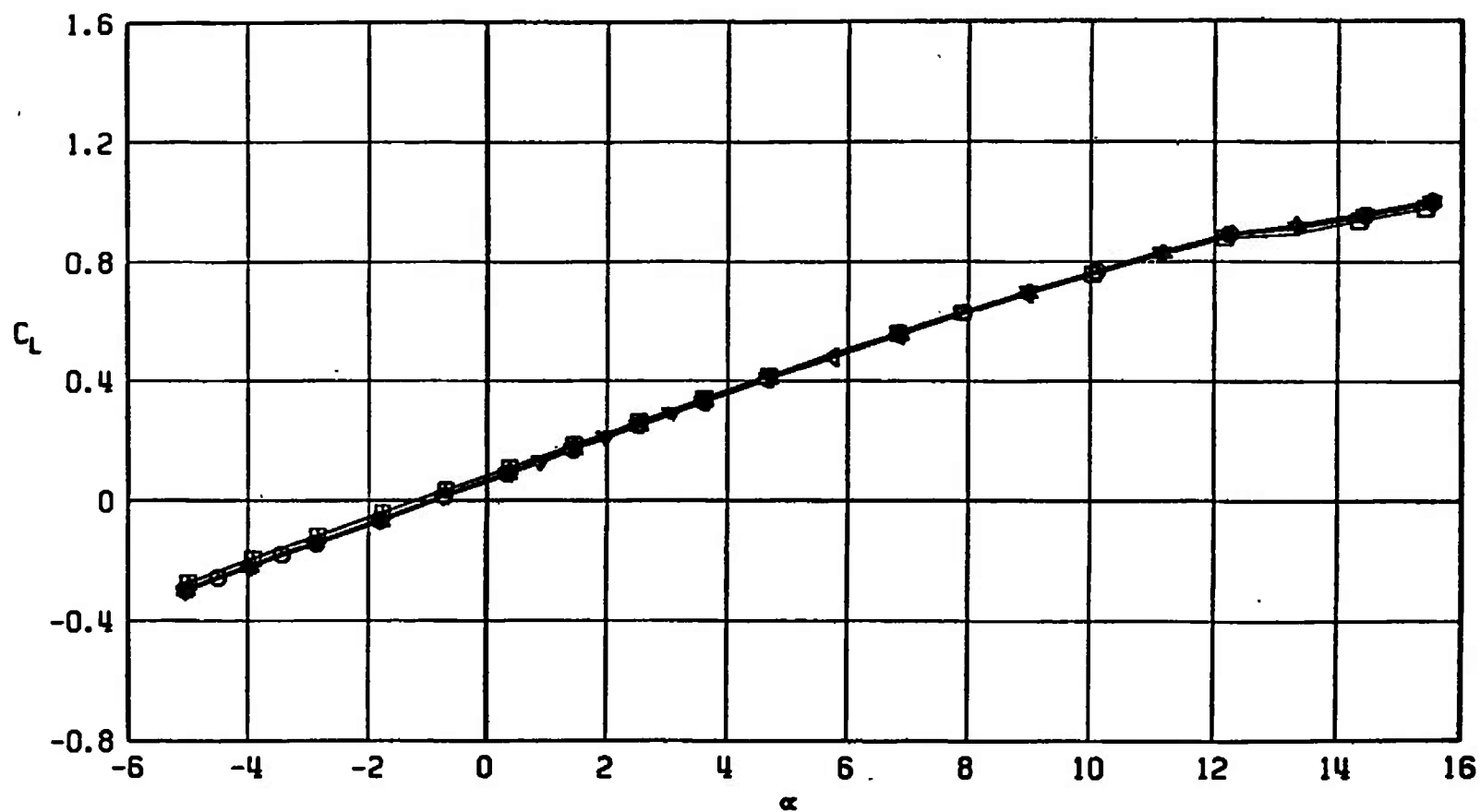
d.  $M_\infty = 1.05$   
Fig. 44 Continued

SYMBOL	CONFIGURATION
□	F401
○	F411
△	F410
▽	F408
◊	F409



e.  $M_\infty = 1.10$   
Fig. 44 Continued

SYMBOL	CONFIGURATION
□	F401
○	F411
△	F410
▽	F408
▼	F409



f.  $M_\infty = 1.20$   
Fig. 44 Concluded.

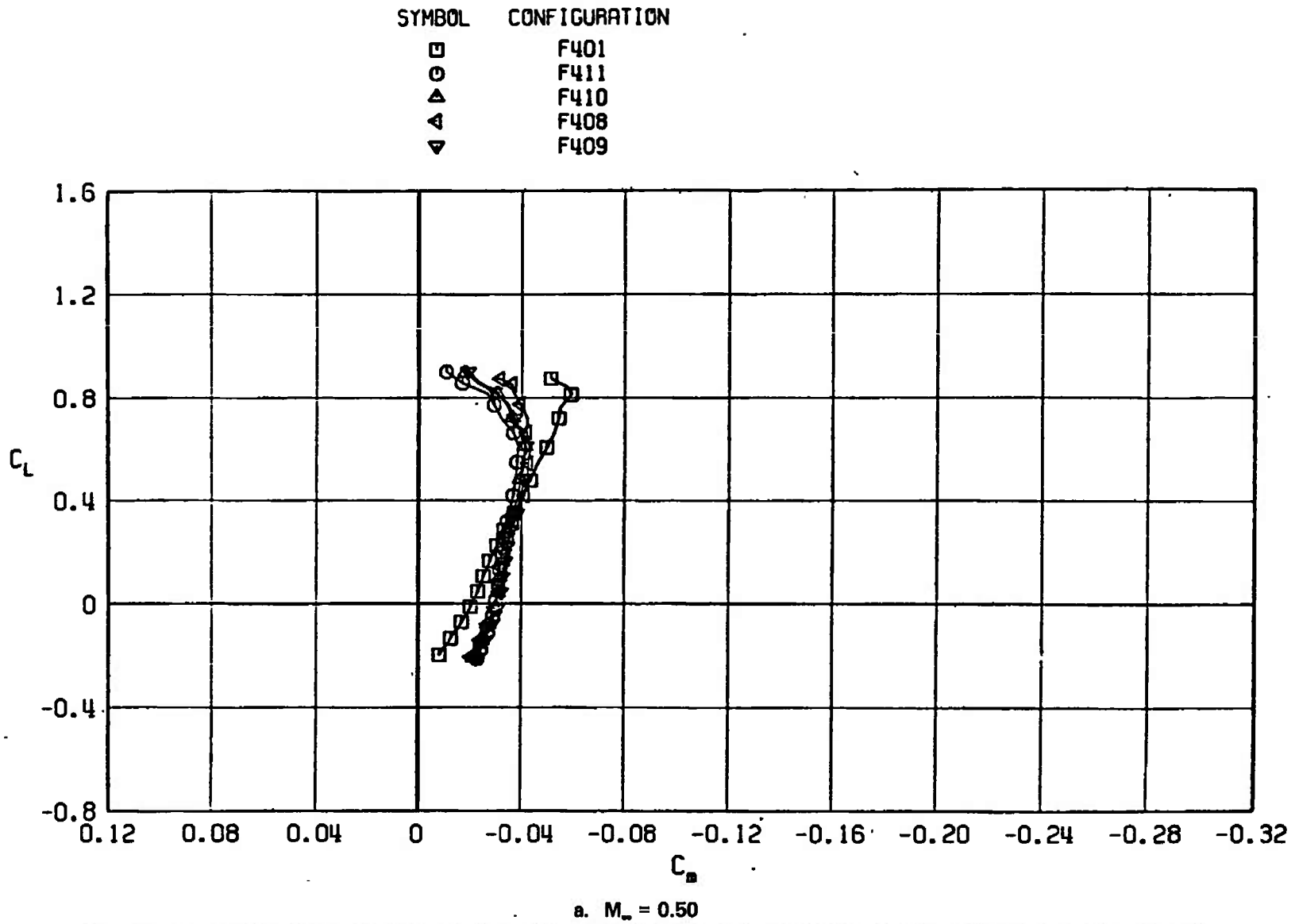
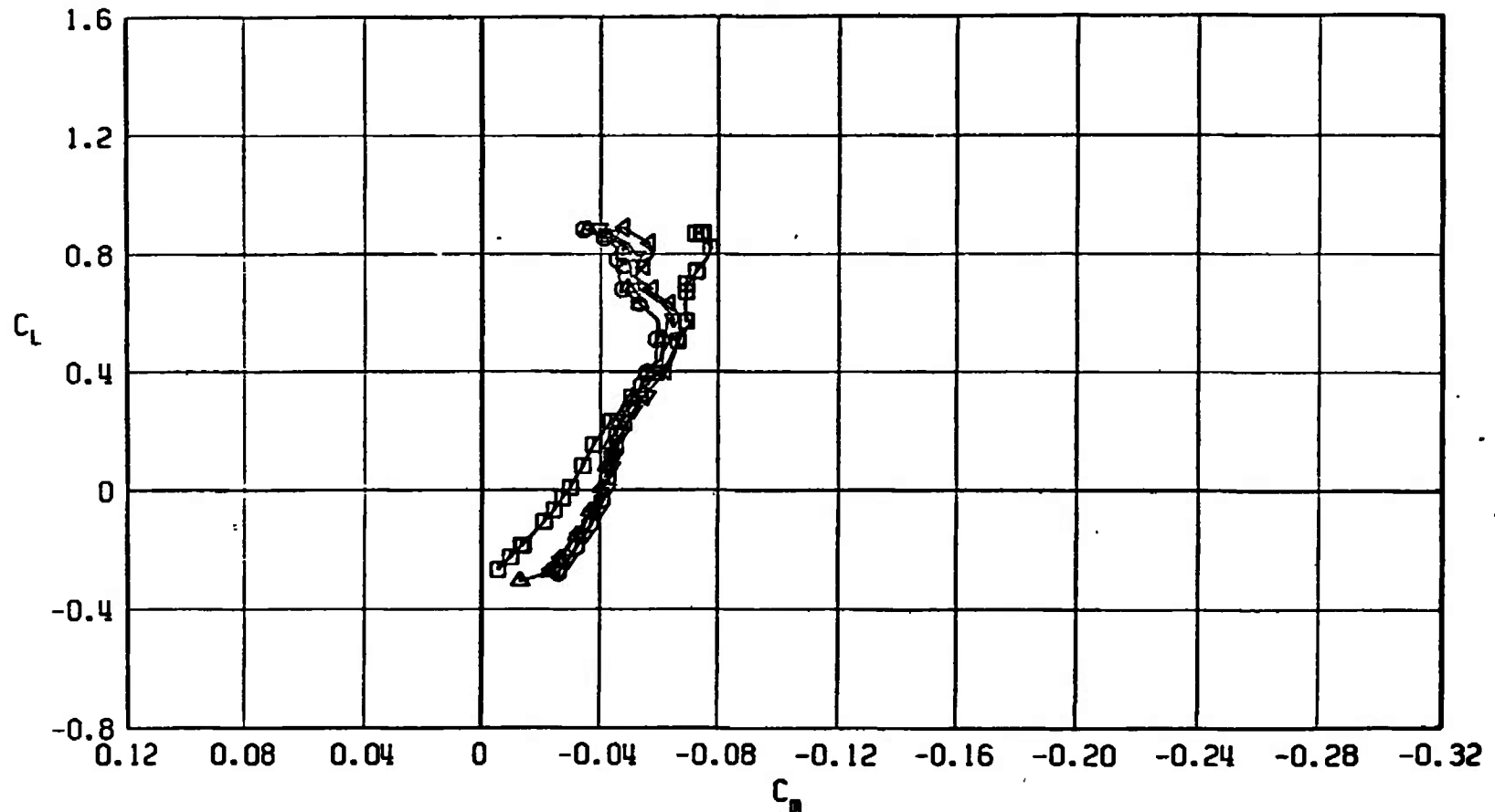


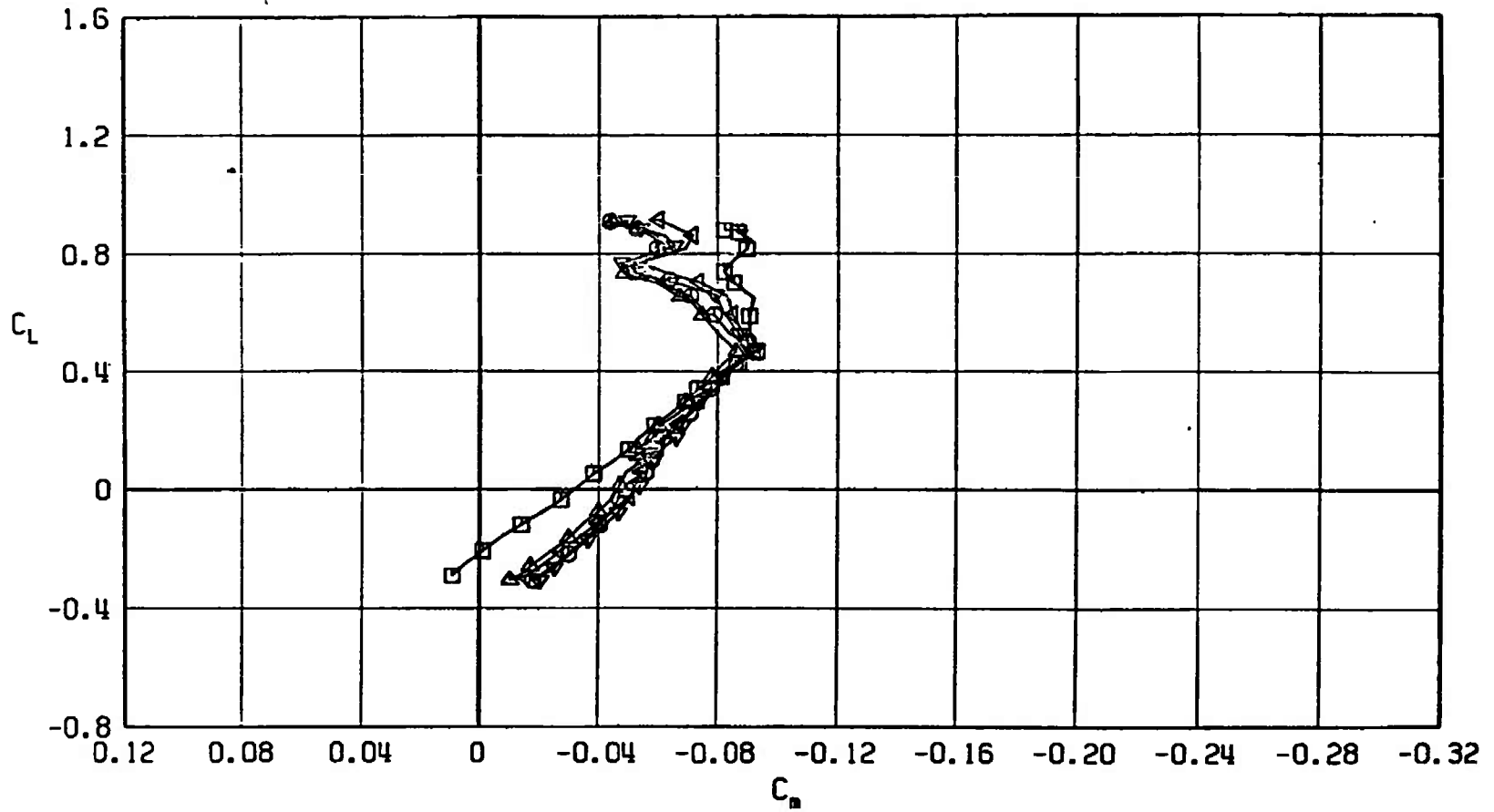
Fig. 45 Pitching-Moment Coefficient Variation with Lift Coefficient for Configurations F401, F408, F407, F410, and F411

SYMBOL	CONFIGURATION
□	F401
○	F411
△	F410
◀	F408
▼	F409



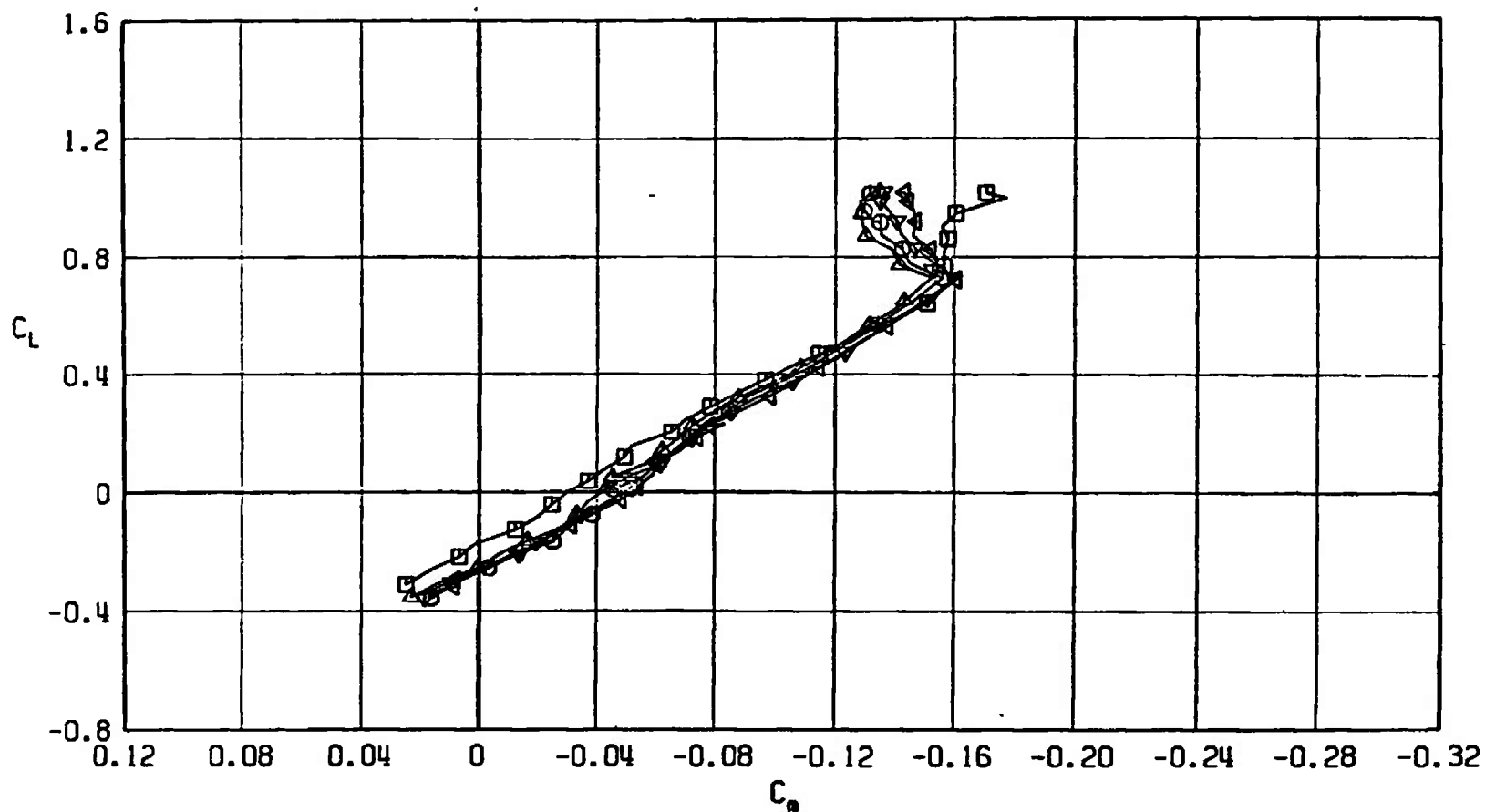
b.  $M_\infty = 0.90$   
Fig. 45 Continued

SYMBOL	CONFIGURATION
□	F401
○	F411
△	F410
◀	F408
▽	F409



c.  $M_\infty = 0.95$   
Fig. 45 Continued

SYMBOL	CONFIGURATION
□	F401
○	F411
△	F410
◀	F408
▼	F409

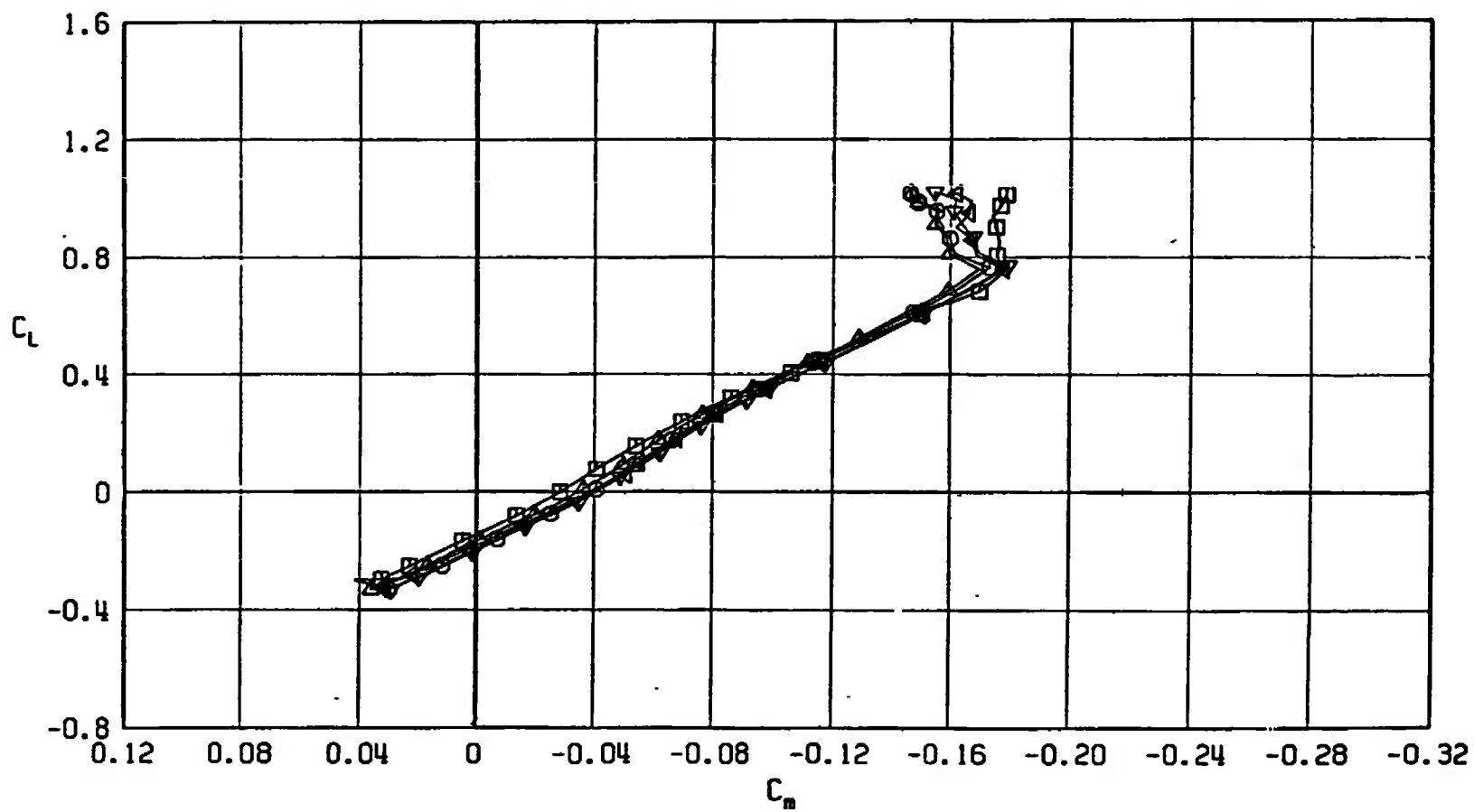


d.  $M_\infty = 1.05$   
Fig. 45 Continued



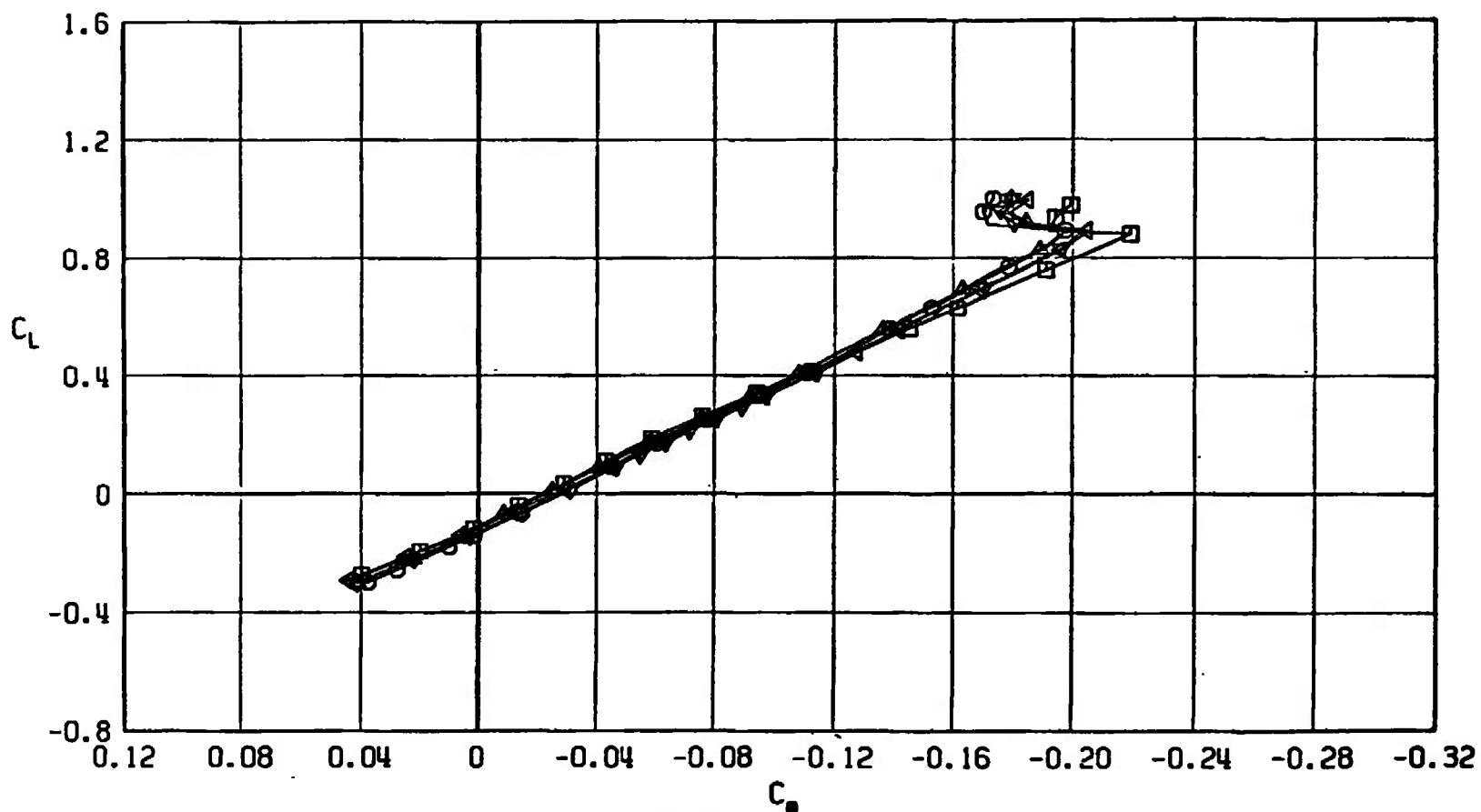
## SYMBOL - CONFIGURATION

□	F401
○	F411
△	F410
▽	F408
▲	F409



e.  $M_\infty = 1.10$   
Fig. 45 Continued

SYMBOL	CONFIGURATION
□	F401
○	F411
△	F410
▽	F408
▼	F409



f.  $M_\infty = 1.20$   
Fig. 45 Concluded

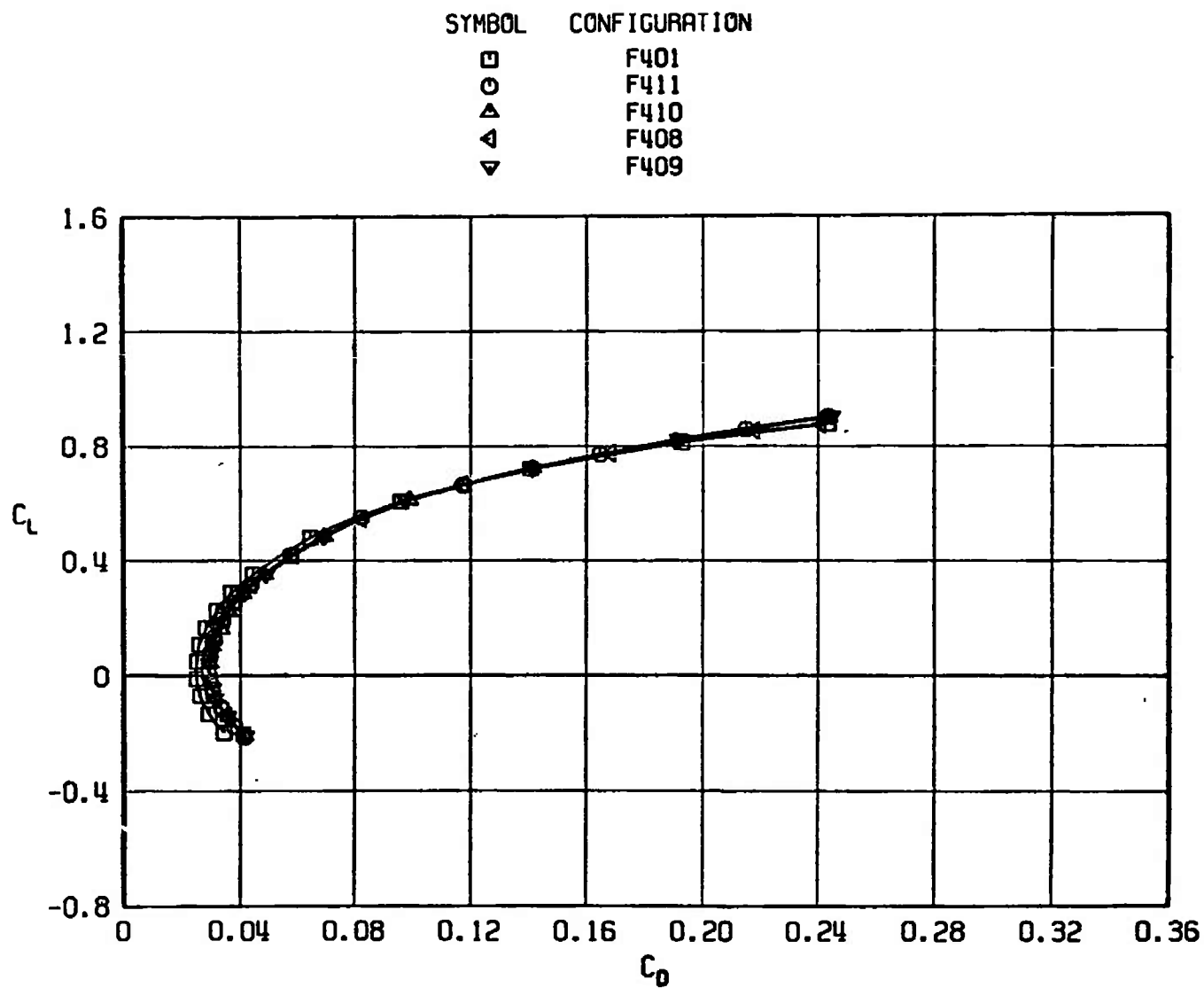
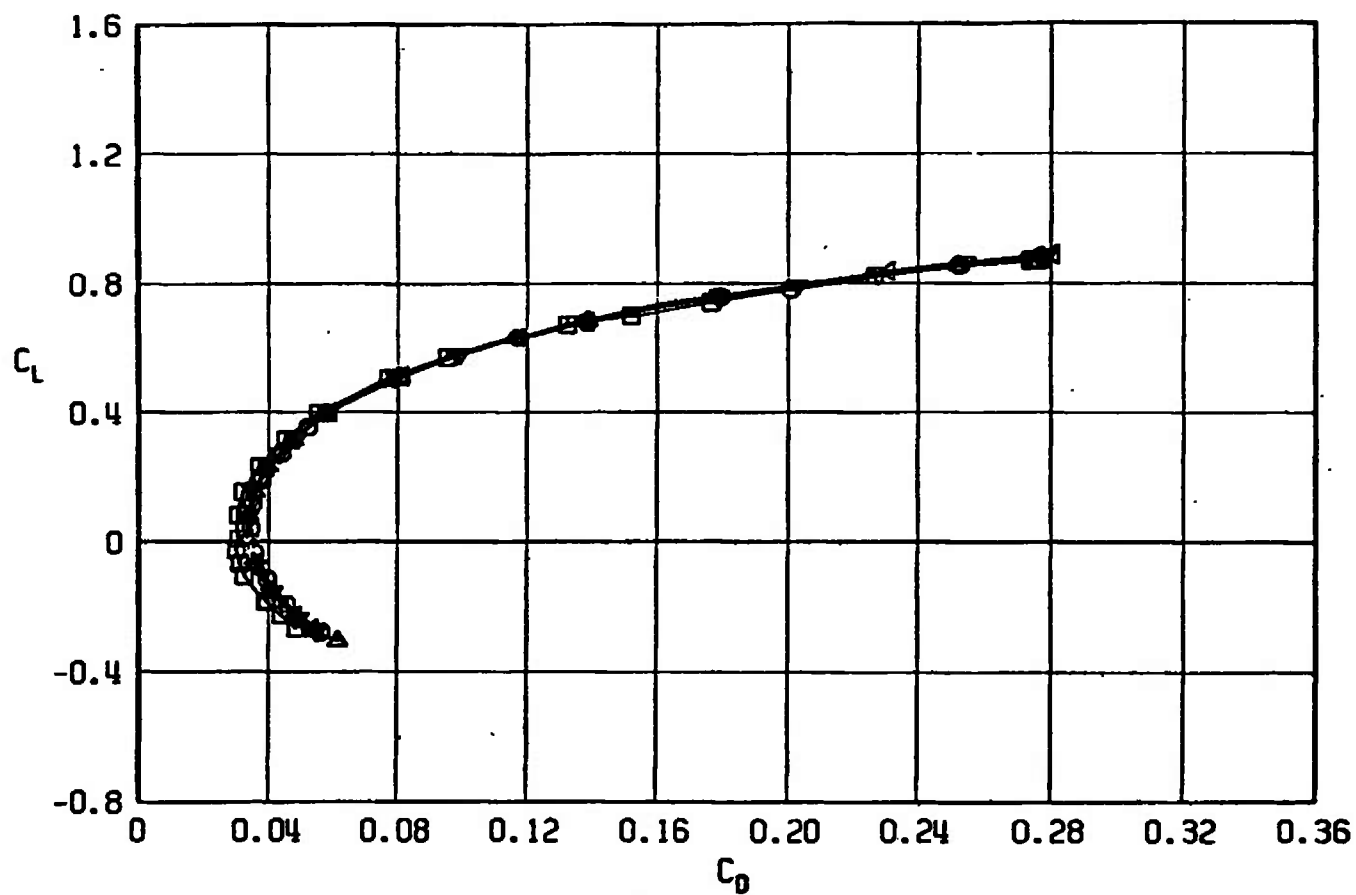
a.  $M_\infty = 0.50$ 

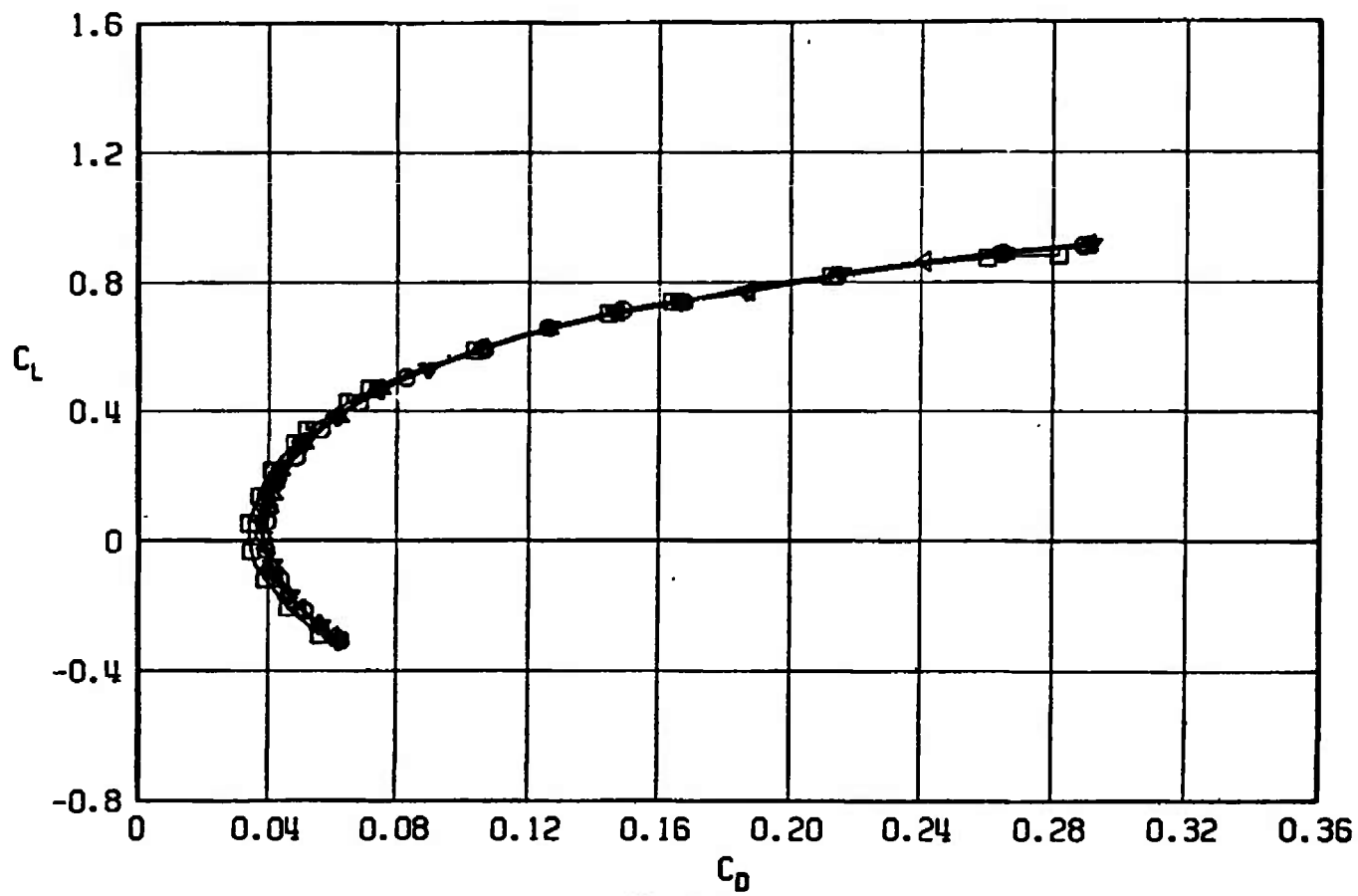
Fig. 46 Drag Coefficient Variation with Lift Coefficient for Configurations F401, F408, F407, F410, and F411

SYMBOL	CONFIGURATION
□	F401
○	F411
△	F410
◀	F408
▼	F409

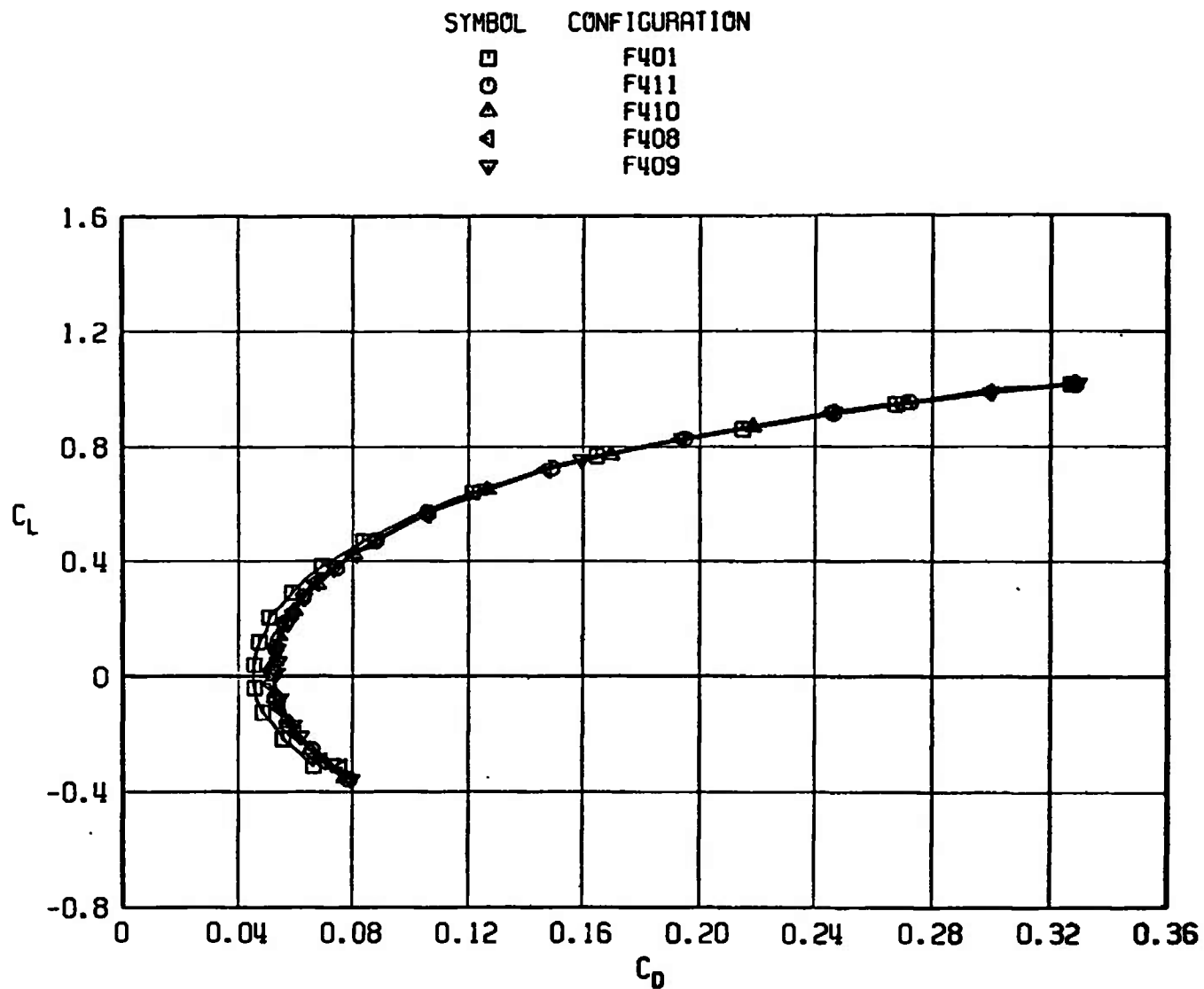


b.  $M_\infty = 0.90$   
Fig. 46 Continued

SYMBOL	CONFIGURATION
□	F401
○	F411
△	F410
▽	F408
▲	F409

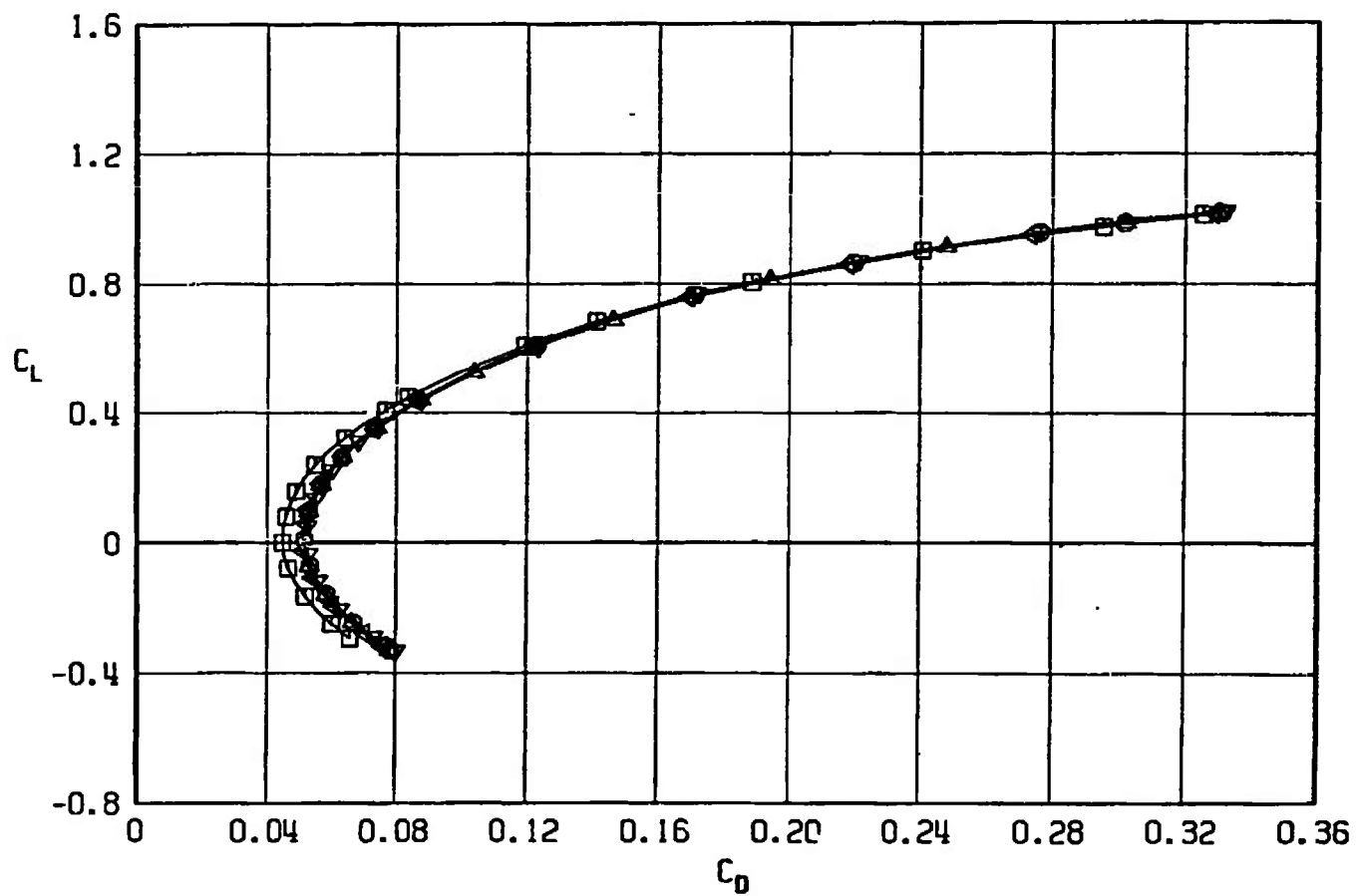


c.  $M_\infty = 0.95$   
Fig. 46 Continued

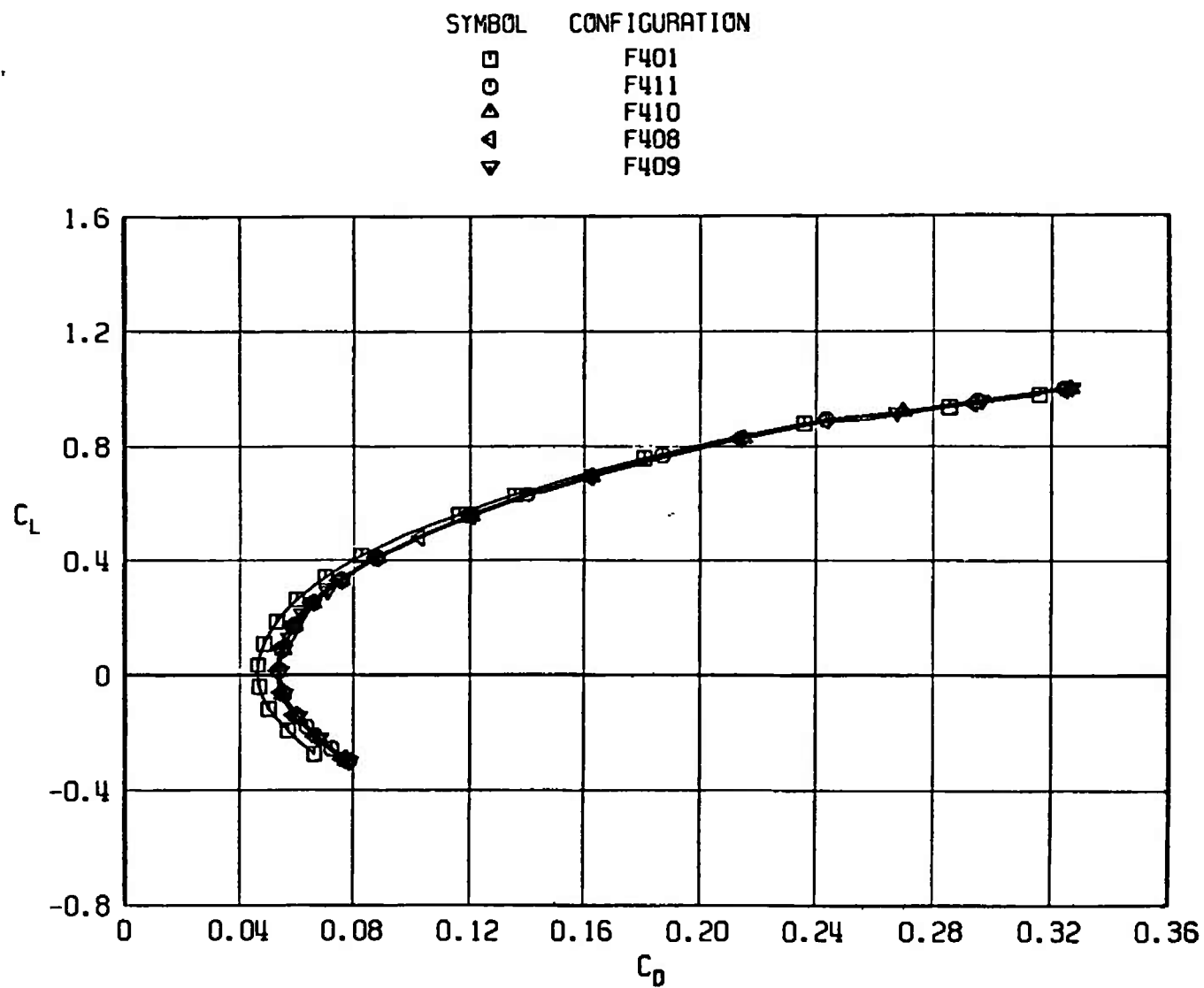


d.  $M_\infty = 1.05$   
Fig. 46 Continued

SYMBOL	CONFIGURATION
□	F401
○	F411
△	F410
▽	F408
◊	F409



e.  $M_\infty = 1.10$   
Fig. 46 Continued



f.  $M_\infty = 1.20$   
Fig. 46 Concluded



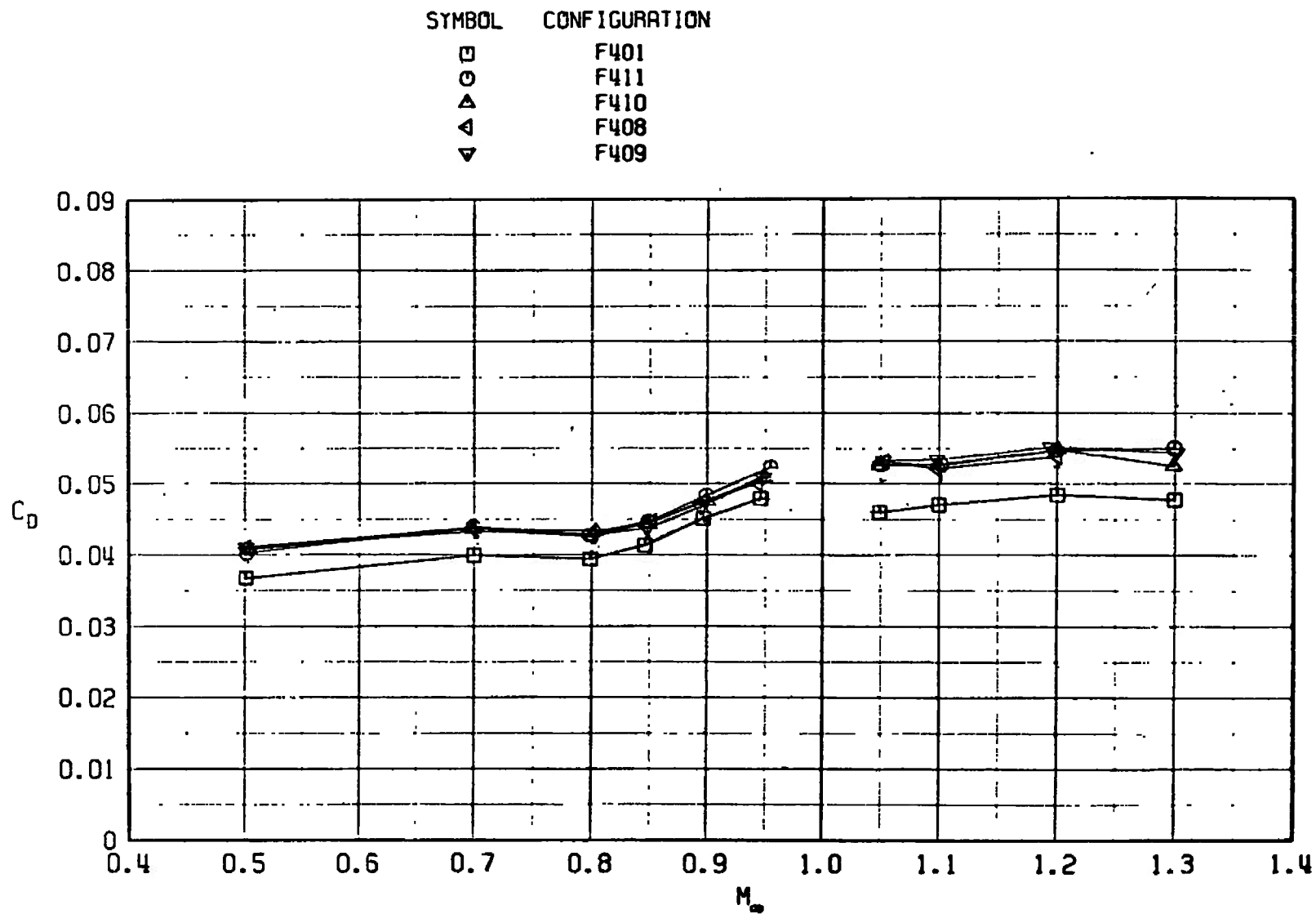


Fig. 47 Drag Coefficient Variation with Mach Number at  $C_L = 0.30$ ,  $M_\infty < 1.0$ , and  $C_L = 0.1$ ,  $M_\infty > 1.0$  for Configurations F401, F408, F407, F410, and F411

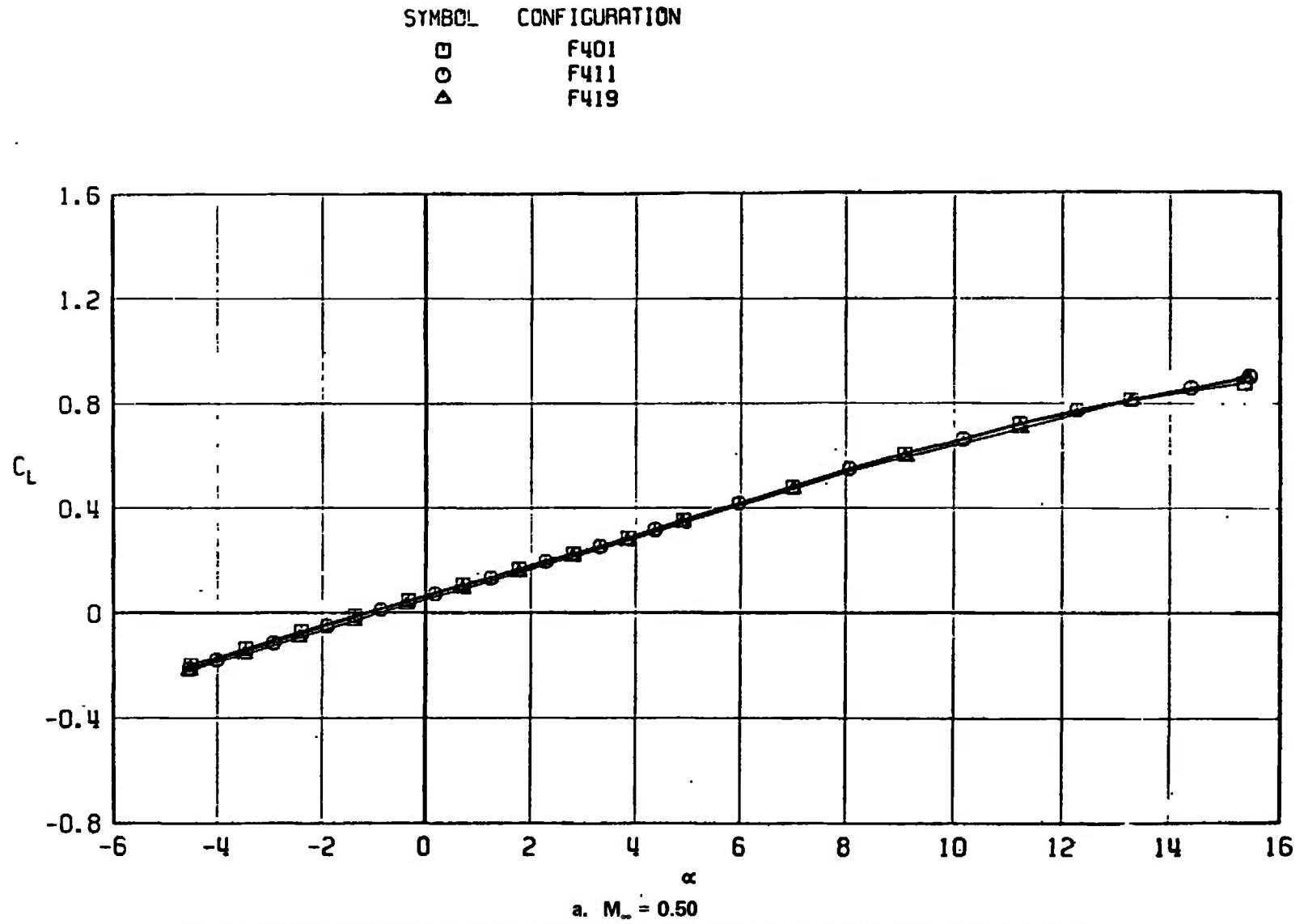
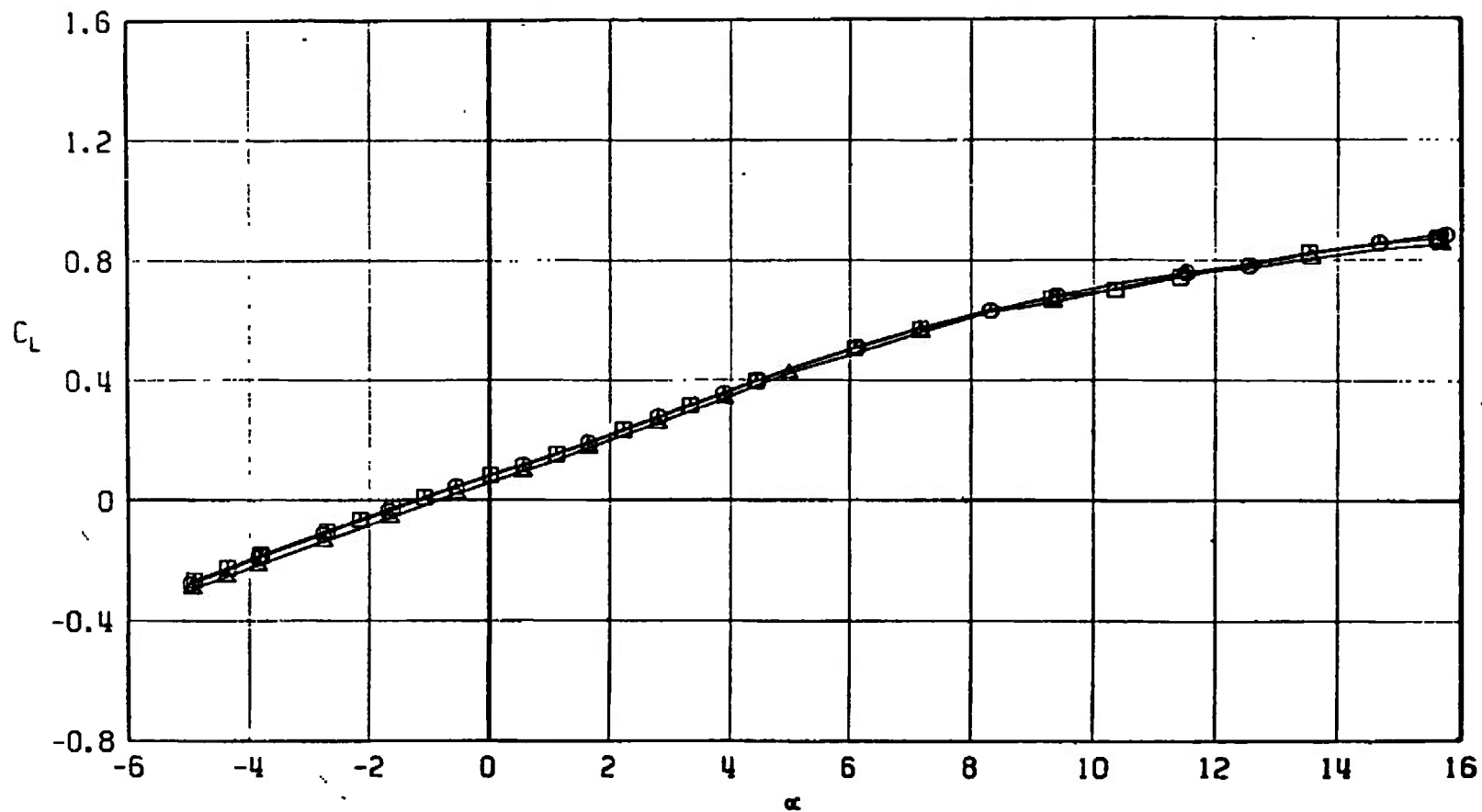


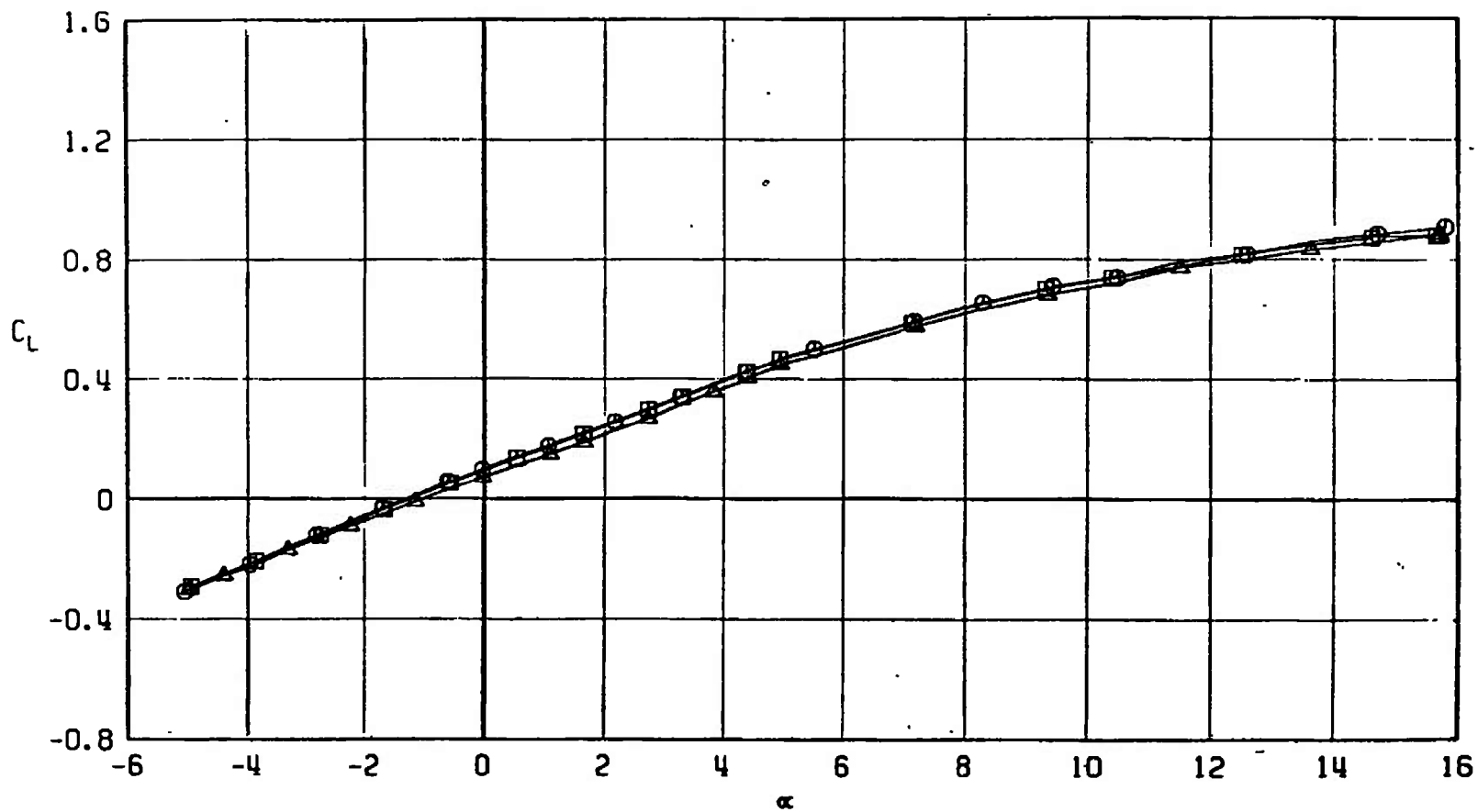
Fig. 48 Lift Coefficient Variation with Angle of Attack for Configurations F401, F411, and F419

SYMBOL	CONFIGURATION
□	F401
○	F411
△	F419



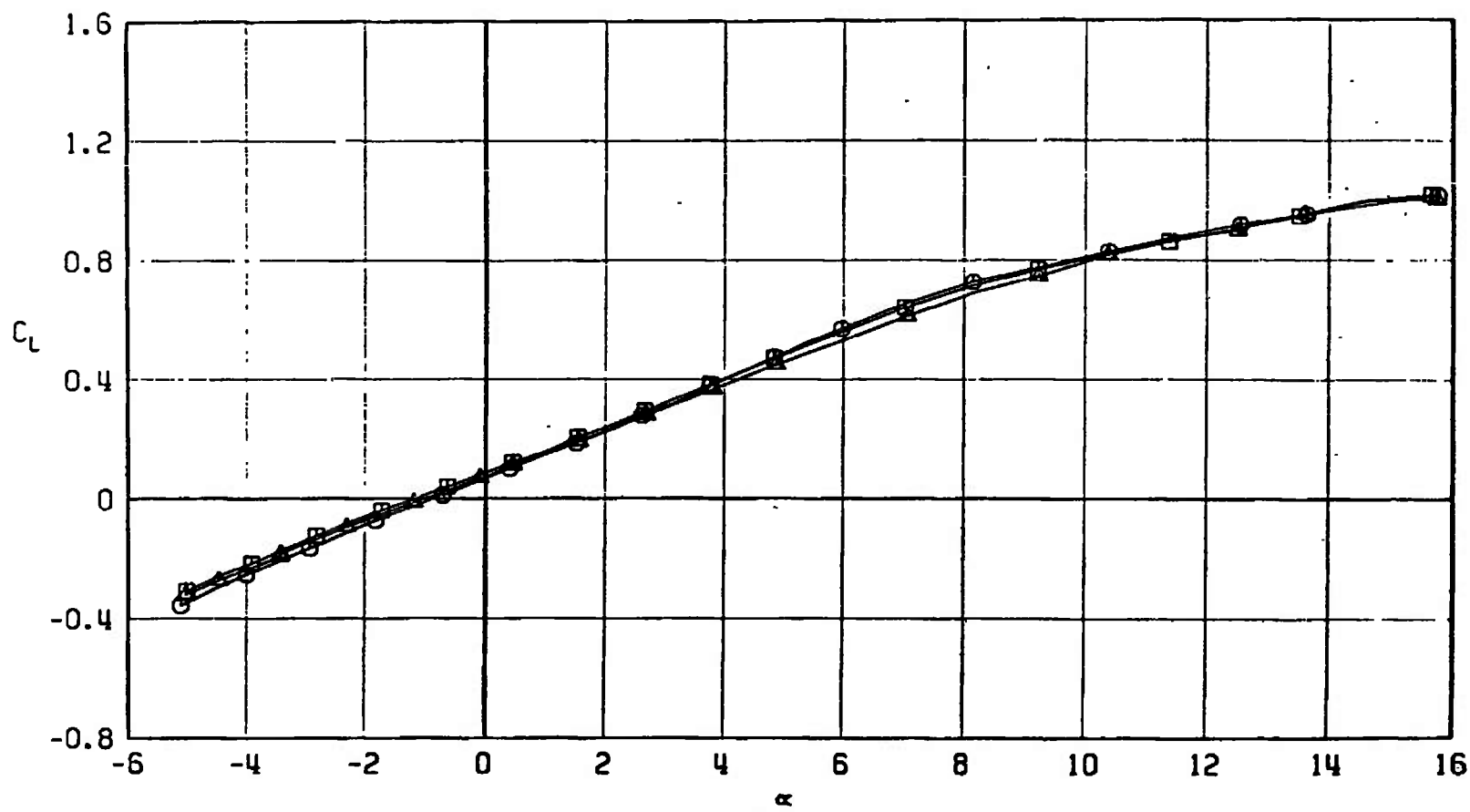
b.  $M_\infty = 0.90$   
Fig. 48 Continued

SYMBOL	CONFIGURATION
□	F401
○	F411
△	F419



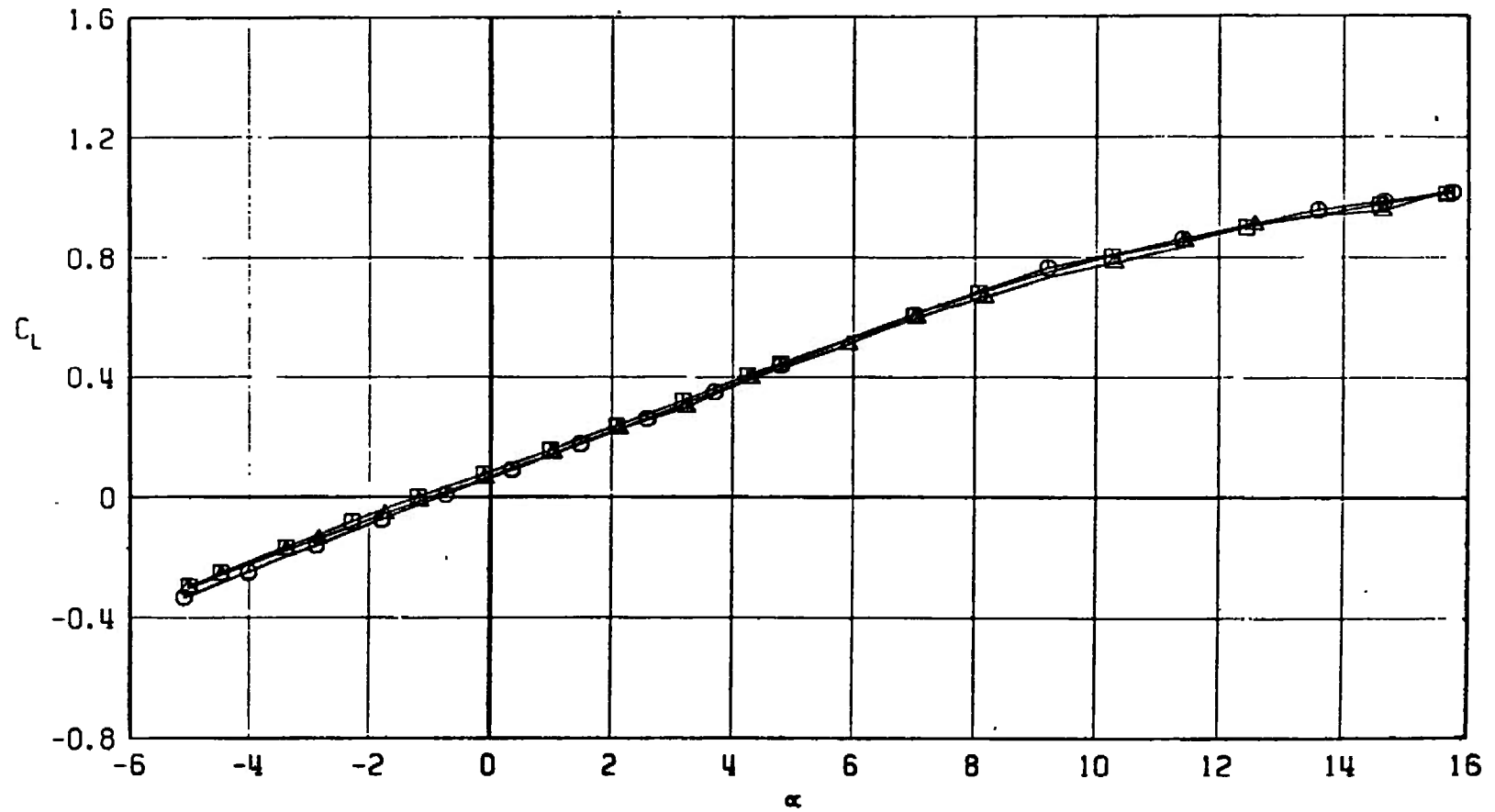
c.  $M_\infty = 0.95$   
Fig. 48 Continued

SYMBOL	CONFIGURATION
□	F401
○	F411
△	F419



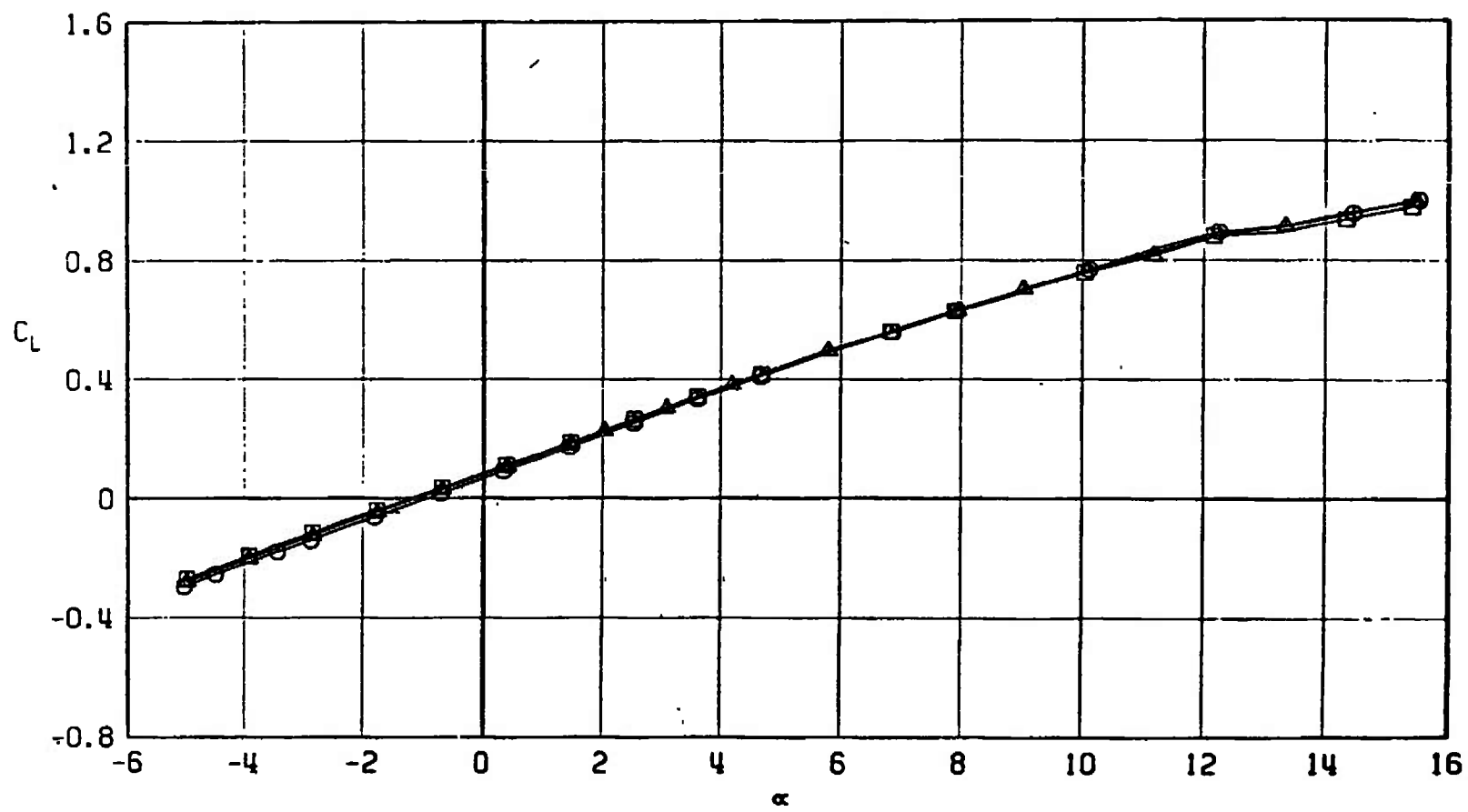
d.  $M_\infty = 1.05$   
Fig. 48 Continued

SYMBOL	CONFIGURATION
□	F401
○	F411
△	F419



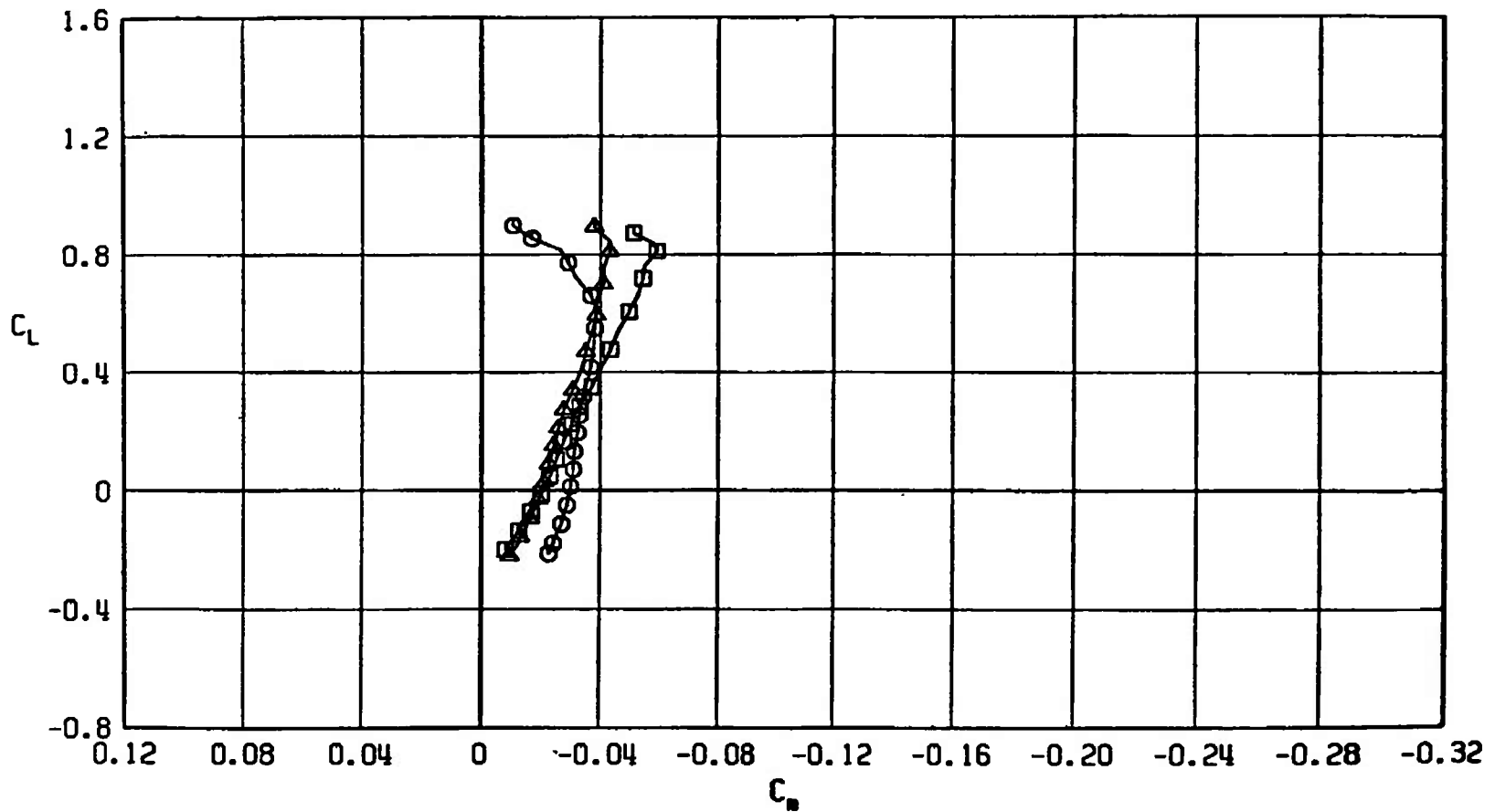
e.  $M_\infty = 1.10$   
Fig. 48 Continued

SYMBOL	CONFIGURATION
□	F401
○	F411
△	F419



f.  $M_\infty = 1.20$   
Fig. 48 Concluded

SYMBOL	CONFIGURATION
□	F401
○	F411
△	F419

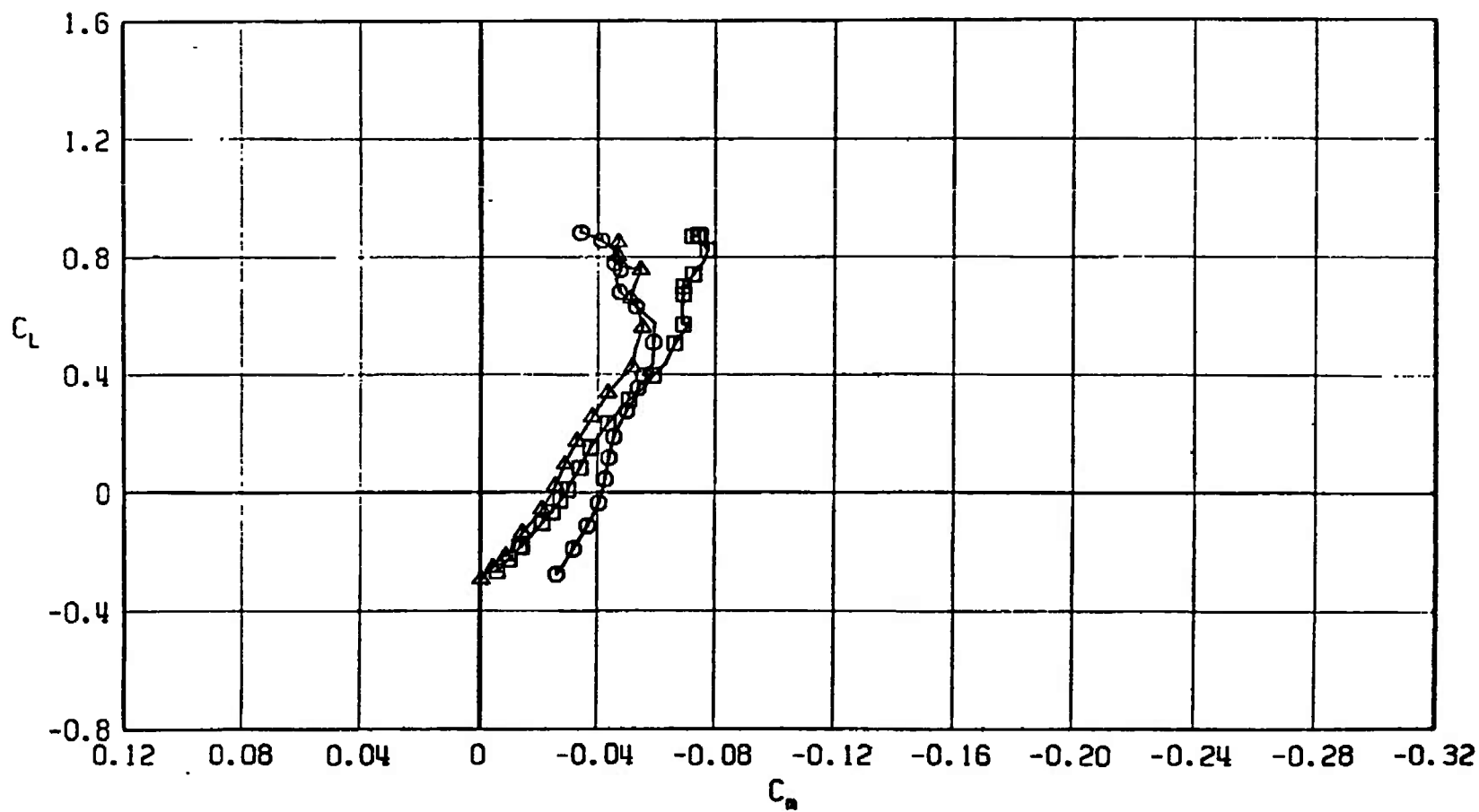


a.  $M_\infty = 0.50$

Fig. 49 Pitching-Moment Coefficient Variation with Lift Coefficient for Configurations F401, F411, and F419

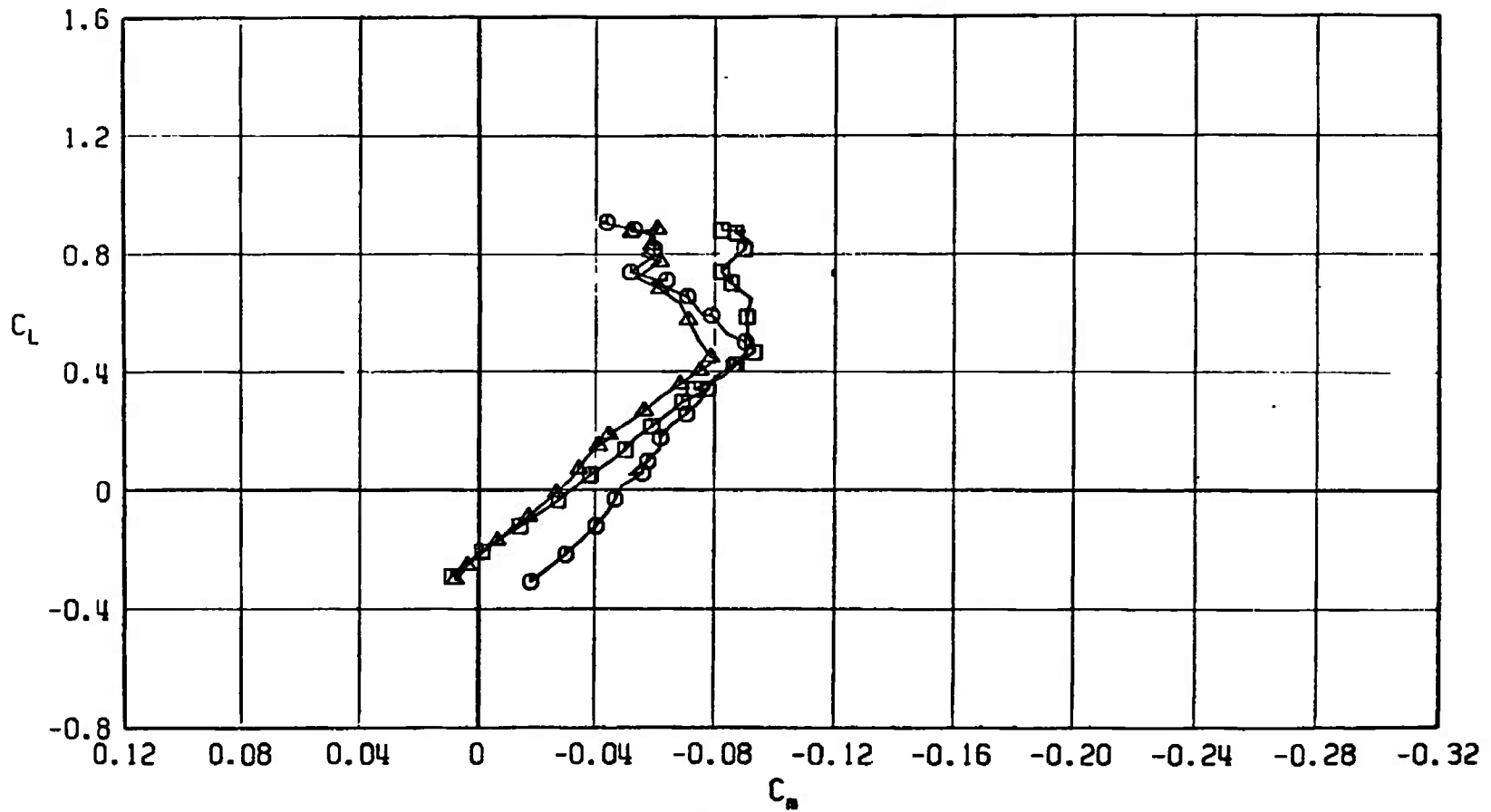


SYMBOL	CONFIGURATION
□	F401
○	F411
△	F419



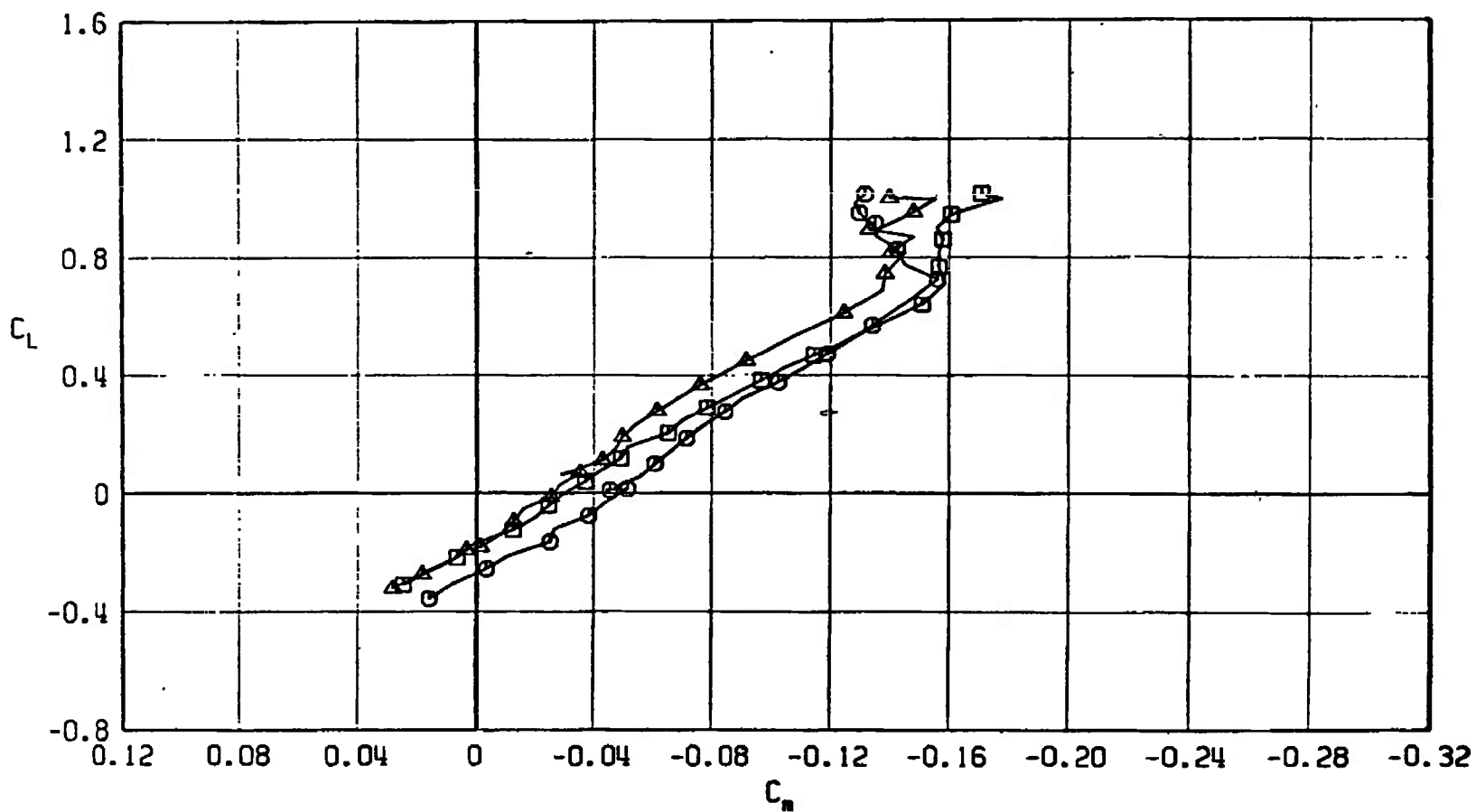
b.  $M_\infty = 0.90$   
Fig. 49 Continued

SYMBOL	CONFIGURATION
□	F401
○	F411
△	F419



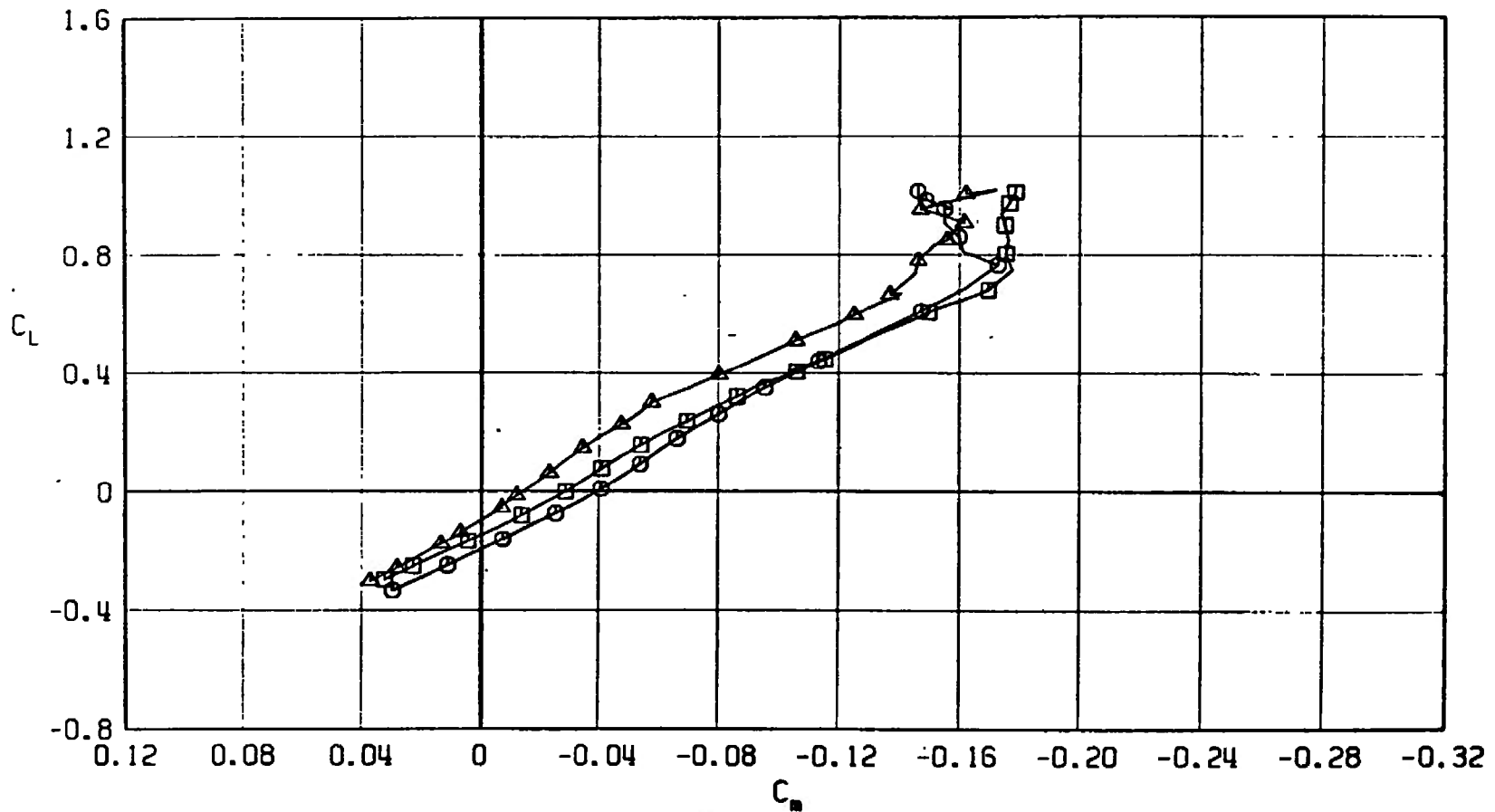
c.  $M_\infty = 0.95$   
Fig. 49 Continued

SYMBOL	CONFIGURATION
□	F401
○	F411
△	F419



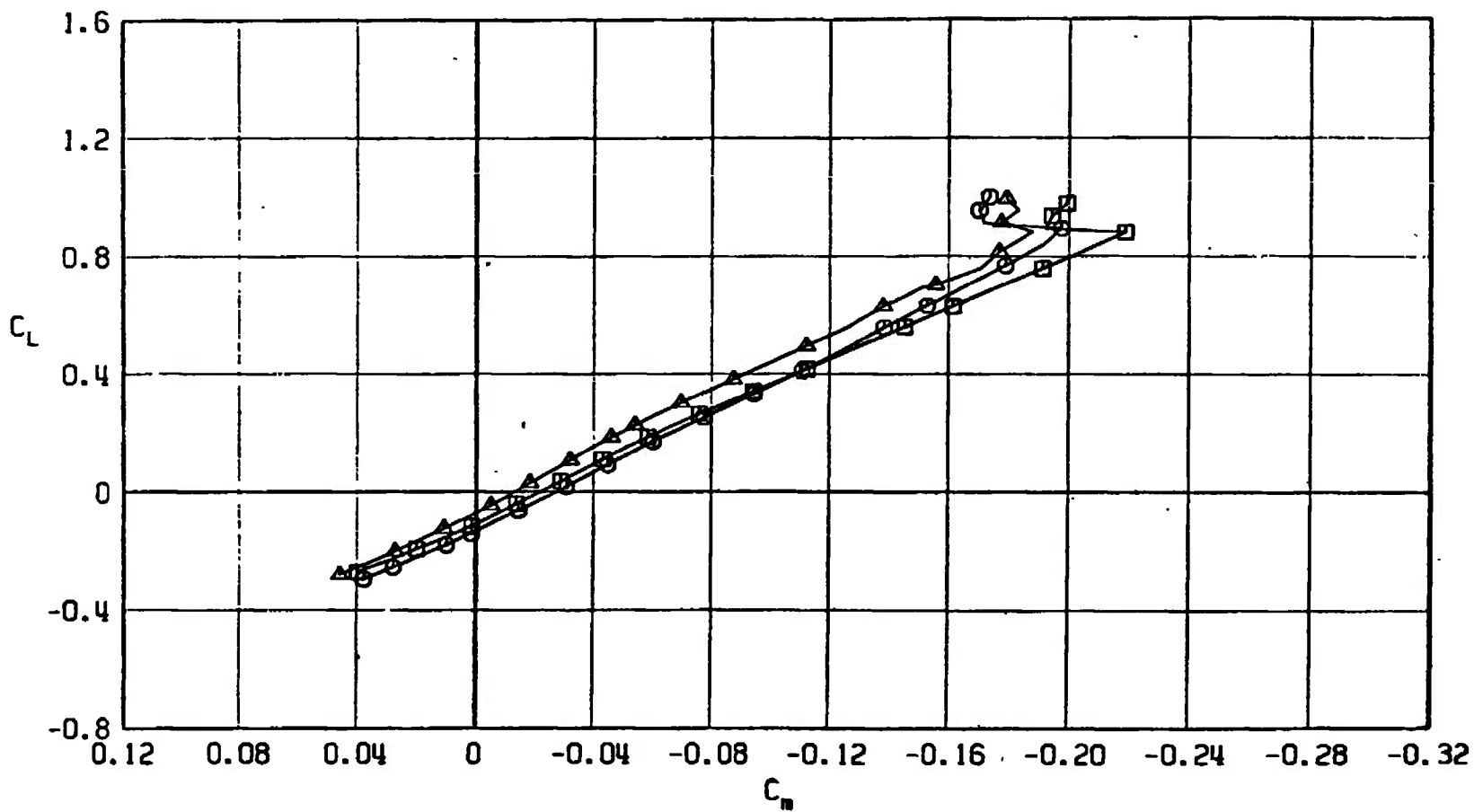
d.  $M_\infty = 1.05$   
Fig. 49 Continued

SYMBOL	CONFIGURATION
□	F401
○	F411
△	F419



e.  $M_\infty = 1.10$   
Fig. 49 Continued

SYMBOL	CONFIGURATION
□	F401
○	F411
△	F419



f.  $M_\infty = 1.20$   
Fig. 49 Concluded

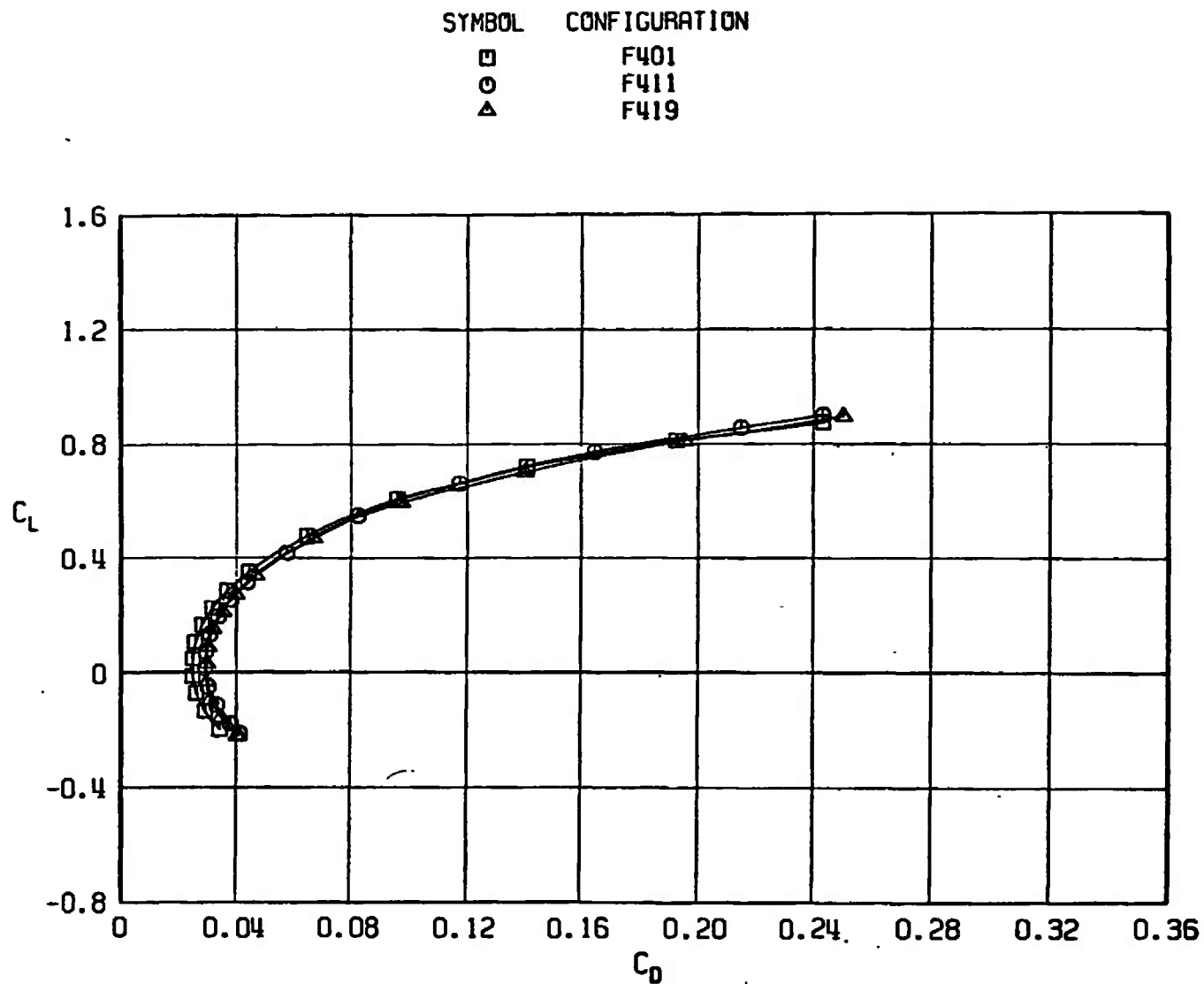
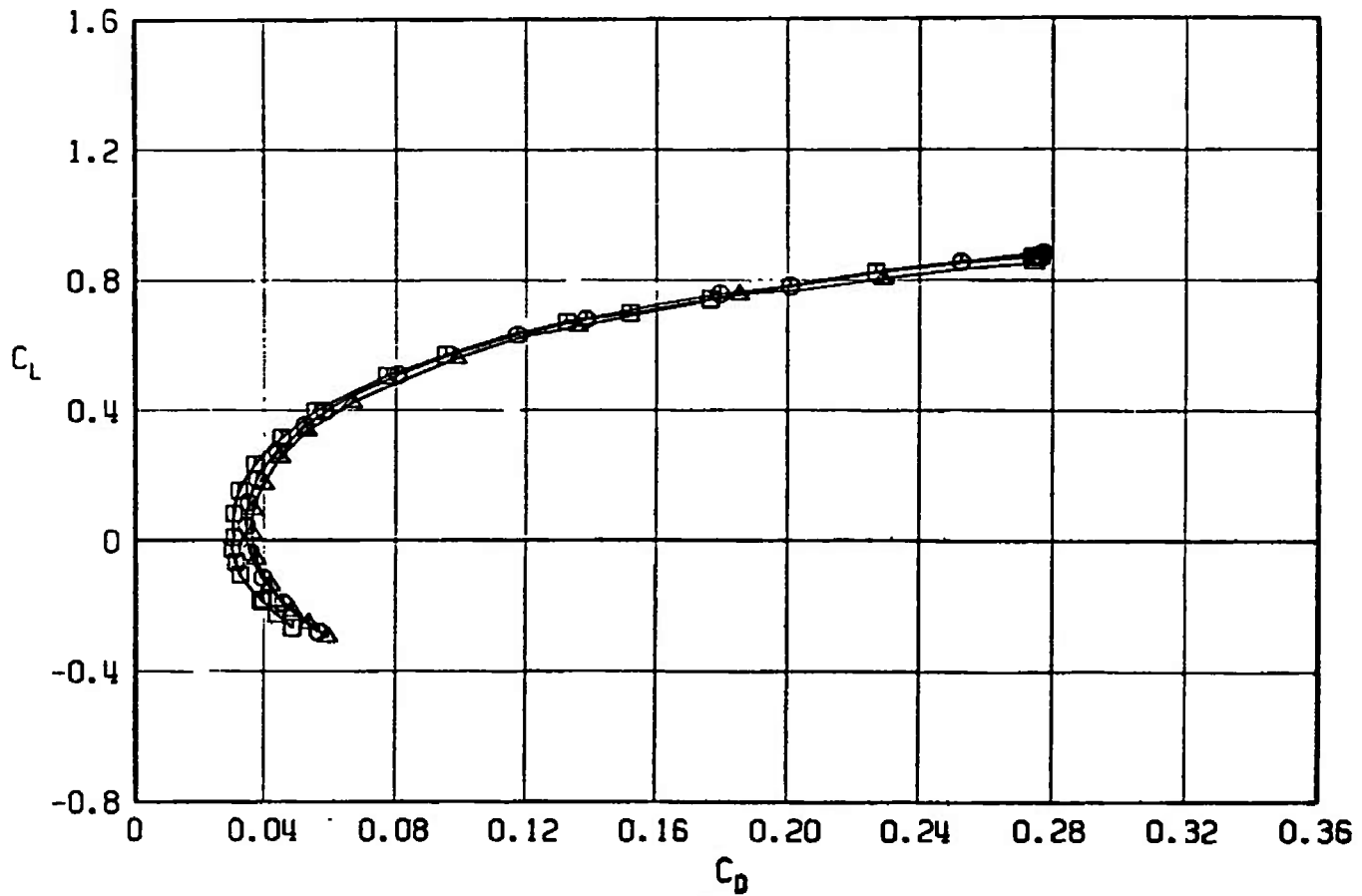
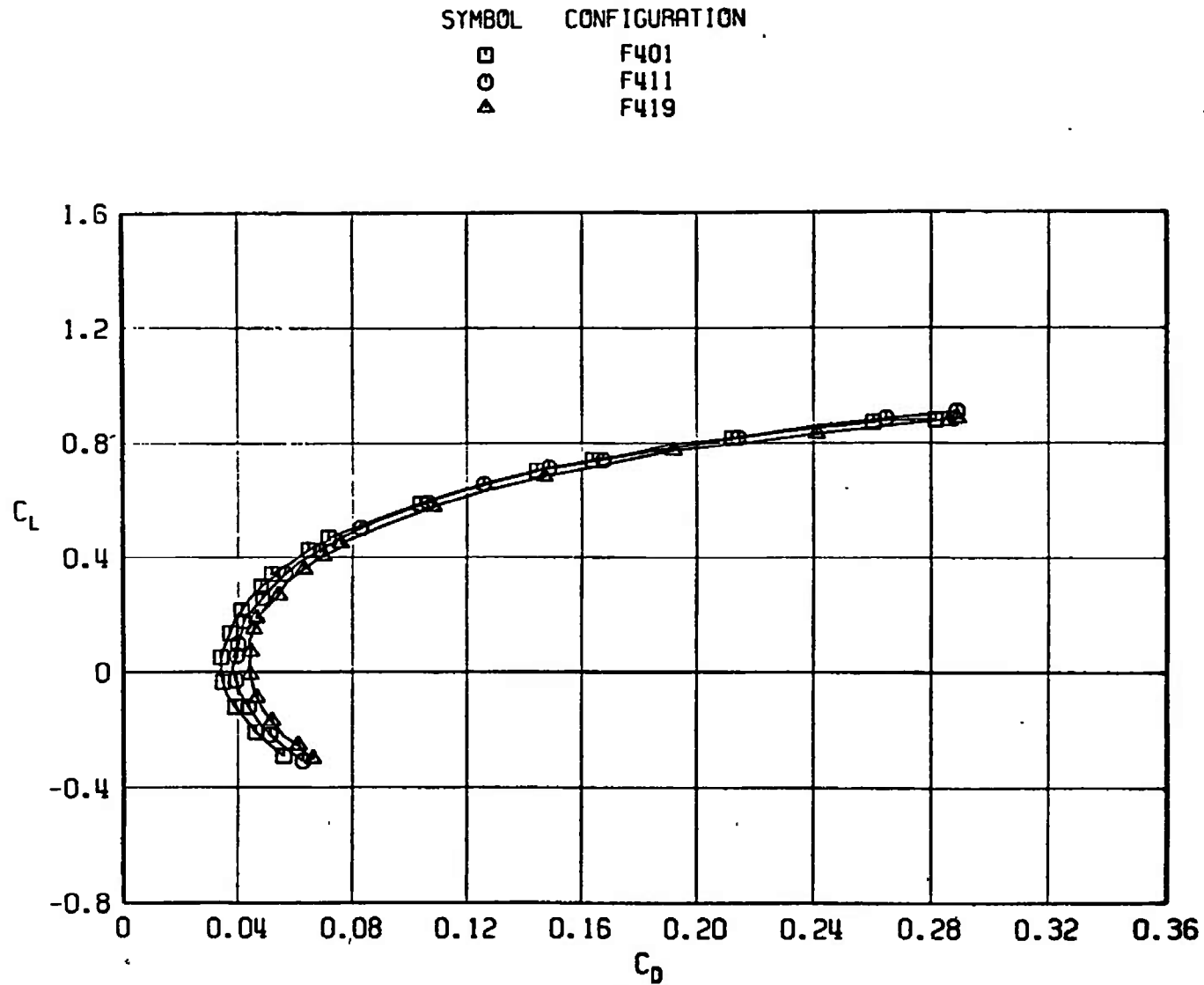
a.  $M_\infty = 0.50$ 

Fig. 50 Drag Coefficient Variation with Lift Coefficient for Configurations F401, F411, and F419

SYMBOL	CONFIGURATION
□	F401
○	F411
△	F419



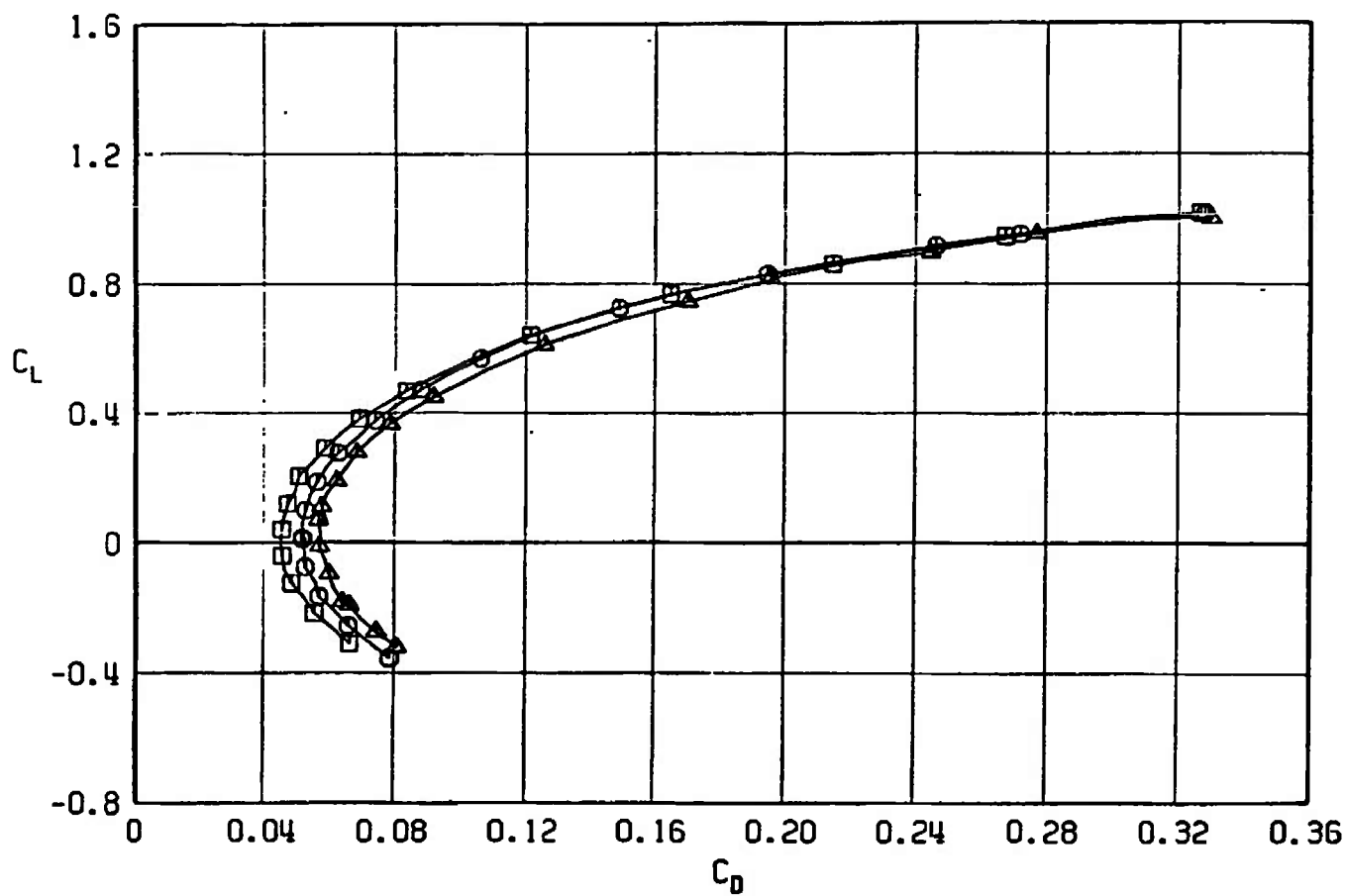
b.  $M_\infty = 0.90$   
Fig. 50 Continued



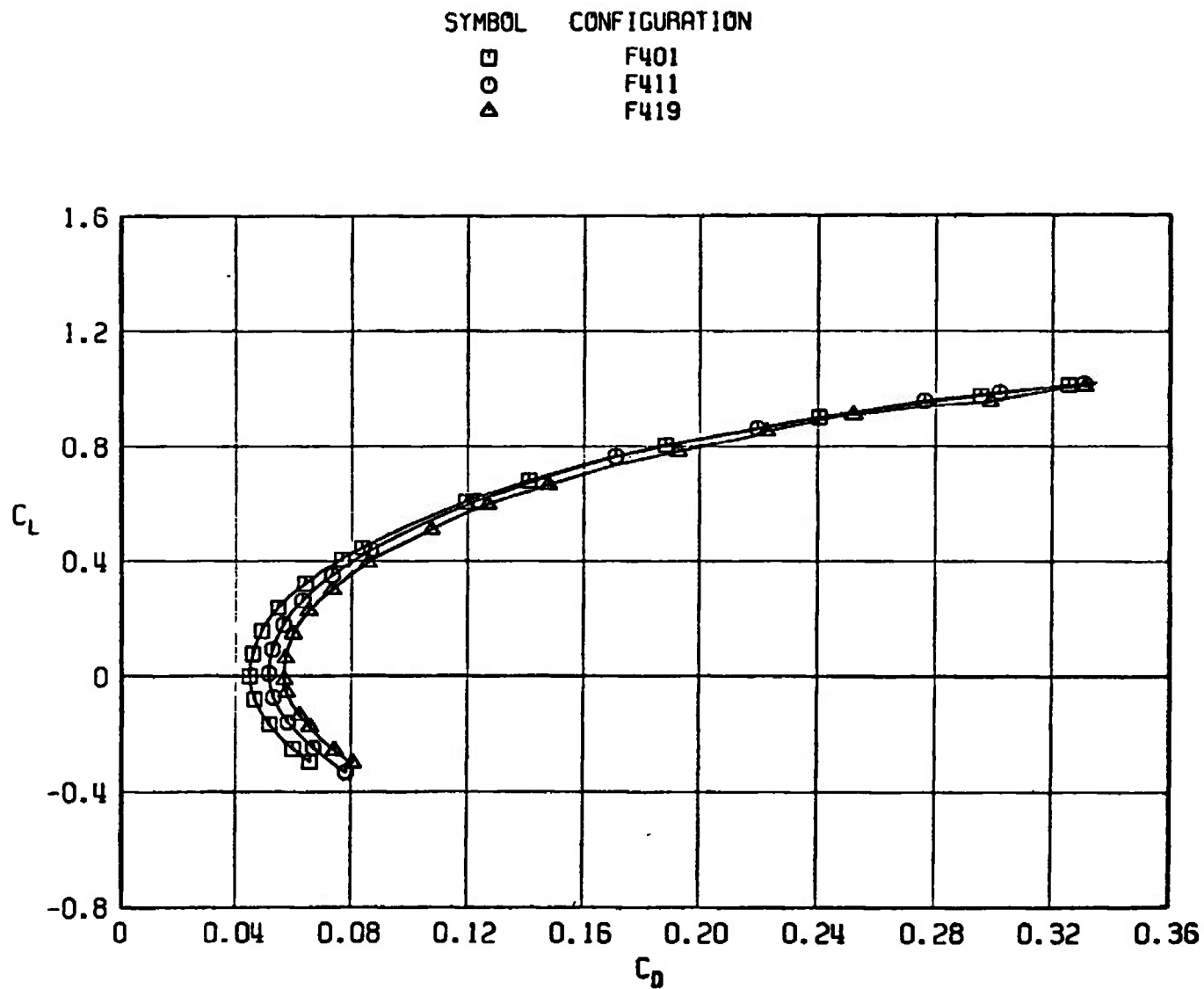
c.  $M_\infty = 0.95$   
Fig. 50 Continued



SYMBOL	CONFIGURATION
□	F401
○	F411
△	F419

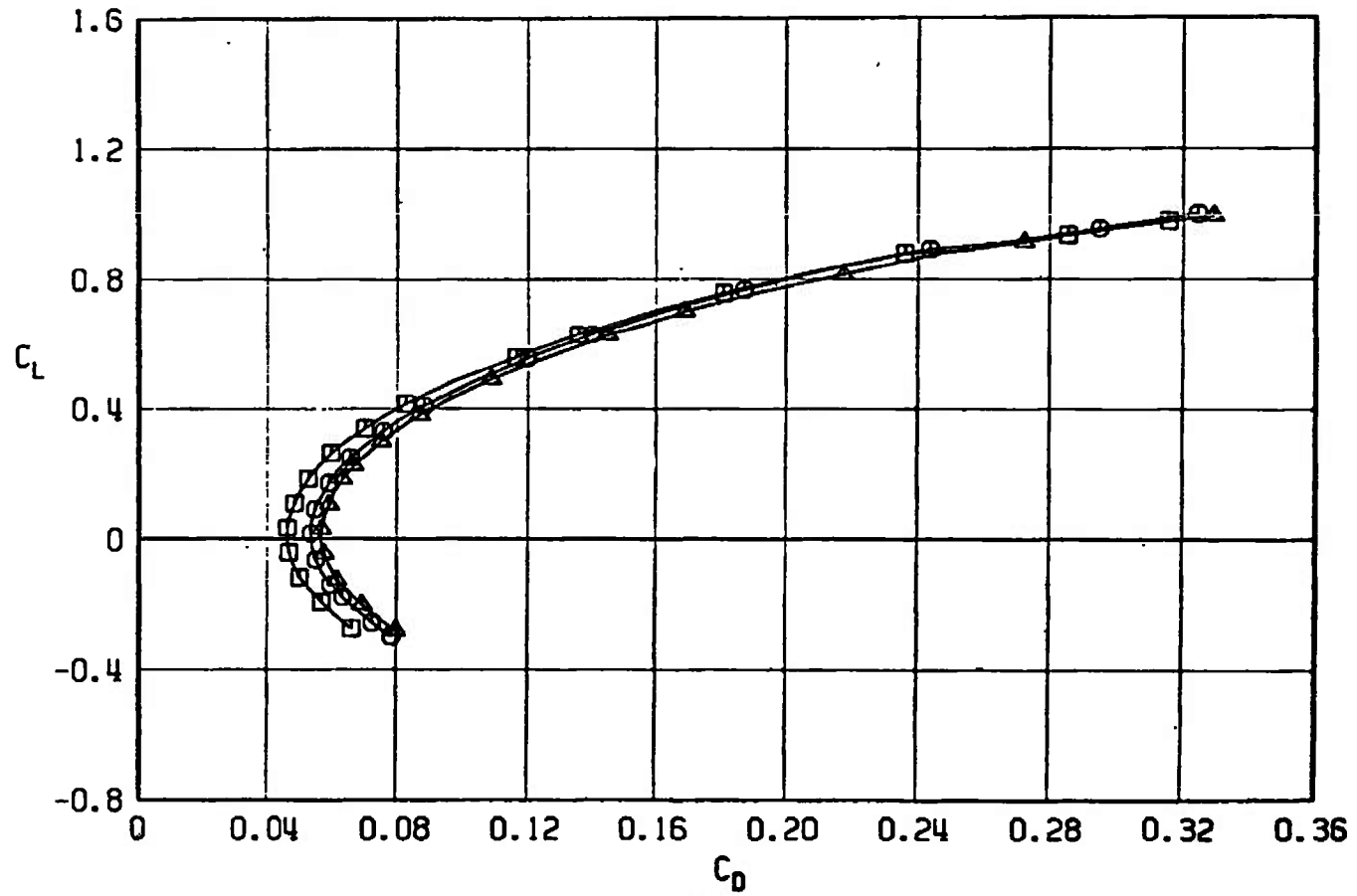


d.  $M_\infty = 1.05$   
Fig. 50 Continued



a.  $M_\infty = 1.10$   
Fig. 50 Continued

SYMBOL	CONFIGURATION
□	F401
○	F411
△	F419



f.  $M_\infty = 1.20$   
Fig. 50 Concluded

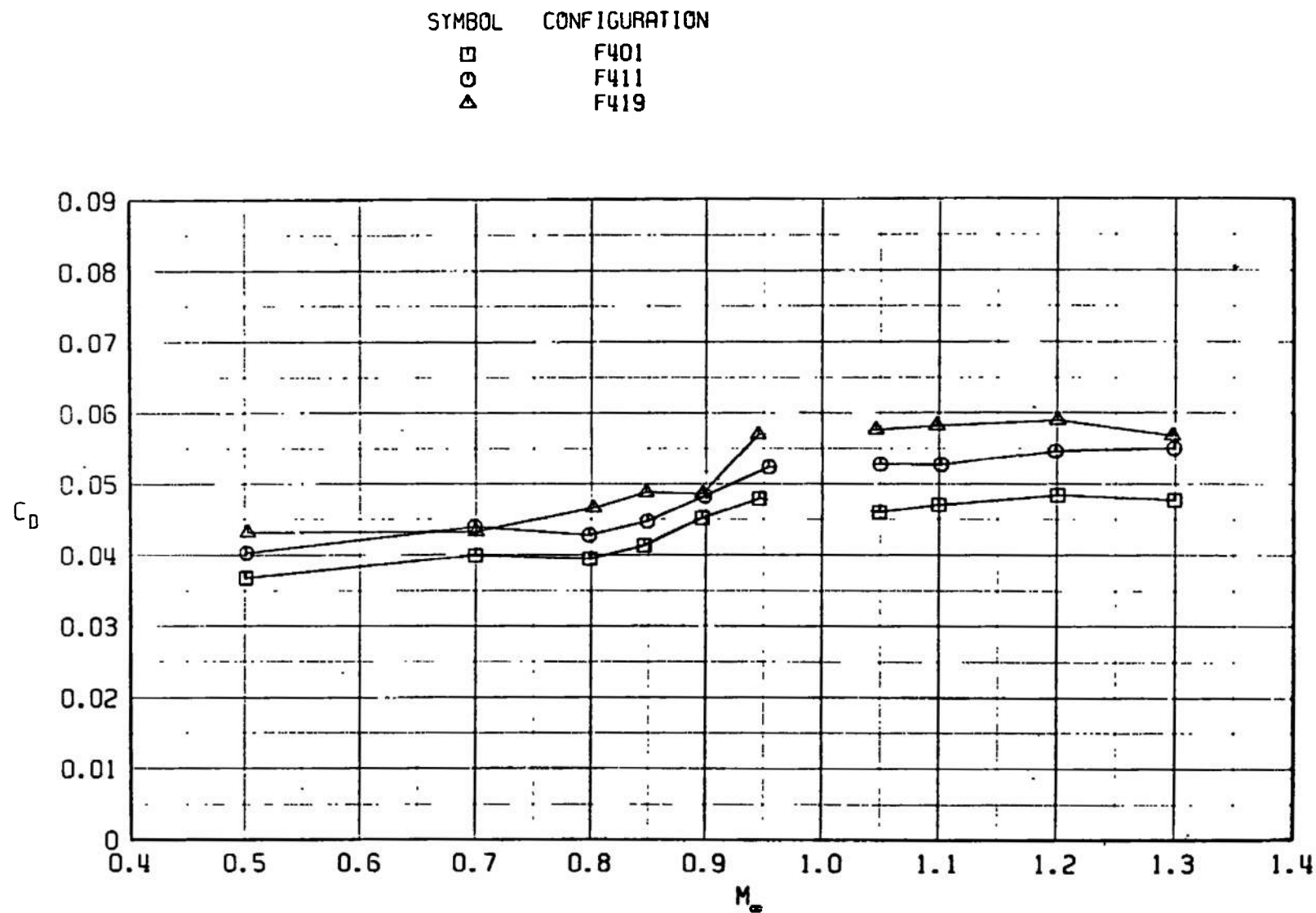


Fig. 51 Drag Coefficient Variation with Mach Number at  $C_L = 0.30$ ,  $M_\infty < 1.0$  and  $C_L = 0.1$ ,  $M_\infty > 1.0$  for Configurations F401, F411, and F419

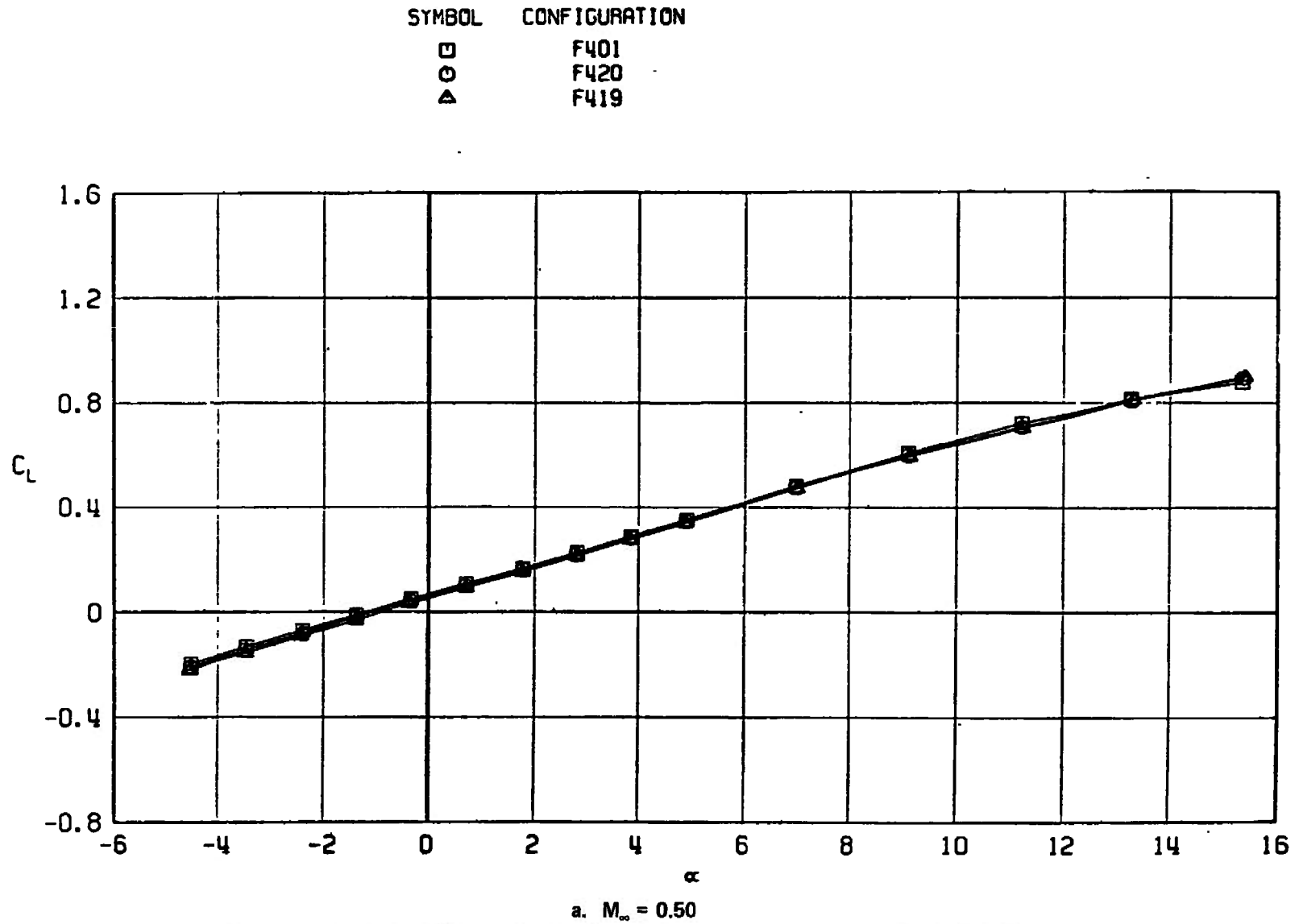
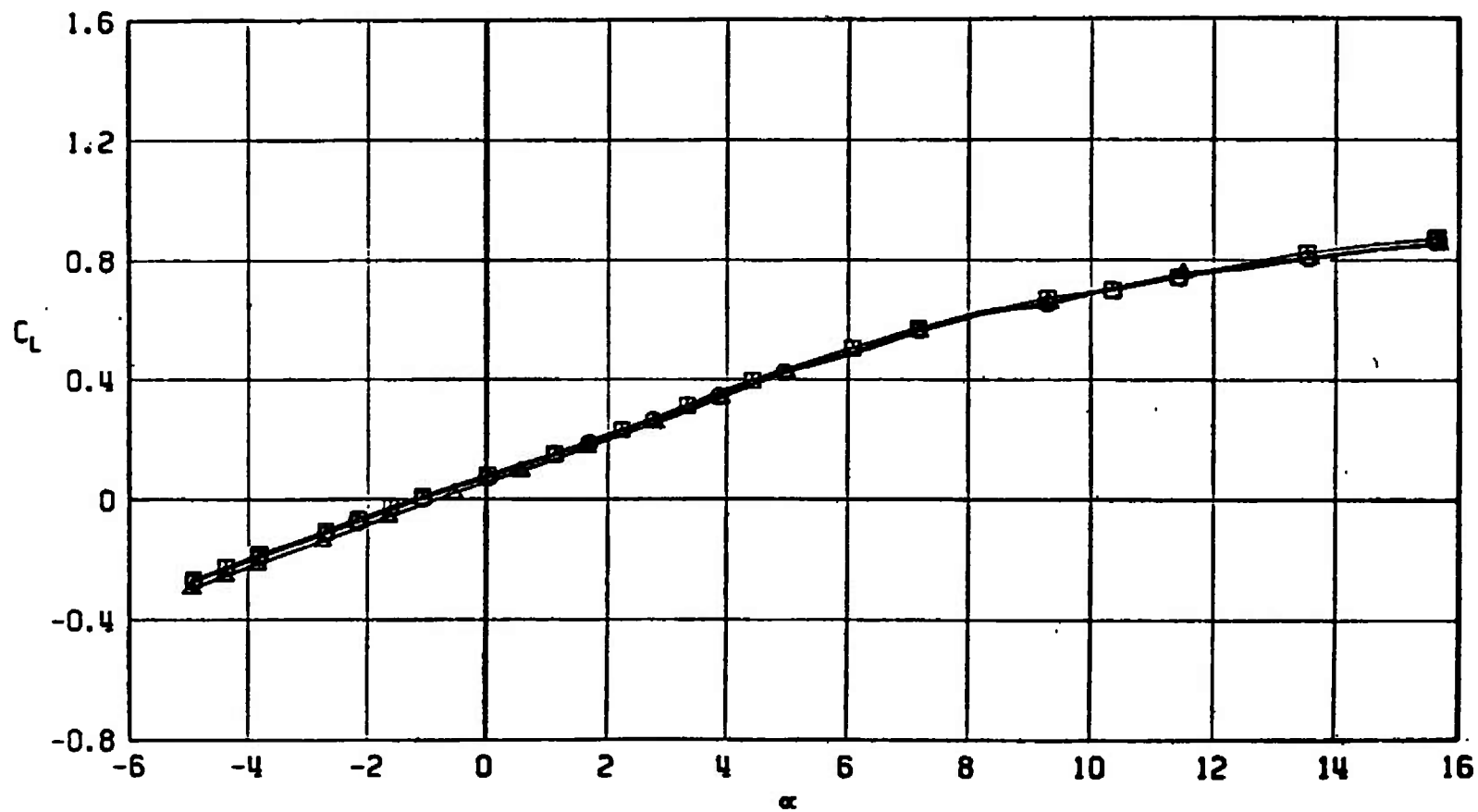


Fig. 52 Lift Coefficient Variation with Angle of Attack for Configurations F401, F419, and F420

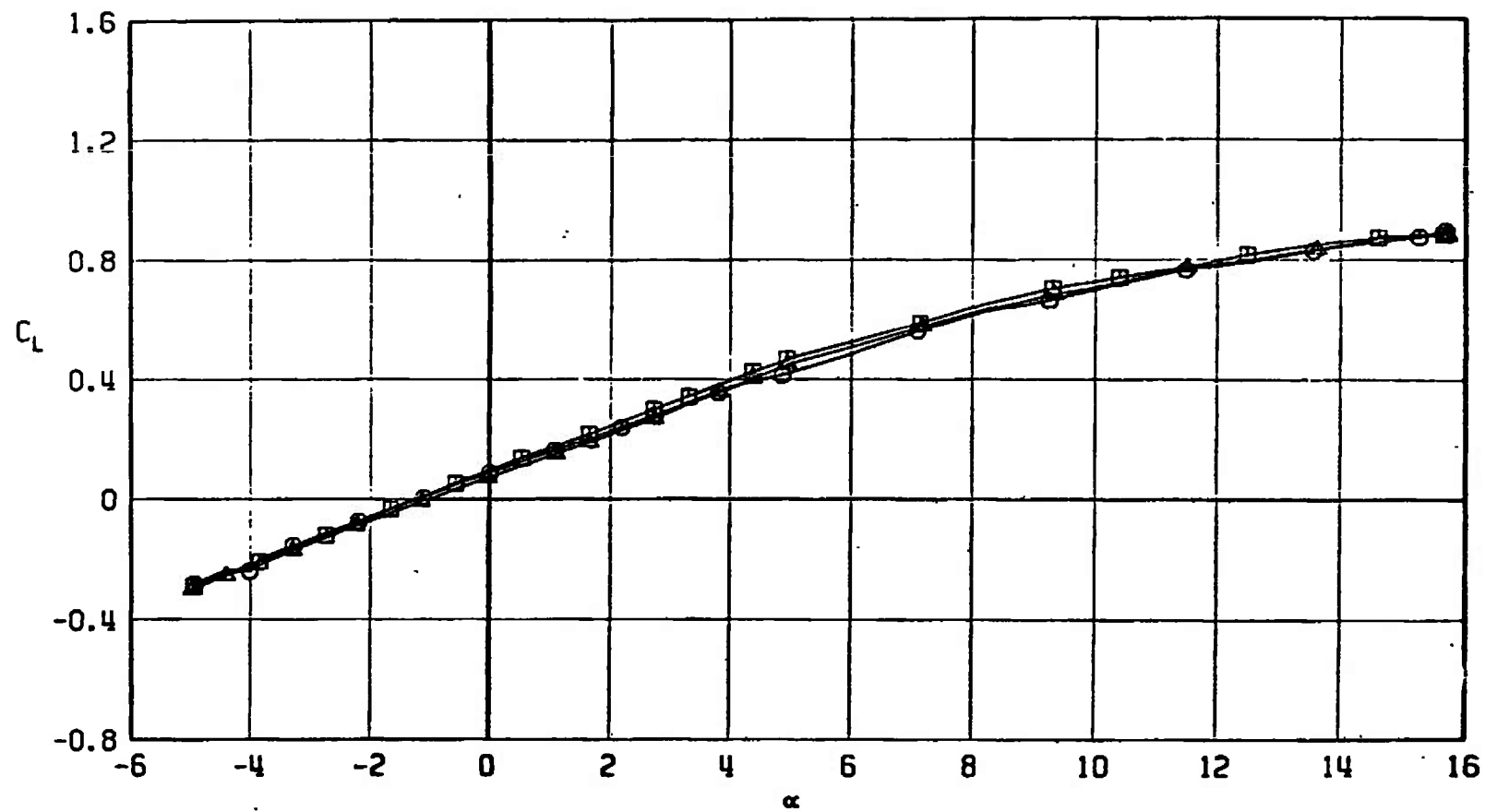
SYMBOL	CONFIGURATION
□	F401
○	F420
△	F419



b.  $M_\infty = 0.90$   
Fig. 52 Continued

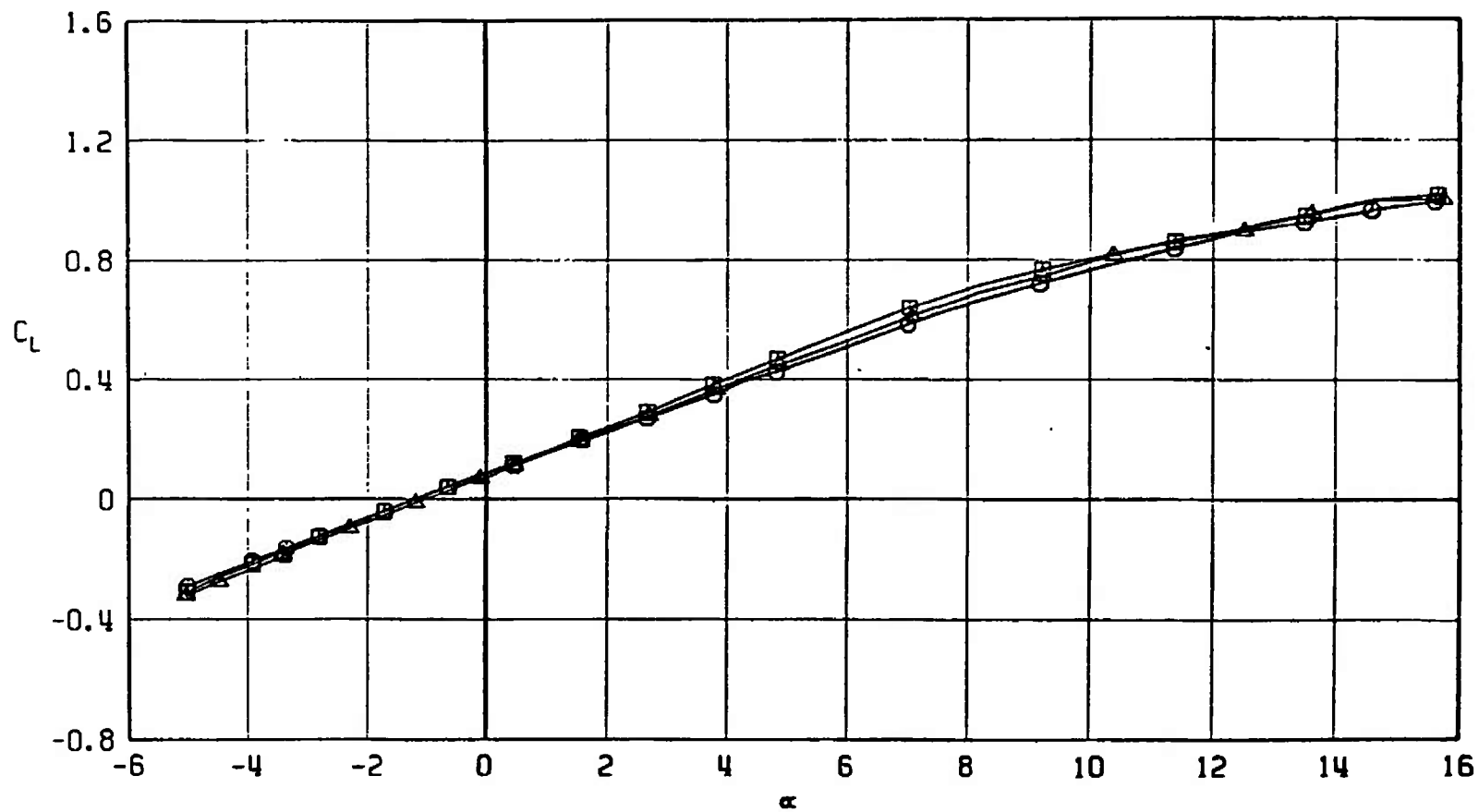
SYMBOL	CONFIGURATION
--------	---------------

□	F401
○	F420
△	F419



$c. M_{\infty} = 0.95$   
Fig. 52 Continued

SYMBOL	CONFIGURATION
□	F401
○	F420
△	F419



d.  $M_\infty = 1.05$   
Fig. 52 Continued



SYMBOL	CONFIGURATION
□	F401
○	F420
△	F419

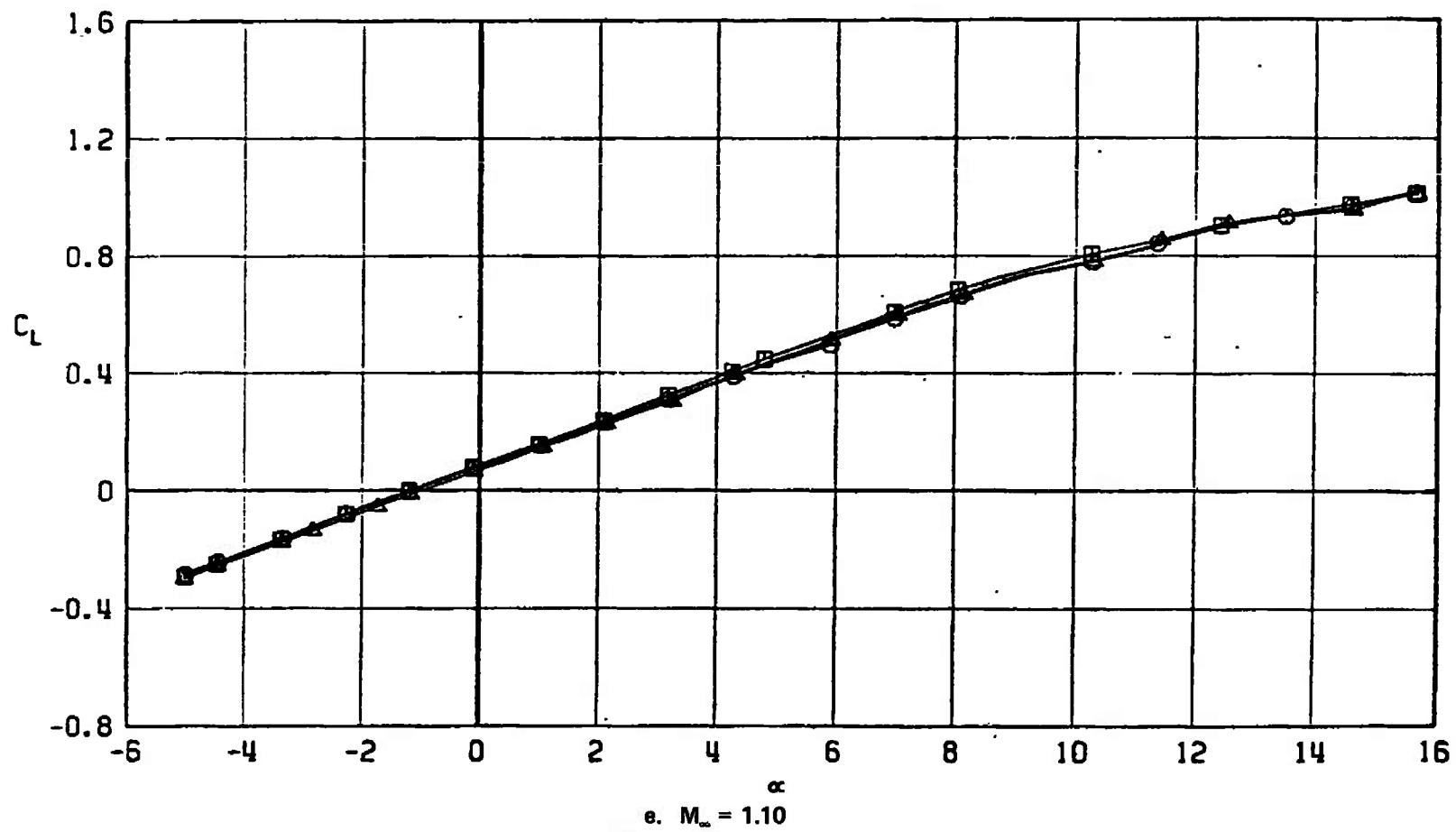
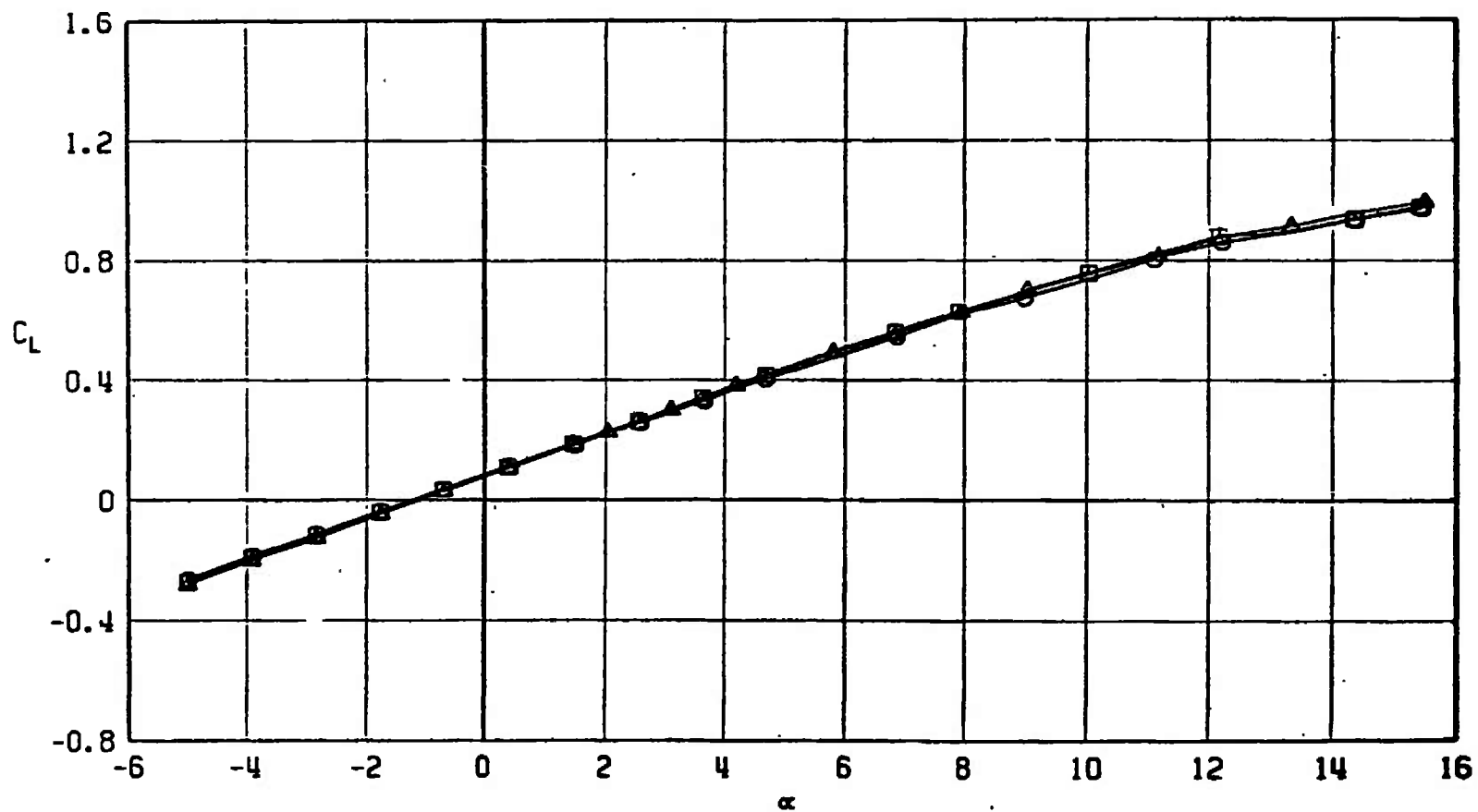


Fig. 52 Continued

SYMBOL	CONFIGURATION
□	F401
○	F420
△	F419



f.  $M_\infty = 1.20$   
Fig. 52 Concluded

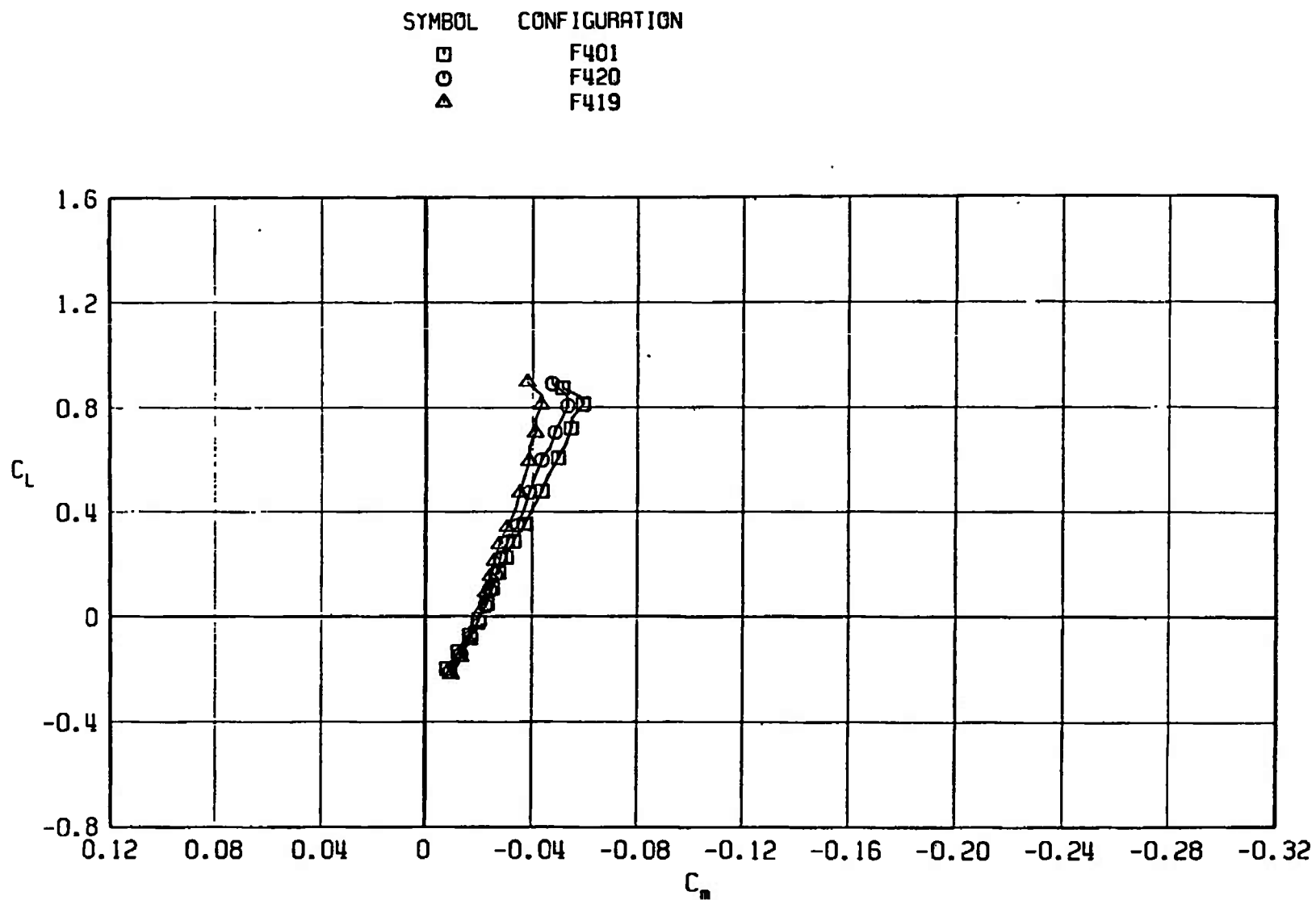
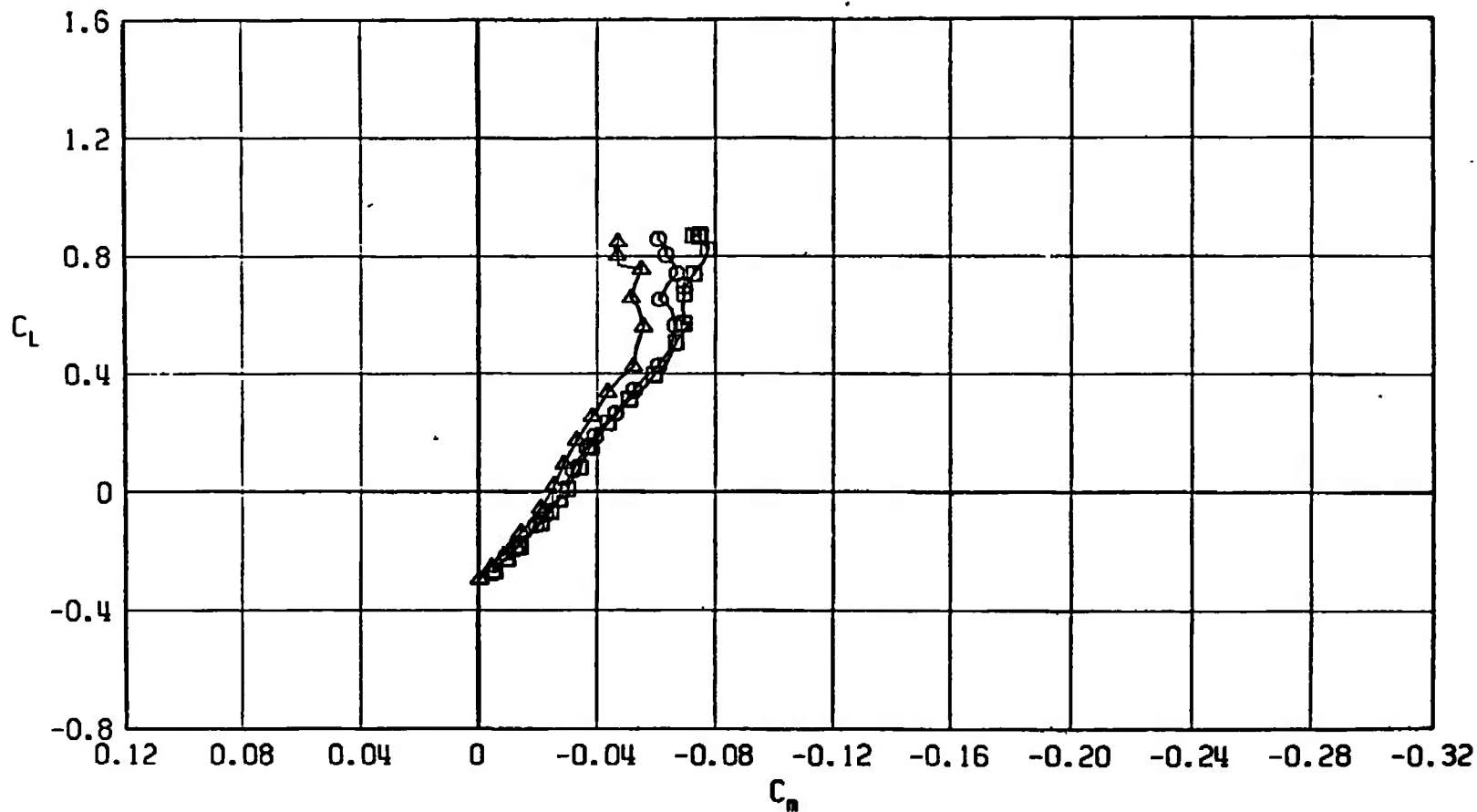
a.  $M_\infty = 0.50$ 

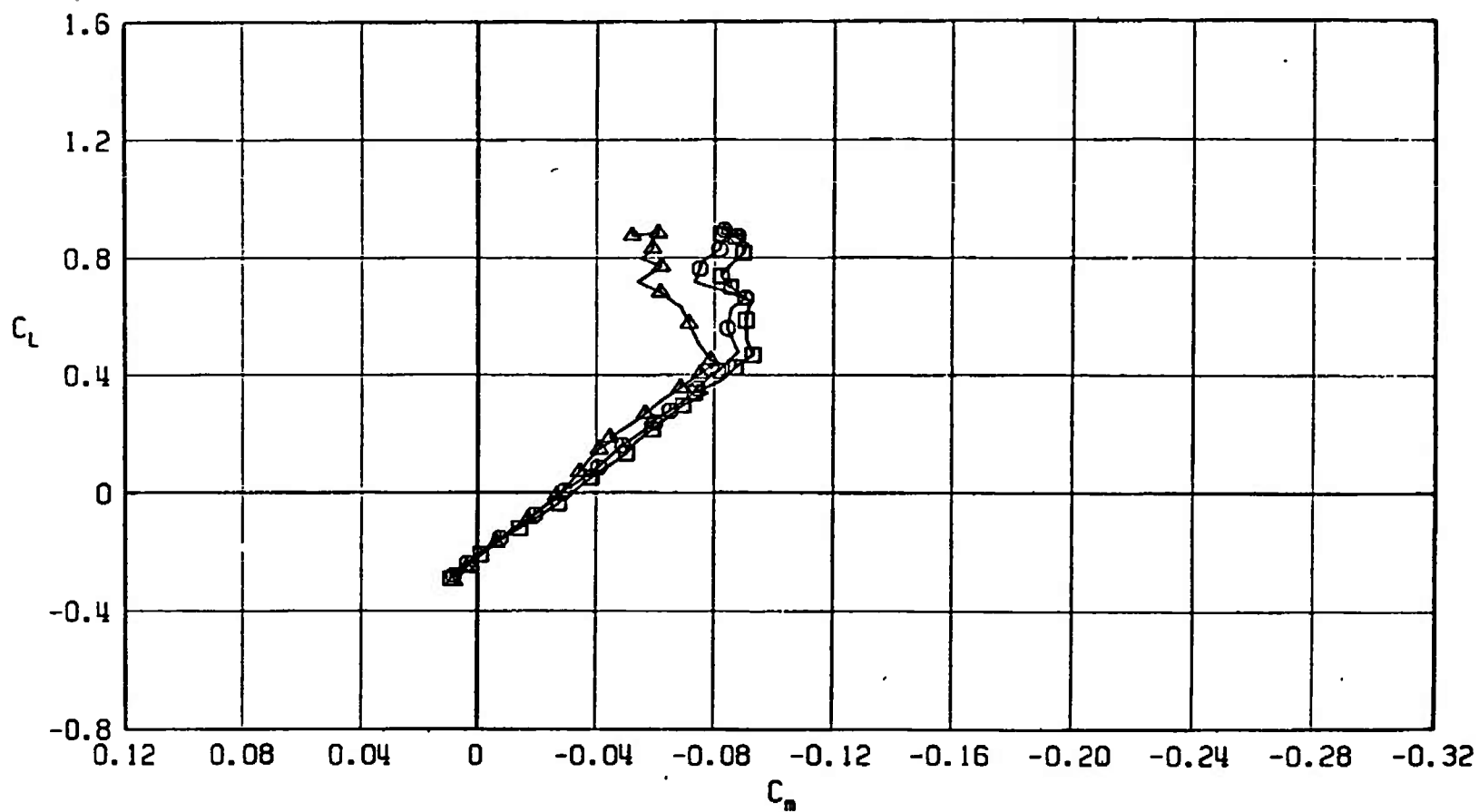
Fig. 53 Pitching-Moment Coefficient Variaton with Lift Coefficient for Configurations F401, F419, and F420

SYMBOL	CONFIGURATION
□	F401
○	F420
△	F419



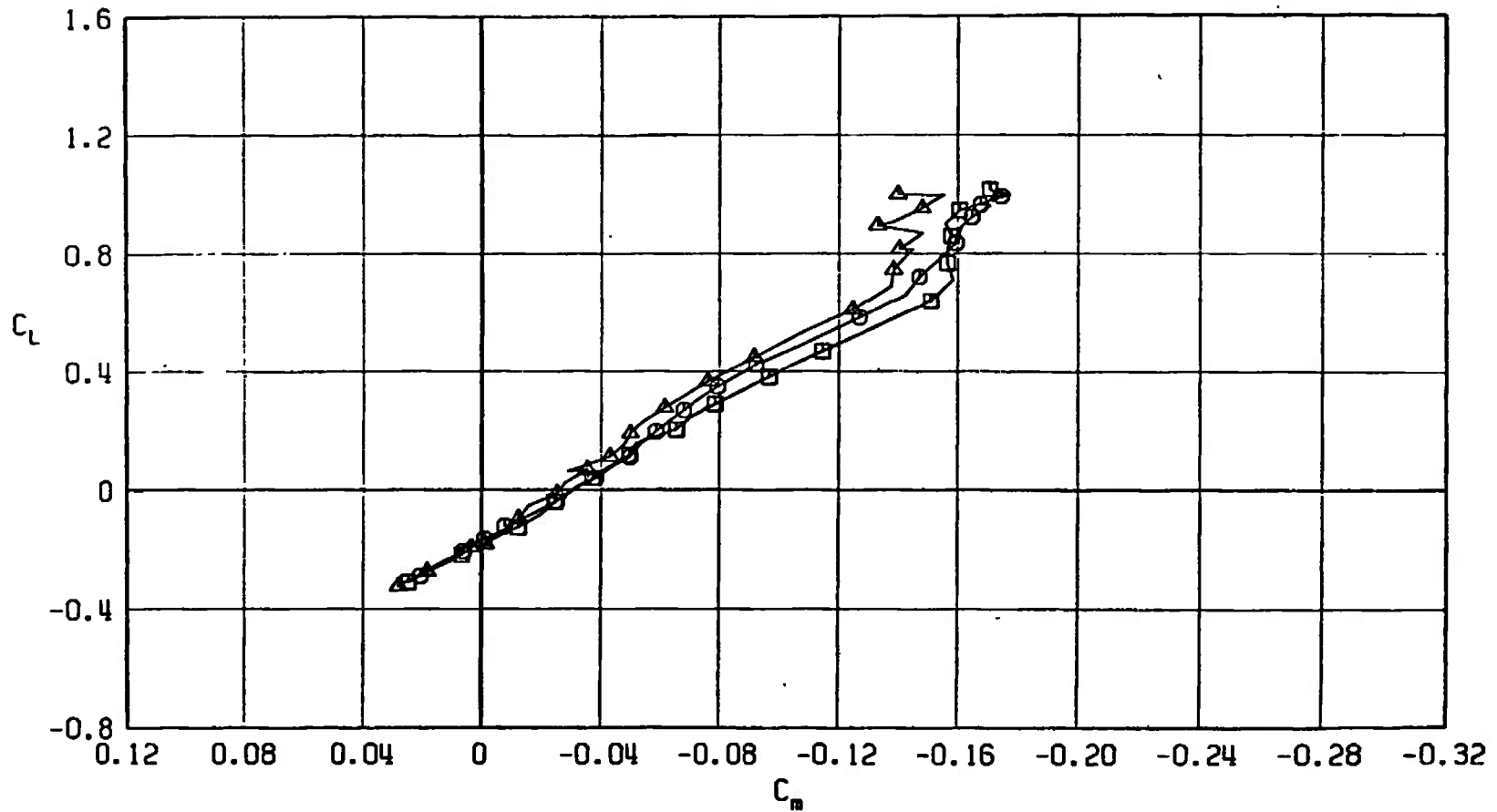
b.  $M_\infty = 0.90$   
Fig. 53 Continued

SYMBOL	CONFIGURATION
□	F401
○	F420
△	F419



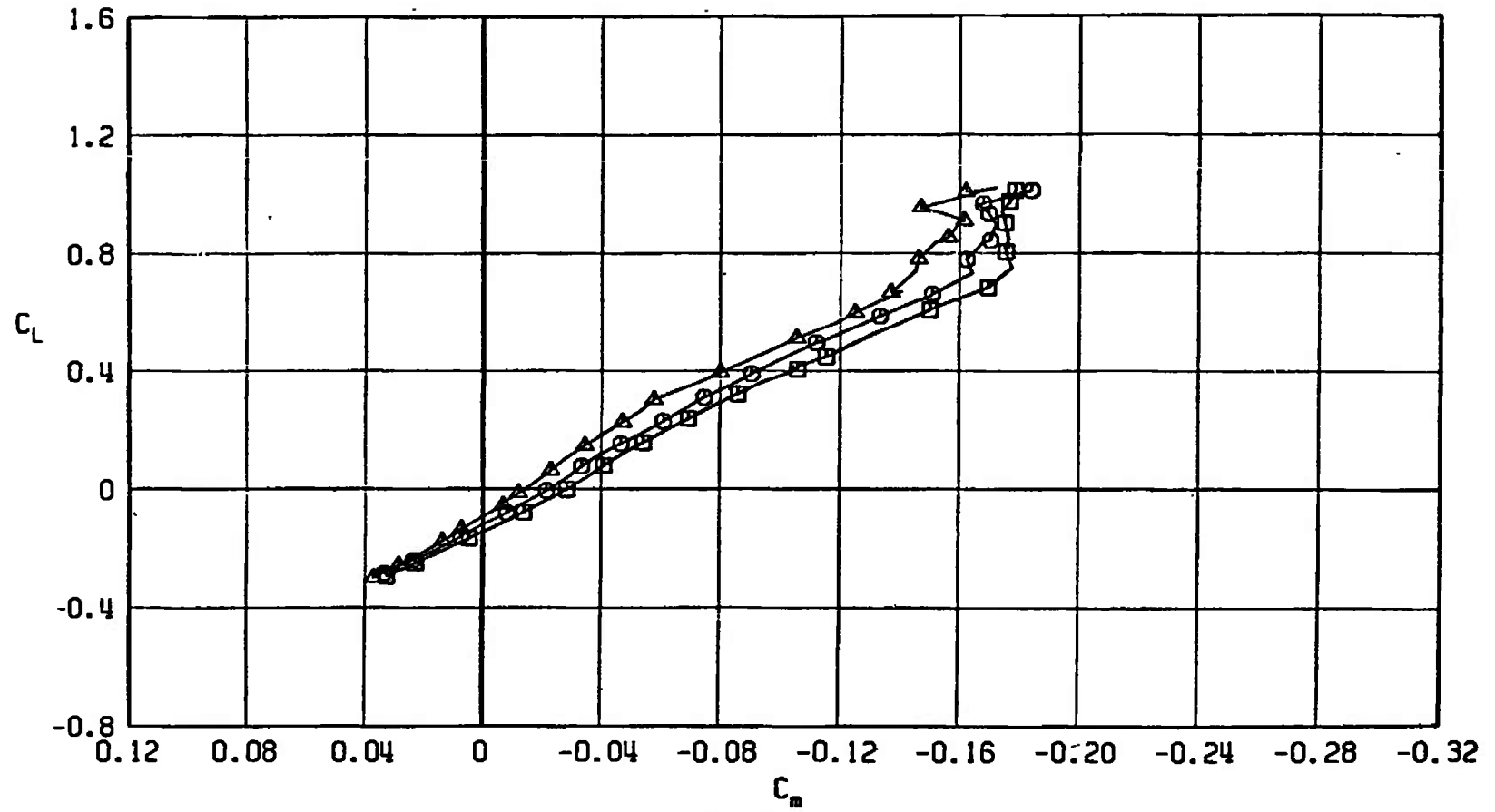
c.  $M_\infty = 0.95$   
Fig. 53 Continued

SYMBOL	CONFIGURATION
□	F401
○	F420
△	F419



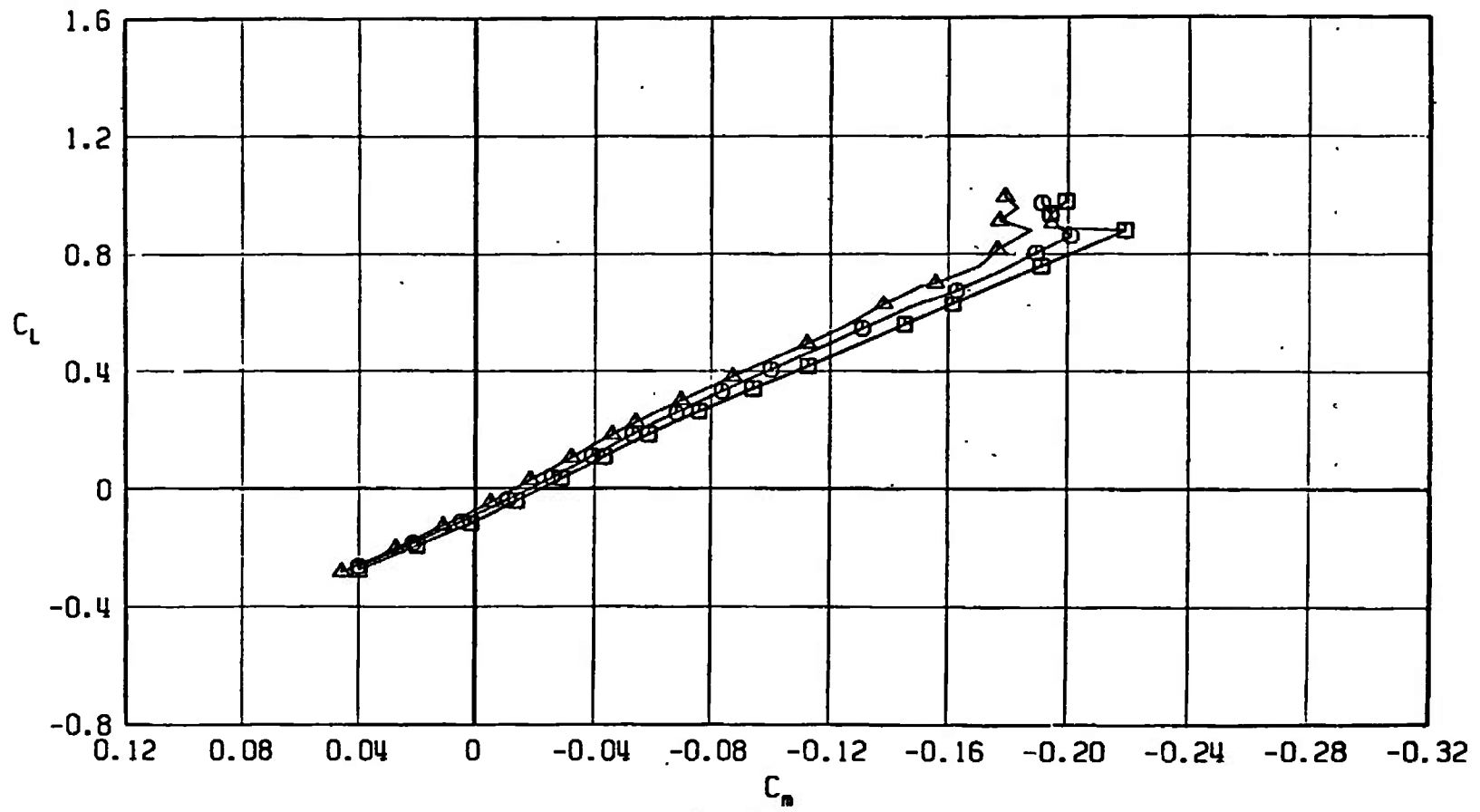
d.  $M_\infty = 1.05$   
Fig. 53 Continued

SYMBOL	CONFIGURATION
□	F401
○	F420
△	F419



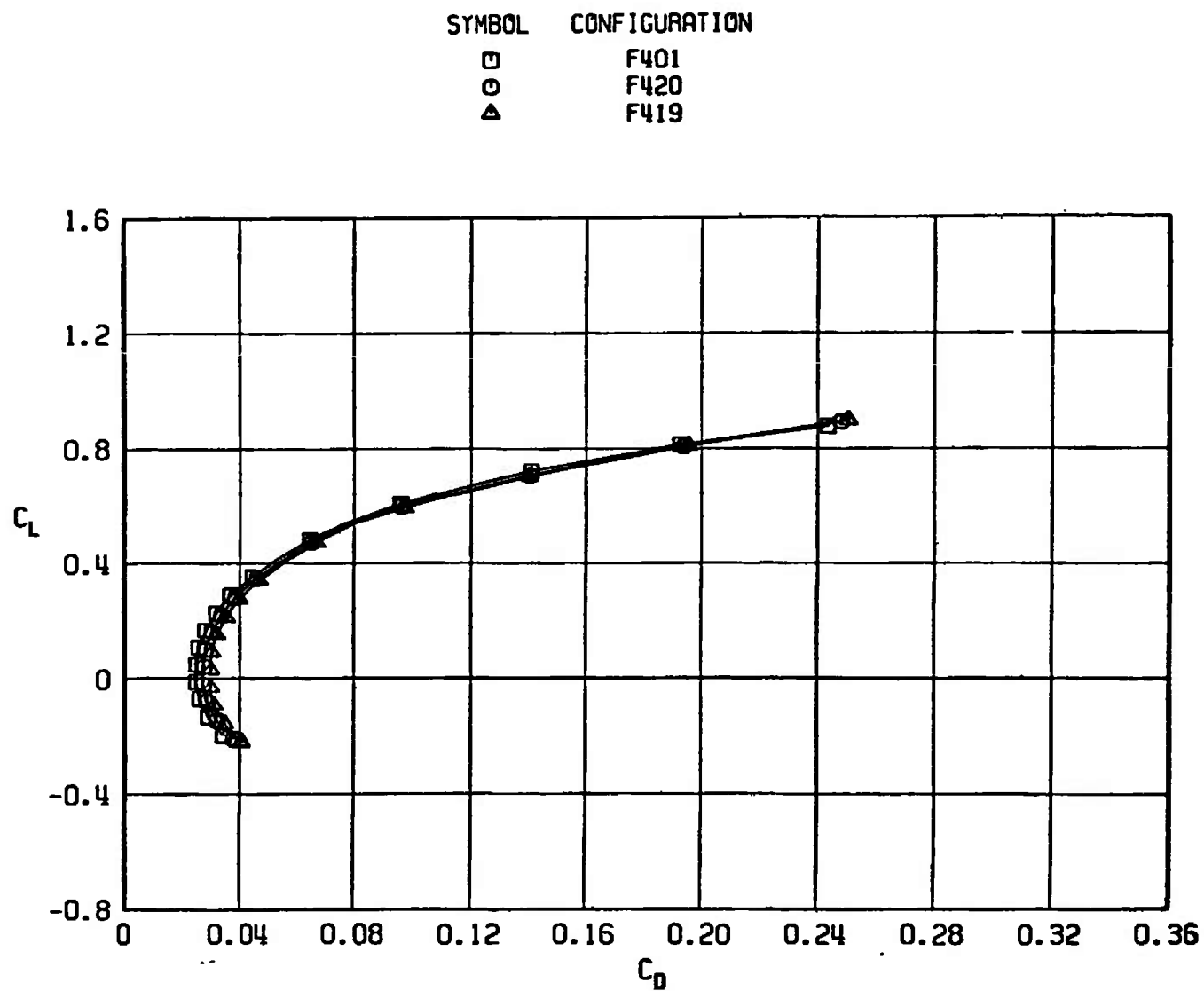
e.  $M_\infty = 1.10$   
Fig. 53 Continued

SYMBOL	CONFIGURATION
□	F401
○	F420
△	F419



f.  $M_\infty = 1.20$   
Fig. 53 Concluded

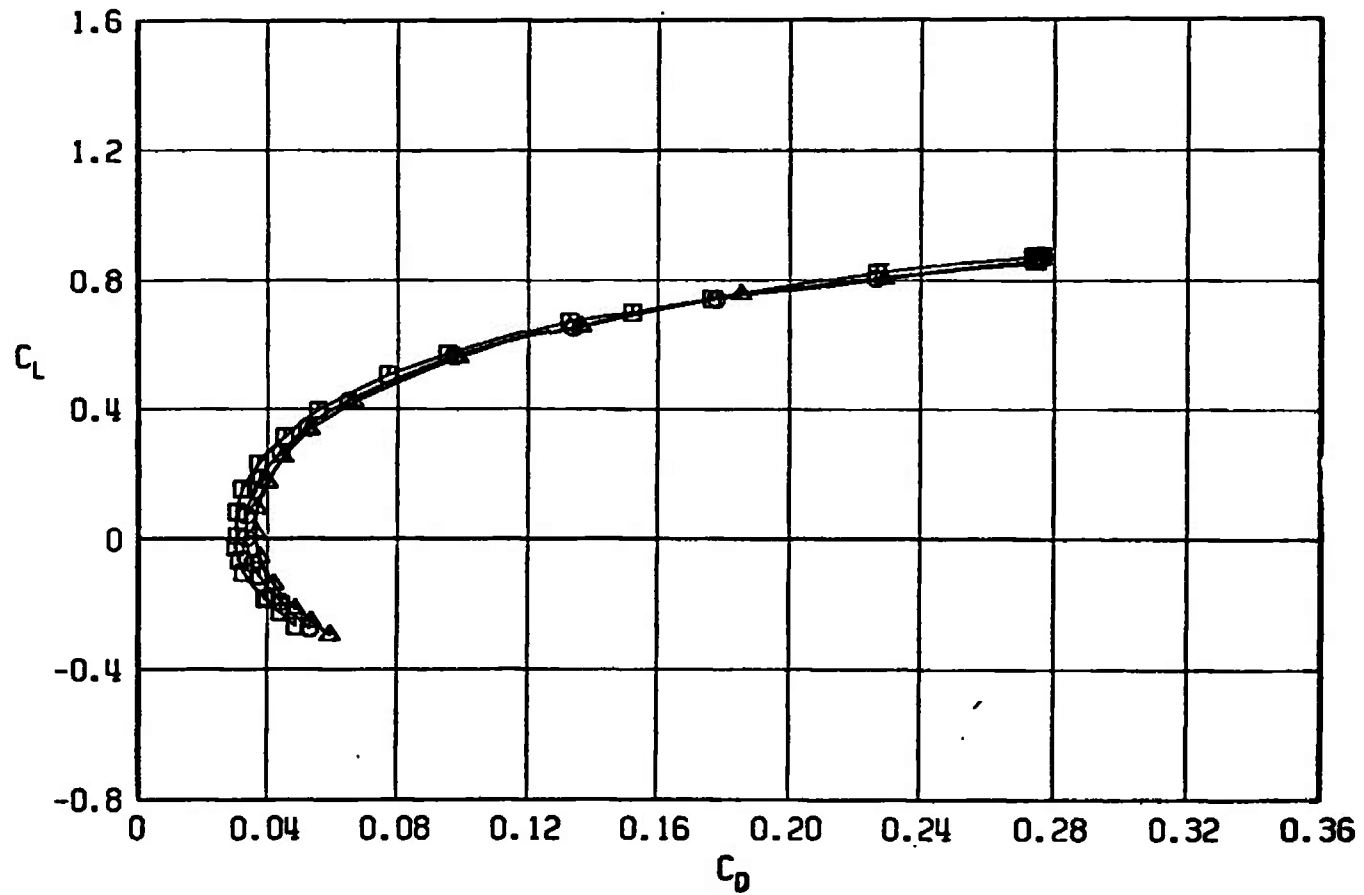




a.  $M_\infty = 0.50$

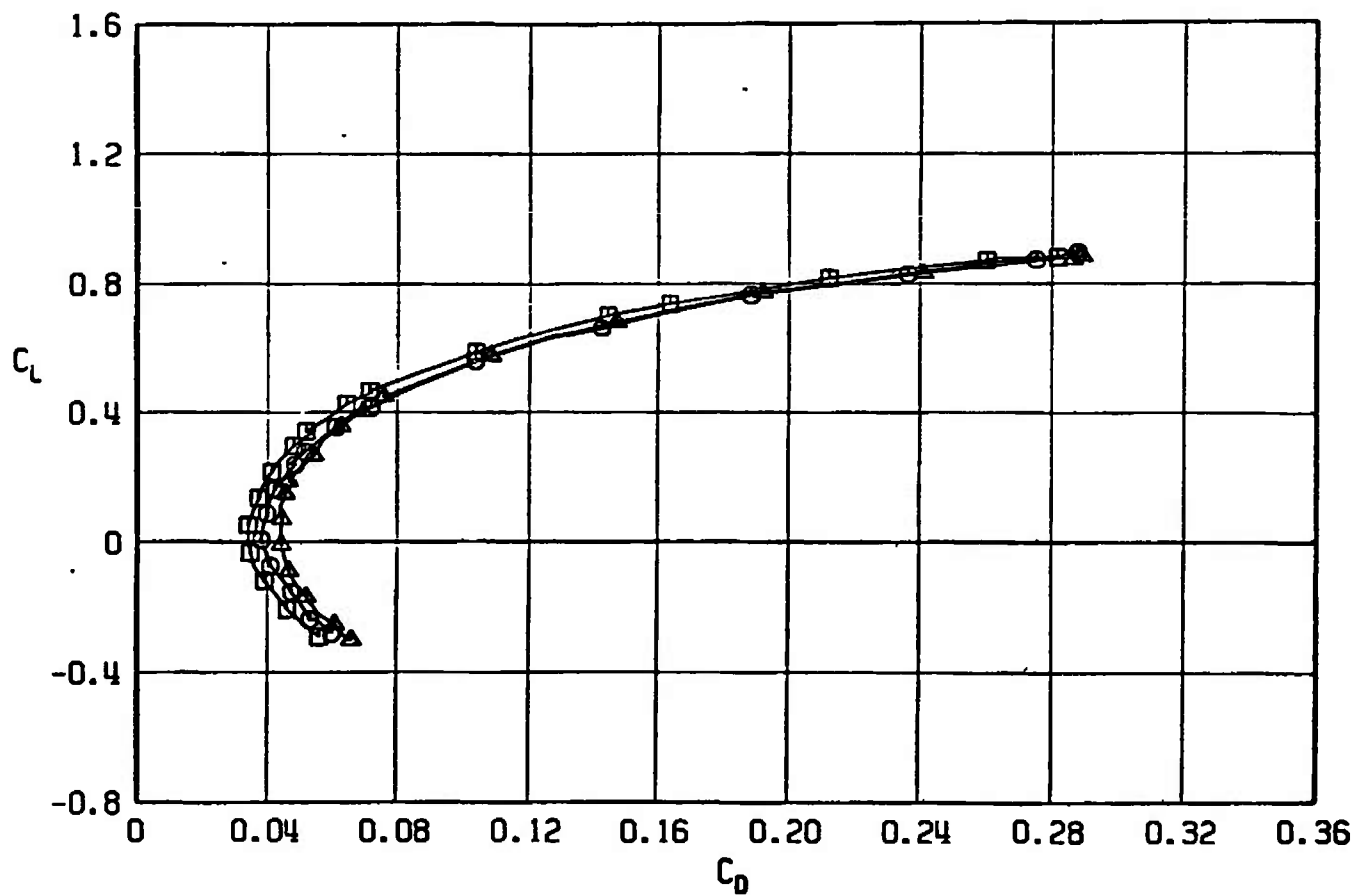
Fig. 54 Drag Coefficient Variation with Lift Coefficient for Configurations F401, F419, and F420

SYMBOL	CONFIGURATION
□	F401
○	F420
△	F419



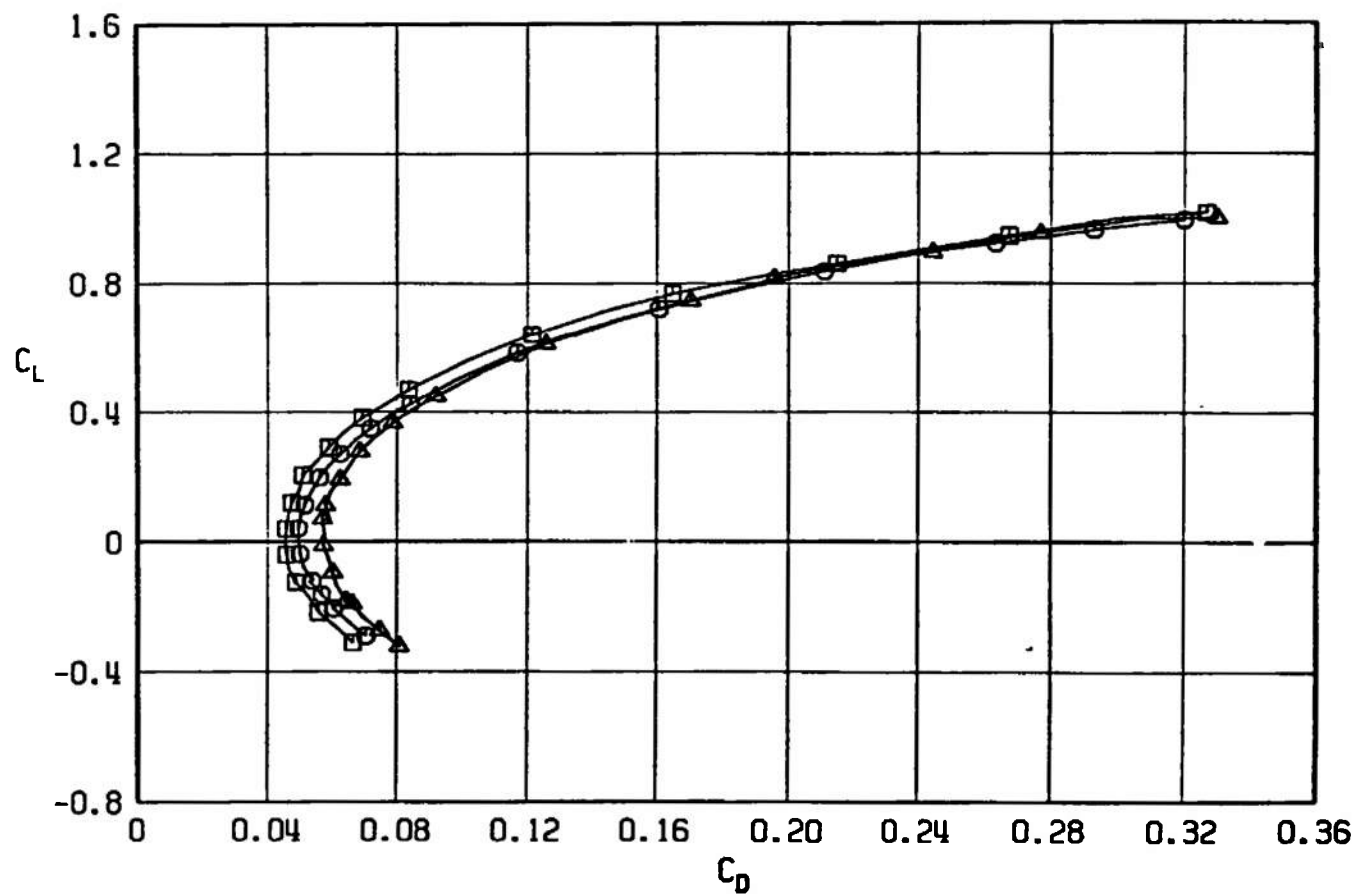
b.  $M_\infty = 0.90$   
Fig. 54 Continued

SYMBOL	CONFIGURATION
□	F401
○	F420
△	F419

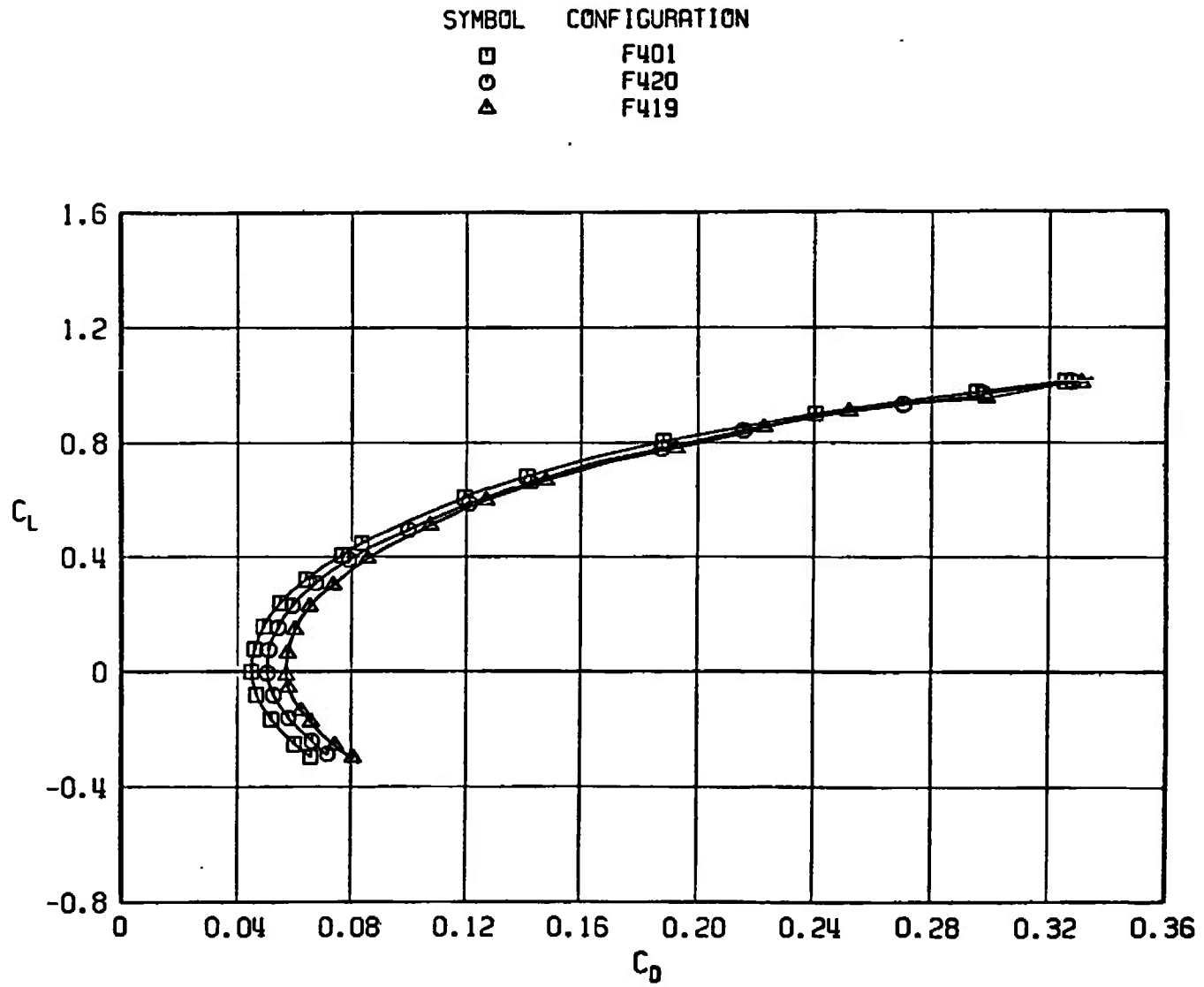


c.  $M_\infty = 0.95$   
Fig. 54 Continued

SYMBOL	CONFIGURATION
□	F401
○	F420
△	F419



d.  $M_\infty = 1.05$   
Fig. 54 Continued



e.  $M_\infty = 1.10$   
Fig. 54 Continued

SYMBOL      CONFIGURATION

□

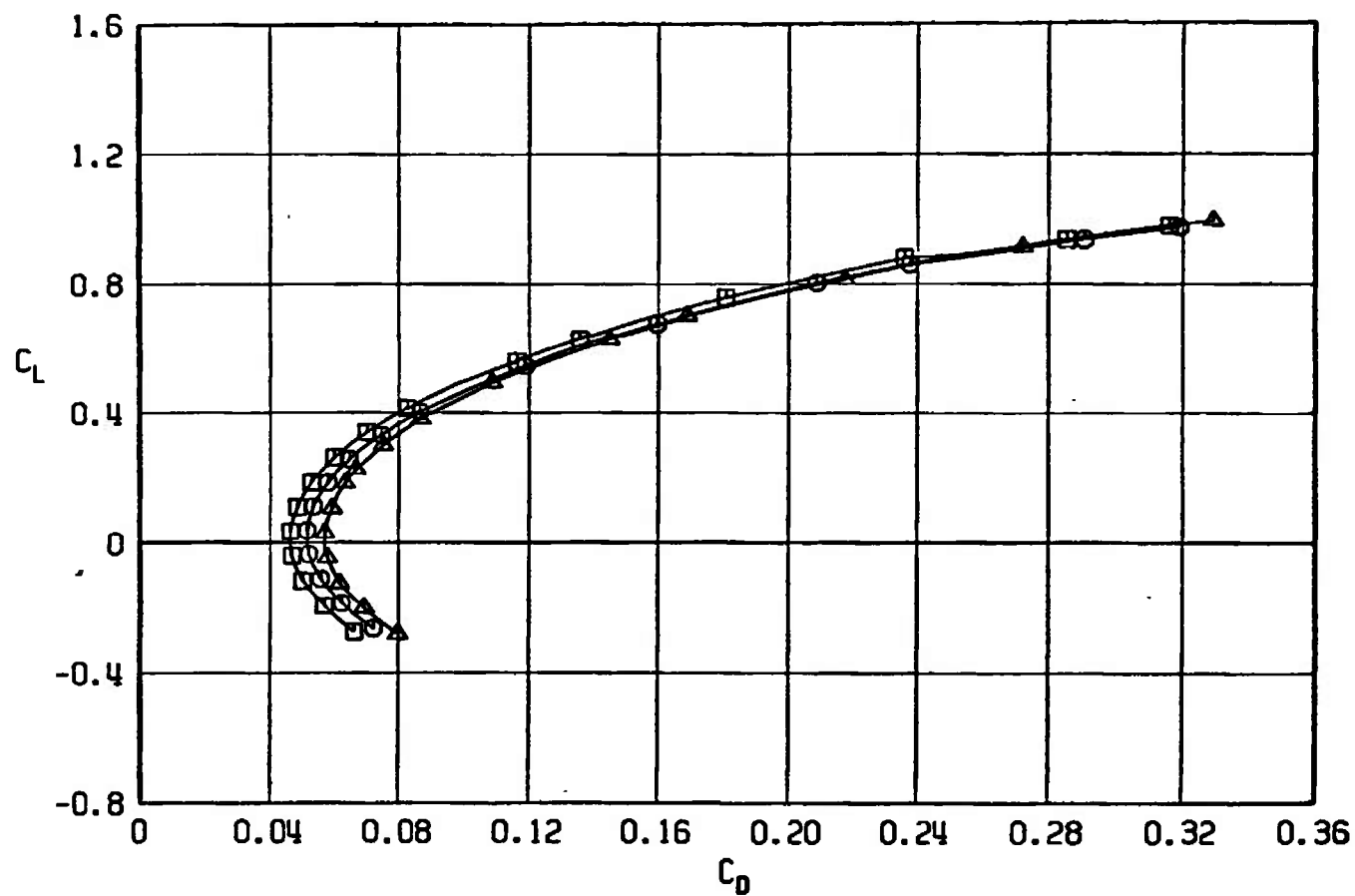
F401

○

F420

△

F419



f.  $M_\infty = 1.20$   
Fig. 54 Concluded

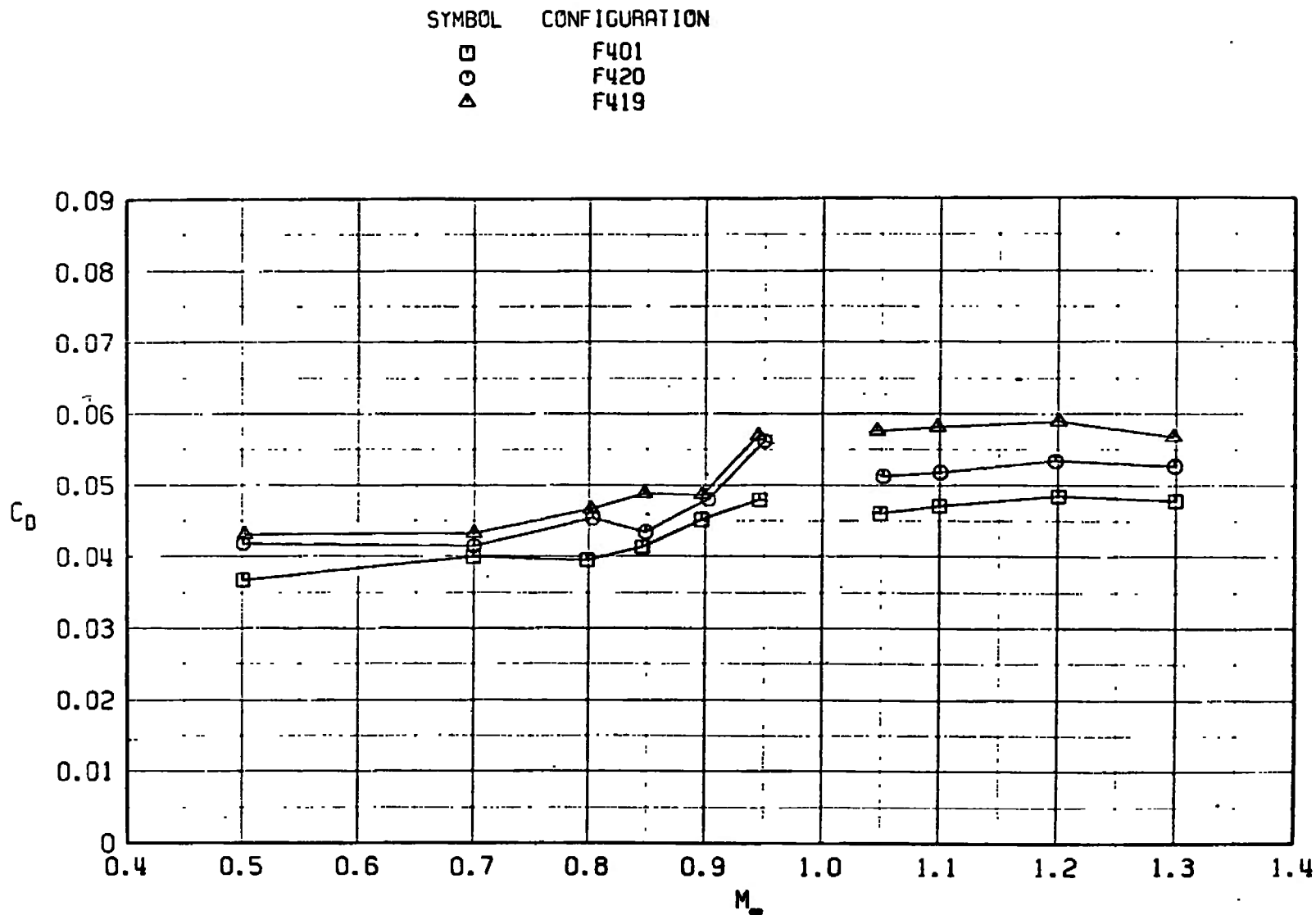


Fig. 55 Drag Coefficient Variation with Mach Number at  $C_L = 0.30$ ,  $M_\infty < 1.0$  and  $C_L = 0.1$ ,  $M_\infty > 1.0$  for Configurations F401, F419, and F420

**TABLE I**  
**AIRCRAFT LOAD CONFIGURATIONS**

A-7D			
<u>Configuration</u>	<u>Inboard</u>	<u>Mid-Wing</u>	<u>Outboard</u>
A701	Clean	Clean	Clean
A702	Clean	Pylon plus MER plus M-117; Sta 2, 3, 4	Clean
A703	Clean	Left wing only plus pylon plus MER plus M-117; Sta 2, 3, 4	Clean
A704	Clean	Pylon plus TER plus M-117; Sta 1, 2, 3	Clean
A705	Case G	Clean	Clean
A706	Clean	Case G	Clean
A707	Clean	Clean	Case G
A710	Clean	Clean	Case D
A711	Left wing only, Case G	Clean	Clean
A712	Clean	Left wing only, Case G	Clean
A713	Clean	Clean	Left wing only, Case G
F-4E			
	<u>Centerline</u>	<u>Inboard</u>	<u>Outboard</u>
F401	Clean	Clean	Clean
F402	Pylon plus MER	Pylon plus TER	370-gal fuel tank
F403	Clean	Pylon plus TER plus MK-82; Sta 1, 2, 3	370-gal fuel tank
F404	Clean	Pylon plus TER plus M-117; Sta 1, 2, 3	370-gal fuel tank
F405	Clean	Case A	Clean
F406	Clean	Case B	Clean
F407	Clean	Case C	Clean
F408	Clean	Case D	Clean
F409	Clean	Case E	Clean
F410	Clean	Case F	Clean
F411	Clean	Case G	Clean
F412	Clean	Left wing only, Case A	Clean
F415	Clean	Left wing only, Case D	Clean
F418	Clean	Left wing only, Case G	Clean
F419	Clean	Clean	Case G
F420	Clean	Clean	Left wing only, Case G



TABLE II  
GUIDE TO FIGURE INTERPRETATION

Figures	Variable	Configurations
12, 13, 14, and 15	Store addition, carriage configuration	A-7D A701, A702, A703, and A704
16, 17, 18, and 19	Parametric-shape configuration	A701, A707, and A710
20, 21, 22, and 23	Parametric-shape carriage position	A701, A711, A712, and A713
24, 25, 26, and 27	↓	A701, A705, A706, and A707
28, 29, 30, and 31	Parametric-shape configuration addition	A701, A707, and A713
32, 33, 34, and 35	Store addition, store configuration	F-4E F401, F402, F403, and F404
36, 37, 38, and 39	Parametric-shape configuration	F401, F412, F415, and F418
40, 41, 42, and 43	↓	F401, F405, F406, and F407
44, 45, 46, and 47	↓	F401, F408, F409, F410, and F411
48, 49, 50, and 51	Parametric-shape carriage position	F401, F411, and F419
52, 53, 54, and 55	Parametric-shape configuration addition	F401, F419, and F420

UNCLASSIFIED

Security Classification

## DOCUMENT CONTROL DATA - R &amp; D

(Security classification of title, body of abstract and indexing annotation must be entered when the overall report is classified)

## 1. ORIGINATING ACTIVITY (Corporate author)

Arnold Engineering Development Center  
ARO, Inc., Operating Contractor  
Arnold Air Force Station, Tennessee

## 2a. REPORT SECURITY CLASSIFICATION

UNCLASSIFIED

## 2b. GROUP

N/A

## 3. REPORT TITLE

LONGITUDINAL STATIC STABILITY AND DRAG CHARACTERISTICS OF A-7D AND F-4E  
AIRCRAFT WITH VARIOUS EXTERNAL STORE CONFIGURATIONS AT TRANSONIC SPEEDS

## 4. DESCRIPTIVE NOTES (Type of report and inclusive dates)

Final Report - November 9 to 17, 1970

## 5. AUTHOR(S) (First name, middle initial, last name)

Ronald E. Davis, ARO, Inc.

## 6. REPORT DATE

April 1971

## 7a. TOTAL NO. OF PAGES

217

## 7b. NO. OF REFS

0

## 8a. CONTRACT OR GRANT NO. F40600-71-C-0002

## b. PROJECT NO. 2567

## c. Program Element 62602F

## d.

## 9a. ORIGINATOR'S REPORT NUMBER(S)

AEDC-TR-71-54

## 9b. OTHER REPORT NO(S) (Any other numbers that may be assigned this report)

ARO-PWT-TR-71-16

10. DISTRIBUTION STATEMENT Distribution limited to U.S. Government agencies only; contains information covering the test and evaluation of military hardware; April 1971; other requests for this document must be referred to AFATL (DLII), Eglin AFB, Florida 32542.

## 11. SUPPLEMENTARY NOTES

Available in DDC

## 12. SPONSORING MILITARY ACTIVITY

Air Force Armament Laboratory  
(DLII), Eglin AFB, Florida 32542

## 13. ABSTRACT

Longitudinal aerodynamic characteristics of 0.05-scale models of A-7D and F-4E aircraft were obtained at Mach numbers from 0.50 to 1.30 to determine the effects of store configuration and location on stability and drag. Prototypes, as well as a family of proposed store configurations, were tested.

Distribution limited to U.S. Government agencies only; contains information covering the test and evaluation of military hardware; April 1971; other requests for this document must be referred to AFATL (DLII), Eglin AFB, Florida 32542.

This document has been approved for public release  
its distribution is unlimited. Per AF letter H 4  
12 April, 1976-  
William O. Cook-

UNCLASSIFIED

Security Classification

14.	KEY WORDS	LINK A		LINK B		LINK C	
		ROLE	WT	ROLE	WT	ROLE	WT
	A-7D aircraft F-4E aircraft scale models external stores aerodynamic characteristics transonic flow bombs wind tunnels						

APSC  
Arnold AFB Tenn

UNCLASSIFIED

Security Classification